

**ACOUSTIC CHARACTERIZATION OF ULTRASOUND CONTRAST
MICROBUBBLES AND ECHOGENIC LIPOSOMES:
APPLICATIONS TO IMAGING AND DRUG-DELIVERY**

by

Shirshendu Paul

A dissertation submitted to the Faculty of the University of Delaware in partial fulfillment of the requirements for the degree of Doctor of Philosophy in Mechanical Engineering

Fall 2013

© 2013 Shirshendu Paul
All Rights Reserved

UMI Number: 3640166

All rights reserved

INFORMATION TO ALL USERS

The quality of this reproduction is dependent upon the quality of the copy submitted.

In the unlikely event that the author did not send a complete manuscript and there are missing pages, these will be noted. Also, if material had to be removed, a note will indicate the deletion.



UMI 3640166

Published by ProQuest LLC (2014). Copyright in the Dissertation held by the Author.

Microform Edition © ProQuest LLC.

All rights reserved. This work is protected against unauthorized copying under Title 17, United States Code



ProQuest LLC.
789 East Eisenhower Parkway
P.O. Box 1346
Ann Arbor, MI 48106 - 1346

**ACOUSTIC CHARACTERIZATION OF ULTRASOUND CONTRAST
MICROBUBBLES AND ECHOGENIC LIPOSOMES:
APPLICATIONS TO IMAGING AND DRUG-DELIVERY**

by

Shirshendu Paul

Approved: _____

Suresh G. Advani, Ph.D.
Chair of the Department of Mechanical Engineering

Approved: _____

Babatunde A. Ogunnaike, Ph.D.
Dean of the College of Engineering

Approved: _____

James G. Richards, Ph.D.
Vice Provost for Graduate and Professional Education

I certify that I have read this dissertation and that in my opinion it meets the academic and professional standard required by the University as a dissertation for the degree of Doctor of Philosophy.

Signed: _____

Kausik Sarkar, Ph.D.
Professor in charge of dissertation

I certify that I have read this dissertation and that in my opinion it meets the academic and professional standard required by the University as a dissertation for the degree of Doctor of Philosophy.

Signed: _____

Lian-Ping Wang, Ph.D.
Member of dissertation committee

I certify that I have read this dissertation and that in my opinion it meets the academic and professional standard required by the University as a dissertation for the degree of Doctor of Philosophy.

Signed: _____

Liyun Wang, Ph.D.
Member of dissertation committee

I certify that I have read this dissertation and that in my opinion it meets the academic and professional standard required by the University as a dissertation for the degree of Doctor of Philosophy.

Signed: _____

Sanku Mallik, Ph.D.
Member of dissertation committee

PREFACE

The successful completion of this dissertation was made possible by contributions from several people. This is a humble attempt to recognize their support and encouragement that was the driving force during my graduate studies. Anything that I had achieved during my doctoral studies would not have been possible without them.

First and foremost, I will like to thank my adviser, Prof. Kausik Sarkar, for everything he has done for me. Words fail to describe his immense contributions to my life, both personally and professionally. He made an undergraduate, fresh out of college, a part of his research group and transformed him into a thoughtful researcher by providing careful guidance and tireless encouragement. He made sure that my doctoral studies would help me imbibe all the qualities required to achieve the professional success I desired without taking away the enjoyments of being a part of the academic research environment. Under his guidance, not only did I learn how to approach a problem and come up with creative ways to solve it, but also how to formulate a problem worth solving — the most essential skill to be a successful researcher. He also gave invaluable suggestions to improve my technical writing and presentation skills. I will always be grateful to him for providing me a memorable Ph.D. experience.

I am also grateful to Prof. Sanku Mallik for his continued support both as our collaborator and as a member of my thesis committee. He has been the driving force behind the implementation of several novel and creative ideas during my doctoral research. He has always been extremely supportive in providing me with everything that I required from his side for the successful completion of our research goals. A significant portion of this thesis and several of my publications have been the result of our collaborative work with Prof. Mallik and his students.

I am thankful to Prof. Lian-Ping Wang, for his guidance as a member of my thesis committee. Prof. Wang's insightful questions had always motivated me to critically analyze the results and understand their physical significance. Prof. Wang has also been a great teacher during the two graduate level courses I took under him — *Multiphase Flows* and *Computational Fluid Mechanics*. Both these courses have been extremely beneficial in improving my understanding of fluid mechanics and its numerical implementation. The vigor with which he taught both the courses was truly astounding.

I also owe my sincere gratitude to Prof. Liyun Wang, for her contributions as a member of my thesis committee and as my teacher. She introduced me to the rapidly expanding field of biomedical engineering during her courses on *Cell and Tissue Transport* and *Cytomechanics*. She always encouraged the students to pursue a thorough and methodical review of the literature and interactive group discussions in her courses — two skills that have been immensely beneficial during the later stages of my doctoral research.

I am thankful to Prof. Valerie Roy, Prof. Leonard Schwartz, Prof. Pablo Huq, Prof. Anthony Beris, and Prof. Annette Shine for their invaluable contributions to my academic training through various graduate level courses. I am also thankful to the Department of Mechanical Engineering at University of Delaware for providing me the opportunity to pursue my doctoral studies. I am sincerely grateful to the faculty and staff(especially Lisa, Lita, and Ann) at the department for their continued assistance and support throughout the course of my graduate studies. I would also like to acknowledge the help I got from the Mechanical and Aerospace Department at the George Washington University(especially Zephra and Cindy) during the final year of the doctoral studies. I would also like to acknowledge the financial support I got from the UD Mechanical Engineering and NSF during my Ph.D.

My doctoral research is largely the outcome of several collaborations and the guidance from various members of the research community. I am grateful to my coauthors Prof. Dhiman Chatterjee and Prof. Flemming Forsberg for their contributions to

my graduate research. A significant portion of my research (Chapters 4, 5) was inspired by their findings. Much of what I achieved in my research with liposomes would also not have been possible without the help of the various researchers from Prof. Mallik's lab, especially Tapas Nandy, Rahul Nahire, and Dr. Manas Halder. They have been kindly providing me with various liposome samples for my experiments and several other characterization data for the liposome samples. They have also contributed greatly to several of my publications (Chapters 9, 11). I am extremely grateful to Prof. Christy Holland at University of Cincinnati and her students Dr. Jonathan Kopechek and Kirthi Radhakrishnan for their invaluable suggestions. I am especially thankful to Jonatahan who has always welcomed my queries and has patiently responded to them on numerous occasions. I would also like to acknowledge the help from Prof. Shaolin Huang in this regard. Special thanks to Prof. Norman Wagner and Prof. Anne Robinson (also her student Andrea Naranjo) of UD Chemical Engineering Department for letting me use their equipments. I am indebted to our collaborators, Prof. Margaret Wheatley of Drexel University and her student Dr. Michael Cochran, for providing their contrast agents for my experiments. They also provided critical insights that resulted in the successful publication of our results (Chapter 6). I am also thankful to Dr. Jeffrey Ketterling and Dr. Parag Chitnis from Riverside Research Center for providing us with multiple batches of contrast agents for my acoustic experiments. My interactions with Dr. Yanjun Gong and his adviser Prof. Tyrone Porter of Boston University have also contributed to my doctoral research.

During my graduate studies, the support from my friends and colleagues have also made these past few years even more enjoyable. I will like to thank all the members of the research group under Prof. Sarkar — Dr. Amit Katiyar, Dr. Swarnajay Mukherjee, Dr. Rajesh Singh, Daniel Russakow, Priyesh Srivastava, Krishna Nandan, Nima Mobadersamy, Lang Xia, and Mitra Aalee — for a providing a memorable Ph.D. experience and for their friendship. I am sincerely thankful to Daniel and Tyler, the two undergraduate members of our lab, who have helped me a lot with the acquisition of the experimental data that constitute a significant portion of this dissertation. I

have also benefited through my interactions with several fellow graduate students at UD and beyond like Ananth, Harman, Himanshu and others. I have also been lucky to have the support of several wonderful friends I made over the years — Ambudhi, Seema, Sapan, Roshni, Samir, Prathamesh, Vignesh, Priyanka, Nikhil to name a few. I will also like to express my gratitude to Dr. Ohm Divyam for his recommendations that helped me acquire a job.

I will forever be grateful to my teachers in India, Prof. Amitava Datta and Prof. Ranjan Ganguly, for encouraging me to pursue graduate studies. I am also indebted to my friends in India — Madhuparna, Debajyoti, Susanta, Sreemoyee, Sayani, and Krishanu — for their encouragement and support in this regard.

Finally, I will like express my deepest love and sincere regards to my parents, Indira and Samir Paul. Without their unconditional love, support, tireless encouragement, sincere guidance, and invaluable sacrifices, I would not have achieved anything that I have today. They have been patiently waiting alone and praying every day for the successful completion of my doctoral studies. I am also grateful to my family members, especially my uncle Mr. Pijush Ranjan Saha and my cousin Anirvan Saha, for their guidance and support.

Dedicated to my loving parents, Indira Paul and Samir Kumar Paul.

TABLE OF CONTENTS

LIST OF TABLES	xix
LIST OF FIGURES	xxi
ABSTRACT	xxvii
Chapter	
1 INTRODUCTION	1
1.1 Motivation	1
1.2 General Aims of this Study	2
1.3 Specific Objectives	3
1.4 Organization of this dissertation	4
2 BACKGROUND AND BASIC CONCEPTS	6
2.1 Ultrasound and Its Applications in Medicine	6
2.1.1 Basics of Ultrasound and Acoustics	6
2.1.2 History and Medical Applications	8
2.2 Ultrasound Contrast Agents	9
2.2.1 Ultrasound Contrast Agents in Imaging	11
2.2.2 Ultrasound Contrast Agents in Therapy	13
2.3 Echogenic Liposomes and Polymersomes	14
2.4 Single Bubble Dynamics	15
2.4.1 Uncoated Bubbles	15
2.4.2 Encapsulated Bubbles	18
2.4.3 Small-Amplitude Oscillations	21
2.4.3.1 Acoustic Cross-Sections	24

2.4.3.2	Damping Factors	25
2.4.3.2.1	Viscous Damping in Compressible Liquid	26
2.4.3.2.2	Thermal Damping and Choice of Polytropic Index	27
2.4.3.3	Resonance Frequency	28
2.4.4	Large-Amplitude Oscillations	32
2.4.4.1	Resonance Behavior and Damping Factor	32
2.4.4.2	Nonlinear Behavior	32
2.4.4.2.1	Second-Harmonics	34
2.4.4.2.2	Subharmonics	35
2.4.4.3	Modeling the Scattered Acoustic Pressure Field	35
2.5	Dynamics of a Suspension of Bubbles	36
2.5.1	Attenuation	36
2.5.1.1	Multiple Scattering Effects	38
2.5.1.2	Attenuation and Resonance Frequency	39
2.5.2	Speed of Sound	40
2.5.3	Scattering	41
2.5.4	Bubble Dissolution and Bubble Destruction	41
2.6	Experimental Characterization of Ultrasound Contrast Agents	43
2.6.1	Acoustic Attenuation and Scattering	43
2.6.2	Radial Dynamics	45
2.6.3	Experimental Strategies to Avoid Polydispersity	47
2.7	Material Characterization of the Encapsulation	47
3	EXPERIMENTAL METHODS	49
3.1	Size Measurements	50
3.1.1	Dynamic Light Scattering	50

3.1.2	Coulter Counter	51
3.2	Microscopic Imaging of the Particles	51
3.2.1	Transmission Electron Microscopy	51
3.2.2	Atomic Force Microscopy	52
3.3	Acoustic Experiments	52
3.3.1	Details of Transducer Used in this Study	52
3.3.2	Transducer Calibrations	53
3.3.2.1	Experimental Procedure and Data Reduction	54
3.3.3	Attenuation and Phase Velocity Measurements	58
3.3.3.1	Setup Description	58
3.3.3.2	Experimental Procedure and Data Reduction Technique	59
3.3.4	Scattering Measurements	61
3.3.4.1	Setup Description	61
3.3.4.2	Experimental Procedure and Data Reduction Technique	63
3.3.5	Time Dependent Attenuation and Scattering Experiments . .	63
3.3.6	Ultrasound Imaging	65
3.3.7	Ultrasound Mediated Release Studies	65
3.3.7.1	Setup Description	65
3.3.7.2	Quantification of Release	67
3.4	Summary	68
Part I	CHARACTERIZATION OF ULTRASOUND CONTRAST MICROBUBBLES	69
4	A STRAIN-SOFTENING INTERFACIAL RHEOLOGICAL MODEL OF THE ULTRASOUND CONTRAST AGENT ENCAPSULATION	70
4.1	Introduction	70

4.2 Mathematical Formulation	73
4.2.1 Assumptions	73
4.2.2 Bubble Dynamics	74
4.2.3 Interfacial Rheology	75
4.2.3.1 Newtonian Rheology	76
4.2.3.2 Viscoelastic Rheology with a Constant Elasticity	76
4.2.3.3 Viscoelastic Rheology with a Quadratic Elasticity	79
4.2.3.4 Viscoelastic Rheology with a Exponentially Varying Elasticity	81
4.2.3.5 Marmottant Model	82
4.3 Prediction of Bubble Dynamics	84
4.3.1 Radial Dynamics	85
4.3.2 Subharmonic Generation Thresholds	89
4.4 Summary and Conclusions	91
5 CHARACTERIZATION OF LIPID COATED MICROBUBBLES	93
5.1 Introduction	93
5.2 Experimental Methods	94
5.3 Material Characterization of the Encapsulation Using Attenuation	95
5.3.1 Method	95
5.3.2 Results and Discussion	97
5.3.2.1 Sonazoid Microbubbles	97
5.3.2.2 Definity Microbubbles	100
5.4 Prediction of Scattered Fundamental and Subharmonic Response	103
5.4.1 Method	103
5.4.2 Results and Discussion	104
5.4.2.1 Sonazoid Microbubbles	104
5.4.2.2 Definity Microbubbles	108
5.4.2.3 Near-Chaotic or Chaotic Oscillations	111
5.5 Summary and Conclusion	112

6 CHARACTERIZATION OF POLYMER SHELLLED MICROBUBBLES	114
6.1 Introduction	114
6.2 Materials and Methods	116
6.2.1 Preparation Protocol	116
6.2.1.1 PLA Microbubble Preparation	116
6.2.1.2 PB-127 and Philips Bubbles	117
6.2.2 Size Distribution Measurements	118
6.2.3 Acoustic Experiments	118
6.2.4 Mathematical Modeling	120
6.3 Results and Discussion	120
6.3.1 Size Measurements	120
6.3.2 Material Characterization of the Encapsulation Using Attenuation	122
6.3.2.1 PLA microbubbles	122
6.3.2.1.1 Resonance Frequency of PLA Bubbles . .	127
6.3.2.2 PB-127 and Philips Bubbles	129
6.3.3 Time Dependent Attenuation and Destruction Thresholds for PLA Microbubbles	134
6.3.4 Scattering and Comparison with Model Predictions	137
6.3.4.1 PLA Microbubbles	137
6.3.4.1.1 Fundamental and second harmonic responses	137
6.3.4.1.2 Subharmonic Response	141

6.3.4.1.3	Model validation and their Predictive capability	142
6.3.4.2	PB-127 and Philips Microbubbles	146
6.4	Summary and Conclusions	149
7	DESIGN AND IMPLEMENTATION OF MODIFIED <i>IN VITRO</i> EXPERIMENTAL SETUPS FOR THE CHARACTERIZATION OF ULTRASOUND CONTRAST MICROBUBBLES	152
7.1	Motivation	152
7.2	Materials and Methods	153
7.2.1	Smaller Sample Volume Experimental Setup	153
7.2.2	Ambient Pressure Dependent Subharmonic Measurements	154
7.3	Results and Discussion	157
7.3.1	Smaller Sample Volume Experimental Setup	157
7.3.2	Ambient Pressure Dependent Subharmonic Measurements	159
7.4	Summary and Conclusion	161
Part II	DESIGN AND DEVELOPMENT OF ‘DUAL-PURPOSE’ ECHOGENIC LIPOSOMES AND POLYMERSOMES	163
8	A REVIEW OF ECHOGENIC LIPOSOMES	164
8.1	Echogenic Liposomes	164
8.1.1	The Preparation Protocol for Making Echogenic Liposomes	164
8.1.2	Acoustic Characterization of Echogenic Liposomes	167
8.1.3	Ultrasound Triggered Release from Echogenic Liposomes	169
9	ACOUSTIC CHARACTERIZATION OF ECHOGENIC LIPOSOMES: <i>IN VITRO</i> ATTENUATION AND SCATTERING MEASUREMENTS	172
9.1	Introduction	172

9.2 Materials and Methods	173
9.2.1 Preparation of Echogenic Liposomes and Reconstitution Procedure	173
9.3 Results and Discussion	174
9.3.1 Size Distribution	174
9.3.2 Attenuation	176
9.3.3 Scattering	179
9.4 Summary and Conclusions	185
10 ACOUSTIC CHARACTERIZATION OF <i>POLYMERIZED ECHOGENIC LIPOSOMES</i>	187
10.1 Materials and Methods	188
10.1.1 Preparation of Polymerized Echogenic Liposomes	188
10.2 Results and Discussion	189
10.2.1 Size Distribution	189
10.2.2 Ultrasonic Imaging	189
10.2.3 Attenuation Measurements	190
10.2.3.1 Time Dependent Attenuation Studies and Destruction	191
10.2.4 Scattering Measurements	196
10.3 Summary and Conclusions	202
11 ‘DUAL-PURPOSE’ ECHOGENIC LIPOSOMES AND POLYMERSOMES: PROOF OF CONCEPT	203
11.1 Motivation	203
11.1.1 MMP-9 Cleavable ELIPs	205
11.1.2 Polymer Coated Redox Triggered ELIPs	205
11.1.3 pH Sensitive Liposomes with Tunable Echogenicity	206

11.1.4 Redox Sensitive Echogenic Polymersomes	207
11.2 Materials and Methods	208
11.2.1 Preparation Protocol	208
11.2.1.1 MMP-9 Cleavable ELIPs	208
11.2.1.2 Polymer Coated Redox Triggered ELIPs	210
11.2.1.3 pH Sensitive Liposomes with Tunable Echogenicity .	211
11.2.1.4 Redox Sensitive Echogenic Polymersomes	211
11.2.2 Size Distribution Measurements and Microscopic Imaging . . .	212
11.2.3 Ultrasonic Measurements	212
11.3 Triggered Release Studies	212
11.4 Results and Discussion	214
11.4.1 Size Distribution and Microscopic Images	214
11.4.1.1 MMP-9 Cleavable ELIPs	214
11.4.1.2 Polymer Coated Redox Triggered ELIPs	216
11.4.1.3 pH Sensitive Liposomes with Tunable Echogenicity .	218
11.4.2 Proof of Echogenicity	218
11.4.2.1 MMP-9 Cleavable ELIPs	219
11.4.2.2 Polymer Coated Redox Triggered ELIPs	222
11.4.2.3 pH Sensitive Liposomes with Tunable Echogenicity .	224
11.4.2.4 Redox Sensitive Echogenic Polymersomes	227
11.4.3 Proof of Ultrasound Enhanced Stimuli Responsive Release .	231
11.4.3.1 MMP-9 Cleavable ELIPs	231
11.4.3.2 Polymer Coated Redox Triggered ELIPs	234
11.5 Summary and Conclusions	237
12 CONCLUSIONS AND FUTURE WORK	238
12.1 A Review of the Outcomes	238
12.1.1 Characterization of Ultrasound Contrast Microbubbles	238

12.1.2 Strain-Softening Models of Contrast Agent Encapsulation	239
12.1.2.1 Characterization of Lipid Coated Microbubbles	240
12.1.2.2 Characterization of Polymer Encapsulated Microbubbles	240
12.1.2.3 Experimental Investigation of Ambient Pressure Dependent Subharmonic Response	241
12.1.3 Design and Development of ‘Dual-Purpose’ Echogenic Liposomes and Polymersomes	241
12.1.3.1 Acoustic Characterization of Conventional and Polymerized Echogenic Liposomes	242
12.1.3.2 Experimental Validation of the Concept of ‘Dual-Purpose’ Contrast Agent	243
12.2 Limitations of this Study	243
12.3 Proposed Future Work	244
12.3.1 Scope for Model Improvement	244
12.3.2 Possible Experiments with Contrast Microbubbles	246
12.3.3 Possible Studies with Echogenic Liposomes	246
REFERENCES	249
Appendix	
A DERIVATION OF THE RAYLEIGH-PLESSET EQUATION	287
A.1 Incompressible Form	287
A.2 Compressible Form	288
B DERIVATION OF THE ACOUSTIC CROSS-SECTIONS	291
C DATA ACQUISITION SYSTEM AND MATLAB CODES USED IN THE ANALYSIS OF EXPERIMENTAL DATA	294
D MATLAB CODES USED IN THE PARAMETER ESTIMATION AND FOR SCATTERING PREDICTIONS	305
E REPRINT PERMISSIONS	314
E.1 Reprint Permission for Figure 2.1 in Chapter 2	314
E.2 Reprint Permissions for Chapter 3	319
E.3 Reprint Permissions for Chapter 4	333
E.4 Reprint Permissions for Chapter 5	338

E.5	Reprint Permissions for Chapter 6	348
E.6	Reprint Permission for Figure 8.1 in Chapter 8	351
E.7	Reprint Permissions for Chapter 9	356
E.8	Reprint Permissions for Chapter 11	364

LIST OF TABLES

2.1	Overview of the most commonly referred ultrasound contrast microbubbles [1–3].	12
3.1	Details of unfocused transducers used in this study.	52
3.2	Details of focused transducers used in this study.	53
5.1	Estimated interfacial rheological properties of the encapsulation of Sonzaoid and Definity microbubbles for different interfacial models.	99
5.2	Threshold pressure (in MPa) for subharmonic scattering obtained experimentally and from different interfacial models for Sonazoid bubbles.	108
6.1	Size distributions, z-averaged diameters and number-averaged diameters for three separate measurements of poly(DL-lactic acid)-encapsulated microbubbles obtained using dynamic light scattering. Reprinted with permission from [4].	121
6.2	Shell thickness and concentration of bubbles per milligram of powder for various polymer shelled bubbles used in this study.	123
6.3	Estimated model parameters of poly(DL-lactic acid)-encapsulated microbubbles for different interfacial models and using three different size distributions. Reproduced from [4] with permission from Elsevier.	126
6.4	Estimated material properties of the polymeric encapsulation for PB-127 and Philips microbubbles using different interfacial models.	133
6.5	Subharmonic generation thresholds for PLA-encapsulated microbubbles.	144
9.1	Average diameter and the polydispersity index of ELIPs	174

9.2	Comparison of previously reported size distribution measurements with ELIPs.	175
10.1	Average diameters and polydispersity indices of Pol-ELIPs.	190
11.1	Amino acid sequence of LP4	209
C.1	Purpose of Matlab codes/functions included in this appendix.	295
D.1	Purpose of Matlab codes/functions included in this appendix.	305

LIST OF FIGURES

2.1	Schematic representation of a contrast microbubble constructed for drug-delivery.	10
2.2	Hypothesized structures of echogenic liposomes (ELIPs).	15
2.3	The plot of the response function $Q(\omega, b)$ for a linear oscillator with varying damping factors.	31
2.4	Schematic representation of attenuation of an acoustic wave	37
3.1	Transducer bandwidth explained.	54
3.2	Experimental setup for transducer calibrations.	55
3.3	Calibration results showing linear relationship between input voltage and output pressure for a 3.5 MHz transducer excited at its center frequency	57
3.5	Acquired signal on the oscilloscope during attenuation measurements.	60
3.6	Experimental setup to measure scattering using a large sample volume	62
3.7	Schematic representation of the ultrasound imaging setup.	65
3.8	Schematic representation of the setup used for ultrasound mediated release studies.	66
4.1	A representative figure depicting the change of interfacial elasticity and effective surface tension with fractional change of area for constant (CEM), quadratic (QEM) and exponential (EEM) elasticity models.	80
4.2	Radial dynamics of encapsulated bubbles as predicted by different interfacial models.	86

4.3	“Compression-only” behavior of encapsulated bubbles as predicted by different interfacial models.	87
4.4	Analytical predictions of subharmonic generation thresholds by encapsulated microbubble using different interfacial models.	90
4.5	Prediction of two subharmonic generation threshold (numerically) using the Marmottant model.	91
5.1	Measured and fitted attenuation coefficient for Sonazoid microbubbles	97
5.2	Measured and fitted attenuation coefficient for Definity microbubbles	100
5.3	Size distribution and attenuation data with “fresh” and “expired” Definity microbubbles.	102
5.4	Frequency dependent attenuation coefficient for Definity microbubbles	103
5.5	Fundamental response of Sonazoid microbubbles.	105
5.6	Subharmonic response of Sonazoid microbubbles.	107
5.7	Fundamental response of Definity bubbles at 10 MHz.	109
5.8	Subharmonic response of Definity bubbles at 10 MHz.	109
5.9	Ratio of subharmonic to fundamental response from Definity bubbles at 20 MHz.	110
6.1	Three independent measurements of the size distribution of poly(DL-lactic acid)-encapsulated contrast microbubbles obtained using dynamic light scattering.	121
6.2	Size distributions of PB-127 and Philips microbubbles obtained using dynamic light scattering.	123
6.3	<i>In vitro</i> attenuation measurements with PLA microbubbles.	124
6.4	Experimentally measured and fitted attenuation data for PLA microbubbles.	126
6.5	Experimentally measured attenuation data for PB-127 and Philips bubbles.	130

6.6	Experimentally measured dispersion data for PB-127 and Philips bubbles.	130
6.7	Experimentally measured and fitted attenuation data for PB-127 microbubbles.	131
6.8	Experimentally measured and fitted attenuation data for Philips bubbles.	132
6.9	Experimentally measured time dependent normalized total attenuation for PLA microbubbles at 200 kPa.	136
6.10	Experimentally measured time dependent normalized total attenuation for PLA microbubbles at various excitation pressures. .	136
6.11	Experimentally measured fundamental and second-harmonic response from PLA	137
6.12	Comparison of predicted and measured fundamental response from PLA	139
6.13	Comparison of predicted and measured second-harmonic response from PLA	140
6.14	Experimentally measured subharmonic response from PLA microbubbles	142
6.15	Comparison of predicted and measured subharmonic response from PLA	143
6.16	Comparison of experimentally measured and predicted scattered subharmonic responses of PLA-encapsulated microbubbles for the Newtonian model (NM).	145
6.17	Subharmonic responses of PB-127 microbubbles at 20 MHz excitation. .	148
7.1	Experimental setup to measure scattering using a small sample volume	155
7.2	A 3-D view of the acoustic setup for measuring ambient pressure dependent subharmonic response.	156

7.3	Comparison of the scattered response from Definity using the small and large sample volume acoustic setups.	158
7.4	Experimentally measured ambient pressure dependent subharmonic response from Definity microbubbles.	160
7.5	Experimentally measured ambient pressure dependent subharmonic response from PLA microbubbles.	161
8.1	ELIP Preparation protocol	166
9.1	TEM and AFM images of ELIPs	176
9.2	Experimentally measured frequency dependent attenuation coefficient of echogenic liposomes.	177
9.3	Experimentally measured concentration dependent attenuation coefficient for ELIPs.	179
9.4	FFT of the experimentally acquired scattered signal from ELIPs. . .	180
9.5	Experimentally measured fundamental and second harmonic response from ELIPs.	181
9.6	Experimentally measured scattered response from ELIPs with and without lyophilization.	183
9.7	Experimentally measured scattered response from ELIPs with varying mannitol content.	184
10.1	Size distribution of Pol-ELIPs	190
10.2	Ultrasound images of Pol-ELIPs.	191
10.3	Attenuation measured through a suspension of Pol-ELIPs	192
10.4	Time dependent normalized total attenuation due to Pol-ELIPs. .	193
10.5	Attenuation due to PC-PE-CH Pol-ELIPs.	195
10.6	Comparison of Scattered response from both versions of Pol-ELIPs (PC-PE and PC-PE-CH) and ELIPs.	198

10.7	FFTs of the scattered signal from different ELIP formulations.	199
10.8	Scattered response from Pol-ELIPs with varying acoustic pressure. .	200
10.9	Scattered subharmonic response from Pol-ELIPs with varying acoustic pressure.	201
10.10	Mannitol dependence of the echogenic response from Pol-ELIPs. . .	202
11.1	Particle size distribution of MMP-9 cleavable ELIPs using DLS and TEM.	215
11.2	Particle size distribution of polymer coated redox triggered ELIPs using DLS.	216
11.3	Transmission Electron Microscopic images of negatively stained redox triggered ELIPs.	217
11.4	Atomic Force Microscopic images of polymer coated redox triggered ELIPs.	217
11.5	Particle size distribution of pH sensitive liposomes with tunable echogenicity using DLS and TEM.	218
11.6	Acoustic backscattered response from MMP-9 cleavable ELIPs. . .	220
11.7	Ultrasound images of MMP-9 cleavable ELIPs.	221
11.8	Acoustic backscattered response from redox triggered ELIPs.	223
11.9	Ultrasound images of redox triggered ELIPs.	223
11.10	Time dependent acoustic backscattered response from pH sensitive ELIPs.	225
11.11	Ultrasound images of pH sensitive liposomes with varying pH values.	226
11.12	Gray scale values of ultrasound images of pH sensitive echogenic liposomes.	227
11.13	Acoustic backscattered response from redox sensitive echogenic polymersomes.	228

11.14	Time dependent acoustic backscattered response from redox sensitive echogenic polymersomes.	229
11.15	Ultrasound images of redox sensitive echogenic polymersomes.	230
11.16	Mean gray scale values from ultrasound images of echogenic polymersomes.	230
11.17	Frequency and time dependent ultrasound triggered release from MMP-9 cleavable ELIPs.	232
11.18	Role of exposure time in ultrasound triggered release from MMP-9 cleavable ELIPs at 3 MHz excitation.	232
11.19	Ultrasound enhanced MMP-9 triggered release of contents from MMP-9 cleavable ELIPs.	233
11.20	Redox triggered and ultrasound enhanced redox triggered release of the contents from polymer coated ELIPs.	236
C.1	The LabView program GUI interface utilized for the data acquisition.	294

ABSTRACT

Micron- to nanometer - sized ultrasound agents, like encapsulated microbubbles and echogenic liposomes, are being actively developed for possible clinical implementations in diagnostic imaging and ultrasound mediated drug/gene delivery. Contrast microbubbles (1-10 micron in diameter) contain a low solubility gaseous core stabilized by an encapsulation made of lipids/proteins/polymers/surfactants. Echogenic liposomes (ELIPs), which combine the advantages of liposomes such as biocompatibility and ability to encapsulate both hydrophobic and hydrophilic drugs with a strong reflection of ultrasound, are also excellent candidates for concurrent ultrasound imaging and drug delivery applications. The primary objective of this thesis is to characterize the acoustic behavior and the ultrasound-mediated content release of these contrast agents for developing multi-functional ultrasound contrast agents. The first part of this thesis reports the investigation of encapsulated microbubbles utilized as ultrasound contrast agents, whereas the second part reports the experimental characterizations of echogenic liposomes (ELIPs) and echogenic polymersomes.

Contrast microbubbles are nonlinear systems capable of generating a subharmonic response i.e., response at half the excitation frequency, which can improve image quality by providing a higher signal to noise ratio. However, design and development of contrast microbubbles with favorable subharmonic behavior requires accurate mathematical models capable of predicting their nonlinear dynamics. To this goal, ‘strain-softening’ viscoelastic interfacial models of the encapsulation were developed and subsequently utilized to formulate a modified form of the Rayleigh-Plesset equation to model the nonlinear dynamics of these encapsulated microbubbles. A hierarchical two-pronged approach of modeling — a model is applied to one set of experimental data to obtain the model parameters (material characterization), and then the model is

validated against a second independent experiment — is demonstrated in this thesis for two lipid coated (Sonazoid™ and Definity®) and a few polymer (polylactide) encapsulated microbubbles. We performed *in vitro* acoustic characterization with these contrast microbubbles, i.e., determined the material properties of their encapsulations and compared model predictions with experimental observations. The nonlinear elastic models developed were successful in predicting several experimentally observed behaviors e.g., low subharmonic thresholds and “compression-only” radial oscillations. Results indicate that neglecting the polydisperse size distribution of contrast agent suspensions, a common practice in the literature, can lead to inaccurate predictions and unsatisfactory results.

Recent numerical investigations of the nonlinear dynamics of encapsulated microbubbles from our group contradicted previously published experimental results on the dependence of subharmonic behaviors on ambient pressure. We wanted to investigate this issue through new *in vitro* acoustic experiments by designing a modified experimental setup. Preliminary results indicate that the previously published conclusion that subharmonic response from contrast microbubbles linearly decreases with increasing ambient pressure might not be correct under all excitation conditions; it may both increase or decrease under appropriate excitations in conformity with the results of numerical investigations.

Experimental characterization of the ELIPs and polymersomes was performed with the goal of demonstrating their potential as ultrasound agents with simultaneous imaging and drug/gene delivery applications — ‘dual-purpose’ contrast agents. Carefully performed experiments conclusively demonstrate the ultrasound reflectivity (echogenicity) of the liposomes prepared using an established protocol. Although, no subharmonic response from these ELIPs was observed, altering the constituents of the lipid bilayer and polymerizing it generated a subharmonic response indicating that the echogenic properties of ELIPs can be controlled by altering the preparation protocol. Our results indicate that the freeze-thaw cycle and lyophilization in presence of mannitol followed by reconstitution in a buffer was critical for generating echogenic

response from these liposomes. A finite amount of mannitol (above 100 mM) proved critical for echogenicity, but increasing the mannitol concentration above that amount did not change the echogenicity. Lyophilized powders create a polydisperse suspension of liposomes upon reconstitution, which in turn results in a response without a distinct resonance peak. We believe that the echogenicity of the liposomes results from the larger diameter liposomes present in this polydisperse suspension. In spite of the conclusive experimental evidence of echogenicity, the underlying mechanisms are not completely understood primarily due to the uncertainty regarding the exact location of the gas pockets. An accurate knowledge of the locations and dimensions of the gas pockets is critical for developing improved mathematical models of their acoustic behaviors.

For the experimental validation of the concept of ‘dual-purpose’ contrast agents, four novel formulations were investigated — a lipopeptide conjugated ELIP formulation that can be triggered by the extracellular enzyme matrix metalloproteinase-9 (MMP-9), a polymer coated redox triggered ELIP formulation for cytosolic drug delivery, pH sensitive liposomes with tunable echogenicity capable of drug-release in mildly acidic micro-environment and redox sensitive echogenic polymersomes. Both in vitro acoustic studies and ultrasound imaging (the latter performed in NDSU by our collaborators) demonstrated the echogenicity of each of these formulations. Although, ultrasound excitation (< 5 MHz) alone was incapable of causing optimal release of contents, a dual-triggering strategy proved successful. Application of ultrasound in conjunction of other triggers (e.g., enzyme, pH, redox) showed significant enhancements (10-20%), which resulted in a total release of up to 80-90%. Considering these experimental results, it can be concluded that these novel formulations have the potentials for simultaneous imaging and therapeutic applications. These contrast agents hold the potential of providing powerful treatment strategies for many diseases, including cardiovascular ones and various cancers.

Chapter 1

INTRODUCTION

1.1 Motivation

According to the Centers for Disease Control and Prevention, USA, cardiac diseases and cancer were the two leading causes of death in the U.S in 2009 [5]. Cardiovascular diseases(CVD) accounted for 599,413 deaths closely followed by cancer which resulted in 567,628 fatalities [5]. The total cost associated with CVD and cancer amounts to \$312.6 billion [6] and \$201.5¹ billion, respectively. Improved diagnostic tools and state of the art treatment strategies can help in reducing the immense burden of these diseases. Diagnostic ultrasound is an attractive choice for the detection cardiovascular diseases and their treatment. Other clinical applications include improved imaging of the heart and liver. Microbubble based ultrasound contrast agents — comprised of micron sized gas bubbles with a stabilizing layer made of lipids/proteins/polymers/surfactants — and echogenic liposomes (ELIPs) — which are lipid bilayer encapsulated vesicles with entrapped gas pockets — have been developed over the last 30 years to enhance the image quality (or contrast), and reduce the sub-optimality associated with ultrasound images. These contrast agents can also be used for diagnosis and detection of several types of cancer. Rapid progress has been made in the last few decades in developing newer generation contrast agents with a wide range of imaging and therapeutic applications e.g., targeted drug-delivery, enhanced thrombolysis, blood-brain barrier disruption, noninvasive blood-pressure estimation etc.

However, the widespread clinical acceptance of contrast agents is primarily limited by the inadequacy of our knowledge of contrast agent behavior. Although, a

¹ <http://www.cancer.org/cancer/cancerbasics/economic-impact-of-cancer>

significant amount of theoretical and experimental investigations are available in the literature, there is no unified unambiguous explanation for most of them. A lot of the proposed clinical applications of ultrasound contrast agents, like those mentioned above, offer no satisfactory understanding of the underlying mechanisms even under *in vitro* experimental conditions. This gap in knowledge is potentially dangerous and limits the efficacy of these techniques in a clinical environment. Hence, there is a substantial scope for improving our fundamental knowledge of contrast agent behavior that is critical for the rapid evolution of their applications and their widespread adoption. This motivated us to study the contrast agent behavior in great detail, both theoretically and experimentally. We examined and compared the behavior of several microbubble based contrast agents and echogenic liposomes in an attempt to provide an in depth physical understanding of the underlying mechanisms. We have also put significant effort in the design and development of novel contrast agent formulations with the potential to treat cardiovascular diseases and cancer. Thus, the fundamental insights gained through this study can greatly contribute to the design and development of contrast agents and equip us with more reliable predictive tools for characterizing their behavior.

1.2 General Aims of this Study

Investigating the dynamics of ultrasound contrast agents was the central premise of this research. For this, we formulated some general aims of this research. Since, it is critical to have a knowledge of its acoustic properties, for the design and development of contrast agents, a significant part of this research was dedicated to the experimental characterization of the acoustic properties of ultrasound contrast agents. A robust mathematical formulation can significantly improve our physical understanding of the experimental observations. Hence, we also developed a new interfacial rheological model characterizing the stabilizing shell of the microbubble based contrast agents. The predictive capabilities, applicability, and shortcomings of this model were also studied through numerical investigations and by the validation of experimental results.

For a broader understanding of the role of the shell material, several contrast agents formulations were included in this study.

We were also interested in developing novel contrast agent formulations through our collaborative efforts with pharmaceutical scientists. To this goal we decided to study a novel class of contrast agent already proposed in the literature — echogenic liposomes. The experimental evidence demonstrating the acoustic properties of these liposomes were contradictory and ambiguous in some cases. Hence, we pursued a rigorous *in vitro* characterization of these liposomes. Our *in vitro* studies were also helpful in understanding the underlying mechanisms of the reported acoustic behavior of these contrast agents. With a satisfactory knowledge of their dynamics, we then focused on developing novel therapeutic applications by studying both their acoustic properties and payload release characteristics. We also explored the possibility of developing newer liposome based ultrasound contrast agents. Possible modeling aspects of these different class of contrast agents were also explored.

Apart from characterizing the behavior of contrast agents utilizing existing experimental setup, we were also interested in improving their efficiency and novelty.

1.3 Specific Objectives

Based on our overall goals, the following specific objectives were formulated.

1. Characterize the dynamics of microbubble based ultrasound contrast agents.
 - Develop an interfacial rheological model of the contrast agent encapsulation.
 - Experimentally characterize the behavior of contrast agents with different encapsulation materials e.g., lipids (Definity™ and Sonazoid®), polymers (polylactic acid shelled bubbles) etc.
 - Use the experimental data for the material characterization of the encapsulation.
 - Evaluate the performance and predictive capabilities of the model by comparing its predictions with experimental observations.
 - Design and implement modified *in vitro* experimental setups for addressing the issues encountered during the course of this research and provide newer experimental tools for better understanding of contrast agent behavior.

2. Develop novel echogenic liposomes and polymersomes with simultaneous imaging and drug-delivery potential ('dual-purpose' ultrasound agents).
 - Characterize the acoustic properties of echogenic liposomes prepared by following the existing protocol.
 - Investigate the role of lipid compositions on the acoustic properties by characterizing the behavior of a polymerized version of the echogenic liposomes.
 - Experimentally validate the concept of 'dual-purpose' contrast agents for four new formulations, capable of either extracellular drug-delivery or cytosolic drug-delivery.

1.4 Organization of this dissertation

To facilitate the understanding of the research undertaken during this study this dissertation is segregated into four sections.

The first section will include this introductory chapter followed by Chapters 2 and 3. Chapter 2 will provide a detailed discussion of the background relevant to this research. It will also include a comprehensive review of the existing literature along with a discussion of the essential concepts of acoustics frequently referred to in the subsequent chapters. Chapter 3 will discuss in detail the various experimental setups and data reduction techniques utilized in this study. Any experimental method excluded there will be discussed later in the relevant chapters.

The second section, defined as Part I, will focus on the characterization of the dynamics of microbubble based contrast agents. Chapter 4 will introduce the modeling strategy, first proposed by our group, where the encapsulation is treated as a two dimensional interface with intrinsic rheological properties. A new strain-softening model of the interface will then be introduced that was developed to predict the nonlinear behavior of contrast agents under ultrasonic excitation more accurately. Several favorable properties of the models will also be demonstrated using the numerical solutions of the formulated equations. Chapter 5 will implement this model for the material characterization of two different lipid shell bubbles — Definity® and Sonazoid™. The model's ability to predict contrast agent dynamics will also be discussed by comparing numerical predictions with experimental results. Chapter 6 will utilize the same

strategy for characterization of several polymer shelled microbubbles. The last chapter of this part, Chapter 6, will present the work done for the design and development of newer and modified *in vitro* experimental for better characterization of contrast agent behavior.

The third section, defined as Part II, will report the characterization studies of echogenic liposomes and polymersomes. Chapter 8 will provide a thorough review of the existent experimental data characterizing the acoustic behavior and release characteristics of the echogenic liposomes. It will also present a brief overview of polymersomes and their potential applications. This will help in understanding the motivation of our research presented in the following chapters. Chapter 9 will present the *in vitro* acoustic experiments for characterizing the behavior of echogenic liposomes prepared by following an existing protocol. A polymerized version of these liposomes was also developed to understand the role of lipid composition on acoustic properties and enhance stability. The experimental findings of their acoustic properties will be discussed in Chapter 10. Chapter 11, the last chapter of this section, will introduce three new formulations of echogenic liposomes and one echogenic polymersomes, all with simultaneous imaging and drug-delivery potential. The chapter will provide detailed discussion of the properties of these formulations for *in vitro* experimental validations of the concept of ‘dual-purpose’ ultrasound contrast agents.

The conclusions highlighting the significant contributions of this research will be presented in the final chapter of this dissertation, which constitutes the final section of this thesis. The scope for future continuation of this research will also be discussed by providing specific proposals along with a discussion of the limitations.

Chapter 2

BACKGROUND AND BASIC CONCEPTS¹

2.1 Ultrasound and Its Applications in Medicine

2.1.1 Basics of Ultrasound and Acoustics

In the simplest terms, ultrasound refers to “waves which transport mechanical energy through the local vibration of particles, with no net transport of the particles themselves” at a frequency greater than 20 kHz that is usually the upper limit of human hearing [8]. However, T. G. Leighton also emphasized the limitations of such simplified definition by noting that “there may indeed be a net transport of particles, and the frequency content of the tonal wave may change in such a way that it becomes misleading to assign to it a single frequency and, further, to compare it to 20 kHz when protecting individuals” [8].

Acoustic waves can be encountered in different forms such as longitudinal compressional waves, shear transverse displacement wave, torsional wave etc. However, longitudinal compressional wave is the most commonly encountered form among these. These waves also have different propagation characteristics e.g., phase and group velocity, dispersion, attenuation etc. For the simplest longitudinal compressional wave, a single phase speed (c_ϕ) can be defined as the speed at which the wave is traveling from left to right. Wavelength (λ) is defined as the distance between two points on the wave with same disturbances. Wavelength and phase speed are related as

$$c_\phi = \nu\lambda, \quad (2.1)$$

¹ Certain parts of the text in this chapter have been adapted from an under review article [7].

where ν is the linear frequency in hertz. This can also be related to the angular frequency (ω) as $2\pi\nu = \omega$. If the particle velocity (v) and acoustic pressure (P) are in phase we can define acoustic impedance for the compressional wave as

$$Z = \frac{P}{v} = \rho_0 c_\phi, \quad (2.2)$$

where ρ_0 is the equilibrium density of the medium. Although, this simple relation is only valid for linear waves they are commonly used to estimate various acoustic parameters. Specifically, for plane and spherical waves (as will be generated from the transducers used in this study), the acoustic intensity of the wave can be assumed to be proportional to the square of the acoustic pressure i.e.,

$$I = \frac{P_{\text{acous}}^2}{2Z} = \frac{P_{\text{rms}}^2}{Z}, \quad (2.3)$$

where P_{acous} and P_{rms} are, respectively, the zero-to-peak and the rms acoustic pressure amplitudes of the wave. When the wave travels from one media to another there will be transmission losses at the interface due to reflections — if no losses occur the system is called ‘impedance matched’ system. However, loss can also occur due to other factors. The total contribution due to various losses is referred to as the attenuation of the wave. Such losses can be formulated using a complex form of wavenumber ($k = 2\pi/\lambda$) given by $k = q - ib$ with $i = \sqrt{-1}$. The parameter b characterizes the absorption of the system. The absorption loss can be modeled to fall off as $1/r$, r being the distance from the point considered as reference. Thus, for a plane wave we can write

$$P = P_{\text{acous}} e^{i(\omega t - qx)} e^{-bx} \Rightarrow \frac{dI}{I} = -2bx \Rightarrow I_2 = I_1 e^{-2b(x_2 - x_1)}, \quad (2.4)$$

where x_1 and x_2 are the locations with intensity values I_1 and I_2 respectively. Usually the change in intensity is expressed in decibels (dB) in acoustics and the absorption

coefficient (also referred to as attenuation coefficient) can be written as

$$\alpha_{\text{absorp}} = \frac{10 \log_{10}(I_1/I_2)}{x_1 - x_2} = 20b \log_{10} e. \quad (2.5)$$

The concept of scattering is more difficult to explain. It can be understood as the spreading of the wave occurring in all directions due to an inhomogeneity in its path. The quotient representing the power scattered per unit solid angle per unit incident intensity, can be referred to as the scattering cross-section.

2.1.2 History and Medical Applications

The knowledge of acoustic waves beyond the regime of human hearing was recognized as early as 18th Century, when Spallanzani and Jurine studied bats. The modern theory of acoustic was developed by Lord Rayleigh in 1877. A major thrust in this area was the discovery of the piezo-electric effect in 1880 by Curie brothers. By 1915, ultrasound was being used for detection of icebergs and submarines pioneered by innovations of Richardson, Fessenden and Langevin. Karl Dussik is generally regarded as the first physician to have used ultrasound in medical diagnosis [9]. Ludwig and Struthers were the first investigators who reported pulse-echo technique for tissues. This work was utilized to show that ultrasound can be used to diagnose gallstones. Soon ultrasound was being widely implemented in a range of medical applications. Ian Donald pioneered OB-GYN ultrasound in 1958 [10]. The reflection of acoustic waves described the previous section is utilized to generate images from the reflected echo in ultrasound scanners. The medical applications of ultrasound can be broadly classified as [11]

- **Diagnosis** - Clinical evaluation of organs or conditions. It can involve imaging/diagnosis of abdomen, uterus, heart, eye, neuromuscular injuries.
- **Therapy** - Use ultrasound for beneficial biological effects. It includes physiotherapy, homostasis, bone growth stimulation, drug-delivery etc.
- **Surgery** - Tissue disruptio, destruction or ablation. Generally includes high power techniques like High Intensity Focused Ultrasound (HIFU) for burning

out tissues or tumor ablation, break kidney stones by shock waves (lithotripsy), soft tissue disruption e.g., cataract removal, tumor-debulking for neurosurgery, ultrasound controlled scalpels, dental instruments etc.

2.2 Ultrasound Contrast Agents

Although diagnostic imaging with ultrasound offers a safe, portable, low cost alternative, its applicability is often limited by inferior image quality and lack of spatial resolution in comparison to other imaging modalities like Computed Tomography or Magnetic Resonance Imaging [12]. A major breakthrough in this regard was the accidental discovery of the effectiveness of micron sized gas bubbles in enhancing ultrasound image quality/contrast [13]. The presence of the gaseous core results in a mismatch of acoustic impedance in the liquid in which they are suspended. The high compressibility of the gas also enables the microbubbles to undergo volumetric oscillations under an ultrasonic excitation field. Consequently, these bubbles can reflect, absorb and re-radiate sound energy significantly more than a similar sized liquid filled particles (e.g., blood cells) and surrounding tissues. These gas bubbles are also required to be less than $10 \mu\text{m}$ for passing through small capillaries. Fortunately, the resonance frequency of such bubbles coincides with the frequencies suitable for diagnostic ultrasound imaging (1-10 MHz), maximizing their response under diagnostic conditions. However, the potential for clinical applications of such uncoated microbubbles was severely restricted by their highly unstable nature. The pressure inside a gas bubble is higher than the outside pressure due to the surface tension forces at the air-water interface. This results in their rapid dissolution — in orders of milliseconds to seconds for micron sized air bubble at room temperature [14, 15]. Further investigations demonstrated the improvement of bubble stability through the formation of a thin coating (also referred to as encapsulation/shell) at the interface [16, 17]. This led to the development of Albunex[®], Echovist[®], and Levovist[®], the first generation of commercial contrast agent. Ultrasound contrast agents were first approved for clinical use in Germany (1980s) and later in the United States (1990s) [18].

The earliest contrast agents were air filled bubbles, usually with a stabilizing coating of galactose or albumin. These contrast agents were often too big to pass through the pulmonary and thereby failed to opacify the left chamber of the heart. They also had half life (defined as the time period over which only half of the contrast agent population remains active i.e., responsive to acoustic excitation) in order of seconds resulting in enhancements too transient to be of any practical use. This led to the development of the next generation of contrast agents with less soluble and less diffusive higher molecular weight gases inside e.g., perfluorocarbons, sulfur hexafluoride etc. The stiffness of albumin shells also reduced the amplitude of oscillations of these bubbles in comparison to similar sized uncoated bubbles. Hence, significant research efforts were invested to find more effective coating material for the encapsulation, such as phospholipids, surfactants, polymers etc. Presently, only two contrast agents formulations are approved by the United States Food and Drug Administration (FDA) — Definity® and Optison™. Table 2.1 below provides details of a selected number of ultrasound contrast agents, most commonly cited in the literature. Recently, the microbubble based contrast agents are being actively developed for a wide range of applications extending beyond the scope of diagnostic imaging by utilizing ligand-mediated targeting and loading microbubbles with both hydrophilic and hydrophobic drugs. Figure 2.1 shows a schematic representation of the structure and the constituents of such contrast agents.

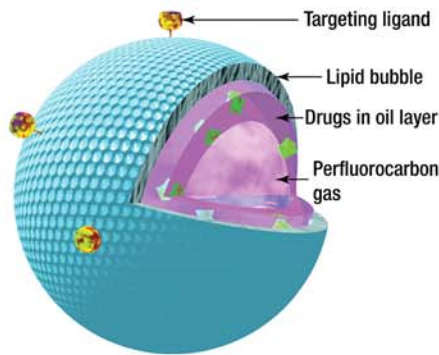


Figure 2.1: Schematic representation of a contrast microbubble constructed for drug-delivery (Reprinted from [19] with permission from BMJ Publishing Ltd.).

In spite of the rapid development of microbubble based ultrasound contrast agents, clinical applications are often limited due to potential safety concerns [20–22] and lower circulation time (defined as the period of time over which the contrast agent can circulate along with the blood flow before it gets dissolved or is taken out of the body) [23]. The relatively larger size of microbubbles in comparison to nanometer sized pores observed in the leaky vasculature associated with cancerous tissues [23], and the constraints on the amount of drug loading [24] also reduces their applicability for the treatment of cancer. Consequently, various other formulations have also been investigated for their potential use as ultrasound contrast agents, such as nanodroplets of liquid fluorocarbon [25–31], liposome based formulations [24, 32–40], bubbicles [41, 42], silica nanoparticles [43], polymersomes [44] etc.

Echogenic liposomes and polymersomes are two such variations of ultrasound contrast agents. Since, a significant portion of this research was dedicated to the acoustic characterization of such novel contrast agent formulations, they will be discussed separately in Section 2.3. Note that, although this dissertation makes a distinction between ultrasound contrast agents (we will use it to refer to the conventional microbubble based agents) and liposomes or polymersomes, the last two are essentially a subset of the first group.

2.2.1 Ultrasound Contrast Agents in Imaging

Since the introduction of ultrasound contrast agents, it has been utilized in different imaging applications. They were initially introduced for enhancing contrast of conventional B-mode (brightness mode) imaging. Subsequently, they were also implemented for use with for enhancing the sensitivity of Doppler imaging [45]. Clinical applications for contrast agents are approved only for contrast echocardiography in the United States [46]. Furthermore, they can only be used for left ventricular opacification and border delineation [20]. However, they are widely used for other radiological imaging applications in Europe and Asia. They are also used for diagnosis of cardiovascular, hepatic, renal, gastrointestinal and pancreatic diseases [12, 47, 48]. However,

Table 2.1: Overview of the most commonly referred ultrasound contrast microbubbles [1–3].

Agent	Manufacturer	Shell Material	Filling Gas
First Generation			
Albunex®	Molecular Biosystems	Albumin	Air
Levovist®	Schering AG	Galactose	Air
Echovist®	Schering AG	Galactose	Air
Sonavist®	Schering AG	Cyanoacrylate	Air
Second Generation and Third Generation agents			
BR14	Bracco Diagnostics Inc.	Phospholipid	C_4F_{10}
Definity®	Lantheus Medical Imaging	Phospholipid	C_3F_8
EchoGen®	Sonus Pharma. Inc.	Surfactant	C_5F_{12}
Imagent®	Alliance Pharma.l Corp.	Phospholipid	N_2/C_6F_{14}
Imavist™	Schering AG	Surfactant	Air and C_6F_{14}
Optison™	GE Healthcare	Albumin	C_3F_8
Quantison™	Upperton Ltd.	Albumin	Air
SonoVue®	Bracco Diagnostics Inc.	Phospholipid	SF_6
Sonazoid™	GE Healthcare	Phospholipid	C_4F_{10}
BiSphere®	POINT Biomedical Corp.	Polylactide	N_2
AI-700	Acusphere, Inc.	Phospholipid	C_4F_{10}
BR38	Bracco Diagnostics Inc.	Phospholipid	C_4F_{10}/N_2

most of these imaging applications utilized the linear response from the microbubbles. It was soon demonstrated that significant improvements can be achieved by harnessing the nonlinear properties of these microbubbles. Since, the tissues surrounding these contrast agents usually generate considerably weaker or almost no nonlinear response, a much higher signal to noise ratio could be obtained. This led to the development of harmonic imaging techniques like Pulse Inversion (PI), Power Modulation (PM) [49]. In spite of its advantages, harmonic imaging can often suffer from signal corruption due to nonlinear propagation effects in tissues and nonlinearity of the tissue itself at higher excitation amplitudes. Hence, subharmonic and ultraharmonic imaging modalities are also being actively developed for potential clinical applications [50]. Subharmonic imaging has drawn significant attention due to the exclusive capability of bubbles for generating such response. Subharmonic imaging can also be utilized for noninvasive blood pressure estimation/monitoring [51–55]. Doppler mode has also improved by implementation of harmonic imaging [56]. Other modalities, like perfusion imaging, rely on destruction of microbubbles [57].

Microbubble based contrast agents can also be used for ligand-mediated targeted imaging or molecular imaging allowing noninvasive detection of physiological changes in diseased patients at the molecular and cellular level [58–61].

2.2.2 Ultrasound Contrast Agents in Therapy

Microbubbles under ultrasonic excitation results in several interesting effects like stable and inertial cavitation [20, 62, 63], microstreaming [63], radiation force generation [64–68], ultrasound-mediated destruction [69–74]. A wide range of therapeutic applications like modulation of vascular and cellular permeability (or sonoporation) [75, 76], thrombolysis [77–79], gene delivery [80, 81] etc., are based on such acoustic behaviors associated with pulsating contrast microbubbles. Although, there are increasing reports of the effectiveness of such therapeutic applications, their underlying mechanisms rare poorly understood. Also, their clinical implementation will be difficult owing to the potential for harmful bioeffects. Microbubbles can also be used as

drug delivery vehicles for both hydrophobic [82] and hydrophilic [83, 84] molecules, and achieve localized or targeted delivery through ultrasound-mediated destruction and/or other external triggers. Such drug release strategies can be used for treatment of cancer and atherosclerotic plaques [23]. Interested readers can refer to the significant number of extensive reviews published in this field every year [23, 58, 85–90].

2.3 Echogenic Liposomes and Polymersomes

Since their discovery by A.D. Bangham [91, 92] in 1965, liposomes have been used extensively as drug delivery vehicles. Liposomes are typically nanometer sized vesicles with a hydrated lipid bilayer encapsulating an aqueous phase. The bilayer membrane is spontaneously formed due to thermodynamic interactions when phospholipids are dispersed in an aqueous phase. Structurally, the liposomes are very similar to biological cells. Hence, liposomes offer several favorable properties like longer circulation time in the blood stream, lesser toxicity, and increased uptake by target organs/tissues. These properties make them suitable for use as drug delivery vehicles [93–96]. Currently, the United States Food and Drug Administration approve about 10 liposomal drug formulations for human use [93, 94]. Liposomes conjugated with targeted ligands can achieve active targeting of indented sites for drug delivery and imaging [97]. Several exogenous (e.g., temperature [98], light [99]) and endogenous (e.g., pH [100], enzymes [101–103], redox [104]) triggers have been used to make stimuli-responsive drug delivery vehicles. Such formulations offer local control over payload release resulting in reduced system toxicity. Recently, ultrasound has also been investigated as a possible external trigger for releasing liposomal contents [94–96, 105].

Acoustically responsive liposomes were first reported in 1996 [32], and since then been termed as echogenic liposomes (ELIPs). The preparation protocol was later optimized by Huang and co-workers [106, 107], through years of research, to establish a standardized methodology involving 3 to 5 freeze-thaw cycles and lyophilization in the presence of a weak cryoprotectant mannitol. These steps are critical in ensuring the echogenicity (i.e., capability to scatter incident acoustic waves effectively) of these

liposomes. It is hypothesized that the freeze-thaw and lyophilization in the presence of mannitol creates bilayer defects, which later allow the entrapment of air during reconstitution [108, 109]. Presence of entrapped air makes these liposomes echogenic. Although, the echogenicity of liposomes have been conclusively demonstrated through both *in vitro* [109, 110] and *in vivo* [35] experiments, the exact location of entrapped air remains unascertained. Possible explanations are existence of a gas pocket within the bilayer [93, 107, 111] or presence of a lipid monolayer coated bubble floating within the aqueous compartment [93] or existence of lipid coated microbubbles in the suspension [112]. Since, ELIPs retain all favorable properties of the conventional liposomes [93], they have also been investigated for simultaneous imaging and ultrasound mediated drug release studies [111, 113–119]. Figure 2.2 below shows two hypothetical structures of echogenic liposomes. ELIPs can be loaded with both hydrophilic and lipophilic drugs [113] represented in the figure by fluorescent green circles and red boxes respectively. Like microbubbles, liposomes can also be prepared with ligand mediated targeting properties — the targeting ligands are represented by the squiggly lines in the figure.

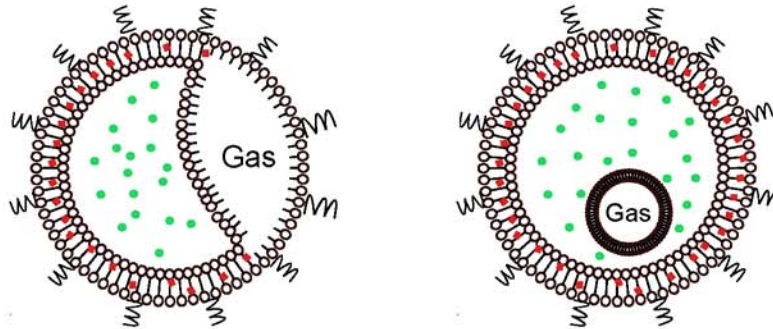


Figure 2.2: Hypothesized structures of echogenic liposomes (ELIPs). The red boxes and green spheres represent lipophilic and hydrophobic drugs respectively.

2.4 Single Bubble Dynamics

2.4.1 Uncoated Bubbles

“Vanitas vanitatum et omnia vanitas: bubbles are emptiness, non-liquid, a tiny cloud shielding a mathematical singularity. Born from chance, a violent and brief

life ending in the union with the (nearly) infinite” is how Prof. Andrea Prosperetti described bubbles in the abstract of one of his papers [120]. Gas bubbles are an intriguing physical system primarily due to the complex nonlinear dynamics associated with them. The dynamics uncoated gas bubbles have been studied extensively both mathematically and experimentally [121–124]. In spite of the staggering amount of information recorded in numerous books [121, 122, 125–127] and reviews [1, 123, 124, 128–132], our knowledge of bubble dynamics continues to increase. The mathematical modeling of bubble dynamics dates back to 1859, when Besant [133] first considered the collapse of a spherical cavity. The problem was again considered by Lord Rayleigh in 1917 [134], when he was appointed by the Royal Navy to understand the reason behind the damages sustained by the propellers of ships. In his pioneering work, he formulated the following equation describing the motion of the bubble wall by considering a single spherical bubble in an infinite, inviscid, incompressible liquid.

$$R\ddot{R} + \frac{3}{2}\dot{R}^2 = \frac{p(R) - p_\infty}{\rho_L}, \quad (2.6)$$

where R is the instantaneous radius of the bubble, \ddot{R} and \dot{R} denote the bubble wall acceleration and velocity respectively, ρ_L is the density of the surrounding liquid, p_∞ is the pressure in the liquid at a very large distance (infinity) from the bubble, and $p(R)$ is the pressure in the liquid at the interface of the bubble. Plesset [130] derived the same expression for a vapor filled bubble from the equation of motion and the continuity equation. He also incorporated the surface tension of the interface in his formulation. Noltingk [135] and Neppiras [136] derived the equation of motion of a gas bubble in an oscillating pressure field. This model was extended by Poritsky [137] to account for liquid viscosity. The resulting equation 2.7 was a generalized form of the Rayleigh equation or also known as the Rayleigh-Plesset-Noltingk-Neppiras-Portisky equation [138], which describes the motion of a oscillating bubble in a viscous, incompressible

fluid of infinite extent. For a complete derivation of the equation see Appendix A

$$R\ddot{R} + \frac{3}{2}\dot{R}^2 = \frac{1}{\rho_L} \left\{ p_i - p_\infty(t) - \frac{2\sigma}{R} - \frac{4\mu\dot{R}}{R} \right\}, \quad (2.7)$$

where σ is the surface tension at the interface/wall, p_i is the pressure inside the bubble, μ is the viscosity of surrounding liquid, $p_\infty(t)$ is the time varying pressure field far away from the bubble. The other symbols are same as defined above. The pressure far away from the bubble can be represented as sum of the static ambient pressure and the time varying dynamic pressure (usually due to the acoustic excitation)

$$p_\infty(t) = p_0 + p_{Ac}(t) \quad (2.8)$$

The inside pressure can also be written as the sum of the contributions from the gas pressure (p_G) and vapor pressure (p_v). A polytropic law can be used to calculate the gas pressure such that

$$p_G = p_{G0} \left(\frac{R_0}{R} \right)^{3\kappa}, \quad (2.9)$$

with $p_{G0} = \left(p_0 + \frac{2\sigma}{R_0} - p_v \right).$

Although, other gas laws like the Van der Waals law can also be used [139], they do not show any significant improvement of predictions for contrast microbubble dynamics [2, 140]. With these assumptions, Equation 2.7 takes the following form

$$R\ddot{R} + \frac{3}{2}\dot{R}^2 = \frac{1}{\rho_L} \left\{ \left(p_0 + \frac{2\sigma}{R_0} - p_v \right) \left(\frac{R_0}{R} \right)^{3\kappa} + p_v - \frac{2\sigma}{R} - \frac{4\mu\dot{R}}{R} - p_0 - p_{Ac}(t) \right\}, \quad (2.10)$$

where R_0 is the initial radius of the bubble, κ is the polytropic constant of the inside gas. More detailed discussion on the appropriate choice of the polytropic index will be considered in a later section.

Note that, Equation 2.10 does not account for liquid compressibility. This assumption will not be valid in situations where the velocity of the bubble wall is comparable with the velocity of sound in the surrounding liquid. Several versions of Rayleigh-Plesset equations, e.g., Keller-Miksis equation [141], Trilling Equation [142], Herring equation [143], and Gilmore equation [144], have been suggested to include liquid compressibility. Prosperetti and Lezzi [145–147] in their pioneering work proved that these equations are essentially the member of the same family of differential equations with a maximum accuracy in the order of $\frac{\dot{R}}{c}$, c being the velocity of sound in the liquid. It is however, difficult to ascertain which equation will give the most accurate numerical results under a given condition. The generalized form of the equations is given as

$$\rho_L R \ddot{R} \left[1 - (\lambda + 1) \frac{\dot{R}}{c} \right] + \frac{3}{2} \rho_L \dot{R}^2 \left[1 - \left(\lambda + \frac{1}{3} \right) \frac{\dot{R}}{c} \right] = \left[1 + (1 - \lambda) \frac{\dot{R}}{c} \right] (p_G - p_\infty) + \frac{R}{c} \frac{dp_G}{dt} - \frac{2\sigma}{R} - \frac{4\mu \dot{R}}{R}, \quad (2.11)$$

where λ is an arbitrary parameter of small order. $\lambda = 0$ gives the original for the Keller-Miksis equation, while $\lambda = 1$ gives the Herring equation. Note that compressibility is more important for studying bubble collapse and shock wave generation or for sonoluminescence studies. Brenner et al. [128] have suggested that the following form of compressible RP equation, which is very accurate and stable even at high Mach numbers, and this form has been used throughout this dissertation [See Appendix A for more details].

$$R \ddot{R} + \frac{3}{2} \dot{R}^2 = \frac{1}{\rho_L} \left\{ p_G - \frac{2\sigma}{R} - \frac{4\mu \dot{R}}{R} - p_0 - p_{Ac}(t) - \frac{R}{c} \frac{dp_G}{dt} \right\} \quad (2.12)$$

2.4.2 Encapsulated Bubbles

Dynamics of coated bubbles were studied even before the introduction of contrast agents in an attempt to understand the effects of coating on the behavior of

oceanic bubbles. Since the implementation of micron sized bubbles with a stabilizing layer as contrast agents, researchers have attempted to model the dynamics of contrast microbubbles by incorporating *ad hoc* terms in the RP type equations or through rigorous derivation from first principles. We present here a very brief discussion of the various models of contrast microbubble encapsulation. Interested readers are referred to two recent articles [3, 148] that present an excellent review of the various models for encapsulated bubbles. The most prominent effect of the encapsulation will be to increase the damping and change the stiffness of the system. Stiffness can be increased by elastic effects of coating or can decrease due reduced surface tension effects caused by surfactant based coatings. The earliest attempt to model the dynamics of contrast microbubbles dates back to 1990, where Roy and co-workers modeled the encapsulation as a viscous liquid [149]. de Jong and others [150–153] modeled Albunex, the first clinically approved contrast agent, by including *ad hoc* terms in the RP equation to model the shell as a viscoelastic solid with a shell elasticity and a shell friction. The first rigorous theoretical model was developed by Church [154], where he assumed the encapsulation to be a thin incompressible solid shell, and modeled it using the Kelvin-Voigt constitutive law. Hoff et al. [155], Hoff [156] refined this model with the assumption of an infinitesimal thickness of the encapsulation, and matched the model predictions with the experimental data for a contrast agent Nycomed. Morgan et al. [157] proposed a modified Herring equation, with an elastic term derived using the model by Glazman [158] for organic film coating, to describe the encapsulated bubble dynamics. Khismatullin and Nadim [159], introduced compressibility and viscoelasticity of the surrounding liquid in Church’s model, and theoretically proved that those have negligible effect on their dynamics. Allen et al. [160] assumed the encapsulation to be a purely viscous liquid layer, with bulk viscosity parameters, to model the encapsulation of a new therapeutic microbubble named MRX-552 (ImaRx Therapeutics, Tucson, AZ). Allen and Rashid [161] later proposed another model to predict the large amplitude oscillations of polymeric spheres that can also be used to model polymer coated microbubbles. In 2003, our group proposed, for the first time, an interfacial rheological

model for contrast agent encapsulations [162]. Although, the proposed model treated the interface as viscous fluid, an elastic term was included in a later publication [163]. Marmottant et al. [164] introduced a model for large amplitude oscillations of lipid-shelled bubbles with incorporation of a radius dependent surface tension term inspired by previous experimental measurements. This model has gained wide acceptability because of its ability to account for shell rupture and the capability to predict several nonlinear behaviors of lipid shells that have been observed experimentally. Doinikov and Dayton [165], in 2007, proposed a model for lipid shelled microbubbles assuming the shell to be a viscoelastic Maxwell fluid. Tsiglifis and Pelekasis [166] implemented three different constitutive laws, viz., Kelvin-Voigt, Mooney-Rivlin, and Skalak models to describe the elastic properties of the encapsulating shell. Stride [167], in 2008, proposed a model for contrast agent encapsulation by treating it as a homogenous insoluble molecular monolayer with both viscosity and interfacial tension varying with the instantaneous molecular concentration at the interface . Doinikov et al. [168] proposed another model with a nonlinear viscosity term in addition to the Kelvin-Voigt elasticity term to better predict nonlinear behavior of lipid shells. To account for the large amplitude oscillations and the nonlinear behavior of contrast agent encapsulations, we proposed an improved version of our constant elasticity model in 2010 [169]. A nonlinear variation of interfacial elasticity with the area fraction was proposed by the implementation of a quadratic elasticity model (elasticity a linear function of area fraction) and an exponential elasticity model (elasticity varies exponentially with area fraction) [detailed discussion provided later]. Marmottant et al. [170] have also proposed a recent modification of their existing model for lipid encapsulation to extend its applicability to solid like encapsulating shells. In an attempt to explain the variation of estimated properties with bubble size, Li et al. [171] have proposed an integration of the nonlinear elasticity model by Marmottant and co-workers with the nonlinear viscosity model by proposed Doinikov and co-workers to have a ‘nonlinear shell elasticity and viscosity’ model (NSEV).

The different models to describe dynamics of encapsulated microbubbles discussed in the preceding paragraph are essentially the modified versions of the classical Rayleigh-Plesset equation that can be represented in a single interfacial framework [172] as given below

$$R\ddot{R} + \frac{3}{2}\dot{R}^2 = \frac{1}{\rho_L} \left\{ p_G - \frac{2\sigma(R)}{R} - \frac{4\dot{R}}{R^2}\kappa^s(R, \dot{R}) - \frac{4\mu\dot{R}}{R} - p_0 - p_{Ac}(t) - \frac{R}{c} \frac{dp_G}{dt} \right\}, \quad (2.13)$$

where $\sigma(R)$ or the effective interfacial tension and $\kappa_s(R, \dot{R})$ or the surface dilatational viscosity are the interfacial contributions due to the encapsulation. With the assumption of a polytropic law and neglecting the vapor pressure (typically much smaller than the ambient pressure) inside the bubble, we have the following form of modified RP equation for describing the dynamics of encapsulated microbubbles

$$\begin{aligned} \rho_L \left[R\ddot{R} + \frac{3}{2}\dot{R}^2 \right] &= \left(p_0 + \frac{2\sigma(R_0)}{R_0} \right) \left(\frac{R_0}{R} \right)^{3\kappa} \left(1 - \frac{3\kappa\dot{R}}{c} \right) \\ &\quad - \frac{2\sigma(R)}{R} - \frac{4\dot{R}}{R^2}\kappa^s(R, \dot{R}) - \frac{4\mu\dot{R}}{R} - p_0 - p_{Ac}(t) \end{aligned} \quad (2.14)$$

2.4.3 Small-Amplitude Oscillations

The RP equation given in 2.14 is a nonlinear equation and has to be solved numerically. However, the small amplitude oscillations of a gas bubble in liquid can be modeled using the linearized form of the governing equation. Such linearized analyses can provide critical insights into the behavior of the bubbles, like its resonance frequency, extinction or absorption cross-section etc.

One can write a generalized form of 2.12 as given by Prosperetti [173]

$$\rho_L \left[R\ddot{R} + \frac{3}{2}\dot{R}^2 \right] = \left(1 + \frac{R}{c} \frac{d}{dt} \right) P(R, \dot{R}) - \frac{4\mu\dot{R}}{R} - p_0 - p_{Ac}(t) - \Sigma(R, \dot{R}) \quad (2.15)$$

where inside gas pressure (p_G) is written as a function of bubble radius ($P(R, \dot{R})$) and

velocity allowing heat exchange with surrounding liquid, and the interfacial terms are clubbed together, such that

$$\Sigma(R, \dot{R}) = \frac{2\sigma(R)}{R} + \frac{4\kappa^s \dot{R}}{R^2}.$$

Note that $\Sigma(R, \dot{R})$ can accommodate other rheological models with nonlinear viscosity terms. We also define

$$\frac{R(t)}{R_0} = 1 + X(t)$$

With these definitions 2.15 becomes

$$\begin{aligned} \ddot{X} + \frac{3}{2} \frac{\dot{X}^2}{1+X} &= \frac{1}{\rho_L R_0^2 (1+X)} \left[P(X, \dot{X}) - p_0 - p_{Ac}(t) - \Sigma(X, \dot{X}) \right] \\ &\quad - \frac{4\mu}{\rho_L R_0^2} \frac{\dot{X}}{(1+X)^2} + \frac{1}{\rho_L c R_0} \frac{dP}{dt} \end{aligned} \quad (2.16)$$

Now, for small-amplitude oscillations the following Taylor series expansions can be made for a perturbative approach

$$P(R, \dot{R}) \approx P_0 + P_X X + P_{\dot{X}} \dot{X} + \frac{1}{2} P_{XX} X^2 + \frac{1}{2} P_{\dot{X}\dot{X}} \dot{X}^2 + P_{X\dot{X}} X \dot{X}, \quad (2.17)$$

where $P_0 = P(R_0, 0)$ with subscripts denoting differentiation. Similarly, we can write another expansion for the interfacial terms as

$$\Sigma(R, \dot{R}) \approx \Sigma_0 + \Sigma_X X + \Sigma_{\dot{X}} \dot{X} + \frac{1}{2} \Sigma_{XX} X^2 + \frac{1}{2} \Sigma_{\dot{X}\dot{X}} \dot{X}^2 + \Sigma_{X\dot{X}} X \dot{X}, \quad (2.18)$$

where $\Sigma_0 = \Sigma(R_0, 0)$. Note that for a polytropic gas law we have

$$P_X = -3\kappa P_0, \quad P_{XX} = 3\kappa(\kappa+1)P_0 \quad (2.19)$$

Allowing the condition of pressure equilibrium

$$P_0 - p_0 - \Sigma_0 = 0,$$

and a sinusoidal acoustic excitation pressure

$$p_{Ac}(t) = -p_A \cos(\omega t),$$

[2.15](#) can be truncated to a second order expression given below

$$\ddot{X} + 2b\dot{X} + KX = 2p_A \cos \omega t + AX^2 + B\dot{X}^2 + CX\dot{X} - 2p_AX \cos \omega t, \quad (2.20)$$

where the following definitions have been implemented

$$p_A = \frac{p_{Ac}}{2\rho_L R_0^2} \quad (2.21a)$$

$$K = \frac{-P_X + \Sigma_X}{\rho_L R_0^2}, \quad (2.21b)$$

$$2b = 4 \frac{\mu}{\rho_L R_0^2} - \frac{P_X}{\rho_L R_0} - \frac{P_{\dot{X}} - \Sigma_{\dot{X}}}{\rho_L R_0^2}, \quad (2.21c)$$

$$A = \frac{1}{\rho_L R_0^2} \left[\frac{1}{2} (P_{XX} - \Sigma_{XX}) - (P_X - \Sigma_X) \right] = \frac{1}{2\rho_L R_0^2} (P_{XX} - \Sigma_{XX}) + K \quad (2.21d)$$

$$B = \frac{P_{\dot{X}\dot{X}} - \Sigma_{\dot{X}\dot{X}}}{2\rho_L R_0^2} - \frac{3}{2} \quad (2.21e)$$

$$C = \frac{P_{X\dot{X}} - \Sigma_{X\dot{X}} - P_{\dot{X}} + \Sigma_{\dot{X}}}{\rho_L R_0^2} + \frac{8\nu}{R_0^2} \quad (2.21f)$$

Note that, the negative sign in front of the acoustic pressure is convenient for starting the bubble oscillation at $t = 0$ with an expansion. Also, dP/dt was approximated as $P_X \dot{X}$, which is a valid assumption because of the large velocity of sound in liquid. The physical significance of the terms K and $2b$ will be explained in the following sections. Second order truncations are important in weakly nonlinear analysis of bubble dynamics and will be discussed later. For small-amplitude oscillations we can use the linearized version of [2.20](#) which is given below

$$\ddot{X}_l + 2b\dot{X}_l + KX_l = 2p_A \cos \omega t, \quad (2.22)$$

with X_l , the solution of the linear truncation [2.22](#).

2.4.3.1 Acoustic Cross-Sections

For the analysis of the linearized dynamics of bubbles, it is critical to have a fundamental understanding of the concept of acoustic cross-sections and damping factors. The acoustic scattering (σ_s) and absorption (σ_a) cross-sections are defined as the ratio of scattered and the absorbed powers, respectively, to the intensity corresponding to a plane acoustic wave incident on a single bubble. The extinction cross-section (σ_e) is defined as the sum of these two cross-sections and represents the total work done by the acoustic wave on the bubble. Several expressions for these cross-sections exist in the literature [174] which can be represented in the following generalized format

$$\sigma_s = \frac{4\pi R_0^2}{(\omega_{\text{res}}^2/\omega^2 - 1)^2 + \delta^2}, \quad (2.23)$$

$$\sigma_e = \frac{4\pi R_0^2}{(\omega_{\text{res}}^2/\omega^2 - 1)^2 + \delta^2} \frac{\delta}{\omega R_0/c}, \quad (2.24)$$

where ω_{res} is the resonance frequency of bubble pulsation (yet to be defined) and δ is a dimensionless frequency dependent parameter known as damping coefficient with contributions from liquid viscosity (δ_{vis}), thermal dissipation (δ_{th}), acoustic re-radiation (δ_{rad}), and other contributions (δ_{oth}), which for our case will be due to the encapsulation (δ_{encap}). Although, the form of the scattering cross-section is very similar to the particular solution of the linear model, the exact relationship between damping coefficient (δ) and damping factor (b) will depend on the precise definitions and must be used consistently to avoid errors [174]. Ainslie and Leighton [174] also defined a complex variable $\Omega(R_0, \omega)$ assuming a complex polytropic index (Γ) given below and used it to rigorously define ω_{res}

$$\omega_0(R_0, \omega) \equiv \sqrt{\text{Re} [\Omega(R_0, \omega)^2]}, \quad (2.25a)$$

$$\Omega(R_0, \omega) = 4\pi \frac{\Gamma(R_0, \omega)p_0R_0}{\rho_L V_0(R_0)}, \quad (2.25b)$$

where $V_0(R_0)$ is the unperturbed bubble volume. The exact form of ω_0 will vary depending on the choice of Γ , which is a complex function. However, for a real valued frequency independent polytropic index, which is true for adiabatic and isothermal pulsations, ω_0 equals bubble's natural frequency (ω_{nat}). To avoid any further ambiguity or confusion, we will use ω_0 to denote the resonance frequency of bubble pulsations for the rest of this dissertation. Our final task is to relate ω_0 and K , which will be done in a later section.

We have also used the following definitions for the linearized acoustic cross-sections in our study [See Appendix B for derivation]

$$\sigma_s = \frac{4\pi R_0^2}{(1 + \varepsilon^2) [(K/\omega^2 - 1)^2 + (2b/\omega)^2]}, \quad (2.26)$$

$$\sigma_e = \frac{4\pi R_0^2}{(K/\omega^2 - 1)^2 + (2b/\omega)^2} \frac{2b}{\varepsilon\omega}, \quad (2.27)$$

b , K are same as defined earlier. ε is the dimensionless frequency, which is defined as $\omega R_0/c$. The second order corrections in ε have also been neglected in our published results reproduced here as they did not improve the accuracy of our solution. Also note that the acoustic cross-sections have been represented in terms of damping factor rather than the damping coefficient. This approach helps in avoiding some of the inconsistencies and errors that have been reported in the literature [174].

2.4.3.2 Damping Factors

While defining acoustic cross section we introduced a term called damping coefficient (δ) with viscous, thermal, acoustic re-radiation, encapsulation and other constituents. Damping factor (b) was also defined and the need to use its precise relationships with δ was pointed out. We have used the following definitions which are consistent with 2.26 and 2.27

$$\delta_{\text{tot}} = 2b/\omega_0, \quad (2.28a)$$

$$\delta_{\text{vis}} = \frac{4\mu}{\rho_L \omega_0 R_0^2}, \quad (2.28b)$$

$$\delta_{\text{rad}} = -\frac{P_X}{\rho_L c \omega_0 R_0} = \frac{3\kappa P_0}{\rho_L c \omega_0 R_0} \quad (\text{for polytropic case}), \quad (2.28c)$$

$$\delta_{\text{thm}} = -\frac{P_{\dot{X}}}{\rho_L \omega_0 R_0^2}, \quad (2.28d)$$

$$\delta_{\text{enc}} = \frac{\Sigma_{\dot{X}}}{\rho_L \omega_0 R_0^2}, \quad (2.28e)$$

where all the symbols are same as defined earlier. Since, we have considered a compressible version of RP equation, the radiation damping term is easily determined. The encapsulation damping will be dependent on the choice of the rheological model. In reality, damping due to the encapsulation has the most significant contribution[175] and can be as high as 70 % of the total damping [176]. The role of viscous damping in compressible liquids is discussed below, followed by a discussion of on the appropriate choice of the thermal damping and the polytropic index.

2.4.3.2.1 Viscous Damping in Compressible Liquid

For a Newtonian incompressible liquid the viscous damping, given by 2.28b, can be derived easily from the normal stress calculations — shear viscosity does not manifest itself in spherically symmetric momentum equation. However, the viscous damping term should in principle be corrected when considering a compressible liquid where the velocity field is no longer divergence free. The compressible versions of RP equation do not consider this effect. In contrast microbubble modeling literature, the correction terms are neglected citing negligible contributions. Hoff [156] showed that the correction term was indeed second order in $1/c$. Ainslie and Leighton [174] also pointed out two additional complications due to introduction of liquid compressibility — one due to exponential decay of scattered and incident acoustic waves and the other due to modification of the other damping terms and the stiffness factor as shown by

Yang and Church [177]. These effects are not considered in the present study as such corrections are expected to play negligible role in the analysis presented here.

2.4.3.2.2 Thermal Damping and Choice of Polytropic Index

The choice of the polytropic index will now be justified in context of thermal damping. A closure of the RP equation requires a knowledge of the inside gas pressure. The validity of ideal gas behavior of the inside gas can be verified by calculating the compressibility factor for the gas. Stride [2] has shown that for practical cases assumption of ideal gas behavior is accurate for contrast microbubbles. The pressure variation inside the bubble is also negligible [124, 178]. This assumption of quasi-static oscillations will be valid when $\sqrt{R_0/\lambda_g}$ is small, where $\lambda_g = 2\pi(\gamma R_g T_\infty/M)^{1/2}/\omega$ [124]. R_g is the universal gas constant, M is the molecular weight of the gas, γ is the adiabatic gas constant and T_∞ is the undisturbed liquid temperature. Under these conditions, the pressure-volume relationship for the gas is primarily determined by the heat transfer across the bubble wall [128, 179]. Hence, there are two time scales — a time scale of bubble oscillations and the other for heat transfer. If the former is smaller, the volumetric bubble pulsations are effectively isothermal. For smaller heat transfer time scale, the oscillations are close to adiabatic conditions. The Peclet number defined as $Pe = R_0^2\omega/D_g$ can be used to distinguish between these two regimes, where D_g is the thermal diffusivity of the gas. When $Pe \gg 1$, adiabatic oscillations can be assumed, while an isothermal assumption will be valid for $Pe \ll 1$ [148].

A more careful analysis of the problem was presented by Prosperetti et al. [179] as described below. A heat flux balance at bubble interface can be written as

$$K_g \frac{\partial T}{\partial r} = K_L \frac{\partial T_L}{\partial r}, \quad (2.29)$$

where K_g and K_L are thermal conductivities of the gas and liquid respectively, and T_L is the liquid temperature. By considering a thermal boundary layer thickness in the

gas (δ_g) and the liquid (δ_L), the temperature gradients can be calculated as

$$\frac{\partial T_g}{\partial r} \sim \frac{T_g - T_s}{\delta_g}, \quad \frac{\partial T_L}{\partial r} \sim \frac{T_s - T_\infty}{\delta_L}, \quad (2.30)$$

where T_g is the temperature at the “core” of the bubble and T_s is the temperature at the interface. Now, the boundary layer thickness can be calculated for the respective regions using $\delta \sim \sqrt{D\Delta t}$, where D is the thermal diffusivity of the region considered. Hence, we obtain

$$\frac{T_s - T_\infty}{T_g - T_s} = \left(\frac{K_g \rho_g C_{p,g}}{K_L \rho_L C_{p,L}} \right)^{1/2}, \quad (2.31)$$

where $C_{p,g}$ and $C_{p,L}$ the specific heats of the gas and liquid respectively. Since, liquid density and specific heat are usually much larger than those for the gas, the right-hand side is typically of the order of $10^{-3} - 10^{-2}$. Hence, the surface temperature equals liquid temperature and the temperature drop occurs only inside the bubble. This explains why Peclet number defined above determines the regimes of bubble oscillations at small-amplitudes.

It will be shown in subsequent chapters, based on the above argument, that for contrast microbubbles oscillations are either isothermal (i.e., $\kappa = 1$) or adiabatic (i.e., $\kappa = \gamma$). For both these cases the polytropic constant is a real-valued function independent of excitation frequency which makes $P_{\dot{X}} = 0$. *Hence, thermal damping for both adiabatic and isothermal cases is identically zero.* It is difficult to estimate the polytropic constant for intermediate Peclet numbers and requires a more rigorous approach[178, 180–182]. Prosperetti et al. [179] has shown that for small-amplitude oscillations, a complex polytropic index can be defined which will give us the exact expression for thermal damping for those cases.

2.4.3.3 Resonance Frequency

A characteristic of any dynamical system is its resonance behavior and bubbles are no exception. It is evident from the linearized form of the equation of motion that

resonance behavior will play an important role in determining its dynamics. Resonance behavior of contrast microbubbles is even more important because of the fortuitous coincidence of the diagnostic ultrasound frequency with the resonance frequency of these bubbles. The linearized version of RP equation is analogous to a forced spring-mass-damper system. The frequency at which the system undergoes unforced oscillations is defined as its natural frequency(ω_{nat}). For unforced oscillations, 2.22 becomes

$$\ddot{X}_l + 2b\dot{X}_l + KX_l = 0, \quad (2.32)$$

and the solution is

$$X_0 = a_1 \exp((i\omega_{\text{nat}} - b)t) + a_2 \exp((-i\omega_{\text{nat}} - b)t), \quad (2.33)$$

where both K and β can be functions of the natural frequency in general for pulsating bubbles and they follow the relation given below

$$\omega_{\text{nat}}^2 = K(\omega_{\text{nat}}) - b(\omega_{\text{nat}})^2. \quad (2.34)$$

Usually, the damping factor(b) is small and hence the damped natural frequency is not significantly different from undamped natural frequency. Moreover, for most cases with small amplitude oscillations for contrast microbubbles K and b are constants [Will be shown later]. Hence, for constant damping factor (b) and stiffness (K), $\omega_{\text{nat}}^2 = K - b^2$. With these assumptions, let us now reexamine the forced oscillator problem. The solution to 2.22 is given by

$$X_l(t) = a_0 e^{-bt} \cos \left[(K - b^2)^{\frac{1}{2}} t + \Psi_0 \right] + Q(\omega, b) \cos(\omega t + \phi), \quad (2.35)$$

where a_0, Ψ_0 are constants determined by the initial conditions and $Q(\omega, b)$ and ϕ are given by:

$$Q(\omega, b) = 2p_A \left[(K - \omega^2)^2 + 4b^2\omega^2 \right]^{-\frac{1}{2}}, \quad (2.36a)$$

$$\phi = \tan^{-1} [2b\omega / (\omega^2 - K)]. \quad (2.36b)$$

Note that, $Q(\omega, b)$, which is the response function of the oscillator, will have a maximum at $\omega^2 = K - 2b^2$ indicating resonance. Hence, we can now write for constant damping factor (b) and stiffness (K), $\omega_0^2 = K - 2b^2$, recalling our earlier definition of resonance frequency. $Q(\omega, b)$ is also the steady state response of the system. The concept of resonance can be easily understood by substituting the forcing term by $2\epsilon P'_A$ and considering small damping i.e., $b = \epsilon b'$, such that $|\epsilon| \ll 1$ with P'_A and b' order one terms. Substituting these values in 2.36a we have

$$Q(\omega, \epsilon b) \simeq P'_A / b' K \quad \text{when} \quad \omega \simeq K, \quad (2.37)$$

to be of order one. Hence, resonance allows amplification of the excitation amplitude. This concept of resonance will also be critical for understanding the nonlinear response of the system later. Typical resonance curves for varying damping is shown in Figure 2.3. We observe the increase of the damping factor reduces the peak amplitude of the resonance and tends to make the response curve broader. The shift in resonance frequency due to increasing damping is however minimal under small amplitude oscillations. This again justifies that undamped natural frequency can be used to estimate the resonance frequency of the bubble.

Let us now consider the resonance behavior for encapsulated microbubbles. Lets introduce the assumption that the gas inside follows a polytopic gas law with a real valued frequency independent polytopic index. This makes both K and b to be constant. As explained in preceding sections, we can safely approximate the resonance frequency of bubbles (ω_0) by the undamped natural frequency obtained from the linear

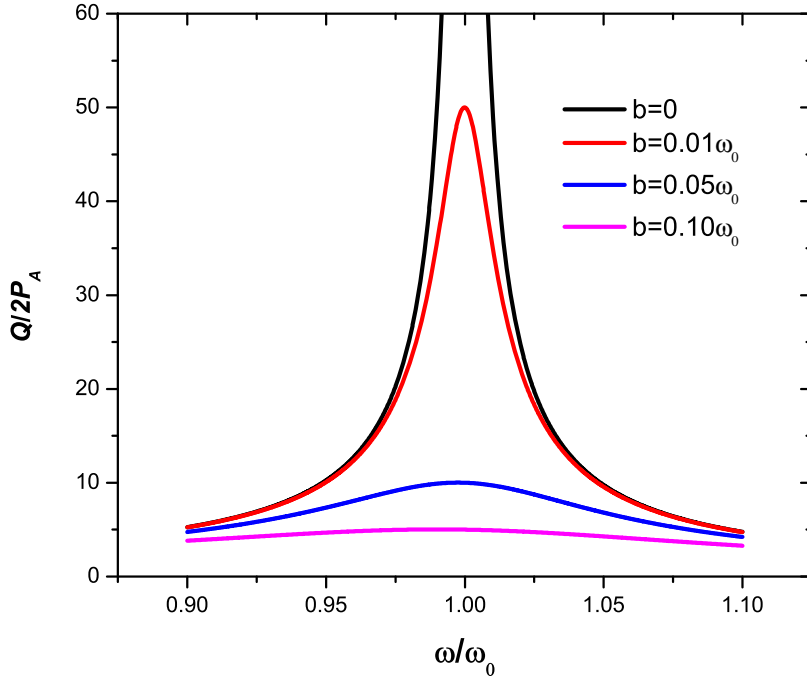


Figure 2.3: The plot of the response function $Q(\omega, b)$ for a linear oscillator with varying damping factors.

model, i.e., $\omega_0^2 = K$. Hence, we can now write an expression of resonance frequency using 2.21b as

$$K = \omega_0^2 = \frac{3\kappa P_0 + \Sigma_X}{\rho_L R_0^2}, \quad (2.38)$$

where Σ_X will change based on our choice of rheological model. Since, the usual tendency of the encapsulation to increase the stiffness, Σ_X increases beyond its value for uncoated bubbles, which is $2\sigma_{\text{water}}/R_0$. This causes the resonance of a similar sized contrast microbubble to shift to a higher value in comparison to an uncoated bubble of same size. Specific examples will be shown in the later sections.

2.4.4 Large-Amplitude Oscillations

The full nonlinear form of RP equation does not have any exact analytical solution and hence has to be solved numerically to obtain solutions for large amplitude oscillations. The dynamics of large amplitude oscillations will be determined by the acoustic excitation pressure and several interesting behaviors have been reported. But, certain nonlinear phenomena can also be understood by applying a weakly nonlinear analysis.

2.4.4.1 Resonance Behavior and Damping Factor

The expression for resonance frequency [2.38](#) derived earlier is strictly valid for small-amplitude oscillations. It has been shown, for both uncoated [\[138\]](#) and coated bubbles [\[183\]](#), that with increasing amplitude of acoustic excitation the resonance curve skews towards smaller bubbles. Hilgenfeldt et al. [\[129\]](#) explains this by noting that a third order expansion of RP equation modifies the expression for resonance frequency making it smaller than the linear approximation. Since, the attenuation theory given by [2.27](#) is strictly valid for small-amplitude oscillations, it is critical to ensure that any acoustic attenuation experiments are performed at low excitation pressure for a correct comparison with theoretical predictions. For large amplitude oscillations, thermal damping can be incorporated by considering an effective thermal viscosity. Stride [\[2\]](#) has shown that such corrections have almost no effect on the dynamics of contrast microbubbles.

2.4.4.2 Nonlinear Behavior

The nonlinear behavior of the bubble will now be discussed using a weakly nonlinear analysis, invoking the concept of resonance. Let us consider the second order truncated version of the RP equation [2.20](#), and substitute the following in it

$$X(t) = X_l(t) + Y(t), \quad (2.39)$$

where $X_l(t)$ has already been defined and solved for. Using 2.39 in 2.20 and substituting 2.38, we have

$$\ddot{Y} + 2b\dot{Y} + \omega_0^2 Y = A(X_l + Y)^2 + B(\dot{X}_l + \dot{Y}) + C(X_l + Y)(\dot{X}_l + \dot{Y}) - 2p_A(X_l + Y) \cos \omega t, \quad (2.40)$$

where A, B, C are same as defined earlier and Y on both sides are the same. Note that there is a striking similarity between 2.22 and 2.40. The latter can be interpreted as an equation governing the dynamics of a linear oscillator, albeit with a more complicated forcing term with more frequency components than the exciting ultrasound pulse. Hence, there can be a possibility of a resonant amplification when either of the frequency components of the right hand side is close to ω_0 and the forcing term p_A is significantly larger. Such resonances can be termed as nonlinear resonances. It remains difficult to determine for what frequency components will we have this resonance behavior, which can be easily derived, as explained below. This heuristic argument is key to understanding the nonlinear dynamics of any system and was introduced by Prosperetti in his pioneering dissertation [184] and several subsequent publications [173, 185–187].

For a nonlinear resonance, Y will have dominant frequency components which can be expressed as $e^{\pm in\omega t}$, where $n\omega \sim \omega_0$. Note that, due to the chosen form of Y and the previously derived form of the linear solution, X_l , the right hand side can only produce the following frequencies:

$$0, \quad 2\omega, \quad \omega \pm n\omega, \quad 2n\omega. \quad (2.41)$$

Hence, the only possible cases when a nonlinear resonance can occur (i.e., $\omega_0 \sim n\omega$)

are given by:

$$2\omega \sim n\omega, \quad \text{i.e.,} \quad n = 2, \quad (2.42)$$

$$(1 - n)\omega \sim n\omega, \quad \text{i.e.,} \quad n = \frac{1}{2}, \quad (2.43)$$

where 2.42 gives the second-harmonic component of the system and 2.43 gives the first subharmonic component of the system. In principle, the above methodology can be expanded to higher orders to incorporate other harmonics, subharmonics, and ultra-harmonics [184].

2.4.4.2.1 Second-Harmonics

When a second-harmonic resonance occurs, it is sufficient to consider that component in the solution of Y , as all other components will have negligible contributions. Hence, the solution can be expressed as

$$Y \simeq Y_2 = Y_{2,0}e^{2i\omega t} + \text{c.c}, \quad (2.44)$$

where c.c is the complex conjugate of $Y_{2,0}$. The solution $Y_{2,0}$ is given as [173]

$$|Y_{2,0}|^2 = \left(\frac{p_A}{\sqrt{(\omega_0^2 - \omega^2) + 4b^2\omega^2}} \right)^4 \frac{[A + (1 - B)\omega^2 - \omega_0^2]^2 + (C + 2b)^2\omega^2}{(\omega_0^2 - 4\omega^2)^2 + 16b^2\omega^2}, \quad (2.45)$$

with all symbols are same as defined earlier. Two important observations must be noted

1. Second-Harmonic solution does not have any generation threshold i.e., $Y_{2,0} = 0$ is not a solution.
2. The amplitude of second-harmonic oscillation is proportional to the square of the amplitude of the excitation pressure i.e., $Y_{2,0} \propto p_A^2$

2.4.4.2.2 Subharmonics

Similar to the second-harmonic resonance, we can write the dominant part of the solution for the first subharmonic resonance as

$$Y \simeq Y_{\frac{1}{2}} = Y_{\frac{1}{2},0} e^{i\omega t/2} + \text{c.c.} \quad (2.46)$$

Putting 2.46 in 2.40, we can obtain a solution for $Y_{\frac{1}{2},0} = 0$. Non-zero solutions can only be obtained once a threshold condition is satisfied which is given below following [173]

$$\left(\frac{p_A}{\sqrt{(\omega_0^2 - \omega^2) + 4b^2\omega^2}} \right)^2 = \frac{(\omega_0^2 - \frac{1}{4}\omega^2)^2 + b^2\omega^2}{[2A + (B + 1)\omega^2 - \omega_0^2]^2 + \left(\frac{C}{2} - 2b\right)^2\omega^2}. \quad (2.47)$$

This threshold is for the subharmonic generation to be possible. The presence of subharmonic signal in the solution is determined by the initial conditions. Another threshold, known as the absolute threshold [173, 188], has to be exceeded for subharmonic components to be necessarily present and a clear distinction should be made as far as possible while comparing numerical/experimental predictions with analytical theory.

2.4.4.3 Modeling the Scattered Acoustic Pressure Field

Most of the experimental measurements record the scattered pressure field far away from the bubble — hence, the name far-field scattered pressure. Note that the scattering cross-section derived in Section 2.4.3.1 is valid for small-amplitude oscillations only. The acoustic pressure scattered by the bubble can easily be calculated using calculations in Appendix B and is given by [See Brennen [122] pg. 83]

$$P_s(r, t) = \frac{\rho_L R}{r} \left(R \ddot{R} + 2\dot{R}^2 \right). \quad (2.48)$$

Stride [2] gives a more accurate form of above equation as given below

$$P_s(r, t) = \frac{\rho_L R}{r} \left(R \ddot{R} + 2 \dot{R}^2 - \frac{\dot{R}^2 R^3}{2r^3} \right) \quad (2.49)$$

Note that, far away from the bubble with $r \rightarrow \infty$ 2.49 reduces to 2.48. Since, we are interested in the far-field scattered acoustic pressure we used 2.48 for all our calculations. The scattering cross-section can be defined as

$$\sigma_s = \frac{W_{\text{scattered}}}{I_{\text{incident}}} = \frac{4\pi \langle r^2 P_s(r, t)^2 \rangle / \rho_L c}{\langle p_{\text{incident}}(t)^2 \rangle / \rho_L c} = \frac{4\pi \langle r^2 P_s(r, t)^2 \rangle}{p_A^2}, \quad (2.50)$$

where the angular brackets indicates average over a time period.

2.5 Dynamics of a Suspension of Bubbles

The previous section described the mathematical formulations describing the dynamics of a single bubble. In reality, however, suspensions have a range of bubble/particle sizes. Hence, our mathematical modeling must be extended to incorporate the cumulative effects of a polydisperse suspension of bubbles. Acoustic characterization of such suspensions involves various experimental approaches like attenuation measurements, backscatter measurements, detection of ultrasound mediated destruction etc. The underlying physical mechanisms and relevant mathematical models used in this study are described in the following few sub-sections.

2.5.1 Attenuation

Attenuation through a medium measures the loss of energy experienced by an incident acoustic wave as it travels through it. Figure 2.4 below shows a schematic representation of the effect of attenuation on an acoustic wave. The decay in the acoustic wave occurs both due to absorption of the energy and scattering of the waves by the constituents of the medium under consideration, such that the total loss of

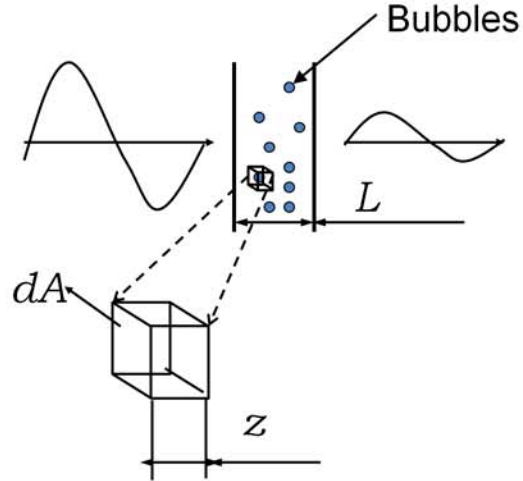


Figure 2.4: Schematic representation of attenuation of an acoustic wave. A small cubical volume within the suspension is also shown outside in a magnified form.

energy from the incident acoustic beam (P_e) can be written as

$$P_e = P_a + P_s \quad (2.51)$$

where P_e , P_a , and P_s are directly related to the σ_e , σ_a and σ_s respectively. Thus, the calculation of attenuation due a single bubble is fairly straightforward. The total attenuation is usually expressed as energy lost per unit length — for ultrasound imaging it is expressed in terms of decibels per unit length e.g., dB/cm. Let us now assume the bubbles in the suspension are in low concentrations such that each bubble scatters and absorbs independently of one another. With this assumption the loss of energy of the incident wave can be calculated simply as a sum of the energy lost due to each individual bubbles (P_n). Considering a small volume in the suspension $dV = dA_z$ as shown in Figure 2.4. The total power lost due to the bubbles can then be written as

$$dP_i = \sum_{n=1}^N P_n = I_i \left(\int_{a_{\min}}^{a_{\max}} \sigma_e(\omega, a) n(a) da \right) dV, \quad (2.52)$$

where N is the total number of bubbles in dV , I_i is the intensity of the incident wave, $n(a)da$ is the number of bubbles per unit volume with their radius in the interval $(a, a + da)$, (a_{\min}, a_{\max}) is the range of bubble sizes in the suspension. The change in the intensity due to attenuation is thus given by

$$dI_i = -\frac{dP_i}{dA} = -I_i \left(\int_{a_{\min}}^{a_{\max}} \sigma_e(\omega, a) n(a) da \right) dz. \quad (2.53)$$

So the intensity of the acoustic wave can now be written as a function of the distance traveled through the suspension as

$$I_i(z) = I_i(0) \exp \left(- \int_{a_{\min}}^{a_{\max}} \sigma_e(\omega, a) n(a) da z \right), \quad (2.54)$$

which gives us the frequency dependent attenuation coefficient ($\alpha(\omega)$) in dB per unit length as

$$\begin{aligned} \alpha(\omega) &= -\frac{1}{z} 10 \log_{10} e \left(\frac{I_i(z)}{I_i(0)} \right) = 10 \log_{10} e \int_{a_{\min}}^{a_{\max}} \sigma_e(\omega, a) n(a) da \\ &= 10 \log_{10} e \sum_{a_{\min}}^{a_{\max}} \sigma_e(\omega, a) n(a) da, \end{aligned} \quad (2.55)$$

where the integration is expressed evaluated as a summation for a discrete size distribution.

2.5.1.1 Multiple Scattering Effects

The above formulation relies on a critical assumptions that the cumulative effects of the bubble population can be expressed simply as a sum of individual contributions. This is a valid assumption only for small volume fractions in the range of $10^6 - 10^{-5}$. With increasing volume fractions bubbles will start to interact and the scattered wave from one bubble might be interfered by the presence of a neighboring

bubble. This results in fluctuations in the velocity of sound in water about a mean velocity. The average effect is a frequency dependent sound velocity along with attenuation. These average effects can be modeled using a continuum approach [189–192], multiple scattering theory [192–194] and diagram methods [194]. Stride [2] extended this theory to propose a more accurate model for contrast microbubbles valid upto a concentration of 10^6 particles/ml. It was shown that even with an improved model there was no significant differences from the linearized attenuation theory given above upto particle concentrations of 10^5 /ml. Since, most of our experiments are performed well below this limit, we can safely neglect the multiple scattering effects in attenuation for our analysis. A simple test for validating this assumption will be to observe the peak attenuation coefficient as a function of bubble concentration — a linear increase will validate absence of multiple scattering effects.

2.5.1.2 Attenuation and Resonance Frequency

Equation 2.55 can be written in the following form for a monodisperse bubble population as

$$\alpha(\omega) = 10 \log_{10} eN\sigma_e(\omega). \quad (2.56)$$

Hence, the peak of the attenuation curve will coincide with the peak of the extinction cross-section, which occurs at the resonance frequency. Hence, experimentally measured attenuation coefficient will help us determine the resonance frequency of a monodisperse suspension if small-amplitude oscillations are valid and bubble concentrations are lower than 10^5 /ml. For a polydisperse suspension, however, the comparison will not be direct. The peak of the attenuation will represent a weighted averaged resonance frequency of the suspension. This point will be critical in analyzing the experimental results presented later in this thesis.

The critical significance of small-amplitude assumption must be reiterated in this context. As shown earlier, an increase in excitation pressure skews the resonance curve,

thereby deviating from the linearized predictions. Hence, one must be extremely careful to avoid such pressure dependent attenuation effects. Chatterjee et al. [195] showed that when the excitation pressure is sufficiently low, further reduction in excitation amplitude did not change the attenuation curve obtained in broadband measurements. This is used as a test for validating small-amplitude assumption in this thesis. Note that for certain lipid coated microbubbles (e.g., BR14, SonoVue), as low as 10 kPa acoustic excitation pressure amplitude might be required for meeting the above mentioned criteria [183].

2.5.2 Speed of Sound

It was mentioned in the previous section, that presence of bubble changes velocity of sound in the fluid also known as dispersion effect. Hoff [156] showed that even at moderate volume fractions ($10^{-5} - 10^{-4}$) the dispersion effects are significant without causing notable variation from the linearized multiple scattering free attenuation predictions. Hence, while modeling changes to sound velocity through suspension of bubbles, measured experimentally, multiple scattering effects should be considered. Commander and Prosperetti [191] gives the following expression for dispersion of an acoustic wave traveling through a bubbly suspension.

$$\left(\frac{c}{c_m}\right)^2 = 1 + 4\pi c^2 \int_{a_{\min}}^{a_{\max}} \frac{an(a)}{\omega_0^2 - \omega^2 + 2ib\omega} da, \quad (2.57)$$

where c_m is the frequency dependent, complex phase velocity of a wave propagating through the suspension of bubbles. If $c_m = u - iv$, we have

$$c_m(\omega) = \frac{c}{u}, \quad (2.58a)$$

$$\alpha(\omega) = 10 \log_{10} e \left(\frac{\omega v}{c} \right), . \quad (2.58b)$$

Note that the attenuation coefficient predicted by 2.55 and 2.58b give exactly similar results for the volume fractions considered in this study. Equations 2.58a and 2.57 will

be used to predict frequency dependent velocity of sound through a bubbly suspension for comparison with experiments.

2.5.3 Scattering

Scattered acoustic pressure can be calculated using the expression for radiated field given in Equation 2.48, which can then be used to calculate scattering cross-section using 2.50. Neglecting multiple scattering effects the effective scattering cross-section for a suspension of bubbles can be expressed as

$$S_s(\omega) = \int_{a_{\min}}^{a_{\max}} \sigma_s(a; \omega) n(a) da = \sum_{a_{\min}}^{a_{\max}} \sigma_s(a; \omega) n(a) da. \quad (2.59)$$

To detect nonlinear components in the scattered pressure a Fourier transform of the scattered power will be utilized using a Fast Fourier Algorithm. The amplitude of scattered spectrum will be expressed in dB with unit reference. Since, attenuation experiments requires measurable change in the amplitude of the incident acoustic wave, considerable higher particle concentrations have to be used in experiments. Scattering measurements require much lower particle concentrations. Hence, multiple scattering effects can be safely neglected for modeling *in vitro* experimental results. However, *in vivo* experiments typically utilize much larger concentrations, and it will be appropriate under those circumstances to utilize a multiple scattering model as proposed by Stride [2].

2.5.4 Bubble Dissolution and Bubble Destruction

As mentioned earlier, a free air-bubble in water can dissolve in a matter of milliseconds due to Laplace pressure effects. Such effects will be important in polydisperse suspension with smaller bubbles dissolving at a much faster rate. Contrast microbubble are more stable because of the presence of low solubility gases and the stabilizing encapsulation. A study of encapsulated microbubble dissolution is beyond the scope of this study. However, previous research by our group has indicated that presence of

a viscoelastic coating can provide stable equilibrium of bubbles under static conditions thereby providing prolonged shelf-life [14, 15, 196]. Since, the time scale of bubble oscillations under ultrasonic pulses are orders of magnitude smaller than the static dissolution rate, they will not affect the dynamics of bubbles. The validity of this assumption under dynamic conditions needs to be ascertained. Acoustically driven diffusion generally increases rate of bubble dissolution [69, 197]. Lipid coated microbubbles are found to be critically affected by acoustically driven dissolution at 400-600 kPa acoustic excitation pressure [198] and they can fragment above 800 kPa acoustic pressure [198]. Other interesting phenomena like lipid shedding [72, 198–201] from microbubbles and stabilization of bubble size at intermediate acoustic pressure [198, 201, 202] have also been reported [198]. Several groups have been studying these effects with the goal of developing reliable mathematical models of such behaviors that can be incorporated in the bubble dynamics of encapsulated microbubbles [197, 203–205]. The present study neglects such effects in the mathematical modeling of contrast microbubbles and hence, can be a basis of future research.

Contrast microbubbles can undergo ultrasound mediated destruction. Several modes of destruction have been reported in the literature [69], which are: bubble growth at low acoustic pressure (for non-air-filled bubbles only), excitation amplitude dependent destruction at intermediate acoustic pressure and excitation independent rapid fragmentation at high acoustic pressures. Incorporation of destruction mechanisms in theoretical modeling is difficult and often done using *ad hoc* criteria. The popular model due to Marmottant et al. [164] considers break-up and rupture of the encapsulation by introducing an upper cut-off in their interfacial tension term. It will be shown in later sections, that our models, which do not model bubble rupture or break-up, can successfully capture experimentally observed behavior of contrast microbubbles. This indicates that bubble destruction probably had negligible influence in most of our *in vitro* experiments. Nevertheless, incorporation of destruction mechanisms should be considered to accurately model contrast agent behavior and can be the basis

of future improvements. This study also includes acoustic experimental study of bubble destruction utilizing the technique developed in our research group by Chatterjee et al. [69].

2.6 Experimental Characterization of Ultrasound Contrast Agents

2.6.1 Acoustic Attenuation and Scattering

The number of papers published every year on acoustic characterization of ultrasound contrast agents through attenuation and scattering experiments is astounding. However, none of them make propose any substantial modification from the basic experiments that were developed during the early days of contrast agent characterization. Hence, only a short overview is given for this topic, which should be sufficient for understanding the results of this study.

Attenuation measures the loss of energy of an acoustic wave as it travels through a medium. It is enhanced in presence of microbubbles. If the attenuation due the contrast microbubbles is too high, the scattered signal can be lost completely before being received by the transducers. Hence, the earliest standardized measurements of contrast agent efficacy utilized a parameter called STAR (scattering to attenuation cross-section ratio) [206]. For a good contrast agent this value should be as high as possible indicating a high backscatter of signal with minimal loss of energy of the scattered wave during transmission. Apart from a measure of contrast agent efficacy, the frequency dependent attenuation measurement can also capture the resonance behavior of a monodisperse bubble population as evident from. The peak in such a curve will indicate the resonance frequency. For a polydisperse suspension the peak will indicate a weighted average. Attenuation setups either employ a single transducer in transmit-receive mode [50, 207] or a pair of transducers, one in transmitting mode and the other in receiving mode [195, 208]. The receiver can also be a needle hydrophone [209, 210], which offers greater sensitivity and increased receiving bandwidth. While the former setup is less prone to signal corruption due to the excitation pulse, it is restricted by the receiving bandwidth of the exciting transducer. A two transducer setup is more

flexible in this regard but it might lead to more noisy data if the received signals are not properly filtered and extracted to avoid interference from the incident pulse. But, both setups should give equivalent results if appropriate precautions are taken during experimental measurements. Note that both focused and unfocused transducers have been used for attenuation measurements. However, an unfocused transducer will generate a pulse, which will have greater resemblance with a plane wave. The attenuation theory is based on the assumption of plane waves traveling through the suspension. Attenuation measurements can either be broadband or narrowband. While broadband experiments can be performed faster with the application of a single pulse with a broad bandwidth (e.g., a short duration impulse), it suffers from lack of uniformity of pressure across the pulse bandwidth. This issue can be addressed by using multiple transducers with overlapping bandwidth to check consistency of the acquired data — the data should match in regions of overlapping bandwidth. An alternate to broadband attenuation measurements is the implementation of narrowband pulses. Pulses are generated at small frequency intervals, each having the same output pressure. However, this technique requires more time for the completion of a single run and also requires more careful calibrations. For most general characterization a broadband measurement should be sufficient. However, if one needs to characterize any specific behavior of the contrast agent likely to be affected by uncertainties of broadband measurement a narrowband approach can be followed e.g., for determination of excitation pressure dependent resonance frequency of monodisperse bubble suspensions [210].

Measurement of acoustic backscattering can also be done using a single transducer, a pair of transducers or a transducer-hydrophone pair. The single transducer setup will utilize a pulse-echo setup to detect backscattered signals from the bubbles. If one needs to obtain the backscattering coefficient, scattered signal a perfect reflector also has to be acquired preferably using a flat, polished metallic surface [109]. Note that, although, backscatter experiments are usually performed with focused transducers, unfocused transducers can also be used. Most two transducer system implements

confocal alignment of two focused transducers facing each other in the horizontal direction. Shi and Forsberg [50] introduced an improved method to obtain backscattered response with high spatial resolution and higher signal-to-noise ratio. The transducers were confocally aligned at right angles, which helped in acquiring signal generated only from bubbles in the focal volume of the transducers. Due to spherically symmetric oscillations of the bubbles, these signals were equivalent to pure backscattered echoes. Scattering experiments will typically utilize single frequency sinusoidal excitation pulse. However, use of chirp coded pulse have also been reported [211]

For both attenuation and scattering experiments the sample can be placed can be dispersed in the entire chamber [50, 162] or contained in a smaller sample chamber with acoustically transparent window immersed in a larger bath of water [109, 210, 211]. While the former arrangement is less prone to noise from wall reflections it utilizes a larger amount of sample per run and is limited by its ability to characterize dense suspension of bubbles. A setup involving acoustically transparent windows however, can be corrupted by reflections from the wall — the window is not completely transparent. Such smaller setup also violates the theoretical assumption of bubbles placed in a liquid of infinite extent and suitable modifications must be invoked for comparison with analytical/numerical results.

2.6.2 Radial Dynamics

Measuring material properties by using attenuation measurements through a bulk suspension of microbubbles have several limitations e.g., the polydispersity of microbubbles critically affects the predictions, linearized dynamics might not be a valid assumption, the material properties might not be the same over the entire range of bubble population etc. Due to these limitations associated with attenuation measurements, experimentally obtained radius-time signatures of microbubble are also used for the estimation of interfacial properties. The radial dynamics of individual microbubble can be captured directly using high speed cameras [212–214] and streak cameras [157, 215–217] or indirectly e.g., using light scattering measurements [218–220] and an

acoustical camera [221]. Although, direct optical observations of microbubbles offer several advantages like more accurate measurement, isolation of response from individual microbubble, minimal effects of signal attenuation and no requirement of accurate calibration, they often have limited optical resolution, constraints over data collection, and require ultra-fast cameras that are expensive and not easily accessible. Indirect measurements provide an inexpensive, less complicated, real-time alternative with no limitations on the data acquisition. However, they cannot provide the wide range visual information obtained from direct optical observations. Techniques using radius-time data have been successful in accurately capturing the radial dynamics of several different contrast microbubbles like Quantison [222], Definity [219, 223], SonoVue [212, 213, 218, 224], BR14 [176, 188, 221] Sonazoid [220], Optison [220], Targestar [225] etc. The numerical solution of the RP type equation can be fitted with these experimentally measured radius-time curves to obtain the material properties using an error minimization algorithm. The fitting can be done with just the knowledge of the bubble's initial radius and the excitation pulse. It has been successfully implemented to estimate model parameters for different encapsulated microbubbles using several different rheological models of encapsulation [168, 171, 176, 213, 218, 219]. Several interesting observations have been made during experimental investigations of the radial dynamics of contrast microbubbles like compression-only behavior [164, 183, 224], existence of a threshold for the onset of oscillations [183, 226], mode vibration of bubbles [227, 228], non-spherical oscillations [228–230], buckling of shells [231] etc. These observations reflect the nonlinearity of the encapsulated bubble dynamics even at low acoustic excitation pressures, which is neglected in fitting of linearized dynamics with experimental attenuation data. This gives a definite advantage to this kind of property estimation technique to assess the applicability and validity of various models. To illustrate this we can consider the compression-only behavior — at low excitation pressures, certain phospholipid coated bubbles (e.g., BR14, SonoVue) show asymmetric oscillations, more compression than expansion, about the initial diameter. This behavior has been attributed the buckling of the phospholipid shells [231]. Most models

for encapsulated bubble dynamics cannot capture this behavior except Marmottant's model [164], Doinikov's nonlinear viscosity model [168], the NSEV model [171] and the exponential elasticity model with non-negative surface tension. Thus, comparison with experimentally observed radius-time curves can also assess the capabilities of various rheological models and can be used for characterization of contrast agents.

2.6.3 Experimental Strategies to Avoid Polydispersity

Scattering experiments using a polydisperse suspension can be corrupted by multiple scattering effects and is also trickier to model. Experimental observation of radial dynamics can circumvent this problem, but it cannot provide a direct measurement of acoustic scattering by microbubbles which is the primary purpose of these contrast agents. Hence, significant efforts have been made to develop several single bubble acoustic characterization techniques [197, 232–242]. Single bubble acoustic characterization can be a useful tool to validate the predictions of the models for encapsulated bubble dynamics without encountering the problem of polydispersity. An alternate approach has been to produce monodisperse bubble suspensions [210, 243–246] and characterize them with standard attenuation and scattering experiments [210, 244, 247, 248]. Both these kind of experimental data is critical for better understanding the dynamics of contrast microbubbles and for making further improvements in the rheological models of microbubble encapsulations. Removing the uncertainty in model predictions due to polydispersity will significantly improve our theoretical understanding of these models.

2.7 Material Characterization of the Encapsulation

Estimation of model parameters for material characterization of the encapsulation remains a difficult problem till date. Standard low frequency techniques for direct measurement of interfacial properties such as Langmuir trough are of limited validity for measuring material properties of contrast agents oscillating at megahertz frequencies. Hence, several different approaches have been utilized to measure material

properties using various experiments, e.g., backscattering measurements [249], attenuation measurements [155, 156, 250], light scattering experiments [218, 219], high-speed optical observations [176, 212, 251, 252], atomic force microscopy [253] and measurements using Fluorescence Recovery After Photobleaching (FRAP) [254], fluorescence lifetime imaging [255].

We use the experimentally obtained attenuation data to determine the unknown model parameters and then validate our model predictions against nonlinear scattering in this study. Usually, attenuation experiments are performed at low amplitude excitations. Hence, one can use the linearized version of RP equation to get expressions for both the damping coefficient [See 2.21c] and the resonance frequency [This method will be elaborated later]. Since, use of attenuation requires a fitting through least square optimization, Hughes et al. [256] and Grishenkov et al. [257] suggested a more stringent test by simultaneously fitting both attenuation and phase velocity for PVA-shelled microbubbles. Due to the ill posed nature of the problem, the fitting process is difficult and also very sensitive to several factors like polydispersity of the suspension, initial guess of parameters, etc. Also, attenuation data might not always reflect the linearized dynamics. Recent experimental observations have demonstrated the occurrence of non-linear behaviors e.g., compression only behavior [183], shift of resonance frequency [183], subharmonic generation [188], etc., even at very low acoustic excitation pressures of 50 kPa. This may result in inaccurate predictions and one need to account for these sources of errors in their analysis.

This concludes our discussion of basic concepts and review of the existing literature required for understanding both the motivation behind and outcomes of our research.

Chapter 3

EXPERIMENTAL METHODS¹

In Chapter 2 we reviewed the various techniques employed for the characterization of contrast agents. Since, this research was motivated by the need of a detailed understanding of the contrast agent dynamics through a combined experimental and mathematical modeling approach, we utilized different experimental setups for our studies. A detailed discussion of all the experimental setups and methodologies utilized by us will be presented here to avoid unnecessary repetitions in later chapters. Although, the experimental apparatus used are fairly simple, it will be evident in the following chapters that even simple *in vitro* acoustic studies can provide a rich plethora contrast agent dynamics that are not well understood. Such simple experiments can also provide critical insights into shortcomings of mathematical models, whose performance is expected to degrade further under real world *in vivo* conditions.

The acoustic setups utilized in this study can be broadly categorized as: transducer calibration experiments, low amplitude excitation attenuation experiments (linear dynamics), higher amplitude excitation scattering experiments (both linear and non-linear dynamics), time dependent attenuation and scattering studies, ultrasound imaging with clinical scanners, and ultrasound triggered release studies with liposomes. The release study protocol with triggers other than ultrasound were application specific. Hence, those protocols are excluded in this generalized description and will be mentioned in the relevant chapters of this thesis. Other experiments included size measurements using dynamic light scattering (DLS), Coulter Counter Multisizer and

¹ Certain parts of the text in this chapter have been adapted from the several published articles[4, 110, 114, 115].

imaging of particles using transmission electron microscopy (TEM), atomic force microscopy (AFM), optical microscopy. These characterization studies using sizing instruments and microscopic images are essential for a better understanding of the underlying physical mechanisms observed in our acoustic experiments. *However, the author did not perform these experiments and they were acquired through collaborative efforts. Since, their inclusion is vital to the discussion of results obtained in dissertation, they are presented here with due acknowledgments.*

3.1 Size Measurements

Size distribution data is critical for the acoustic characterization of ultrasound contrast agents. We used DLS for most of our size measurements. However, DLS does not provide the actual number of particles present in a suspension which were determined using a Coulter Counter apparatus.

3.1.1 Dynamic Light Scattering

A dynamic light scattering (DLS) instrument (Zetasizer Nano-ZS90; Malvern Instruments Ltd., Malvern, Worcestershire, UK) controlled with the Zetasizer software (version 6.20) was used for measuring particle size distributions (PSD). DTS 0012 polystyrene latex disposable sizing cuvettes (RI: 1.59) were used and the measurements were performed at a scattering angle of 90°. The powdered form of contrast agents were reconstituted in PBS or HEPES buffer to give a final concentration of 0.1 mg/ml (total lipid concentration) and 1 mg/ml (powder concentration) for echogenic liposomes and PLA microbubbles respectively. The cuvette was equilibrated for 120 s and 10-12 readings were then taken for a single measurement at constant temperature of 25°C. Measurements were repeated 3-5 times to check for reproducibility of the results obtained.²

Size distributions and concentrations of polymer shelled Philips bubbles and PB-127 bubbles were measured using another light scattering based sizing equipment

² Performed by Rahul Nahire at North Dakota State University.

(AccuSizer 770A; Particle Sizing Systems, Santa Barbara, CA). Bubble suspensions were formed by rehydrating the powdered form of polymer microcapsules in 1 ml of DI water. The solutions were gently swirled until they appeared uniform before initiating data acquisitions. The sizing system was sensitive to particles with diameters between 0.5 μm and 100 μm . Measurements were taken in triplicates to check for reproducibility of the results obtained.³

3.1.2 Coulter Counter

Size and bubble concentration measurements were made also with a Coulter Counter Multisizer Z3 (Beckman Coulter Inc., Fullerton, CA, USA) with a 20 μm aperture, which enabled a measurable size range of 0.7–12 μm . The contrast agents were diluted in desired concentrations in DI water or PBS buffer. All measurements were repeated 3–5 times to ensure reproducibility of the results.⁴

3.2 Microscopic Imaging of the Particles

Our microscopic imaging studies were done with echogenic liposomes only as it is difficult to characterize their morphology with conventional sizing techniques.

3.2.1 Transmission Electron Microscopy

Two different TEM apparatus were used in our studies — a JEOL JEM-100CX-II transmission electron microscope operating at 80 kV and a JEOL JEM-2100CX-LaB₆ transmission electron microscope operating at 200 kV. The liposome samples were diluted to 1 mg/ml (total lipid concentration) and dropped onto 300 mesh Formvar coated copper grids previously coated with 0.01% poly-L-lysine and allowed to stand for 1 minutes before wicking off with filter paper. After air drying for 2 minutes, the samples were stained with 1% phosphotungstic acid for 1.5 minutes and subsequently wicked off with filter paper and allowed to dry again before viewing.

³ Performed by Paul Sheeran at University of North Carolina.

⁴ Performed by Brandon Helfield at Sunnybrook Research Institute, Toronto, Canada.

Images were usually captured at low magnification with the beam spread and not converged to reduce the beam interaction per unit area and hence the damage to sample if it were to occur.⁵

3.2.2 Atomic Force Microscopy

Freshly reconstituted ELIP solutions (in PBS or HEPES buffer) was deposited on mica substrates — 200 μl of the solution was used — followed by air drying to prepare the samples for the AFM experiments. AFM images were obtained by using a MultiModeTM atomic force microscope equipped with a Nanoscope IIIa controller and a J-type piezo scanner from Veeco Metrology Group, Santa Barbara, CA. AFM images were acquired in Tapping ModeTM. Tips made from antimony(n) doped Si were used for obtaining the images under laboratory conditions.⁶

3.3 Acoustic Experiments

3.3.1 Details of Transducer Used in this Study

We have used several single element immersion transducers in this study. The unfocused transducers were used for attenuation measurements, whereas focused transducers were used for scattering experiments. The details corresponding to each transducer are summarized in the Tables 3.1 and 3.2 below.

Table 3.1: Details of unfocused transducers used in this study.

Center Frequency	Manufacturer	Part Number	Diameter (cm)	-6dB Bandwidth (%)
2.25	Valpey Fisher		1.6	47.82
3.5	Olympus-NDT	V382-SU	1.6	66.21
5	Olympus-NDT	V309-SU	1.6	65.72
10	Olympus-NDT	V311-SU	1.6	55.18
15	Olympus-NDT	V319-SU	1.6	48.13

⁵ Performed by Rahul Nahire at North Dakota State University.

⁶ Performed by Avinash Ambre at North Dakota State University.

Table 3.2: Details of focused transducers used in this study. Each of them had a focal length of 3.048 cm.

Center Frequency	Manufacturer	Part Number	Diameter (cm)	6dB Bandwidth (%)
2.25	Olympus-NDT	V-306-SU-PTF	3.048	65.73
3.5	Olympus-NDT	V382-SU-PTF	3.048	86.34
5	Olympus-NDT	V-309-SU-PTF	3.048	85.061
10	Olympus-NDT	V-311SU-PTF	3.048	66.05
15	Olympus-NDT	V-319-SU-PTF	3.048	50.32

3.3.2 Transducer Calibrations

Transducer calibration is the first step in any acoustic experiment. Calibration will give us the exact relationship between the amplitude of the input signal and the output pressure amplitude. This knowledge will help us design our experiments and report them correctly, so that anyone using a different setup could in principle repeat the experiments. Every transducer comes with a set of standardized test results done following a standard protocol ASTM E0165: "Standard Guide for Evaluating Characteristics of Ultrasonic Search Units". This provides a focal length (for spherically focused transducers), waveform durations, and spectrum measurements. Waveform duration is measured at different dB levels (-14, -20, and -40 dB), where the time is measured from the first to the last instance in the pulse such that the voltage there rises (or decreases) above (or below) the noise at that specified ratio [See Figure 3.1a]. In this case the dB value is measured as the ratio between the absolute maximum value and the specified level. As an example, -6 dB is half the maximum amplitude of the wave pulse.

Under the standardized testing conditions, a pulser-receiver sends a short duration pulse of a specified energy to excite the transducer. This wave is reflected by a stainless steel reflector (or a ball) and received back by the same transducer. The calibration sheet comes with a plot of the received waveform given in Figure and a Fourier transform (FFT) of the signal Figure 3.1b. This FFT is utilized to calculate the nominal frequency and -6 dB bandwidth. The bandwidth is typically reported as

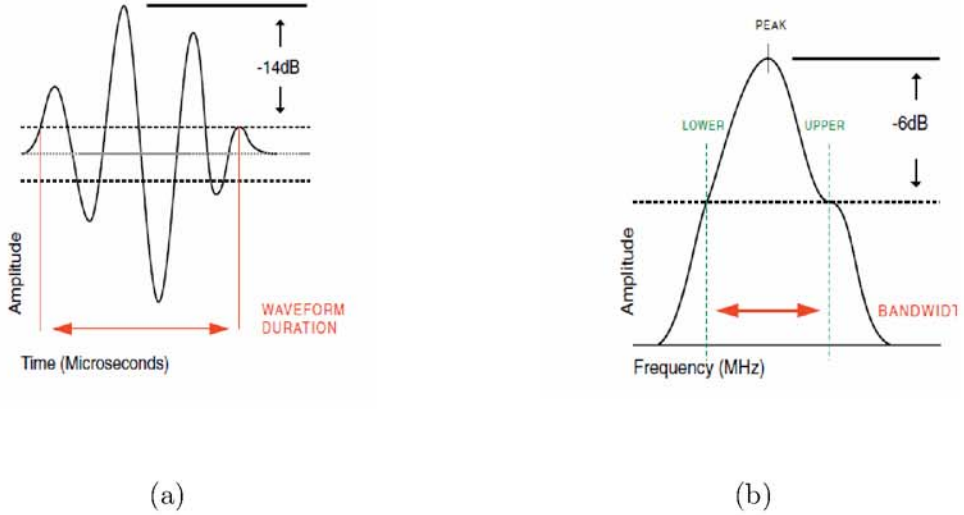


Figure 3.1: (a) Waveform duration at the -14 dB level or 20% amplitude of peak). (b) Peak frequency, upper and lower -6 dB frequencies and MHz bandwidth measurements.

a percentage which is defined as

$$\%Bandwidth = \Delta(f)_{\text{bandwidth}} / f_{\text{peak}}, \quad (3.1)$$

where f_{peak} is the peak in FFT. However, we still need to calibrate the output pressure and verify that the manufacturer reported bandwidth and nominal frequencies are correct. The detailed setup is described below.

3.3.2.1 Experimental Procedure and Data Reduction

One general setup was used for the data acquisition. A 4 mm needle hydrophone (HNC-0400; Onda Corporation, Sunnyvale, CA), was placed in a deionized water bath, held in position by a custom-made, three-dimensional manual positioning stage (Newport Corporation, Irvine, CA), and a machined acrylic attachment [See Figure 3.2]. The transducer to be tested was fixed into a custom made polycarbonate chamber as shown in Figure 3.2. An arbitrary waveform generator (AFG3521; Tektronix, Beaverton, OR) was utilized to generate a single-cycle sine wave, which was amplified by a 55 dB RF power amplifier (Model A300/A150; ENI, Rochester, NY). This amplified wave

was the input to our transducer. The needle hydrophone was connected to a preamplifier (A17dB, Onda Corporation/SEA, Sunnyvale, CA), and its output was viewed on an oscilloscope (TDS2012, Tektronix, Beaverton, OR) in real-time. Signals were acquired from the oscilloscope via a GPIB IEEE 488 cable and a GPIB card, and saved on a desktop computer using LabView (Version 6.0.3; National Instruments, Austin, TX, USA). 5 voltage-time (V-t) radio-frequency (RF) traces were acquired in an averaging mode (64 sequences were averaged) and saved for further analysis. The data were then analyzed using Matlab[®] (Mathworks Inc., Natick, MA, USA). The Matlab code gave us the positive and peak negative amplitude of the waveform. Ideally, they should be same for a sinusoidal output, which is true at low amplitudes. However, increasing the excitation voltage causes deviation from a symmetric waveform due instrumental errors.

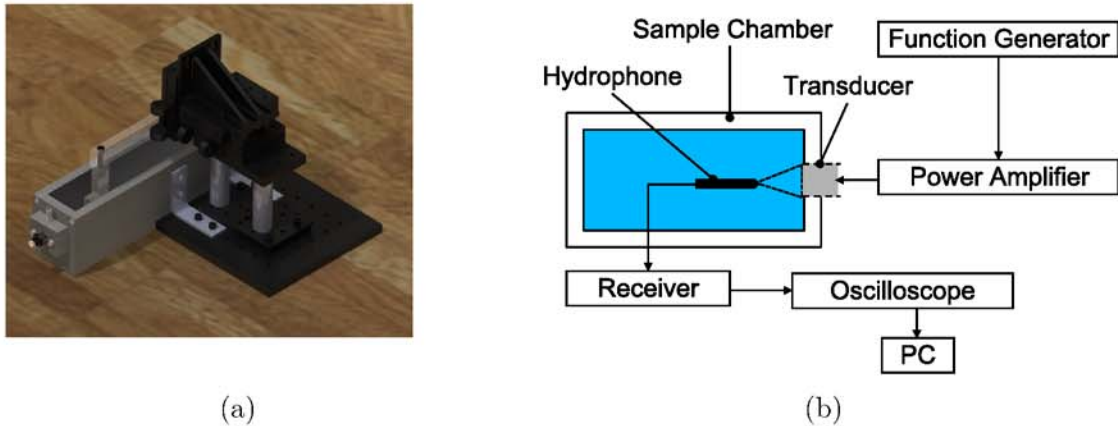


Figure 3.2: (a) Waveform duration at the -14 dB level or 20% amplitude of peak). (b) Peak frequency, upper and lower -6 dB frequencies and MHz bandwidth measurements.

Before acquiring any signal from the transducers, the needle hydrophone was aligned with its focus (or the center point for the unfocused transducer). This can be done by translating the positioning stage to detect the maximum amplitude for the focused transducer and recording the waveforms. For unfocused transducers, the hydrophone was translated across the face of the transducer in three mutually perpendicular directions to detect maximum lengths across which response was detected. These

would correspond to the diameters of the transducer in those three directions. The hydrophone was then positioned at the intersection of these three lines. Pressure (or power) calibration of unfocused transducer also required one additional step. After the hydrophone was positioned at the center, it was translated in all three directions by 1 mm steps. This way the response from the transducer was detected at 61 points, 15 in each direction from the center and the center itself. 15 annular circles can now be imagined on the transducer face each containing 4 points, the difference in diameters between consecutive circles being 1 mm. The response from each annular circle was taken as the average response of the 4 points it contains. For the central point a 1 mm diameter circle is considered about the center. Finally these responses are area averaged to obtain the spatial averaged response from the transducer.

Once the peak (or spatial averaged) amplitudes were obtained for the focused (or unfocused) transducer they were converted to pressure using the calibration chart provided by the hydrophone manufacturer. The chart lists Volts/Pascal for the hydrophone for a range of frequencies. The appropriate value corresponding to our excitation frequency is noted. The pressure can then be calculated using the following formulas

$$\text{Peak Positive Pressure (kPa)} = \frac{\text{Peak Positive Amplitude Recorded (V)}}{\text{V/Pa reading in the calibration chart} \times 10^3} \quad (3.2a)$$

$$\text{Peak Negative Pressure (kPa)} = \frac{\text{Peak Negative Amplitude Recorded (V)}}{\text{V/Pa reading in the calibration chart} \times 10^3} \quad (3.2b)$$

$$\text{Average Pressure (kPa)} = \frac{\text{Peak Positive Pressure} + \text{Peak Negative Pressure}}{2} \quad (3.2c)$$

Typically a linear relationship is obtained [See Figure 3.3] between the input voltage and the output pressure at focus (or spatial average pressure). This linear trend was used for designing experiments. Unfocused transducers used for ultrasound mediated release studies often require us to report a spatial average temporal average

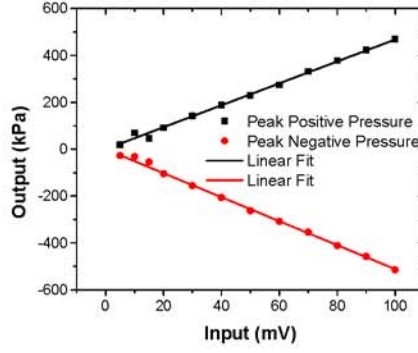


Figure 3.3: Calibration results showing linear relationship between input voltage and output pressure for a 3.5 MHz transducer excited at its center frequency

power (SATA) which was calculated from the as follows

$$P_{i,\text{rms}} = \frac{P_i}{\sqrt{2}} \quad (3.3a)$$

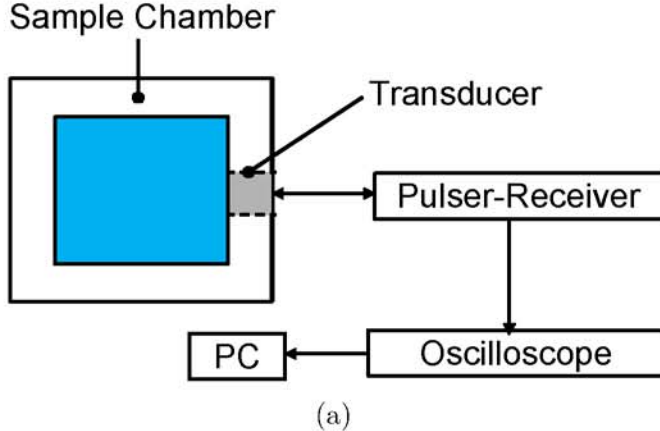
$$I_i = \frac{P_{i,\text{rms}}^2}{\rho_{LC}} \quad (3.3b)$$

$$I_{SA} = \frac{\sum_i I_i A_i}{\sum_i A_i} \quad (3.3c)$$

$$I_{SATA} = I_{SA} \times \text{Duty Cycle} \quad (3.3d)$$

$$(3.3e)$$

where P_i output pressure at i^{th} circle, A_i is the area corresponding to that circle. Duty cycle is defined as the ratio of the active time of the pulse to total duration of the pulse. It can be expressed in terms of the pulse frequency (f), number of cycles (n) and pulse repetition frequency (PRF) as Duty Cycle = $n \times \text{PRF}/f$



(b) Schematic representation of the experimental setup to measure acoustic attenuation *in vitro* using large volume.

3.3.3 Attenuation and Phase Velocity Measurements

3.3.3.1 Setup Description

Attenuation setup employed a large polycarbonate chamber for holding the liquid sample to be investigated. The setup consisted of a custom built polycarbonate chamber with holes drilled through its walls (1.17 cm thick), allowing for the insertion of our ultrasound transducers. The attenuation experiments were based on a pulse-echo measurement technique [See Figure 3.4b] following previous researchers [69, 156, 162]. Attenuation from a suspension of contrast agent (constantly stirred) was measured using unfocused broadband transducers operated in transmit/receive mode [See Table 3.1 for details of the transducers used]. A pulser/receiver (Model 5800; Panametrics-NDT, Waltham, MA, USA) was used to excite the transducers at a PRF of 100 Hz; it generated a broadband pulse with a duration of 440ns. The pulse generated at the face of the transducer traveled a total distance of 12 cm through the contrast agent suspension (from the transducer face to the container wall and back) before being received and fed to the digital oscilloscope (Model TDS 2012; Tektronix, Beaverton, OR, USA) to observe the signal in real time. Signals were acquired from the oscilloscope via a GPIB IEEE 488 cable and a GPIB card, and saved on a desktop computer using LabView (Version 6.0.3; National Instruments, Austin, TX, USA). 20 voltage-time

(V-t) radio-frequency (RF) traces were acquired in an averaging mode (64 sequences were averaged) and saved for further analysis. The data were then analyzed using Matlab® (Mathworks Inc., Natick, MA, USA) to calculate the attenuation coefficient for the contrast agent suspension. The peak negative pressure at the transducer output was calibrated using the calibration techniques described above. An external dB attenuator was also used to reduce the transducer output pressure and ensure the validity of linearized dynamics.

3.3.3.2 Experimental Procedure and Data Reduction Technique

Measured amount of buffer solution (100-150 ml of PBS or PBS-BSA solution) was poured into the large sample chamber, with least possible agitation for avoiding formation of air bubbles, to ensure the complete immersion of the transducer. The solution was left to equilibrate with the atmospheric oxygen for 5 mins that helped get rid of any residual bubbles — smaller bubbles will dissolve and larger bubble will float up. 20 V-t traces were acquired as reference signals i.e., without any contrast and saved on the computer using LabView [More details of acquisitions provided in Appendix C]. The contrast agents were then added to the solution and gently stirred to create a homogeneous solution. A magnetic stirrer was also used during the experiments to maintain sample homogeneity. 5 mins after adding the contrast agents, 20 more voltage-time traces were acquired with the contrast agents. The acquired pulse now had a reduced amplitude due to an attenuation effects as shown in Figure 3.5. This entire process was repeated 5 times to ensure reproducibility of the results.

For the smaller volume, 15 ml of solution was required. The reference signals were acquired with the buffer inside the sample chamber. Contrast agents were then added and mildly stirred without damaging the film. A small spherical magnetic stirrer was used to maintain homogeneity. Rest of the acquisition process remained similar.

The stored data files were then analyzed using a Matlab® code [Appendix C]. The acquired voltage-time responses were converted to the frequency domain using a Fast Fourier Transform Algorithm (FFT). The FFT gave us the frequency dependent

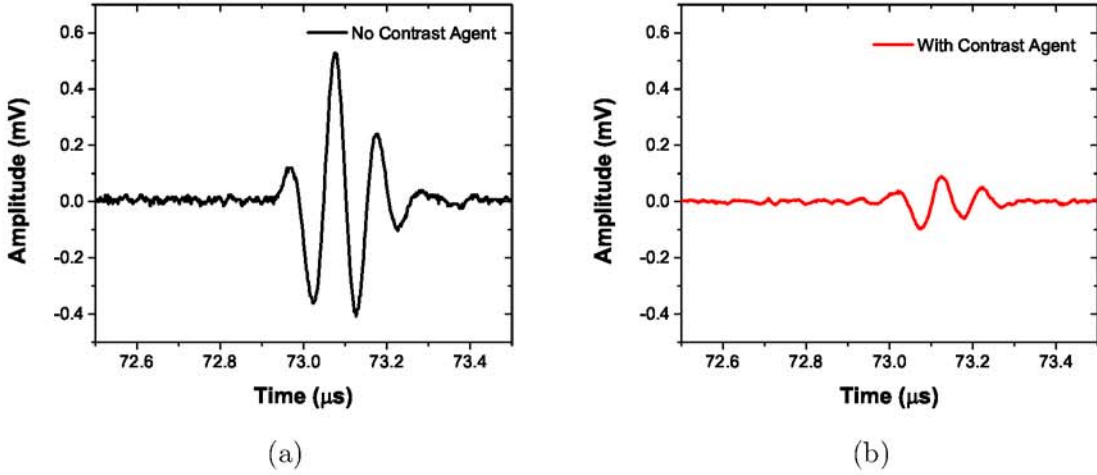


Figure 3.5: Signal acquired on the oscilloscope during attenuation measurements without (a) and with (b) contrast agents.

amplitude and phase associated with the pulses. These were averaged over the 20 acquisitions for both the reference signal and the signal with contrast agents. Using definitions of attenuation and phase velocities given in 2.55 and 2.57, the attenuation coefficient and phase velocity can be calculated using the following expressions

$$\alpha(\omega) = 20 \log_{10} \left(\frac{\bar{V}_{\text{ref}}(\omega)}{\bar{V}_{\text{sig}}(\omega)} \right) / 2L, \quad (3.4a)$$

$$c_m(\omega) = \left(\frac{1}{c_{\text{ref}}} - \frac{\varphi_{\text{ref}}(\omega) - \varphi_{\text{sig}}(\omega)}{2L\omega} \right)^{-1}, \quad (3.4b)$$

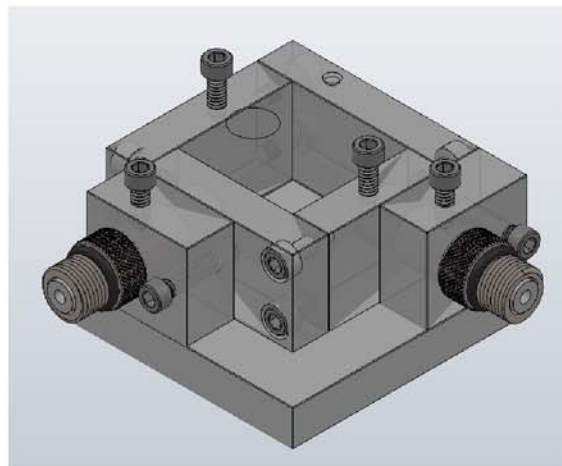
where in 3.4a, L is the distance between the transducer face and the reflecting wall, $\bar{V}_{\text{ref}}(\omega)$ is the response averaged in the frequency domain without any contrast agent in the medium, $\bar{V}_{\text{sig}}(\omega)$ is the response averaged in the frequency domain with contrast agents suspended in the medium. In 3.4b, c_{ref} is the phase velocity in water, $\varphi_{\text{ref}}(\omega)$ and $\varphi_{\text{sig}}(\omega)$ are the phases of the two signals.

3.3.4 Scattering Measurements

3.3.4.1 Setup Description

The scattering setup used was based on a technique similar to the one used by previous researchers [50, 163]. It employed two spherically focused transducers, each having an individual diameter of 1.6 cm and a focal length of 3.05 cm. As with attenuation, two acoustic setups were used — one larger volume setup and one smaller volume setup. The smaller volume setup was a modification pursued based on our experiences with the larger volume setup and will be discussed separately in Chapter 7.

In the larger volume setup [See Figure 3.6], the transmitting and receiving transducers were confocally positioned at right angles by placing them through circular holes drilled through the adjacent walls of a rectangular chamber. This configuration ensures similarity of scattered signals to backscattered echoes [50] along with high spatial resolution [163]. As mentioned above, 100-150 ml of contrast agent suspension was required for complete immersion of both the transducers. Details of the various transducers used are provided in Table 3.2. An arbitrary/function generator (Model AFG 3251; Tektronix, Beaverton, OR, USA) was utilized to generate a 32 cycle sinusoidal pulse of desired frequency at a PRF of 100Hz. This signal was then amplified using a 55dB power amplifier (Model A-300, ENI, Rochester, NY, USA) and fed to the transmitting transducer. Output pressure were determined using calibration technique explained earlier. The contrast agent at the focal volume of the transducer scattered this signal back which was received by the receiving transducer utilizing a pulser/receiver (Model 5800; Panametrics-NDT, Waltham, MA, USA) in receiving mode with a 20dB gain. The amplified signals were then fed to the oscilloscope to view them in real time. Voltage-time RF signals were saved onto the desktop using the same method used for attenuation experiments discussed earlier. For the data analysis of the scattered signals, 50 acquisitions in averaging mode were saved.



(a)

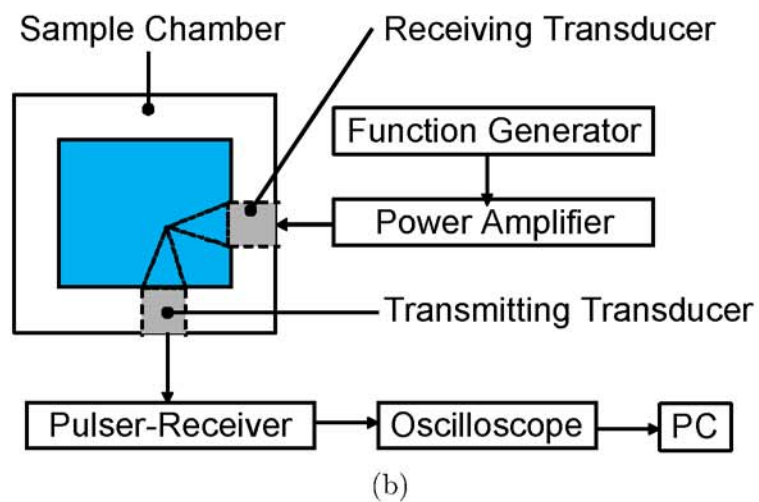


Figure 3.6: (a) A 3-D view of the setup for measuring scattering using a larger volume.
(b) Schematic representation of the experimental setup to measure acoustic scattering *in vitro* using a large sample volume.

3.3.4.2 Experimental Procedure and Data Reduction Technique

The scattering measurements for the control signal i.e., without contrast agents and the response due to the contrast agents were acquired using the same procedure mentioned earlier for attenuation experiments, but with 50 acquisitions for each case. For scattering a similar technique was used to get the average response in frequency domain (50 voltage time acquisitions are used). The scattered response was converted into a dB scale by taking a unit reference. Responses at frequencies of interest are then appropriately extracted from the resultant data set to find the fundamental, second and sub-harmonic scattered responses [See Appendix C for Matlab codes]. The final data is reported as an enhancement over the control.

3.3.5 Time Dependent Attenuation and Scattering Experiments

The attenuation and scattering experiments mentioned above analyzed the average response over a given time period. However, it was also required at times, to look at the time evolution of these properties. Time dependent attenuation studies can be used for acoustic measurement of ultrasound mediated contrast agent destruction [69]. Time dependent scattering studies, on the other hand, were useful to determine variation of acoustic responsiveness of the contrast agents with time. The experimental setup for both these experiments were exactly similar to those discussed above, the only difference being that 100-200 acquisitions with contrast agents were saved instead. The acquisition of reference signals remains unchanged. Also, since we were looking at time evolution of the properties, the acquisitions of the response with contrast agent was started within 30 seconds of their addition and mixing with the buffer solution — previously we used to wait for 5 mins for them to come to a stable state.

For time dependent attenuation studies, the average response over 30 sec-1 min intervals were calculated with a slight modification to the Matlab[®] code [See Appendix C]. Usually this implied averaging over 5-10 consecutive acquisitions. If we denote the start of the acquisitions with contrast agents as $t = 0$ and the averaging interval as Δt . The attenuation calculated using 3.4a for just the first acquisition is denoted by $a(0)$.

We assume that the response at time $t + n\Delta t$ can be approximated as the average over the period $(t + (n - 1)\Delta t, t + n\Delta t)$ and denote as $a(t = n\Delta t)$. Hence, we can write

$$a(0) = 10 \log_{10} \left(\frac{\bar{V}_{\text{ref}}^2(\omega)}{\bar{V}_{\text{sig},0}^2(\omega)} \right) / 2L, \quad (3.5a)$$

$$a(t = n\Delta t) = 10 \log_{10} \left(\frac{\bar{V}_{\text{ref}}^2(\omega)}{\bar{V}_{\text{sig},n-1}^2(\omega)} \right) / 2L, \quad (3.5b)$$

where $\bar{V}_{\text{ref}}(\omega)$ is same as defined earlier, $\bar{V}_{\text{sig},0}(\omega)$ denotes the response calculated with the first acquisition, $\bar{V}_{\text{sig},n-1}(\omega)$ denotes the average over the period $(t + (n - 1)\Delta t, t + n\Delta t)$. With these definitions however, at each instant of time we have an attenuation spectra and we can plot it with time as was done by Shi and Forsberg [50]. However, we were interested in characterizing the destruction with these experiments, which would then corrupt the data by nonlinear energy transfer across frequency spectrum. Hence, a revised definition was proposed by Chatterjee et al. [69], where at each instant in time the signals are summed over the frequencies and represented by a single value, $A(t)$ such that

$$A(0) = 10 \log_{10} \left(\frac{\sum_{\omega} \bar{V}_{\text{ref}}^2(\omega)}{\sum_{\omega} \bar{V}_{\text{sig},0}^2(\omega)} \right) / 2L \quad (3.6a)$$

$$A(t) = 10 \log_{10} \left(\frac{\sum_{\omega} \bar{V}_{\text{ref}}^2(\omega)}{\sum_{\omega} \bar{V}_{\text{sig},n-1}^2(\omega)} \right) / 2L. \quad (3.6b)$$

$A(t)$ was normalized by its value at $t = 0$ and denoted by $NA(t)$ such that

$$NA(t) = A(t)/A(0). \quad (3.7)$$

For time dependent scattering studies we calculated a term similar to $a(t)$ defined above, but with a unit reference. Instead of summing it over entire frequency range, we extracted the fundamental, subharmonic and second harmonic components at each instant from the resultant frequency spectra and plotted their evolution with

time.

3.3.6 Ultrasound Imaging ⁷

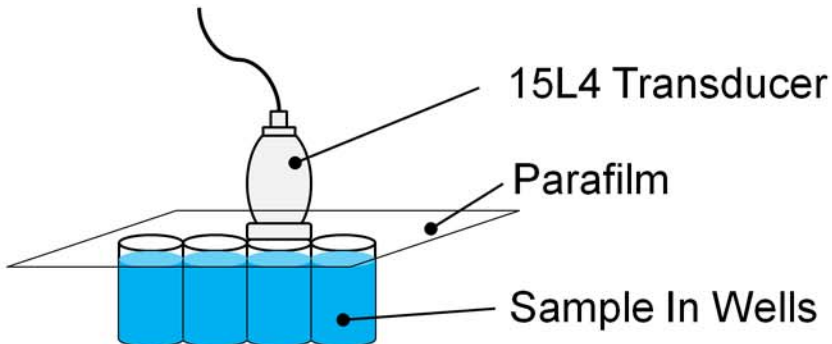


Figure 3.7: Schematic representation of the ultrasound imaging setup.

A Terason t3200™ diagnostic ultrasound scanner (MedCorp LLC., Tampa, FL, USA) was used to acquire ultrasound images of contrast agents reconstituted in phosphate buffered saline. A layer of Aquasonic™ 100 (Parker Laboratories, Inc., Fairfield, New Jersey, USA) ultrasound gel was applied to the 15L4 Linear Array ultrasound transducer (4.0-15.0 MHz) (MedCorp LLC., Tampa, FL) sound plate. The gel coated transducer was placed over the parafilm covering the wells of a 96-well plate, with each well containing 200 µl of the contrast agent solution [See Figure 3.7]. The ultrasound scan properties were set at 0.7 Mechanical Index (MI), 0.6 Thermal Index (TIS), Omni Beam activated, level C Image Map, level 3 Persistence, high (H) frequency, level 3 TeraVision, level 51 2D Gain, level 60 Dynamic Range (DR), 3 cm scan depth, and 22 Hz frame rate. The acquired images were properly labeled and saved for future use.

3.3.7 Ultrasound Mediated Release Studies

3.3.7.1 Setup Description

The in vitro setup for ultrasound enhanced release studies employed a single element unfocused immersion transducer (Model IP301HP; Valpey Fisher Corporation, Hopkinton, MA, USA). The active element of the transducer has a diameter of 1 cm and

⁷ Perfomed by Rahul Nahire at North Dakota State University.

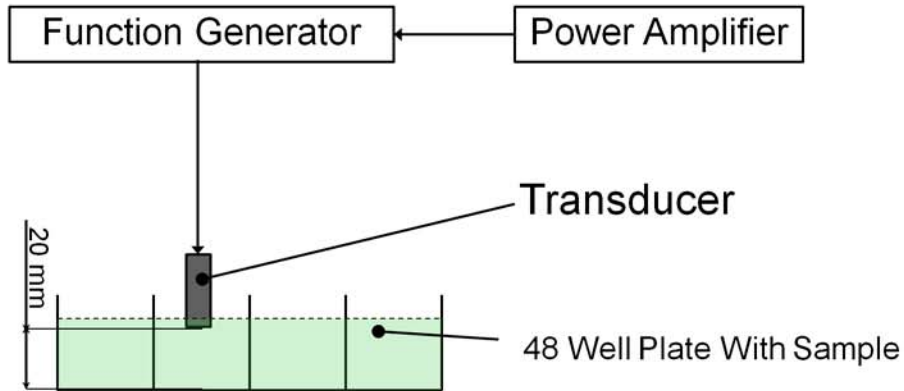


Figure 3.8: Schematic representation of the setup used for ultrasound mediated release studies.

a nominal center frequency of 3.5 MHz with a -6 dB bandwidth of 85%. Some of the release studies presented here were also performed with a 2.25 MHz flat faced transducer 1.27 cm in diameter (Model V 306 SU; Valpey Fisher Corporation, Hopkinton, MA, USA). An arbitrary function generator (Model 33250A; Agilent, Santa Clara, CA, USA) was used to generate a continuous sinusoidal wave with desired parameters, which was then amplified with a power amplifier (Model A-150; ENI, Rochester, NY, USA) and fed to the transducer. The release studies were carried out in a 48 well plate filled with 500 μ l sample (12 well plate with 3 ml sample for 2.25 MHz transducer) with a total lipid concentration of 0.02 mg/ml. The transducer face was always kept immersed in the sample volume at a distance of 20 mm from the base (Figure 3.8). The homogeneity of the sample was maintained using a small magnetic stirrer. The entire plate was kept on an ice bath to minimize the temperature changes. Release studies were performed with a 3 MHz continuous wave. The output pressure, determined from calibrations, and exposure time were varied to obtain optimum release. Although, the current setup has often been used to subject biological cells to ultrasound [258], it allows reflections from the air-water interface. This effect has been studied in detail recently [259, 260] to show that the reflection creates a standing wave pattern giving rise to a spatially varying acoustic field. For the limited goal of demonstrating ultrasound-mediated release here, current setup is adequate. Also note that less than 1% energy

transfer due to stimulation from a transducer positioned in one well was measured at a neighboring well indicating negligible inter-well interference. All experiments were repeated three times to ensure the reproducibility of results obtained. We are currently developing a setup that would address the wall reflection effect, and will be used to determine optimal ultrasound excitation parameters.

3.3.7.2 Quantification of Release

For our release studies, the liposomes under investigation were loaded with fluorescent molecules like calcein and carboxyfluorescein. Two different strategies were implemented — for carboxyfluorescein loaded liposomes used a self-quenching method, whereas the calcein loaded liposomes utilized a CoCl_2 quenching method.

For the former implementation, the fluorescence of the liposomal payload was negligible due to self quenching effect at high concentrations. With the application of a trigger, these molecules will come out and will be detected by the fluorescence detecting instrument. An increase in the readings will indicate a release. Release was monitored by recording fluorescence emission intensity at 518 nm with an excitation wavelength of 480 nm. Background readings were noted before starting the ultrasonic excitation (Initial Intensity). After the completion of ultrasound treatment, another set of readings were acquired (Observed Intensity). Finally, a positive control was obtained by detecting the fluorescence of liposomes treated with Triton-X100. This fluorescence was treated as 100% release (Final Intensity). The percentage reading was then calculated using the following formula

$$\text{Release}(\%) = \frac{\text{Observed Intensity} - \text{Initial Intensity}}{\text{Final Intensity} - \text{Initial Intensity}} \times 100 \quad (3.8)$$

For CoCl_2 quenching strategy, liposomes were loaded with fluorescent molecules at sub-quenching concentrations and hence, were detected during fluorescence measurements. The liposomal suspension had dissolved CoCl_2 , which quenched the fluorescence of the molecules as they came out of the liposomes. Thus, the reading would go down

indicating a release. Fluorescence was monitored at 515 nm with an excitation wavelength of 495 nm. As before three readings were recorded before application of US, after application of US and after application of Triton-X100. However, now the initial fluorescence indicates 100% and the final fluorescence with TritonX-100 represents the background fluorescence. So, the release was calculated using the following expression

$$\text{Release}(\%) = \frac{\text{Initial Intensity} - \text{Observed Intensity}}{\text{Initial Intensity}} \times 100 \quad (3.9)$$

Two different fluorescence measuring instruments were used in this study, a fluorescence microplate multidetection instrument (Model Spectramax-M5; Molecular Devices,Sunnyvale, CA, USA) and a Photon Counting Spectrofluorimeter (Model PC1; ISS, Inc., Champaign, IL, USA). There was no difference between the readings obtained.

3.4 Summary

This section discusses the various experimental methods utilized in this study. Detail descriptions are provided for different size measuring techniques, microscopic imaging techniques, acoustic attenuation and scattering measurements and ultrasound mediated release studies. Protocols for trigger specific release studies, other than US, will be discussed along with relevant sections. Any additional information required in addition to this generalized description will also be provided as and when required.

Part I

CHARACTERIZATION OF ULTRASOUND CONTRAST MICROBUBBLES

Chapter 4

A STRAIN-SOFTENING INTERFACIAL RHEOLOGICAL MODEL OF THE ULTRASOUND CONTRAST AGENT ENCAPSULATION¹

4.1 Introduction

In Chapter 2, we introduced the concept of ultrasound contrast microbubbles with a stabilizing encapsulation, which will play a critical role in determining the dynamics of such microbubbles under acoustic excitation. We reviewed a number of models describing the rheology of the encapsulation and its effects on the dynamics of coated microbubble that have been proposed over that last two decades. A generalized form of the RP equation for different rheological was also mentioned to extend the previously known weakly nonlinear analysis results for uncoated bubbles. This chapter will explain the derivation of the modified RP equations considering an interfacial rheological model of the encapsulation and then discuss its implications of the contrast microbubble dynamics.

Constitutive modeling of material behavior is a difficult task especially for a nanometer thick encapsulation. The task gets even more complicated due to the dynamic nature of the problem where microbubbles are undergoing volumetric pulsations at megahertz frequencies. Most rigorous theoretical description of the rheology of materials will not be valid under such conditions. Hence, earliest modeling approaches for contrast microbubble relied on an *ad hoc* treatment of the rheology by incorporating additional terms in the RP equation for uncoated bubbles [151, 152]. Church [154] provided the first rigorous theoretical treatment of the problem. Following his methods, a number of modifications were proposed each assuming the encapsulation to

¹ Figures and text in this chapter have been adapted from a published [110] and an article under review [7].

be a homogeneous continuum with bulk material properties [155, 156, 159]. However, biochemical analysis of the encapsulation had already demonstrated that the contrast agent encapsulation was essentially a monolayer of molecules [261, 262], which would invalidate the assumption of homogeneity, at least in the radial direction. Clearly the three orders of magnitude separation of length scale between the overall dimension of the microbubble (micrometer) and the thickness of the encapsulation (nanometer) makes it inappropriate to treat both scales simultaneously. This motivated our group to suggest an interfacial modeling approach for this problem in 2003 [162]. We argued that interfacial rheology, where the interface is treated as a zero-thickness surface with complex interfacial properties — as opposed to bulk rheological properties — that effectively represent the thickness averaged material response, is the appropriate approach for modeling the encapsulation. Note that the surface tension used to characterize an air-liquid interface, either pure or contaminated with surfactants, is also an interfacial rheological property . Over the years, we have also developed a two-pronged characterization effort which includes one experiment to determine the characteristic properties of the encapsulation and a second independent experiment that validates the characterization. The independent validation distinguishes this effort from other similar modeling studies. It also incorporates a way to improve a model where sophistication is introduced as warranted by the modeling effort as opposed to prescribed in advance.

In 2003, our adopted the simplest interfacial rheology — Newtonian, i.e. purely viscous with a constant surface tension (σ) and a dilatational viscosity (κ^s). These two parameters were determined for a number of contrast agents using attenuation of ultrasound through a contrast agent suspension. However, an unreasonably large value of surface tension (0.7-40 N/m) was obtained compared to the value (0.072 N/m) of a pure air-water interface, whereas one would expect a lower value to the absorption of the surface-active molecules at the interface. Yet the Newtonian model (NM) predicted the experimentally observed subharmonic response very well for the contrast agent Optison. The unphysical value of surface tension insinuated a non-Newtonian

rheology for the interface with an explicit interfacial elasticity. The constituent surface active molecules in the encapsulation are in close association with each other giving rise to a solid like interface rather than a Newtonian fluid like interface. Accordingly in 2005, we developed a new model — constant elasticity model (CEM) — including an interfacial dilatational elasticity (E^s) [163]. Characterization with this model obtained a more reasonable surface tension value (smaller than the pure air water interface) for a commercial contrast agent Sonazoid™. Also both the NM and the CEM predicted the same value for the dilatational viscosity ($\sim 10^{-8}$ Ns/m), as expected, because introducing elasticity should not change the viscous component. Despite such welcome features, the model performed poorly in validation, i.e. the predicted scattered subharmonic response did not match well with experimental measurement. The failure was attributed to the linear model of interfacial elasticity which presumably does not correctly describe the large oscillation that generates the subharmonic response. Consequently, we pursued a nonlinear extension of our viscoelastic model presented here[169].

To minimize the complications associated with the constitutive modeling, we consider here two simplest extension of the linear Hooke's Law — a quadratic elasticity model (QEM, interfacial elasticity varying linearly with area fraction), and an exponential elasticity model (EEM, elasticity varying exponentially). Meanwhile, another interfacial model with a nonlinear elastic term had been proposed by Marmottant et al. [164], which has gained wide acceptance because of its ability to predict several experimental observations recorded for contrast microbubbles e.g., the compression-only behavior, where the bubbles compresses more than they expand. We will compare the predictive capabilities of our model with model due to Marmottant and co-workers (referred to as MM).

It should also be noted that other nonlinear viscoelastic rheological models have also been proposed for contrast agent encapsulation. Following our investigation of a constant elasticity model, constitutive models appropriate for membranes such as Mooney-Rivlin (strain-softening) and Skalak (strain-hardening) models were applied

to the encapsulation of contrast microbubbles, where the authors performed a parametric investigation of the effects of the various constitutive parameters on the response of a bubble surrounded by such membranes [166]. These models have been widely used for membranes of capsules and biological cells [263, 264], that contain incompressible liquid in contrast to the compressible gas in a microbubble, and therefore do not undergo volume change. Membrane models (e.g. Mooney-Rivlin model for rubbery material) find the membrane stresses using the generalized strain energy, which is a function of the invariants of the finite deformation membrane strains. Different functional forms of the strain energy give rise to different nonlinear constitutive laws for the membrane including strain softening and hardening [263]. Skalak et al. [265] proposed a specific form of nonlinear strain energy function for the membrane of the red blood cells, which has an almost incompressible area; the form is chosen to incorporate the experimental result that “a change of shape at constant area requires relatively small stresses as compared with the stresses required to increase the area of the membrane.” Therefore, it is unclear if such specialized membrane constitutive laws are appropriate for the microbubble encapsulation. Moreover, for the radial oscillation of microbubbles (in contrast to shape deformation of capsules), where area fraction is the only relevant parameter, such general models are not necessary, and using them lead to difficulty in explaining the underlying physics. A Maxwell model appropriate for a “fluid like” membrane (in contrast to a “solid like” membrane where Kevin’s model is more appropriate) with extensions to nonlinear viscosity have also been applied to the modeling of the bubble encapsulation.

4.2 Mathematical Formulation

4.2.1 Assumptions

The mathematical derivations presented here have the following assumptions:

1. Each bubble can be considered being placed in a fluid of infinite extent i.e., multiple scattering effects can be neglected and there are no walls (either rigid or compliant) nearby. As explained in Section 2.5.1.1 this can safely be assumed for contrast agents concentrations less than $10^6/\text{ml}$, which is valid for all our *in vitro* experiments.

2. The surrounding fluid follows Newtonian constitutive laws, which is valid for most buffer solutions used in experiments.
3. Bubble oscillations can be considered to be spherically symmetric. Higher order modes, if present, will decay faster with increasing radial distance from the bubble. Hence, for most far-field measurements this assumption will be valid.
4. Bubble destruction is neglected, which is expected to occur at fairly high pressures, usually beyond the domain of diagnostic applications.
5. Model parameters are independent of the initial bubble size, which should be valid if they are the material properties of the encapsulation.
6. Other effects due to drug loading, lipid shedding, presence of ligands, aggregation of microbubbles, increase of temperature etc. are also neglected.

4.2.2 Bubble Dynamics

The compressible form of bubble dynamics was derived in [A.2](#) and is given as

$$R\ddot{R} + \frac{3}{2}\dot{R}^2 = \frac{1}{\rho_L} \{p_{r=R} - p_0 - p_{Ac}(t)\} + \frac{1}{c} \frac{d^2}{dt^2} \left(R^2 \dot{R} \right), \quad (4.1)$$

where we replaced $p\infty(t) = p_0 + p_{Ac}(t)$. Note that we will need to substitute the jump condition from the interfacial rheology models in the above equation and assume the governing equation for the pressure volume relationship for the gas under volumetric pulsations to close the equation. We have already justified that a polytropic gas law can safely be assumed to describe the inside the gas pressure variation, considering it to be spatially uniform. Also the last term $\frac{1}{c} \frac{d^2}{dt^2} \left(R^2 \dot{R} \right)$ can be handled by using the RP equation itself, which can be further modified following suggestions of [\[128\]](#) to obtain a more stable for compressible RP equation by replacing this term with $\frac{R}{c} \frac{dp_G}{dt}$. Hence, we can write [4.1](#) as

$$R\ddot{R} + \frac{3}{2}\dot{R}^2 = \frac{1}{\rho_L} \{p_{r=R} - p_0 - p_{Ac}(t)\} - 3\kappa \frac{\dot{R}}{c} p_{G0} \left(\frac{R_0}{R} \right)^{3\kappa}. \quad (4.2)$$

We will now replace the appropriate dynamic boundary conditions for each rheological model given below to obtain our final form of RP equation. In Chapter 2, we gave a generalized form of the 4.2 for any rheological model which is again presented here.

$$\rho_L \left[R \ddot{R} + \frac{3}{2} \dot{R}^2 \right] = \left(1 + \frac{R}{c} \frac{d}{dt} \right) P(R, \dot{R}) - \frac{4\mu \dot{R}}{R} - p_0 - p_{Ac}(t) - \Sigma(R, \dot{R}) \quad (4.3)$$

Our goal is to provide the exact expressions for the term $\Sigma(R, \dot{R})$, for different rheological models.

4.2.3 Interfacial Rheology

The derivation of RP equation requires a force balance at the interface which, following Edwards et al. [266] can be written as

$$\tau_s = \sigma I_s + (\kappa^s - \mu^s) (I_s : D_s) I_s + 2\mu^s D_s, \quad (4.4a)$$

$$[\tau \cdot \mathbf{n}]_{\text{surface}} = \nabla_s \cdot \tau_s, . \quad (4.4b)$$

where τ_s is the stress at the surface, σ is the interfacial tension or the surface tension, κ^s and μ^s are the interfacial dilatational and shear viscosities respectively, I_s and D_s are the surface identity and strain rate tensors respectively. The center double dot represents a scalar product of two tensor quantities. For spatially uniform pressure inside the bubble ($p_G(t)$), the radial part of the jump conditions is given by

$$\left(-p + 2\mu \frac{\partial v_r}{\partial r} \right)_{r=R} + p_G \equiv -p_{r=R} - 4\mu \frac{\dot{R}}{R} + p_G = \frac{2\sigma}{R} + \frac{4\kappa^s \dot{R}}{R^2}. \quad (4.5)$$

Note that the shear viscosity term does not appear due to spherical symmetry of the problem. For a free bubble, dilatational viscosity term is zero which reduces 4.5 to the well known Young-Laplace condition. Also, the dilatational viscosity contribution can be understood considering a bubble undergoing dilatation under volumetric pulsation at a rate of $A^{-1} dA/dt = 2\dot{R}/R$, with $A = 4\pi R^2$. This results in an additional uniform tension with a magnitude of $2\kappa^s \dot{R}/R$.

4.2.3.1 Newtonian Rheology

Under this model the encapsulation is considered as a purely viscous interface of infinitesimal thickness. *The interfacial tension and viscosity terms are both constant under Newtonian assumption.* Hence, we have

$$p_{r=R} = p_G - 4\mu \frac{\dot{R}}{R} - \frac{2\sigma}{R} - \frac{4\kappa^s \dot{R}}{R^2} \quad (4.6)$$

At the initial undisturbed state i.e., with $R = R_0$, $\dot{R} = 0$ and $p_{Ac}(t) = 0$, we have $p_{r=R_0} = p_0$. Hence, using 4.5 given above we can write the following expression of the initial gas pressure

$$p_{G0} \equiv p_G(t=0) = p_0 + \frac{2\sigma}{R_0}. \quad (4.7)$$

The interface is strained even at the undisturbed state with a higher gas pressure inside making the bubbles more susceptible to dissolution, which can only be negated by the low solubility of the gas and the diffusional barrier at the interface. After substituting 4.6 in 4.2 and comparing with the generalized form of encapsulated bubble dynamics given by 4.3 in Chapter 2, we have for the Newtonian Model (NM)

$$\Sigma(R, \dot{R}) = \frac{2\sigma}{R} + \frac{4\kappa^s \dot{R}}{R^2}, \quad (4.8a)$$

$$f_0 = \omega_0/2\pi = \frac{1}{2\pi R_0} \sqrt{\frac{1}{\rho_L} \left(3\kappa p_0 + \frac{2\sigma}{R_0} (3\kappa - 1) \right)}. \quad (4.8b)$$

4.2.3.2 Viscoelastic Rheology with a Constant Elasticity

As mentioned earlier, NM gives unphysical surface tension estimates for most contrast agents. It was argued that due to the high concentration of molecules at the bubble interface, a strong attractive interactions would exist amongst the molecules. This would necessitate an introduction of Gibb's elasticity term through a viscoelastic rheological model[163]. The dilatational elasticity or Gibb's elasticity (E^s) can be

introduced, following Edwards et al. [266], as

$$\sigma(R) = \sigma_0 + \beta \left(\frac{\partial \sigma}{\partial \beta} \right)_{\beta=0}, \text{with} \quad (4.9a)$$

$$\beta = \frac{\Delta A}{A} = \left[\left(\frac{R}{R_E} \right)^2 - 1 \right], \quad (4.9b)$$

$$E^s = \left(\frac{\partial \sigma}{\partial \beta} \right)_{\beta=0}, \quad (4.9c)$$

where R_E is the unrestrained equilibrium radius, σ_0 is the surface tension under the unstrained equilibrium condition, and both the elasticity term (E^s) and the dilatational viscosity term (κ^s) were considered to be a constant [163]. Note that, the Newtonian rheology does not permit existence of an unstrained state. Few important things should now be pointed out. Strictly speaking, the introduction of an elasticity term in this manner does not violate Newtonian rheology (Edwards et al. [266], p. 118). However, this terminology was used to distinguish the model from the purely viscous assumption. Hence, we will refer this model as just Constant Elasticity Model (CEM). Moreover, the expression of the effective surface tension ($\sigma(R)$) given by 4.9a is similar to a first order Taylor expansion and hence, should be valid for small amplitude variations about the unstrained radius(R_E). In fact, this is exactly similar to the linear form of Hooke's law. Hence, even though the introduction of elasticity did predict physically realistic surface tension values, it failed to match with subharmonic observations with contrast microbubble Sonazoid, which requires large amplitude oscillations. The jump conditions for the CEM can be written as

$$p_{r=R} = p_G - 4\mu \frac{\dot{R}}{R} - \frac{4\kappa^s \dot{R}}{R^2} - \frac{2\sigma_0}{R} - \frac{2E^s}{R} \left[\left(\frac{R}{R_E} \right)^2 - 1 \right]. \quad (4.10)$$

At the initial undisturbed state we have

$$p_{G0} \equiv p_G(t=0) = p_0 + \frac{2\sigma_0}{R_0} + \frac{2E^s}{R_0} \left[\left(\frac{R_0}{R_E} \right)^2 - 1 \right]. \quad (4.11)$$

Unlike the NM, we can now assume a pressure equilibrium i.e., $p_{G0} = p_0$, which will ensure better microbubble stability as it does not rely on low solubility of gas or the diffusional barrier any more. Thus, the introduction of elasticity can provide a condition for stable equilibrium of contrast microbubbles under static conditions which have been shown both numerically [14, 15] and through linear stability analysis [196]. The equilibrium radius for the CEM is given by

$$R_E = R_0 \left(1 - \frac{\sigma_0}{E^s}\right)^{-\frac{1}{2}}. \quad (4.12)$$

After substituting 4.10 in 4.2 and comparing with the generalized form of encapsulated bubble dynamics given by 4.3 in Chapter 2, we have for the CEM

$$\Sigma(R, \dot{R}) = \frac{2\sigma_0}{R} + \frac{2E^s}{R} \left[\left(\frac{R}{R_E}\right)^2 - 1 \right] + \frac{4\kappa^s \dot{R}}{R^2}, \quad (4.13a)$$

$$f_0 = \omega_0/2\pi = \frac{1}{2\pi R_0} \sqrt{\frac{1}{\rho_L} \left(3\kappa p_0 - \frac{4\sigma_0}{R_0} + \frac{4E^s}{R_0} \right)}. \quad (4.13b)$$

During pulsations of the bubble, the effective surface tension term ($\sigma(r)$) can become negative. Marmottant et al. [164] proposed another interfacial model at the same time when the CEM model was proposed. Although, the models were derived independently, they had the exact same form for the elasticity term. It was also argued that the effective surface tension term should not be negative. This condition for our interfacial elasticity model is obtained by imposing a condition of non-negativity on the effective surface tension term and is given as

$$\sigma(R) = \begin{cases} \sigma_0 + E^s \left[\left(\frac{R}{R_E}\right)^2 - 1 \right] & \text{for } \sigma_0 + E^s \left[\left(\frac{R}{R_E}\right)^2 - 1 \right] > 0 \\ 0 & \text{for } \sigma_0 + E^s \left[\left(\frac{R}{R_E}\right)^2 - 1 \right] \leq 0 \end{cases} \quad (4.14)$$

With this restriction however, we can no longer satisfy the pressure equilibrium mentioned earlier. This makes the effective stresses at the interface zero initially, which Marmottant et al. [164] calls as buckled state.

However, it was also shown by us that the elasticity term can be introduced as an independent property, without relating it to the surface tension [15]. Under those circumstances, the condition of non-negativity need not be imposed. If the non-negativity is not imposed, and dilatational elasticity is independently introduced, 4.10 might lead to a net compressive stress at the interface. Such a state will induce Euler type buckling in the encapsulation [263, 264], as seen for encapsulated bubbles [200]. Wrinkled bubbles were shown to bind better to their target site [267]. However, to accurately describe the buckling behavior, encapsulation rheology needs a bending resistance term. For the present purpose, where only spherical dynamics is considered, it suffices to assume that there is a finite bending resistance that determines the right wrinkling behavior, which however does not play any role in the spherical dynamics [264]. We will consider here, models with and without the constraint of non-negativity imposed on the surface tension and discuss their implications. The model with a non-negative effective surface tension is denoted with (NN).

To address the shortcomings of the CEM we perused two nonlinear extensions with strain-softening rheology, which are discussed below. For both these models dilatational viscosity term (κ^s) is treated as a constant.

4.2.3.3 Viscoelastic Rheology with a Quadratic Elasticity

As the area fraction increases, the constituent molecules in the encapsulation are distended from their close packed conformation. As a result the encapsulation elasticity reduces. The consequent strain-softening can be modeled by a linearly varying elasticity [See Figure 4.1a]

$$E^s = \begin{cases} E_0^s - E_1^s \beta & \text{for } E_0^s - E_1^s \beta > 0 \\ 0 & \text{for } E_0^s - E_1^s \beta < 0 \end{cases}, \quad (4.15)$$

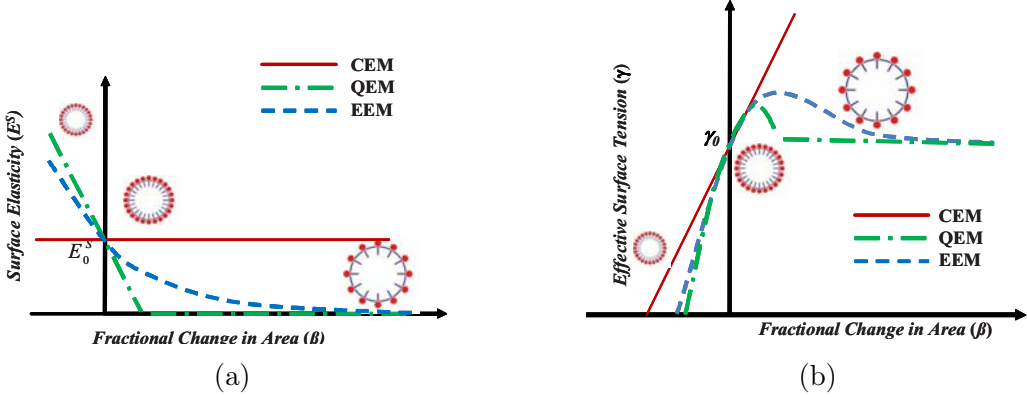


Figure 4.1: A representative figure depicting the change of interfacial elasticity (a) and effective surface tension (b) with fractional change of area for constant (CEM), quadratic (QEM) and exponential (EEM) elasticity models. Reprinted with permission from [169]. Copyright [2010], Acoustical Society of America.

where E_0^s and E_1^s are characterization parameters to be determined. The second condition ensures that the elasticity remains positive (unlike the effective surface tension, negative elasticity would result in an unphysical behavior). The dynamic boundary condition at the bubble interface 4.2 then is replaced by

$$p_{r=R} = \begin{cases} p_G - 4\mu \frac{\dot{R}}{R} - \frac{4\kappa^s \dot{R}}{R^2} - \frac{2\sigma_0}{R} - \frac{2\beta}{R} (E_0^s - E_1^s \beta) & \text{for } E_0^s - E_1^s \beta > 0 \\ p_G - 4\mu \frac{\dot{R}}{R} - \frac{4\kappa^s \dot{R}}{R^2} - \frac{2\sigma_0}{R} & \text{for } E_0^s - E_1^s \beta < 0 \end{cases}, \quad (4.16)$$

where β is same as defined above. Imposing the condition of pressure equilibrium at the initial zero motion state obtains a quadratic equation for β_0 (initial area fraction). Solving it, one obtains

$$R_E = R_0 \left(1 + \frac{E_0^s - \sqrt{(E_0^s)^2 + 4\sigma_0 E_1^s}}{2E_1^s} \right)^{-\frac{1}{2}}, \quad (4.17)$$

where the initial equilibrium radius is chosen to be smaller than the unstrained radius (the correct root of the quadratic equation) so that the resulting compressive strain balances the surface tension leading to a pressure equilibrium.

After substituting 4.15 in 4.2 and comparing with the generalized form of encapsulated bubble dynamics given by 4.3 in Chapter 2, we have for the QEM

$$\Sigma(R, \dot{R}) = \frac{2\sigma_0}{R} + \frac{2E_0^s - E_1^s \left[\left(\frac{R}{R_E} \right)^2 - 1 \right]}{R} \left[\left(\frac{R}{R_E} \right)^2 - 1 \right] + \frac{4\kappa^s \dot{R}}{R^2}, \quad (4.18a)$$

$$f_0 = \omega_0/2\pi = \frac{1}{2\pi R_0} \sqrt{\frac{1}{\rho_L} (3\kappa p_0 + \xi)}, \quad (4.18b)$$

$$\text{where } \xi = 4 \left(1 + \frac{E_0^s - \sqrt{(E_0^s)^2 + 4\sigma_0 E_1^s}}{2E_1^s} \right) \left(\frac{\sqrt{(E_0^s)^2 + 4\sigma_0 E_1^s}}{R_0} \right). \quad (4.18c)$$

4.2.3.4 Viscoelastic Rheology with a Exponentially Varying Elasticity

The quadratic model 4.15 introduces an abrupt change in elasticity to ensure positive dilatational elasticity. With the increasing area fraction, the progressive loss of elasticity could be better modeled by an exponential decay (Figure 4.1) such that

$$E^s = E_0^s \exp(-\alpha^s \beta), \quad (4.19)$$

with α^s and E_0^s to be determined. The dynamic boundary condition is given by

$$p_{r=R} = p_G - 4\mu \frac{\dot{R}}{R} - \frac{4\kappa^s \dot{R}}{R^2} - \frac{2\sigma_0}{R} - \frac{2\beta}{R} E_0^s \exp(-\alpha^s \beta), \quad (4.20)$$

As before, using dynamic boundary condition at the rest state and imposing pressure equilibrium, one obtains

$$\frac{2\sigma_0}{R_0} + \frac{2E_0^s}{R_0} \beta_0 \exp(-\alpha^s \beta_0) = 0 \quad (4.21)$$

Linearizing it for a small value of obtains a quadratic equation similar to the quadratic model above. Equilibrium radius (R_E) is given by (can also be obtained substituting

E_1^s in 4.17 by $\alpha^s E_0^s$)

$$R_E = R_0 \left(1 + \left(\frac{1 - \sqrt{1 + 4\sigma_0\alpha^s/E_0^s}}{2\alpha^s} \right) \right)^{-\frac{1}{2}} \quad (4.22)$$

Substituting 4.19 in 4.2 and comparing with the generalized form of encapsulated bubble dynamics given by 4.3 in Chapter 2, we have for the EEM

$$\Sigma(R, \dot{R}) = \frac{2\sigma_0}{R} + \frac{E_0^s \exp \left(-\alpha^s \left[\left(\frac{R}{R_E} \right)^2 - 1 \right] \right)}{R} \left[\left(\frac{R}{R_E} \right)^2 - 1 \right] + \frac{4\kappa^s \dot{R}}{R^2}, \quad (4.23a)$$

$$f_0 = \frac{1}{2\pi R_0} \sqrt{\frac{1}{\rho_L} \left(3\kappa p_0 + \frac{2E_0^s}{R_0} \left(\frac{\sqrt{1 + 4\sigma_0\alpha^s/E_0^s}}{\alpha^s} \right) \left(1 = 2\alpha^s - \sqrt{1 + 4\sigma_0\alpha^s/E_0^s} \right) \right)}. \quad (4.23b)$$

4.2.3.5 Marmottant Model

The Marmottant model assumes a constant dilatational viscosity term and the effective surface tension to have three distinct regimes: a buckled state of the encapsulation with zero surface tension below a prescribed buckling radius, an elastic state with linearly varying elasticity similar to the CEM, and a ruptured state with surface tension same as that of the air-water interface above a rupture radius. The effective surface tension and the viscosity terms due to this model are given as

$$\sigma(R) = \begin{cases} 0 & \text{for } R \leq R_{\text{buckling}} \\ \chi \left(\left(\frac{R}{R_{\text{buckling}}} \right)^2 - 1 \right) & \text{for } R_{\text{buckling}} \leq R \leq R_{\text{break-up}} \\ \sigma_{\text{water}} & \text{for } R \geq R_{\text{rupture}} \text{ and bubble has ruptured} \end{cases}, \quad (4.24)$$

where χ , the elastic modulus of the shell, is same as E^s in CEM. Also, $R_{\text{buckling}} = R_0 \left[1 + \frac{\sigma(R_0)}{\chi} \right]^{-1/2}$ and $R_{\text{rupture}} = R_0 \left[1 + \frac{\sigma_{\text{water}}}{\chi} \right]^{-1/2}$. Although such an effective surface tension behavior physically quite realistic, the choice for the different limiting

radii remains hard to determine, and typically made so that the results match with experimental observations. The breakup radius is difficult to estimate and is usually considered to be same as the rupture radius. Role of initial bubble state — buckled i.e., $\sigma(R_0) = 0$ or elastic or ruptured i.e., $\sigma(R_0) = \sigma_{water}$ — and the upper limit imposed by the break-up/rupture radius, have been shown to affect bubble dynamics considerably [172, 175, 183, 188]. However, no well defined recipe has been provided till date for the determination of their actual values for different bubbles. An exhaustive parametric study of their effects is beyond the scope of this study and can be found in the above mentioned publications. We assume here the initial surface tension to be zero for all the simulations presented, ensuring a pressure equilibrium at the initial unstrained state. Note that due to the discontinuous variation of effective surface tension with radius, it is difficult to give an expression of resonance frequency. However, one can derive the expression assuming that the bubble exists completely in the elastic regime, which can be written as

$$f_0 = \frac{1}{2\pi R_0} \sqrt{\frac{1}{\rho_L} \left(3\kappa p_0 + \frac{2\sigma(R_0)}{R_0} (3\kappa - 1) + \frac{4\chi}{R_0} \right)}. \quad (4.25)$$

Recently smoother forms of Marmottant model have been proposed that involves a smoothing near the discontinuities [173, 188]. One such form is given below, following Prosperetti [173]

$$\sigma(X) = \chi [H(X - X_{\text{buckling}}) - H(X - X_{\text{rupture}}) + \sigma(R_0)H(X - X_{\text{rupture}})], \quad (4.26)$$

where $R = R_0(1 + X)$ and H is the Heaviside step function which can be smoothed by using a Peskin cosine function to avoid sharp transitions as shown below

$$H_\varepsilon(x) = \frac{1}{2} + \frac{(\varepsilon/\pi)\sin\pi x/\varepsilon}{2\varepsilon}. \quad (4.27)$$

With these definitions, the $\Sigma(X, \dot{X})$ equals $2\sigma(X)/R + 4\kappa^s \dot{R}/R^2$. If we assume that buckling radius and initial radius are the same, or in other words initial surface tension

is zero, we have a set of equations given below for various derivatives of Σ , which can be substituted in the various equations presented in Chapter 2

$$\Sigma_X = \frac{2\chi}{R_0}, \quad (4.28a)$$

$$\Sigma_{\dot{X}} = \frac{4\kappa^s}{R_0}, \quad (4.28b)$$

$$\Sigma_{X\dot{X}} = -\frac{8\kappa^s}{R_0} \quad (4.28c)$$

$$\Sigma_{XX} = \frac{4\chi}{R_0} \left[\frac{1}{\varepsilon} - \frac{1}{2} \right], \quad (4.28d)$$

$$\Sigma_{\dot{X}\dot{X}} = 0. \quad (4.28e)$$

We now have, for all the different interfacial models, the exact expressions for Σ , which when substituted to the generalized form given by Equation in Chapter 2 gives us the full form of the RP equations. These equations can now be solved numerically or analytically using a perturbation method. Since, the perturbation results were also given for the generalized equation in Chapter 2, we can use them directly by simply substituting the appropriate expressions relevant to model being investigated. The discussion for the mathematical formulations for interfacial rheological models for contrast agent encapsulations can now be concluded.

4.3 Prediction of Bubble Dynamics

We can solve 4.3 numerically, provided we know the values of the model parameters characterizing the rheology of the encapsulation material. We mentioned the different material characterization techniques in Chapter 2. Our research group have developed a two pronged approach to this problem by determining material properties from low amplitude attenuation measurements and then using these determined parameters in the numerical solution of 4.3. This strategy was implemented for both lipid and polymeric encapsulations and detailed results will be presented in the subsequent chapter. But before moving into more specific cases, some general behavior and

predictions of these models are presented here to provide the readers a general idea about the predictive capabilities of different interfacial rheological models.

4.3.1 Radial Dynamics

The bubble dynamics equation (4.3) is solved for an initial radius using the material parameters of the encapsulation to obtain the bubble radius as a function of time. We used representative values of parameter for a lipid coated bubble Sonazoid [169]. Figure 4.2 shows them for the constant elasticity (CEM), quadratic (QEM) and the exponential (EEM) elastic models for varied acoustic excitations (0.1, 0.5, 1.5, and 2.0 MPa) all at 3 MHz. Note that for the lowest level of excitation (0.1 MPa), all curves coincide — for weaker oscillations, the nonlinearity remains inactive. However at higher excitations, the curves for nonlinear viscoelastic models deviate from the constant elasticity one due to the strain softening included in the former models. QEM and EEM show very similar behavior for all the frequencies and excitation levels. The strain-softening included in the nonlinear models results in larger radial excursions — as the bubble expands, the surface resists expansion with an effectively smaller elasticity modulus. Previously, our group had reported that unlike the constant elasticity model, a Newtonian model (NM) for the encapsulation fares better in comparing with the measured subharmonic response [162]. To investigate this issue further, the radius vs. time curve according to the NM model is also included in Figure 3. It shows slight deviation relative to the elastic models at 0.1 MPa because of the fundamental difference between the Newtonian and the elastic models. At 0.5 MPa, the radial excursion is smaller than the nonlinear viscoelastic models, but at higher pressures (1.5 and 2.0 MPa), the Newtonian model matches better with the nonlinear models in their amplitude of oscillations. Similar results were obtained at other ($\neq 3$ MHz) frequencies (not shown here for brevity). The higher radial excursion for the NM model can explain its better performance in predicting the subharmonic response of a contrast microbubble compared to CEM.

Recently, de Jong and coworkers found that contrast microbubbles experience

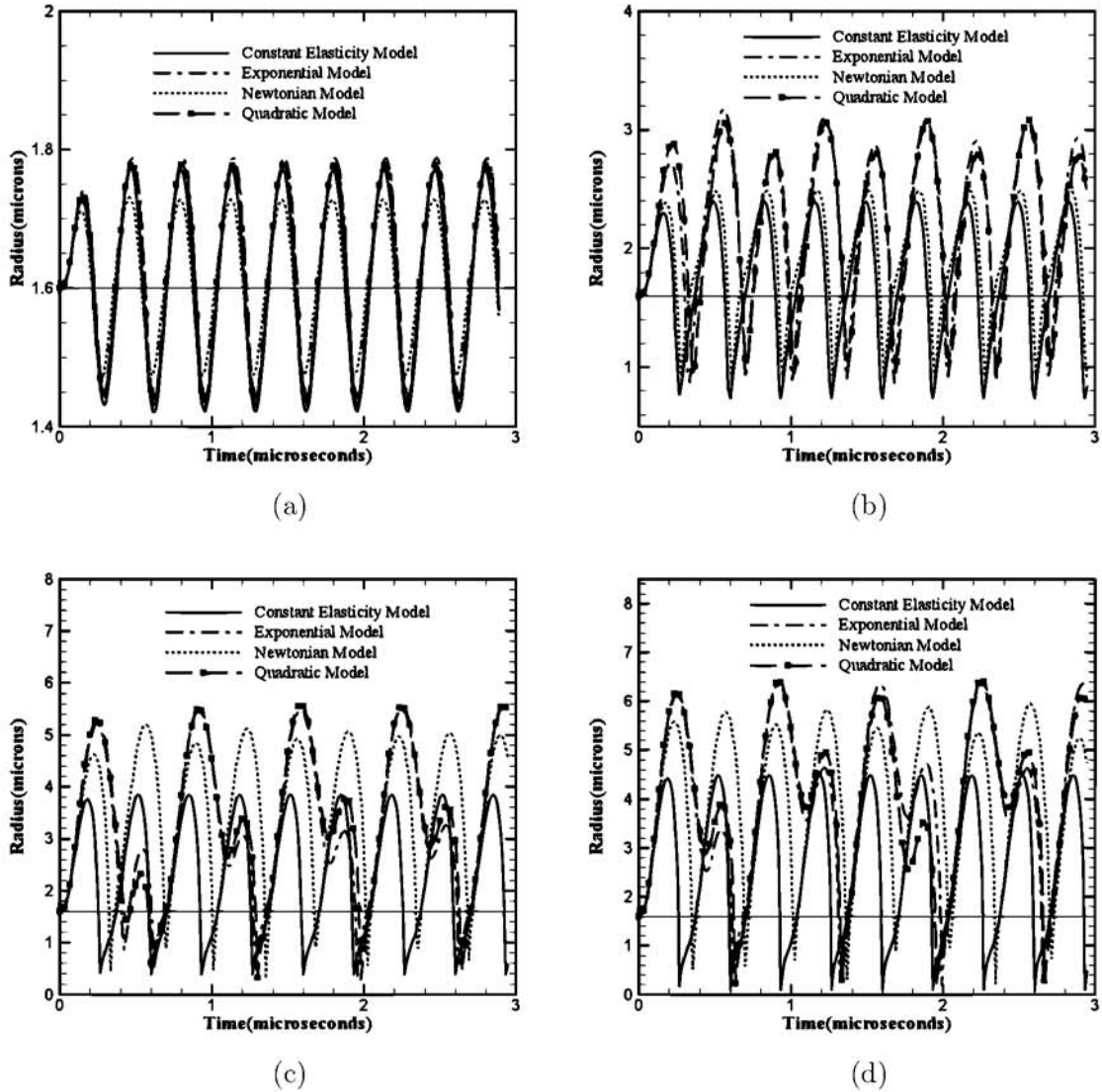


Figure 4.2: Radius-time curves for a $1.6 \mu\text{m}$ Sonazoid bubble as predicted by different encapsulation models at an excitation frequency of 3 MHz and different acoustic pressures of (a) 0.1 MPa, (b) 0.5 MPa, (c) 1.5 MPa, and (d) 2.0 MPa. Reprinted with permission from [169]. Copyright [2010], Acoustical Society of America.

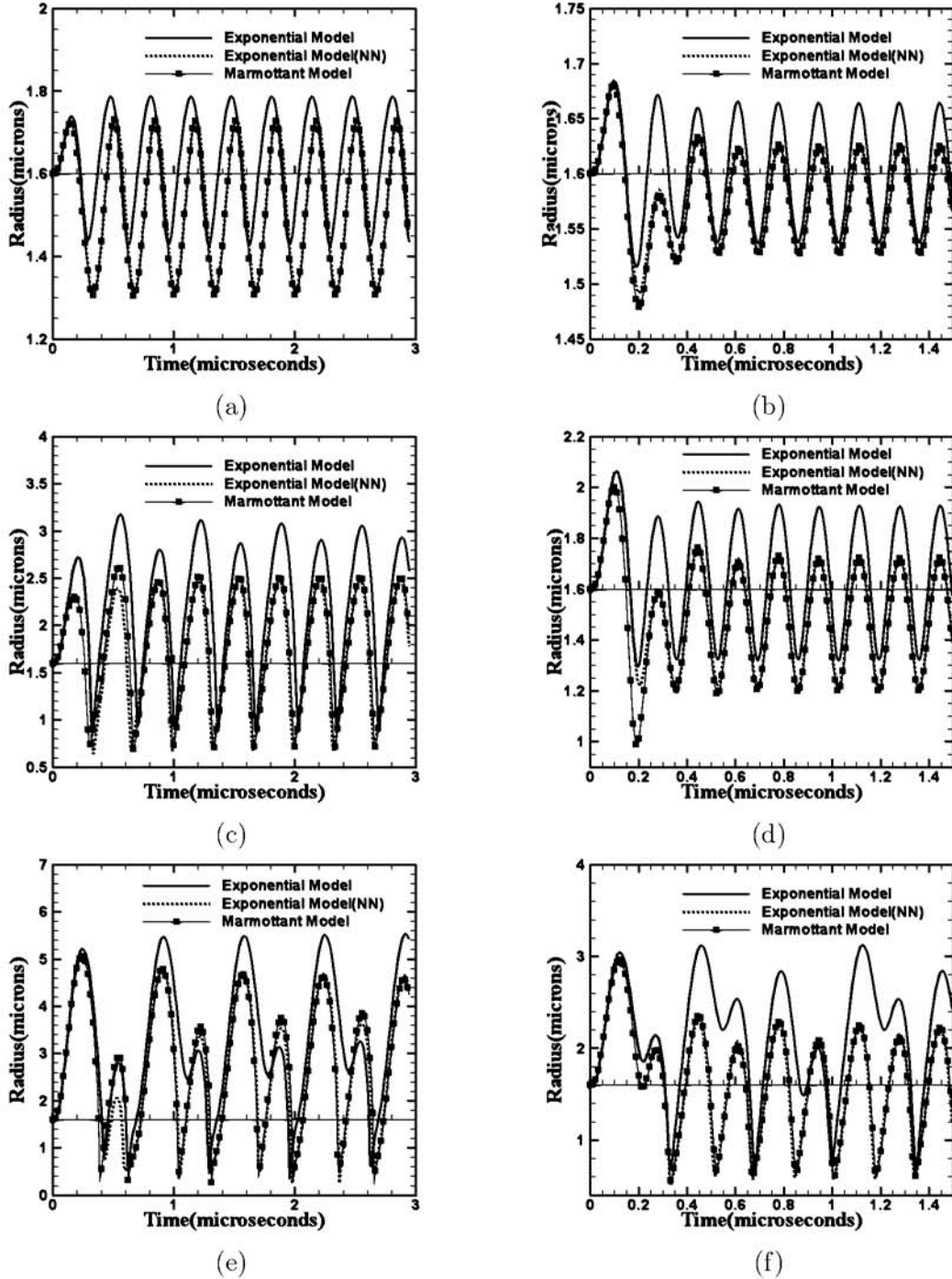


Figure 4.3: Radius-time curves for a $1.6 \mu\text{m}$ Sonazoid bubble as predicted by different encapsulation models at different excitation frequencies and pressures. (a) 3 MHz, 0.1 MPa, (b) 6 MHz, 0.1 MPa, (c) 3 MHz, 0.5 MPa, (d) 6 MHz, 0.5 MPa (e) 3 MHz, 1.5 MPa and (f) 6 MHz, 1.5 MPa. Reprinted with permission from [169]. Copyright [2010], Acoustical Society of America.

a “compression only” behavior for the phospholipid coated agents Sonovue and BR14 (Bracco, Geneva, Switzerland), in that the radial excursion away from the equilibrium radius is not symmetric, but the bubble compresses more than it expands [164, 224]. The compression only behavior is attributed to the buckled state of the encapsulation below R_{buckling} — where the authors assume the surface tension to be zero. As mentioned before, Marmottant et al. [164] assumed the same in their model. The rising surface tension hinders large distension when the bubble expands, but as the bubble compresses into a buckled state, the zero surface tension leads to an asymmetry in dynamics between the expansion and the compression phases. As noted before, in the viscoelastic models proposed here, one can choose to impose the nonnegativity on the surface tension. On the other hand, surface elasticity could be treated as an independent property, and in that case, the effective surface tension could become negative leading to a net compressive stress. In fact, unlike the case of a zero surface tension in the buckled state, such a net compressive stress can be thought of as a direct cause for buckling of the encapsulation. In Figure 4.3, the simulated radial dynamics using the exponential and Marmottant models (the quadratic model’s behavior is similar to the exponential model) are compared. We also include an exponential model, where nonnegativity (NN) has been imposed. Marmottant and the nonnegative exponential models predict very similar results unlike the other exponential model for all cases; they also favor compression only behavior more than the other one. Both at 3 and 6 MHz, one sees a compression only behavior for the Marmottant and the non-negative exponential models but not for the regular exponential model at the acoustic pressure of 0.1 MPa. At 0.5 MPa, compression only behavior is again shown by these two models for 6 MHz but not for 3 MHz. The radial excursion at 3 MHz even for these two models is almost symmetric. At 1.5 MPa excitation, for 3 MHz all curves show larger expansion than compression, and for 6 MHz, the Marmottant and exponential(NN) models predict that bubbles compress marginally more than they expand. According to De Jong et al. [224], compression only behavior is defined as when the maximum expansion to maximum compression is less than 50%. Figure 4.3e shows that the Marmottant model

predicts 85% for this ratio at 3 MHz and 1.5 MPa. Note that the experiments by de Jong and co-workers showing compression only behaviors for Sonovue and BR14 were performed at lower acoustic pressures < 0.25 MPa.

4.3.2 Subharmonic Generation Thresholds

A general expression of subharmonic threshold was as derived by Prosperetti [173] was given in Equation 2.47 of Chapter 2. We can now utilize that expression to comment about the capability of each of the interfacial models to predict subharmonic generation thresholds. For these studies we choose two different sets of parameters — a 3 μm Sonazoid bubbles ($E^s \text{or} \chi = 0.5, \kappa^s = 1.0 \times 10^{-8}$) and a 3 μm polylactide polymer encapsulated bubbles ($E^s \text{or} \chi = 0.02, \kappa^s = 1.0 \times 10^{-9}$). The results are shown in Figure 4.4. We observe that for lipid coated Sonazoid bubbles the interfacial model with nonlinear elasticity term (EEM) clearly performs better. The Newtonian model also predicts lower threshold consistent with previously published results [See Figure 4.4a]. The analytical prediction of subharmonic threshold due to the Marmottant model are extremely small [See Figure 4.4b]. Note that it can be made as small as desired by lowering the smoothing parameter (ε). For polymer encapsulated bubbles with a lower elasticity and dilatational viscosity values, all the interfacial models predicts similar threshold values, with the exception of MM with a smaller smoothing parameter [See Figure 4.4c].

Due to its inherent discontinuity, the MM can predict almost any desired threshold value by a proper choice of smoothing parameter (ε). Experimental results with several contrast agents have indicated that the subharmonic generation thresholds can be lower than that of similar sized uncoated bubbles [268–271]. The MM has been successful in predicting such low subharmonic thresholds [188, 269] for the reasons mentioned above. Although, the analytical results provide a good qualitative match with numerical threshold predictions, one must be careful in directly comparing them to the threshold predictions from numerical solutions. The apparent contradictions can be attributed to several factors such as the polydispersity of the bubble suspension

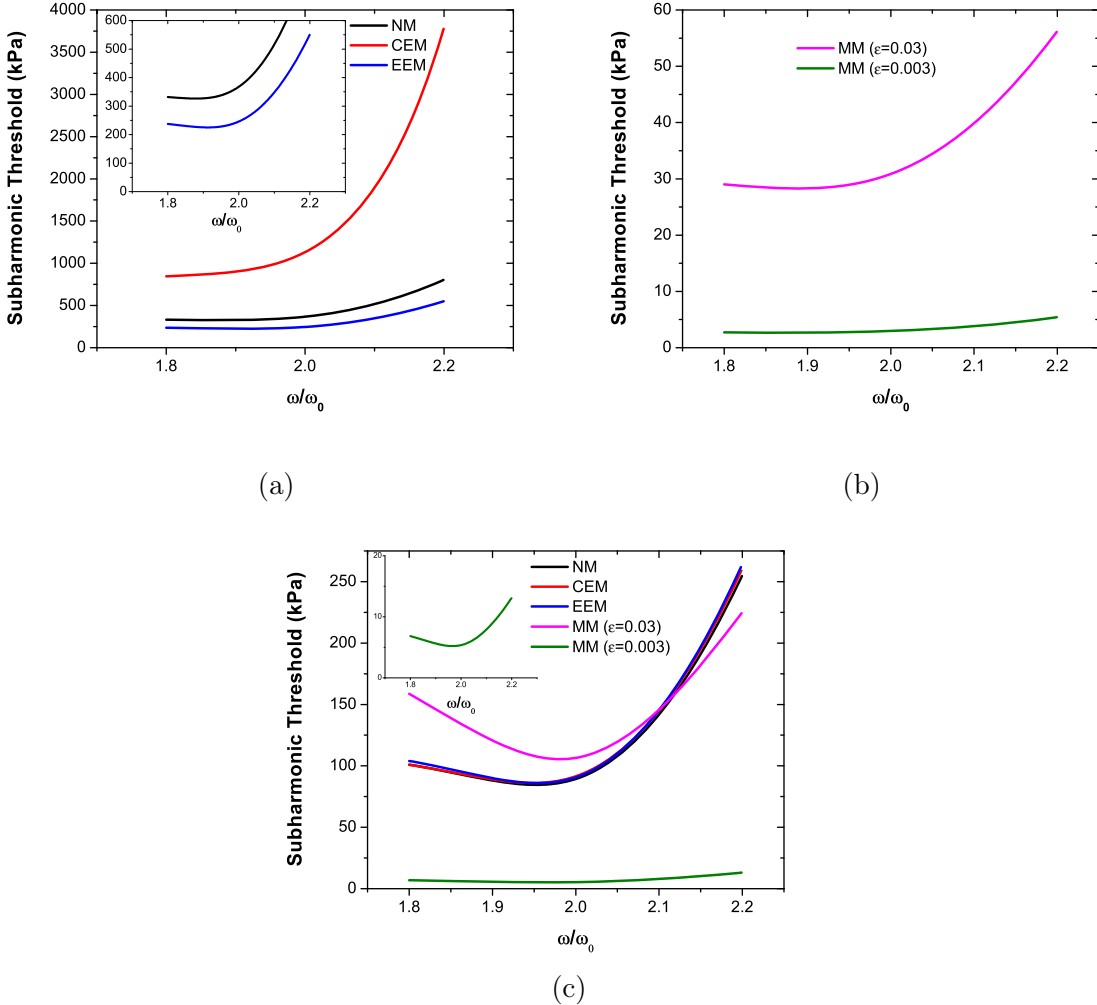


Figure 4.4: Analytical prediction of subharmonic threshold for (a) 3 μm Sonazoid bubble using NM, CEM, EEM [Inset show the magnified view for lower pressures]. (b) 3 μm Sonazoid bubble using MM. (d) 3 μm polyalactide encapsulated bubble using NM, CEM, EEM, MM [Inset show the magnified view for lower pressures].

considered in numerical solutions, the validity of analytical expression only in the vicinity of $2f_0$, the difficulty to distinguish threshold for existence of subharmonic from the necessary condition for presence of subharmonics (or absolute threshold) in numerical simulations, and the occurrence of two thresholds observed in numerical simulations using the MM under certain conditions [See Figure 4.5]. More detailed characterization of the subharmonic behavior of lipid coated and polymer encapsulated microbubbles will be presented in the following chapter.

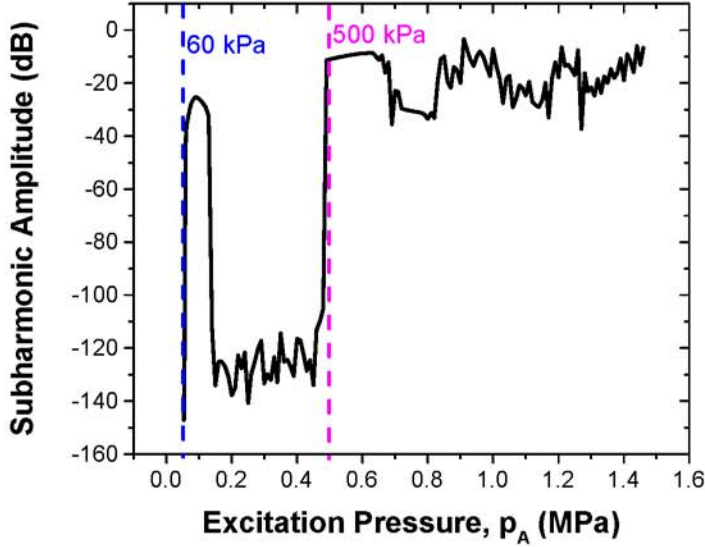


Figure 4.5: Prediction of two subharmonic generation threshold (numerically) using the Marmottant model.

4.4 Summary and Conclusions

This chapter provides the detailed mathematical formulation of the interfacial models of contrast agent encapsulation. Motivated by the previous findings by our research group and strain-softening nonlinear elasticity models were proposed for accurate prediction of encapsulated bubble dynamics. The encapsulation was treated as a complex interface characterized by constitutive parameters such as surface tension (γ_0), dilatational viscosity (κ^s), dilatational elasticity (E_0^s) and new nonlinearity parameters — E_1^s for the QEM model, where the elasticity decreased linearly with area fraction, and α^s for the EEM model, where the elasticity varied exponentially. Both nonlinear models represent the strain softening resulting from the decreased association between constituent molecules in the encapsulation as its area increases. The models are compared with a popular nonlinear elasticity interfacial model proposed by Marmottant et al. [164].

The effects of imposing a constraint of nonnegative effective surface tension (comprising of the reference surface tension and the interfacial elasticity effects) on the

radial dynamics were investigated. The constraint resulted in a behavior very similar to the Marmottant model, because both models prescribe zero surface tension below certain bubble radii. Both (nonnegative exponential and Marmottant) models show ‘compression-only’ behavior at lower acoustic pressures, as reported for certain contrast microbubbles. We have recently shown that effectively non-negative surface tension leads to only neutral stability for an encapsulated contrast bubble against dissolution — as a bubble reaches the compressed state where the surface tension is zero, the bubble does not have any stabilizing force against further shrinking [14, 15, 196]. It therefore can dissolve away by fluctuation.

The subharmonic generation thresholds obtained from small amplitude perturbation analysis was also compared for the various models. The results indicate the superiority of nonlinear elasticity models for prediction of low subharmonic generation thresholds. The Marmottant model in particular can predict almost any desired threshold by a proper choice of the smoothing parameter (ε). However, the numerical predictions from Marmottant model can show the existence of two subharmonic thresholds, which contradict the analytical results. In the subsequent chapters these models will be utilized for the material characterization of lipid coated and polymer encapsulated microbubbles and subsequent comparison of nonlinear dynamics as predicted by the models with those observed in *in vitro* experiments.

Chapter 5

CHARACTERIZATION OF LIPID COATED MICROBUBBLES¹

5.1 Introduction

In Chapter 2, we mentioned the various materials that are used for making the stabilizing layer for ultrasound contrast microbubbles. Lipids or phospholipids are attractive choice for such coatings primarily due to their biodegradability and ease of preparation. Several commercial and experimental microbubbles have lipid encapsulations [See Table 2.1]. We study here two such contrast agents, Sonazoid™ and Definity®. While Sonazoid is not approved for clinical use in the US, the understanding of lipid coated microbubble dynamics was significantly improved during its development in early phases. Definity is still being actively studied for a diverse range of diagnostic imaging and therapeutic applications.

We introduced four different interfacial models for contrast microbubble encapsulation developed by our group and another popular model due to Marmottant and co-worker in Chapter 4. The exact expressions for rheological terms were derived and some of their predictive capabilities and features were also discussed. Here we apply those models to predict experimental observations for both Sonazoid and Definity. Our analysis will be based on the two tier approach mentioned earlier which has the following steps:

- Model parameters are determined by matching predictions of the linearized dynamics of bubble suspensions with low amplitude attenuation experiments
- These model parameters are then substituted in the full nonlinear form of the RP equation for encapsulated microbubbles and solved numerically.

¹ Figures and text in this chapter have been adapted from a published [110] and an article under review [7].

- The model predictions are directly compared with a different set of experimental data for nonlinear scattered response form these bubbles to judge the performance and predictive capabilities of the models and provide suggestions for model improvements and modifications.

5.2 Experimental Methods

Using the method described above, we will determine material properties of the encapsulation, which will be used to predict the acoustic behavior of these contrast agents. For these lipid coated microbubbles, we acquired both attenuation and scattering data either from other published works or through in house experiments. Since, the preparation protocol both these lipid coated bubbles are proprietary, a detailed description of the steps involved cannot be provided here.

The initial development of interfacial models utilized the experimental data for Sonazoid from our collaborators at Thomas Jefferson University, headed by Prof. Flemming Forsberg. Details of the experimental methods utilized can be found in a previously published paper [163]. The attenuation and size distribution data for Definity bubbles were kindly provided by Prof. David Goertz at University of Toronto and his doctoral student Brandon Helfield. The details of the experimental methods involved and the size distribution data can be found in their previous publication [272]. Size measurements and concentration evaluation was done using a Coulter Counter sizer described in Section 3.1.2. The models were validated against two separate sets of experimental data for Definity. One set acquired in our lab and the other was obtained from a previous publication by Cheung et al. [273].

The scattering experiments performed in our lab used the larger volume setup described in Section 3.3.4. A 10 MHz focused transducer was used to excite the bubbles, whereas a 5 MHz focused transducer was used as the receiver. The excitation pressure was varied from 50 kPa to 800 kPa. We had also performed attenuation measurements on our Definity samples using the larger volume setup described in Section 3.3.3. However, we could not use that data for our parameter estimation as we did not have exact concentration and size distribution information for our vials. A 5 MHz

unfocused transducer was used in the attenuation experiments, which were performed at an acoustic excitation pressure of 50 kPa. Definity microbubbles comes in a vial which was reconstituted following the established protocol using Vialmix shaker for 45s [See [195] for more details]. For both type of experiments, a 1:10000 dilution of the microbubble solution was used. 10 μ l of microbubble solution was drawn from the vial, using a microliter syringe, one minute after activation in the shaker and dissolved in 100 ml of PBS buffer.

5.3 Material Characterization of the Encapsulation Using Attenuation

5.3.1 Method

The attenuation of ultrasound measured through a diluted suspension of microbubbles was reported for Sonazoid and Definity, which are used to determine the characteristic parameters pertaining to each model. The experiment was performed at low excitation level (as the classical linear theory of attenuation being invalid at higher excitations). Therefore, one can linearize the nonlinear bubble dynamics equation to obtain a harmonic oscillator equation for periodic excitation which was discussed in details in Section 2.4.3 of Chapter 2. The linearization gives the resonance frequency(ω_0) for each models which are given by Equations 4.8b, 4.13b, 4.18b, 4.23b and 4.25 for NM, CEM, QEM, EEM and MM respectively. The expression for total damping factor ($2b$) is given by 2.21c. The acoustic extinction cross-section can be calculated by using both ω_0 and $2b$ in Equation 2.27. Using this expression of the acoustic extinction cross-section along with the size distribution of the bubbles in the suspension, the total attenuation coefficient can be also be calculated (by neglecting multiple scattering effects) and is given by Equation 2.55. Thus, we can obtain a theoretical expression giving the measure of attenuation coefficient through a suspension of contrast microbubbles, which is dependent on the size distribution and the model parameters corresponding to the chosen rheological model. Size distribution can easily be measured experimentally, which makes this expression only a function of undetermined model parameters which we denote as $\alpha_{\text{calculated}}(\omega_i)$. The experimental data gives us the actual measure

of this quantity which we denote as $\alpha_{\text{measured}}(\omega_i)$. The unknown parameters can now be determined by using a curve fitting algorithm implemented using a Matlab code [SEE Appendix D] by minimizing the following error function

$$Er(\sigma, \kappa^s, E^s, \dots) = \sum_i [\alpha_{\text{calculated}}(\omega_i) - \alpha_{\text{measured}}(\omega_i)]^2. \quad (5.1)$$

If the size distribution is narrow, which is the case for most commercial microbubbles [156, 274] one can just use an average size and the total number of microbubbles in the suspension. We will present our fitting results both with and without the considering the entire distribution and discuss their implications. The values of the other properties used in the fitting were: $\rho_L = 1000 \text{ kg/m}^3$, $\mu = 0.001 \text{ Ns/m}^2$ and $c = 1485 \text{ m/s}$. One outstanding issue is determining the actual value thermal damping. We know that it will identically zero for adiabatic or isothermal oscillations, which can be determined by calculating the Peclet number as discussed earlier. The calculations are given below.

Sonazoid has a relatively narrow size distribution with an average mean diameter of $3.2 \pm 0.2 \mu\text{m}$ with a number concentration of $0.78 \pm 0.38 \times 10^9 / \text{ml}$ [274]. The experiments considered here were conducted at a concentration of $8.1 \times 10^4 \text{ bubbles/ml}$. Sonazoid contains perfluorobutane (C_4F_{10}) gas which has a thermal diffusivity of $2 \times 10^{-6} \text{ m}^2/\text{s}$ [176]. So even at 1 MHz frequencies the Peclet number with the average size is 8 which is much larger than 1 and will increase as the excitation frequency increases. Hence, oscillations can be assumed adiabatic setting the thermal damping term to be identically zero. The adiabatic gas constant for C_4F_{10} is 1.07 [176], which is used in our calculations.

Definity, on the other hand also has a fairly narrow distribution with an average mean diameter of $2.5 \mu\text{m}$ [49, 275] and contains octafluoropropane ($\text{n-C}_8\text{F}_8$) gas inside. The thermal diffusivity of can be calculated to be $1.6 \times 10^{-6} \text{ m}^2/\text{s}$. Hence, at 1 MHz the Peclet number considering the average size is 6 which is also larger than 1. Hence, we can neglect thermal damping and use the gas constant to be the adiabatic value of

C_8F_8 , which is 1.06. [207]

5.3.2 Results and Discussion

Using the error minimization 5.1, we find the properties for different models and report them in Table 5.1. For comparison, we use the same attenuation data to find properties for the model due to Marmottant et al. [164]. The Marmottant Model requires the values of the buckling radius and the break-up radius. These are hard to determine. Following the original reference [164], we take the buckling radius to be equal to the initial radius i.e., zero initial surface tension. The break-up and rupture radii are not explicitly included in the parameter estimation step. Hence, the rupture radius is calculated as $R_{\text{rupture}} = R_0 \left[1 + \frac{\sigma_{\text{water}}}{\chi} \right]^{-1/2}$ and the break-up radius is assumed to be $1.5R_0$.

5.3.2.1 Sonazoid Microbubbles

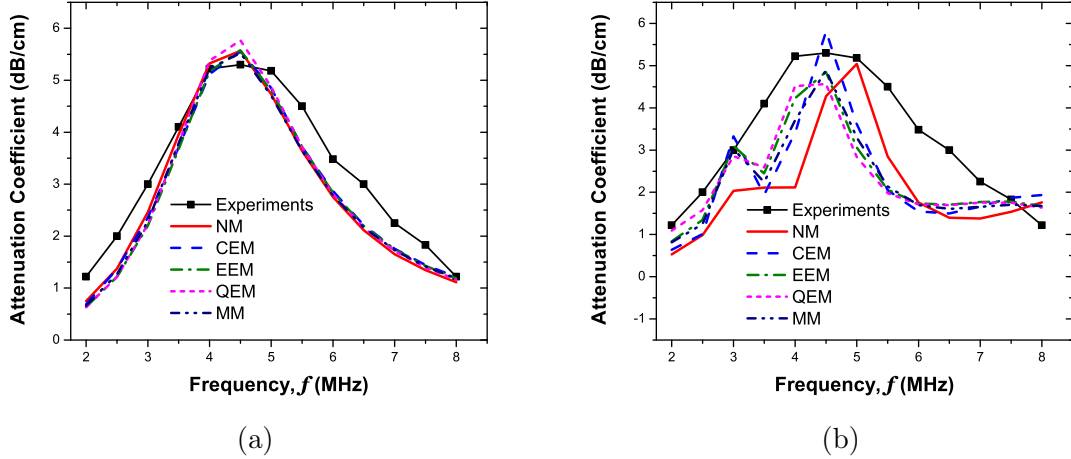


Figure 5.1: Measured and fitted attenuation to determine model parameters for Sonazoid microbubbles using different interfacial models with (a) a mean average size, and (b) the entire size distribution. Concentration was 8.1×10^4 bubbles/ml. Reprinted with permission from [169]. Copyright [2010], Acoustical Society of America.

For Sonazoid microbubbles, parameter estimation using an actual size distribution or using the average radius value lead to the same parameter values (i.e. within the range of experimental scatter). However, using an average radius value, one can

achieve attenuation values from model fairly close to the measured data (Figure 5.1a), while using the actual radius distribution results in a simulated attenuation qualitatively similar to the measured data, but the details remain different (Figure 5.1b). One can understand it by assessing the strict constraints of modeling with a complete distribution — bubbles of different radii lead to different dynamics. This also indicates the sensitivity of the radius distribution in finding the property values. Indeed, if one uses a radius distribution that is 10 times less or more than the measured one, the estimation procedure fails — the model cannot give rise to a low error, i.e. close to measured attenuation for any set of property values. This exercise gives stronger credence to the property determination procedure adopted here. Similar complexities have been reported for parameter estimation using attenuation data for other contrast agents as well [257].

Table 5.1 shows that the value of shell compressibility $\chi=0.53 \text{ N/m}$ obtained for the Marmottant model, in the linear elastic regime ($R_{\text{buckling}}, R_{\text{break-up}}$), is the same as the surface dilatational elasticity values for the elastic models as expected from the fact that they are almost equivalent for small amplitude oscillations. For the QEM and the EEM, one can also note the consistency condition ($E_1^s = \alpha^s E_0^s$) being satisfied by the values listed in Table 5.1. Guan and Matula [220] used light scattering measurements to capture bubble dynamics of Sonazoid microbubbles and showed a very good fit of experimental data with $\kappa^s = 0.6 \times 10^{-9} \text{ kg/s}$, which is close to our estimates. Also, the value of the surface dilatational viscosity for the Marmottant model is of the same order as that of the other models. Note that the parameters obtained for Marmottant model by de Jong and coworkers are of the similar order — van der Meer et al. [176] found $\chi = 0.54 \pm 0.1 \text{ N/m}$ and $\kappa^s = 2.3 \times 10^{-8} \text{ kg/s}$, Marmottant et al. [164] found $\chi = 1.0 \text{ N/m}$ and $\kappa^s = 1.5 \times 10^{-8} \text{ kg/s}$, and Gorce et al. [250] found $\chi = 0.55 \text{ N/m}$ and $\kappa^s = 0.78 \times 10^{-8} \text{ kg/s}$ all for SonovueTM contrast microbubbles.

Table 5.1: Estimated interfacial rheological properties of the encapsulation of Sonzaoid and Definity microbubbles for different interfacial models.

Interfacial Model	Estimated Parameters	
	Sonazoid	Definity
NM	$\sigma = 0.6 \pm 0.14 \text{ N/m}$ $\kappa^s = 1.2 \pm 0.4 \times 10^{-8} \text{ Ns/m}$	$\sigma = 0.9 \pm 0.1 \text{ N/m}$ $\kappa^s = 2.0 \pm 0.5 \times 10^{-8} \text{ Ns/m}$
CEM	$\sigma_0 = 0.02 \text{ N/m}$ $E^s = 0.51 \pm 0.11 \text{ N/m}$ $\kappa^s = 1.2 \pm 0.4 \times 10^{-8} \text{ Ns/m}$	$\sigma_0 = 0.01 \pm 0.01 \text{ N/m}$ $E^s = 1.04 \pm 0.05 \text{ N/m}$ $\kappa^s = 2.6 \pm 0.5 \times 10^{-9} \text{ Ns/m}$
QEM	$\sigma_0 = 0.02 \text{ N/m}$ $E^s = 0.53 \pm 0.1 \text{ N/m}$ $E_1^s = 0.75 \pm 0.015 \text{ N/m}$ $\kappa^s = 1.2 \pm 0.4 \times 10^{-8} \text{ Ns/m}$	$\sigma_0 = 0.02 \pm 0.01 \text{ N/m}$ $E^s = 0.70 \pm 0.2 \text{ N/m}$ $E_1^s = 14 \pm 3.5 \text{ N/m}$ $\kappa^s = 2.6 \pm 0.5 \times 10^{-9} \text{ Ns/m}$
EEM	$\sigma_0 = 0.02 \text{ N/m}$ $E^s = 0.55 \pm 0.1 \text{ N/m}$ $\alpha = 1.5 \pm 0.05$ $\kappa^s = 1.2 \pm 0.4 \times 10^{-8} \text{ Ns/m}$	$\sigma_0 = 0.01 \pm 0.01 \text{ N/m}$ $E^s = 0.70 \pm 0.2 \text{ N/m}$ $\alpha = 20 \pm 5$ $\kappa^s = 2.6 \pm 0.5 \times 10^{-9} \text{ Ns/m}$
MM	$\chi = 0.55 \pm 0.1 \text{ N/m}$ $\kappa^s = 1.2 \pm 0.4 \times 10^{-8} \text{ Ns/m}$ $R_{\text{buckling}} = R_0$ $R_{\text{break-up}} = 1.5R_0$	$\chi = 1.05 \pm 0.05 \text{ N/m}$ $\kappa^s = 2.6 \pm 0.5 \times 10^{-9} \text{ Ns/m}$ $R_{\text{buckling}} = R_0$ $R_{\text{break-up}} = R_{\text{rupture}}$

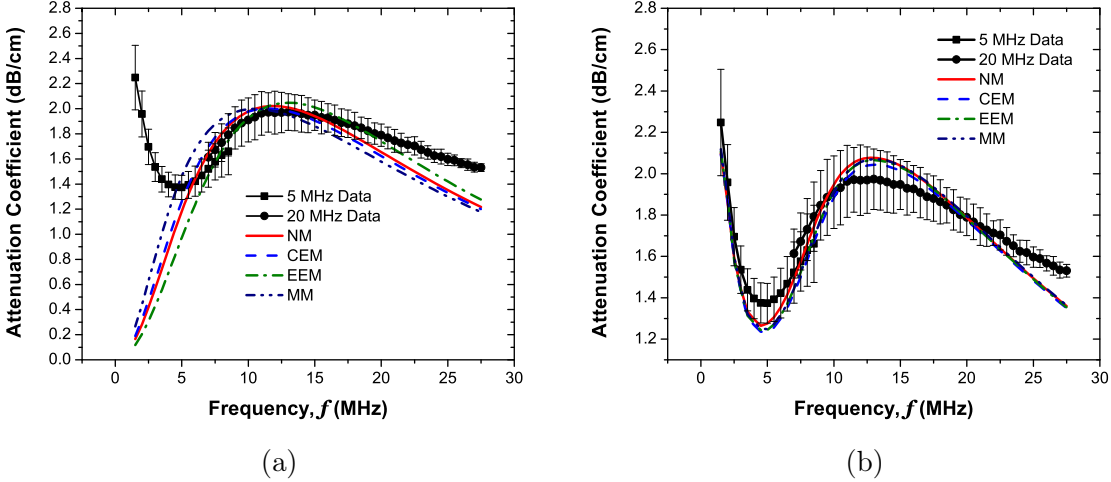


Figure 5.2: Measured and fitted attenuation to determine interfacial model parameters for Definity microbubbles using different interfacial models with (a) a mean average size, and (b) the entire size distribution. Concentration was 7.5×10^5 bubbles/ml.

5.3.2.2 Definity Microbubbles

For Definity microbubble the same estimation technique was employed both with and without considering the entire distribution. The experimentally obtained size distribution for a pre-activation temperature of 22°C had mean number weighted average diameter of 1.17 μm with a concentration of 7.5×10^4 bubbles/ml. We obtained good fit of data both with an average size (Figure 5.2a) and the entire distribution (Figure 5.2b). However, unlike Sonazoid the predicted properties were different indicating the need to use the entire distribution. This is also evident from Figure 5.2a, where the fitting with an average size is unsatisfactory for frequencies less than 5 MHz. Hence, only the property values predicted by considering the entire distribution are reported in Table 5.1.

Table 5.1 also shows the estimated parameters for Definity microbubbles. The elasticity values predicted for our models are close to the shell compressibility (χ) value predicted for the Marmottant model, as was reported for Sonazoid above. The surface dilatational viscosity predicted with different models are also similar. Since, the consistency condition ($E_1^s = \alpha^s E_0^s$) was also satisfied in this case, the QEM model was excluded from the fitting curves and the reported values. Unlike Sonazoid, several

reports of the shell parameter estimates exist for Definity microbubbles. Goertz et al. [207] reported $\chi = 0.85 \pm 0.12$ N/m and $\kappa^s = 0.3 \pm 0.3 \times 10^{-9}$ kg/s for frequency range 12-28 MHz with a 15 second decantation period. They also found that after filtering bubbles above 2 microns in diameter, both the shell compressibility and dilatational viscosity are almost the same ($\chi = 0.75 \pm 0.18$ N/m and $\kappa^s = 0.3 \pm 0.3 \times 10^{-9}$ kg/s). Faez et al. [276] reported that in 7-15 MHz range $\chi = 0.82 \pm 0.16$ N/m and $\kappa^s = 3.0 \pm 0.03 \times 10^{-9}$ kg/s. However, for higher frequencies, 15-25 MHz, $\chi = 1.02 \pm 0.33$ N/m and $\kappa^s = 0.2 \pm 0.2 \times 10^{-9}$ kg/s was reported, indicating an order of magnitude drop in viscosity. Santin et al. [277] reported $\chi = 0.38$ N/m and $\kappa^s = 2.4 \times 10^{-9}$ kg/s for Definity microbubbles. All these estimates are fairly close to our predictions given in Table 5.1, considering we obtained a very good match in the entire frequency range of 1-20 MHz.

Faez et al. [208] had earlier measured attenuation due to “expired” Definity microbubbles — bubbles were used after the expiry date printed on the vials. They showed that the attenuation spectra of “fresh” and “expired” bubbles can be distinctly different [See Figure 5.3b], primarily due to differences in size distributions [See Figure 5.3a]. Note that the peak in the attenuation curve shifts to lower frequencies for the expired bubbles. The Definity vials used in our experiments had also “expired”, and our own attenuation measurements shown in Figure 5.4 is consistent with their measurements. Faez et al. [208] utilized the same fitting strategy used by us to report the following values for expired Definity bubbles: $\chi = 0.79 \pm 0.08$ N/m and $\kappa^s = 8.5 \pm 0.02 \times 10^{-9}$ kg/s. Their estimates indicated negligible changes to shell elasticity but an increase in dilatational viscosity. Hence, we used their size distribution measurements to match our scattering measurements for two different viscosities — one predicted for fresh bubbles (as obtained by us) and one predicted for expired vials (as predicted by Faez et. al.).

Based on the above mentioned findings, we can conclude that our estimation technique gives us fairly reliable and accurate estimation of model parameters characterizing the encapsulation for both Sonazoid and Definity, which will be used for

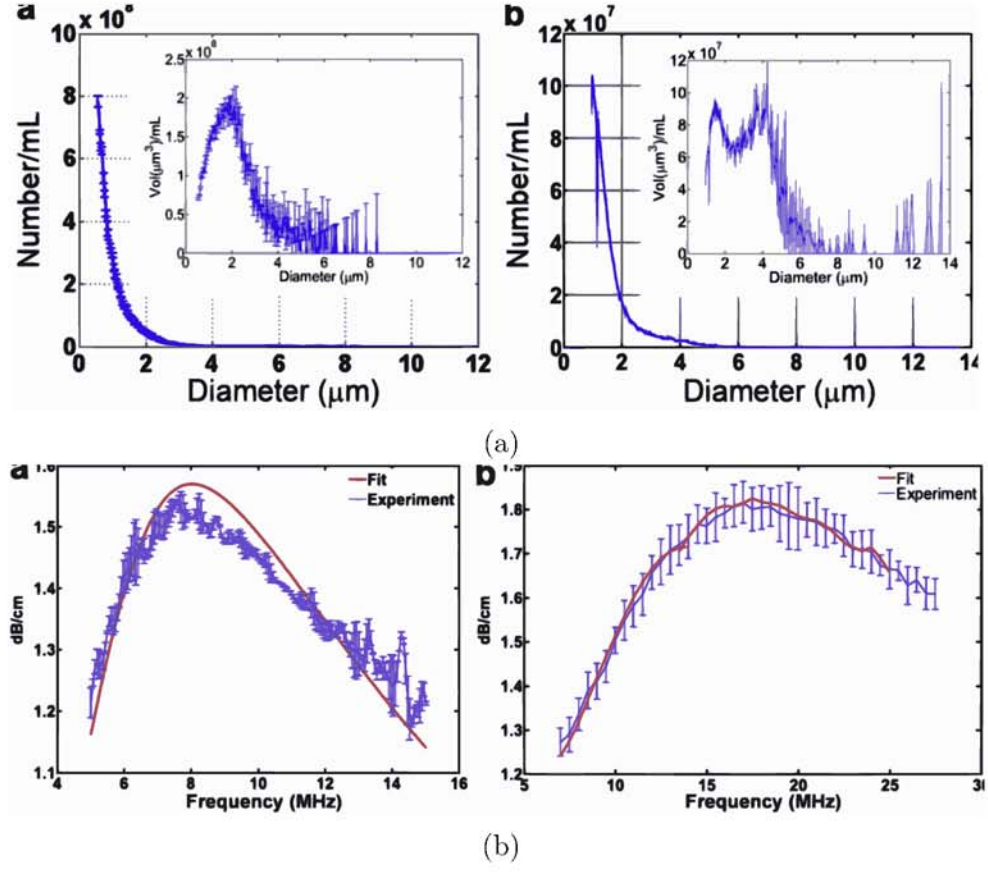


Figure 5.3: (a) Coulter counter size distribution measurement for Definity in number/ml (inset: vol/ml) for “expired” (left) and “fresh” (right) bubbles. (b) Attenuation measurements as a function of frequency for Definity and the fit made for shell properties estimation on “expired” (left) and “fresh” (right) bubbles. Reproduced [208] with permission from Elsevier.

further validation by matching with experimentally measured scattered responses.

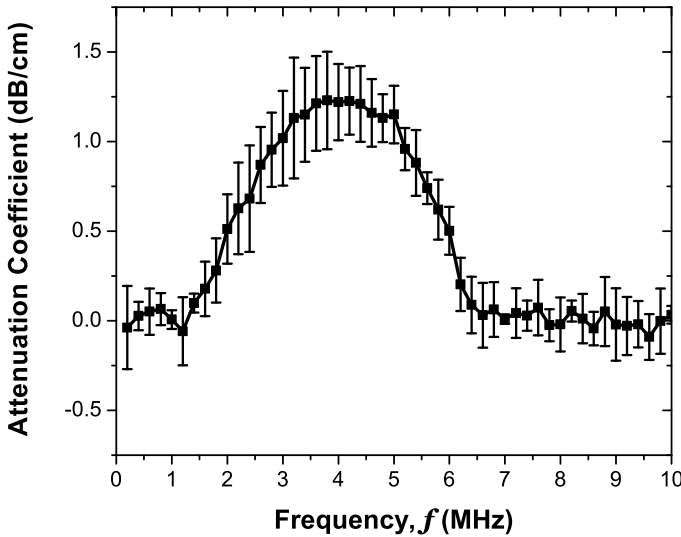


Figure 5.4: Experimentally measured frequency dependent attenuation coefficient for Definity microbubbles measured in our lab. Dilution was 1:10000.

5.4 Prediction of Scattered Fundamental and Subharmonic Response

5.4.1 Method

The full RP equation 4.3 was solved by substituting the model parameters estimated above. A stiff solver (`ode15s`) provided with Matlab[®] package was used to solve the differential equation for each model. A constant amplitude sinusoidal pulse with 64 cycles was used as the excitation pulse ($p_A(t)$) to simulate experimental conditions. The solution for the time dependent radius, obtained for each bubble size in the distribution, was used to calculate the far-field scattered pressure using Equation 2.48, which was subsequently converted to the scattering cross-section of the bubble using Equation 2.50. This cross-section was then converted to the frequency domain by Fourier Transformation using a Fast Fourier Transfer Algorithm implemented in Matlab. The total contribution due to all the bubbles in the suspension was calculated using Equation 2.59, neglecting multiple scattering effects. This assumption is valid as the concentration for the scattering measurements were below 10^5 bubbles/ml. The final result was converted to dB scale with unit reference and the fundamental and

subharmonic components were extracted for comparison with the experimental data. The fundamental response was matched with the experimental data at the lowest excitation pressure to obtain a matching constant. This matching enables us to compare our simulations with the experimental data even without the knowledge of the exact location of the far-field receiver — in logarithmic scale it shifts the response by a constant number. This matching constant was subsequently used to rescale the predicted scattered response for the entire range of excitation pressures. The relevant Matlab codes are provided in Appendix D. The simulations results and the predictive ability of the interfacial models to are discussed below.

5.4.2 Results and Discussion

5.4.2.1 Sonazoid Microbubbles

The fundamental and subharmonic scattered responses from Sonazoid bubbles were measured and reported for four different frequencies — 2, 3, 4.4 and 6 MHz [163]. The scattered fundamental response showed increase with increasing pressure. The subharmonic signal component on the other hand was negligible until a threshold excitation, and then a rapid growth occurred followed by saturation. Plotting the subharmonic data against Mechanical Index [$\text{MI} = P_A/f^{1/2}$, where P_A is the acoustic pressure amplitude measured in MPa and f is the frequency (MHz)] showed an approximate collapse of the data for different frequencies in that paper[163].

Figure 5.5 shows that the fundamental response is modeled very well by all models as was also the case previously. Since, the predictions of the Newtonian model for Sonazoid were reported previously [163], we exclude it in our present study. The prediction of the CEM are given to illustrate the superiority of the strain-softening and non-linear elasticity models. We have also plotted the response from the linearized system for the EEM model, which matches very well the full nonlinear dynamics, except for the 2 MHz excitation Figure 5.5a. This indicates the performance of the models should be judged by their ability to predict the scattered nonlinear response. The

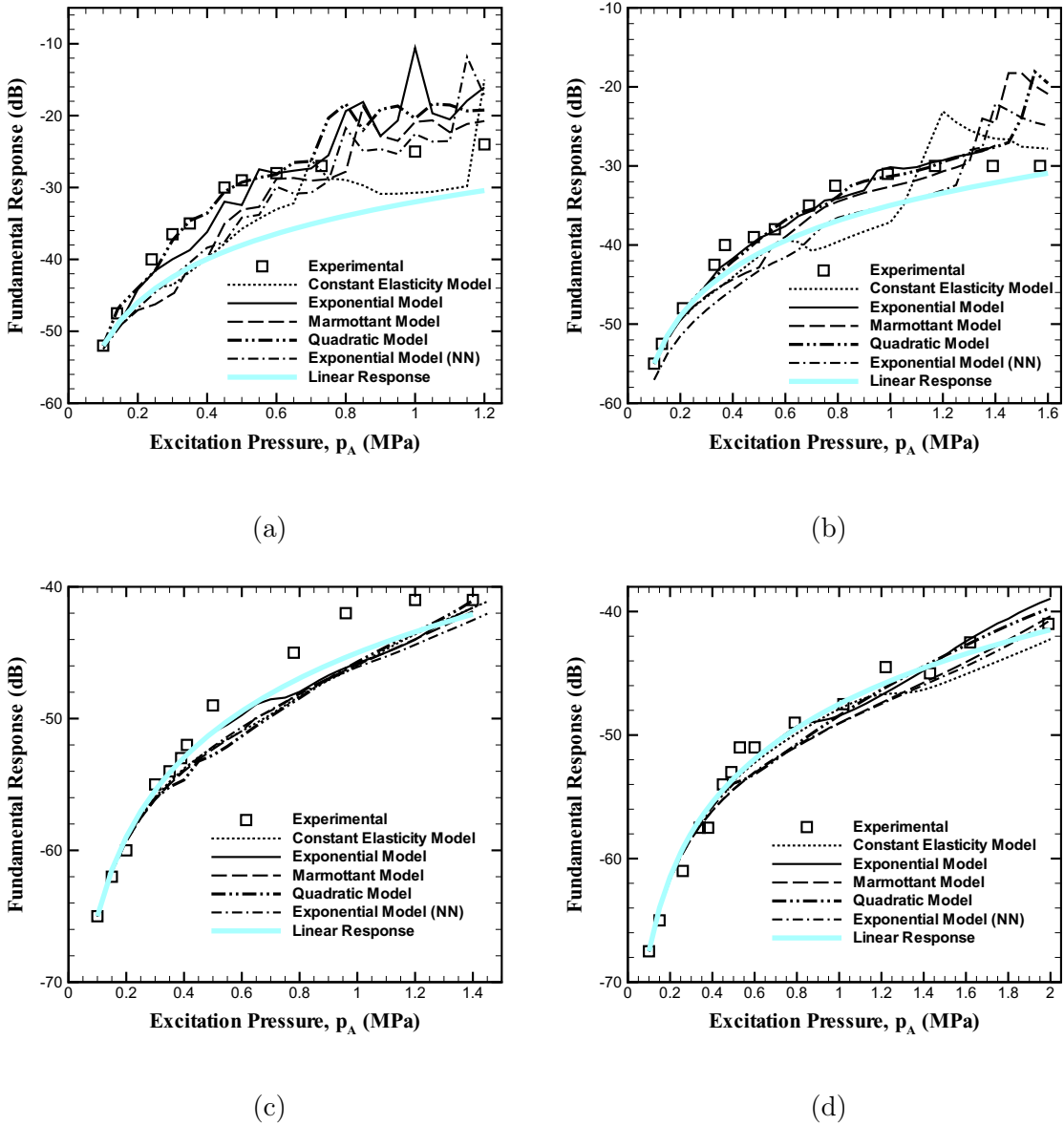


Figure 5.5: Measured and predicted fundamental response of Sonazoid bubbles at various excitation frequencies: (a) 2 MHz, (b) 3 MHz (c), 4.4 MHz, and (d) 6 MHz. Reprinted with permission from [169]. Copyright [2010], Acoustical Society of America.

response due the EEM with non-negativity condition imposed is also shown (denoted by NN).

In Figure 5.6, the subharmonic response from Sonazoid and the predictions from different models are plotted. As noted before, subharmonic response unlike the fundamental remains negligible till a threshold pressure is exceeded. Each of the models similarly generates no subharmonic response until a threshold excitation. At 2 MHz, all models except the constant elasticity perform well. As was shown before [163], the constant elasticity model (CEM) does not predict the subharmonic response well for any frequency. It fails to predict a sharp threshold except at 3 MHz, where it predicts a value twice that found in the experiment. The failure of CEM was thought to result from the model's inability to correctly describe the constitutive behavior of the encapsulation for stronger oscillation. As is evident from the plots, other models show a threshold value for subharmonic excitation and predict the saturation level of subharmonic response very well at each of the frequencies. Although, the Marmottant model is similar to CEM, it effectively incorporates nonlinearity by prescribing a different behavior above the rupture radius. The threshold values predicted by the different models are listed in Table 5.2. Figure 6 shows that the non-negative exponential model results in a response very similar to the Marmottant model. This can be explained by noting that as the bubble shrinks, both prescribe the surface tension to be zero below a certain value of the bubble radius. The QEM and the EEM perform the best in predicting the experimentally measured threshold values. The Marmottant and the EEM (NN) models predict threshold values higher than the measured ones, especially at the higher frequencies of 4.4 and 6 MHz. Although each of the models predicts greater threshold value at the higher frequencies, the EEM and QEM provide better match with experiment. Although, the radial dynamics predicted by the QEM and EEM models was shown to be exactly similar in Chapter 4, the QEM model performs better in matching the experimental results at 4.4 and 6 MHz.

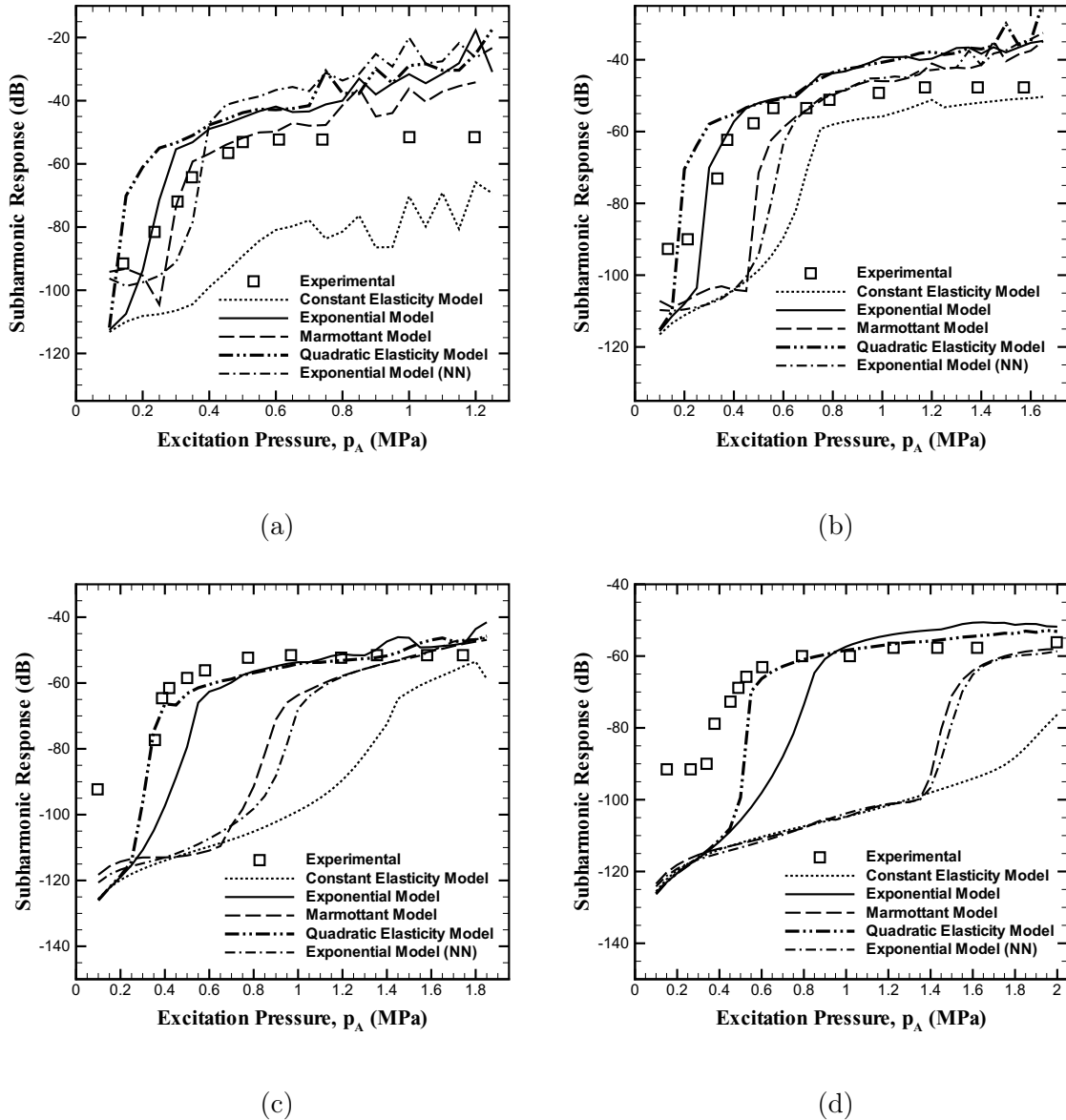


Figure 5.6: Measured and predicted subharmonic response of Sonazoid bubbles at various excitation frequencies: (a) 2 MHz, (b) 3 MHz (c), 4.4 MHz, and (d) 6 MHz. Reprinted with permission from [169]. Copyright [2010], Acoustical Society of America.

Table 5.2: Threshold pressure (in MPa) for subharmonic scattering obtained experimentally and from different interfacial models for Sonazoid bubbles.

	Frequency			
	(MHz)			
	2	3	4.4	6
Experiments	0.24	0.33	0.36	0.4
CEM	...	0.65
QEM	0.15	0.20	0.35	0.50
EEM	0.25	0.35	0.45	0.65
EEM (NN)	0.35	0.55	0.90	1.45
MM	0.30	0.50	0.85	1.45

5.4.2.2 Definity Microbubbles

For Definity microbubbles we will only present the results for the exponential elasticity and the Marmottant model. The Newtonian model is excluded as it predicts unrealistic surface tension values. The constant elasticity model and non-negative EEM is expected to perform worse than the EEM. The quadratic model is not considered as it models the change in elasticity with sharp transitions and discontinuities [See Figure 4.1 in Chapter 4].

Figure 5.7 shows that the predicted fundamental response by both the models. They match very well in for lower acoustic pressure, but unlike Sonazoid, the model predictions diverges at higher pressures. We also show simulations with the dilatational viscosity for “expired” bubbles as estimated by Faez et al. [276]. No significant effect was observed on the model predictions by changing the dilatational viscosity. We believe that at the higher acoustic pressures the response from the bubbles is getting affected by acoustically enhanced diffusion, which is not incorporated by the models. Although, the threshold for such dissolution was determined to be 1.2 MPa for “fresh” Definity bubbles [69], they are expected to change for the “expired” batches studied here. The discrepancies can also be due to the lack of accurate size distribution information for our vials. A more careful study should be undertaken in future to determine to what degree are these factors contributing to our model predictions.

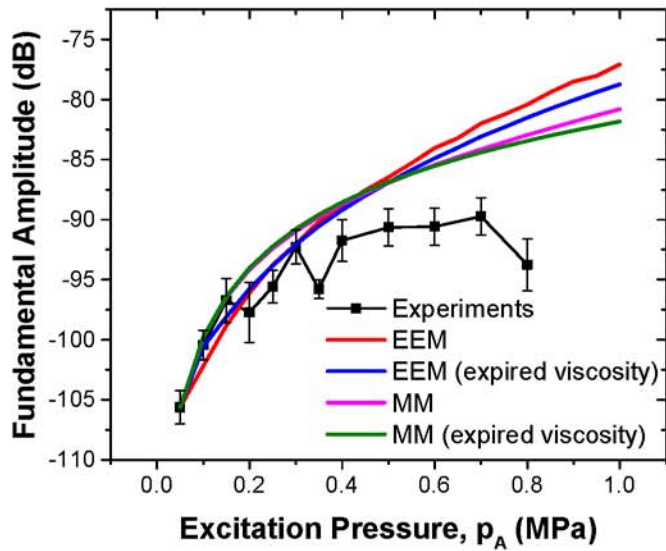


Figure 5.7: Measured and predicted fundamental response of Definity microbubbles at 10 MHz excitation

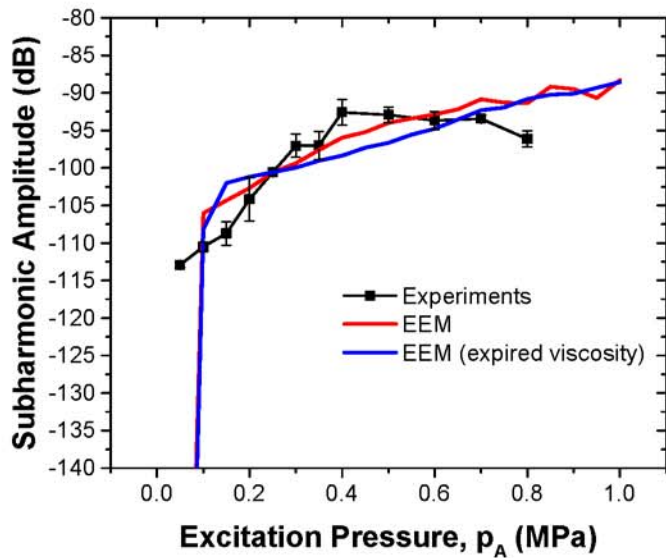


Figure 5.8: Measured and predicted subharmonic response of Definity microbubbles at 10 MHz excitation

Figure 5.8 shows the predicted subharmonic response and their comparison with the experimental measurements at 10 MHz excitation. As before simulations with the

dilatational viscosity predictions for expired bubbles are also shown and the corresponding predictions are virtually equivalent. We also match the experimentally measured subharmonic threshold (~ 150 kPa) very well. However, unlike our observation for Sonazoid we did not find satisfactory match of the saturation level as predicted in our simulations with experimental measurements. Note that beyond 400 kPa, bubble destruction if they were to occur, will also lead to differences between model predictions and experimental data. The predictions from Marmottant model is not shown in Figure 5.8 as it does not show any subharmonic response in the pressure range studied here, which is consistent with our observation for Sonazoid where the MM always predicted higher thresholds.

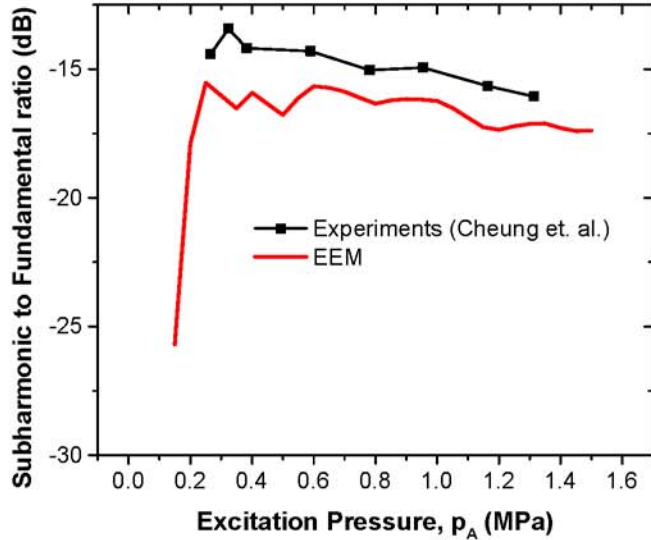


Figure 5.9: Measured and predicted ratios of subharmonic to fundamental response of Definity microbubbles at 20 MHz excitation. Experimental data extracted and reproduced with permission from [273].

Due to the the uncertainties involved in the matching with the 10 MHz data acquired in-house, we did another model validation with the experimental data from Cheung et al. [273] at 20 MHz. They presented their data as ratio of subharmonic to fundamental response in dB. Hence, no matching was required for this case. The comparison of our model predictions and experimental data is shown in Figure 5.9.

We get a very good agreement in this case. The experimental data was only shown in the original paper when a subharmonic was detected and hence it does not show that steep rise. Our predicted subharmonic threshold value also matches exactly with their experimental recordings — threshold for subharmonic generation was 200 kPa. As before, the predictions from Marmottant model is not shown in Figure 5.8 as it does not show any subharmonic response in the pressure range studied here. Hence, we can conclude that our method for characterization of lipid coated bubbles works quite well with a fair degree of accuracy. Further model improvements are required to broaden the applicability of the model e.g., including destruction/dissolution effects, which will be primarily driven by newer experimental observations.

5.4.2.3 Near-Chaotic or Chaotic Oscillations

Note that the excitation pressure dependent response from contrast microbubble obtained by numerical simulations show a lot of structures at higher acoustic pressures instead of a smooth curve [See Figures 5.5, 5.6, 5.9, 5.8]. We believe this is due to the near-chaotic or chaotic behavior of the dynamic system. When an uncoated bubble is excited at high excitation pressures, the response can become unpredictable. This behavior was termed as ‘acoustic chaos’ by [278] to signify the undetermined nature of the bubble response under well defined excitation conditions. In fact, the occurrence of subharmonic components during bubble oscillations can also be utilized as an indicator of the ‘aptitude for chaos of the system’ [121]. Only a few studies have reported the chaotic or near-chaotic behaviors of encapsulated bubbles [279–281]. Nevertheless, the results indicate that in spite of the presence of the shell, contrast microbubble may exhibit chaotic behavior. Such behavior is critically dependent on the encapsulation damping and excitation frequency along with the chosen model of the encapsulation. Note that the chaotic nature of oscillations have not been investigated in the present study and can be a topic of future research to determine the specific conditions and mechanisms for the onset of near-chaotic or chaotic behavior.

5.5 Summary and Conclusion

Nonlinear models for the encapsulation of a contrast microbubble was investigated for lipid coated commercially available contrast agents Sonazoid and Definity. The encapsulation was treated as a complex interface characterized by constitutive parameters such as surface tension (σ_0), dilatational viscosity (κ^s), dilatational elasticity (E_0^s) and new nonlinearity parameters — E_1^s for the QEM model, where the elasticity decreased linearly with area fraction, and α^s for the EEM model, where the elasticity varied exponentially. Both nonlinear models represent the strain softening resulting from the decreased association between constituent molecules in the encapsulation as its area increases. They resulted in very similar overall response for Sonazoid bubbles.

The constitutive parameters are key to the mechanical characterization of a specific contrast microbubble agent. In this chapter, the parameters associated with a commercial contrast agent Sonazoid and Definity were determined (Table 5.1) using measurement of attenuation as a function of frequency. The parameter values pertaining to a recent model due to Marmottant et al. [164] were also found for comparison. Different models are consistent in that the values of constitutive parameters arising in them for the same contrast agent and can be related to each other. The effects of imposing a constraint of nonnegative effective surface tension (comprising of the reference surface tension and the interfacial elasticity effects) were also investigated. The constraint resulted in a behavior very similar to the Marmottant model, because both models prescribe zero surface tension below certain bubble radii.

The models were investigated for their ability to predict the measured nonlinear scattering. Each of the models predicted the fundamental response well for Sonazoid. For Definity however, the model predictions diverged from the experimental data above 400 kPa possibly due to bubble destruction or inaccurate size distribution data. The CEM is shown to perform poorly in predicting the subharmonic response of Sonazoid — it does not predict a threshold value of the acoustic excitation for the subharmonic response seen in experiments. In contrast, introduction of strain softening in QEM and EEM led to the prediction of the threshold value and subsequent saturation, which

clearly indicates their superiority. Hence, we adopted the EEM as the model of our choice for subsequent investigations of Definity due to its realistic modeling of the variation of the dilatational elasticity. The model due to Marmottant et al. [164] also showed a threshold value and saturation, because of its similarity with the nonlinear models presented in this paper. However, the constraint of non-negativity imposed on it as well as a modified EEM model leads to threshold values significantly higher than the experiment at higher frequencies for both Sonazoid and Definity microbubbles. The scattering predictions (both linear and nonlinear responses) using the EEM, utilizing the estimated parameters, determined with a separate set of experiments, show very good agreement with the experimental data.

Chapter 6

CHARACTERIZATION OF POLYMER SHELLED MICROBUBBLES¹

6.1 Introduction

We discussed the characterization of lipid coated microbubbles used as ultrasound contrast agents in the previous chapter. We presented a hierarchical two-pronged approach of modeling, where a model was applied to one set of experimental data to obtain model parameters, and then the model was validated against a second independent experiments. Model improvement/modification was initiated as warranted by the process of validation. Our results indicated a satisfactory match of model predictions with experimentally observed scattered response. This motivated us to further explore this technique for contrast microbubble with other encapsulation materials. Contrast microbubble encapsulations can be made of different materials [See Table 2.1]. Recently, contrast agents with various polymeric shells have been developed that hold promises of enhanced stability [282–285] and improved control of the encapsulation properties [286]. Here we characterize and model linear and nonlinear acoustic several polymer coated microbubbles the details of which are presented in the table below.

Various polymeric microbubbles have been investigated for ultrasonic imaging [242, 257, 286–291] and targeted drug delivery/therapeutics [290, 292–294]. A comprehensive review of the application of polymeric microbubbles to imaging and drug-delivery/therapeutics can be found in a recent publication by Xiong et al. [295].

Poly (D, L-lactide) or poly lactic acid (PLA) as well as PLGA — a block copolymer with varying lactic to co-glycolic acid ratios — have been used to prepare

¹ Figures and parts of the text in this chapter have been adapted from a published [4] and an article under review [7].

air-filled polymeric microcapsules and investigated for potential imaging and drug-delivery applications. Our collaborators at Drexel University, under the guidance of Prof. Margaret A. Wheatley have been actively pursuing design and development of such polymeric air-filled microcapsules. Preliminary acoustic experiments with PLGA (50:50 ratio of lactic to co-glycolic acid) contrast agents have shown around 20dB enhancement both *in vitro* [285, 296] and *in vivo* [287, 296] dose response studies. The Forsberg study also investigated the role of varying ratios of glycolide to lactide in the PLGA *in vivo*. As lactide content was increased the shell became more hydrophobic, which increased the circulation time of the contrast microbubbles. These agents were conjugated with breast cancer targeting ligands [292] making them a potential vehicle for cancer-drug delivery. PLA shelled contrast agents have also been loaded with the chemotherapeutic drug doxorubicin (Dox) for ultrasound mediated delivery [83, 84, 297]. The maximum acoustic response achieved using drug loaded contrast agents showed around 19 dB enhancement *in vitro* (at 5 MHz excitation and 690 kPa peak pressure) and around 14 dB enhancement *in vivo* (with 5 MHz pulsed Doppler ultrasound) [83]. Size measurements on insonated Dox-loaded contrast agents showed a decrease in average size above the peak acoustic excitation pressure of 690 kPa, possibly due to bubble destruction through fragmentation or diffusive loss of gas [84]. Lavisse and co-workers have also independently studied PLA microparticles both *in vitro* and *in vivo* [288] to report 18 dB enhancement in their *in vitro* dose response studies conducted at 10 MHz, 275 kPa excitation.

A complete understanding of the key parameters contributing to the stability, echogenicity and drug release requires reliable mathematical models. Hence, to characterize and analyze of these polymer coated microbubbles, we use here four different interfacial rheological models (first three developed in our lab): 1) Newtonian model, 2) constant elasticity model, 3) strain-softening exponential elasticity model, and 4) Marmottant model. These models have mostly been applied to predict behaviors of lipid coated UCAs. However, polymer coated UCAs have been reported to behave differently for example, to have lower elasticity than lipid- or protein-based contrast

agents [68, 257, 291], or to have a resonance frequency lower than that of a similar sized free bubble [296]; typically presence of a shell increases the resonance frequency. Such distinct behaviors of polymeric microbubbles warrant further investigation.

6.2 Materials and Methods

6.2.1 Preparation Protocol

6.2.1.1 PLA Microbubble Preparation

Poly (lactic acid) ultrasound contrast agents were fabricated using a double emulsion technique [284, 285]. Five hundred milligrams of PLA (100 DL MW=83 kDa, Lakeshore Biomaterials, Birmingham, AL) were dissolved in 10 ml of methylene chloride (Fisher Scientific, Waltham, MA) along with 50 mg of camphor (Sigma-Aldrich, St. Louis, MO). When the polymer was completely dissolved, 1 ml of ammonium carbonate solution (4% w/v, J.T. Baker, Phillipsburg, NJ) was added to the polymer solution, and then immediately sonicated on ice for 30 seconds (10 pulses of 3 seconds each separated by 1 second) with 110 W applied power (Misonix Inc. CL4 tapped horn probe with 0.5 inch tip, Farmingdale, NY). The resulting water in oil emulsion was immediately added to 50 ml of a cold 5% w/v poly(vinyl) alcohol solution (Polysciences, Warrington, PA) and homogenized for 5 minutes at 9500 rpm with a saw tooth homogenizer probe (Brinkmann Instruments, Westbury, NY). Immediately following homogenization, 100 ml of 2% v/v isopropyl alcohol (Fisher Scientific, Waltham, MA) was added to the emulsion, and then stirred for 1 hour to allow the methylene chloride to evaporate. The particles were then collected by centrifugation at 2500 g for 5 minutes and washed three times with hexane (Fisher Scientific, Waltham, MA). After allowing any residual hexane to evaporate the particles were washed in water then flash frozen and lyophilized for 48 hours with a Vitris Benchtop freeze dryer (Gardiner, NY). The water and ammonium carbonate from the core of the particles and the camphor from the polymer shell were allowed to sublime during lyophilization to create a porous polymer shell encapsulating a void which is filled with air when the microbubbles are returned to atmospheric pressure. Contrast agent in the form of a dry powder was

refrigerated and stored until ready for use. *All these contrast agents were fabricated at Drexel University by our collaborator Prof. Wheatley and her student Dr. Michael Cochran.*

6.2.1.2 PB-127 and Philips Bubbles

The PB-127 bubbles and Philips bubbles (denoted by PH) was obtained as lyophilized powders from our collaborators at Riverside Research. *Their preparation protocol is mentioned here briefly to emphasize the role it plays in determining the acoustic and material properties of these contrast agents, which is an essential component of the results presented here.* More detailed description can be obtained in a previous publication [241]. The protocol for PB-127 bubbles is proprietary and hence not available to us but it should be similar to the Philips bubble preparation technique. Unlike the PLA microbubbles, each of these contrast agents were prepared in a specific way to have a distinct shell thickness to radius ratio (STRR) [See Table 6.2 for details]. Poly-L-Lactide with a molecular weight of 2400 and a fluorinated end group was utilized following existing protocols [298]. A stock solution (0.79 g of poly-L-Lactide and cyclodecane in dichloromethane) was emulsified in polyvinyl alcohol (PVA, 3% w/w). This emulsion was added dropwise to 0.3% w/w of PVA in water and pressed through Acrodisk 1- μ m glass filter along with continuous stirring for 3 hours at 500 rpm to evaporate the dichloromethane. After this evaporation, the sample was centrifuged and washed with 5% poly(ethyleneglycol) [PEG] in water twice. The final retrieved sample was mixed with PEG, which was then rapidly frozen at -80°C in a precooled glass vial. Both ice and cyclodecane fractions were removed by freeze-drying 20 hours at 0.2 kPa and again for 20 hours at 0.03 milibars at a shelf temperature of -10°C. The samples were filled with nitrogen to obtain nitrogen filled cores and stored at -4°C till further use. The STRR of the UCA populations obtained in this manner was adjusted through the weight ratio of the polymer in the polymer-cyclodecane stock solution; polymer ratios (%w/w) of 2.85, 1.9, 1.27, and 1.03 yielded shell-to-core ratios of 1:3, 1:5, 1:8, and 1:10, respectively as given in Table 6.2.

6.2.2 Size Distribution Measurements

Size distribution of PLA microbubbles were obtained using dynamic light scattering techniques as described in Section 3.1.1 utilizing the Malvern Zetasizer Nano ZS-90. One milligram of dry contrast agent was suspended in 1 ml PBS by vortexing for 10 seconds then transferred into a disposable cuvette and allowed to equilibrate for 3 minutes before taking measurements. Size distribution measurements of the PB127 and Philips bubbles were also measured using DLS but using the Acusizer 770A.

6.2.3 Acoustic Experiments

For the PLA microcapsules, obtained from Drexel University, we measured both acoustic attenuation and nonlinear scattering by utilizing our own *in vitro* acoustic setups involving a large sample volume discussed earlier in Chapter 3. The details of the attenuation setup can be found in Section 3.3.3, whereas Section 3.3.4 discusses the scattering setup. Contrast agent in the form of a dry powder was refrigerated and stored until ready for use. The dry powder was reconstituted in phosphate buffered saline to make a stock solution with a concentration of 1 mg powder/ml PBS (equivalent to a bubble concentration of 30×10^6 bubbles/ml, See Table 6.2). This stock solution was subsequently used to achieve desired dilutions during acoustic experiments. The stock solution was pipetted into the container with PBS (previously left to equilibrate for 5-10 mins to equilibrate with atmospheric oxygen concentration and for getting rid of any air bubbles created). An aliquot of stock sample was carefully added by automatic pipette and then allowed to mix for around 10 seconds using a magnetic stirrer to ensure a homogeneous suspension before application of ultrasound. The stirring was continued through the entire course of the experiment to maintain homogeneity. Attenuation measurements were acquired for a range of contrast agent concentrations between 0.5 – 3.5 $\mu\text{g}/\text{ml}$ and at a peak negative pressure of 50 kPa. Three different unfocused transducers were used with central frequencies 2.25, 3.5 and 5 MHz. All scattering measurements were conducted at a concentration of 1.33 $\mu\text{g}/\text{ml}$. Two different focused transducers with center frequencies 2.25 and 3.5 MHz were used

as the transmitting transducers at their respective central frequencies. The acoustic excitation pressure was varied from 30-650 kPa capture subharmonic threshold behavior if they were to occur. Since, earlier studies reported a destruction threshold of 690 kPa, no scattering data was obtained beyond this pressure. Reading taken of the sample without contrast agents showed no interference from entrained bubbles. The total volume of gas added with the agent was less than 100 μl in a total volume of 150 ml. Each attenuation and scattering experiment was repeated five times, i.e. five data sets were collected from five new suspensions prepared from the stock solution freshly taken into the experimental setups. The phase velocities, attenuation coefficients and scattered responses were calculated using the techniques mentioned in Sections 3.3.3 and 3.3.4. We also characterized the destruction and stability of PLA microbubbles using the time dependent attenuation experiments described in Section 3.3.5 using a 2.25 MHz unfocused transducer.

The PB-127 and Philips bubbles, provided by our collaborators at Riverside Research, were only characterized using acoustic attenuation at our end using the same setup utilized for PLA microbubbles. The experimental data for the model validation step was taken from a previously published work [241]. As with the PLA bubbles, a stock solution with a powder concentration of 1 mg/ml was prepared and diluted in a manner similar to that for PLA microbubbles. The attenuation experiments were performed at concentration of 10 $\mu\text{g}/\text{ml}$ and at a peak negative acoustic pressure of 50 kPa using a 15 MHz unfocused transducer. For PB-127 bubbles a distinct peak was observed near 5 MHz and hence, the attenuation measurements were repeated with a 5 MHz unfocused transducers. Using a high frequency transducer, we were able to capture their dynamics at higher frequencies 8-24 MHz. This ensured a better agreement with the validation experiments — scattering measurements with these bubbles were performed at an excitation frequency of 20 MHz. The concentration of bubbles per milligram of powder for different contrast agents are provided in Table 6.2.

6.2.4 Mathematical Modeling

For our mathematical modeling, we used the exact same technique utilized for the lipid coated microbubbles. The material characterization was performed by fitting linearized predictions of attenuation coefficients with the experimental data using both an average size and the full distribution. These estimated model parameters were then used to solve the full nonlinear RP equation to obtain scattered response at fundamental, second harmonic and subharmonic frequencies. For these air-filled PLA bubbles, a calculation of the Peclet number based on the average size and at 1 MHz frequencies gives a value of 0.05 which is much less than 1. This allowed us to assume isothermal condition for the oscillations with $\kappa = 1$. For our simulations we used $\rho_L = 1000 \text{ kg/m}^3$, $\mu = 0.001 \text{ Ns/m}^2$ and $c = 1485 \text{ m/s}$. However, the PB-127 and Philips bubble were excited at higher frequencies of 20 MHz which results in a Peclet number of ~ 1 . However, these bubbles have thick encapsulations which should now be accounted for in our heat flux balance. It was suggested that the heat transfer across such thick encapsulation will be negligible thereby giving adiabatic oscillations [Personal Communications with our collaborators]. Hence, for the preliminary simulations presented here, we used both adiabatic ($\kappa = 1.4$) and isothermal ($\kappa = 1.0$) conditions for property estimation and nonlinear scattering simulations. A thermal damping was also incorporated by increasing the liquid viscosity by two folds, which is a general practice in contrast agent literature [3]. A more rigorous calculation of the thermal damping and effective polytropic index value should be undertaken in future to ensure accuracy of the results.

6.3 Results and Discussion

6.3.1 Size Measurements

Figure 6.1 and Table 6.1 show the size distribution measurements with PLA microbubbles for three different samples acquired from the same stock solution using dynamic light scattering equipment as described previously. The number averaged diameters (See Table 6.1) are similar for all three measurements except for slightly

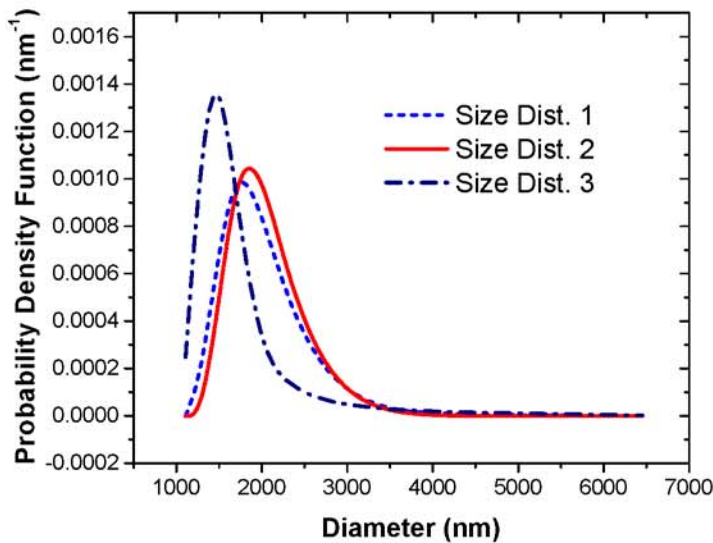


Figure 6.1: Three independent measurements of the size distribution of poly(DL-lactic acid)-encapsulated contrast microbubbles obtained using dynamic light scattering.

Table 6.1: Size distributions, z-averaged diameters and number-averaged diameters for three separate measurements of poly(DL-lactic acid)-encapsulated microbubbles obtained using dynamic light scattering. Reprinted with permission from [4].

Diameter (nm)	Number (%)		
	Size Dist. 1	Size Dist. 2	Size Dist. 3
1106	0	0	4
1281	3	0	21.1
1484	14.9	9.8	33.2
1718	27.4	27.6	21.3
1990	25.1	30.5	7.7
2305	16.1	19.4	4.3
2689	8.3	9.2	2.7
3091	3.4	3	1.8
3580	0.9	0.5	1.3
4145	0.5	0	1
4801	0.4	0	0.8
5560	0	0	0.6
6439	0	0	0.2
Average Diameter			
Number-averaged	1999 nm	2030 nm	1726 nm
z-Averaged	3486 nm	3377 nm	3151 nm

lower value for the third size distribution (Size Dist. 3). However, note that the entire distribution corresponding to Size Dist. 3 is markedly different from the other two with a tighter size distribution, lower peak diameter, and smaller number of bubbles above 1500 nm. Instead of using an average distribution, we use all three size distributions in our analysis and investigate the effects of size distribution variation on property estimation and scattering prediction. We will see below that the difference in size distribution leads to different predictions of subharmonic response.

The size distributions obtained for PB-127 and Philips bubbles did not show any notable variation for multiple runs. Hence, an average distribution could be used in this case. The measured size distributions are presented in Figure 6.2. Both PH37 and PH45 batches show a larger population of sub-micron diameter bubbles. Also none of the bubble suspensions have a monodisperse population, which clearly indicates an average size should not be a representative of the suspension. However, to present an approximate idea of the relative shell thickness differences among these bubbles, we calculate an average shell thickness using the number averaged size, as shown in Table 6.2. The concentrations of the bubbles formed after dissolving 1 mg of powdered contrast agent in buffer were also measured and are presented in the same table. These values were used to calculate the actual number per unit volume ($na(a)da$) corresponding to each bubble size (a) in the distribution for any given dilution. The numbers thus obtained were used as an input in 2.55 during our fitting process.

6.3.2 Material Characterization of the Encapsulation Using Attenuation

6.3.2.1 PLA microbubbles

Attenuation measurements were obtained for five different concentrations of contrast agent using all three transducers. Frequency dependent attenuation coefficients for each measurement were generated using the data reduction technique explained earlier. The value of the attenuation coefficient corresponding to the center frequency of each transducer was then extracted. The average value for each set of five experiments along with the corresponding standard deviation error was then plotted in

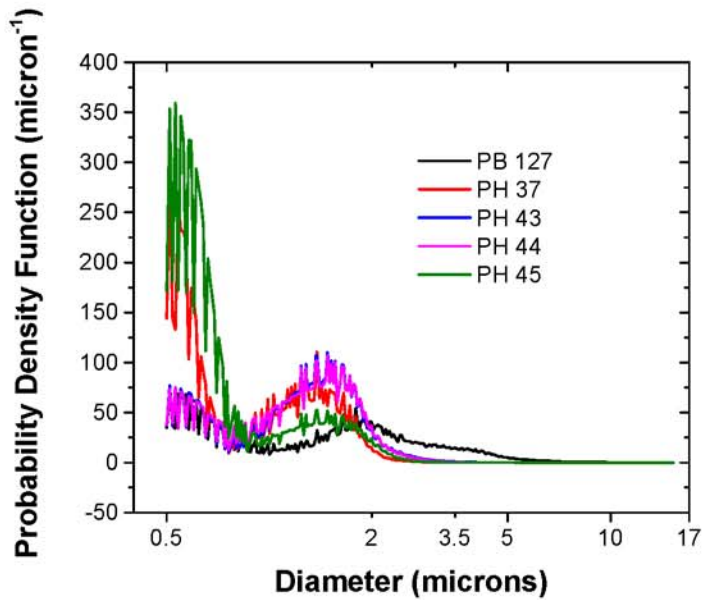


Figure 6.2: Size distributions of PB-127 and Philips microbubbles obtained using dynamic light scattering.

Table 6.2: Shell thickness and concentration of bubbles per milligram of powder for various polymer shelled bubbles used in this study.

UCA Type	Nominal STRR (nm/ μ m)	Average Radius (μ m)	Shell Thickness (nm)	No. of Bubbles 10^6 /mg powder
PLA bubbles	...	0.85	...	30
PB-127	7.5	1.25	9.375	9.9
PH45	30	0.48	14.4	21.8
PH37	40	0.55	22	153
PH44	65	0.66	42.9	99.4
PH43	100	0.68	68	10.4

Figure 6.3a. Note that, for the range of concentrations studied here, the attenuation increases linearly for all three transducers used indicating minimal effects of multiple scattering for the dilute concentrations considered. Figure 6.3b shows the frequency dependent attenuation coefficient obtained for the highest concentration with all three different transducers used. Attenuation coefficients obtained with different transducers are similar in the region of their overlapping frequency bandwidths. The peak of the attenuation curve occurs around 2.5-3 MHz indicating a weighted-average resonance frequency of the polydispersed sample within this range.

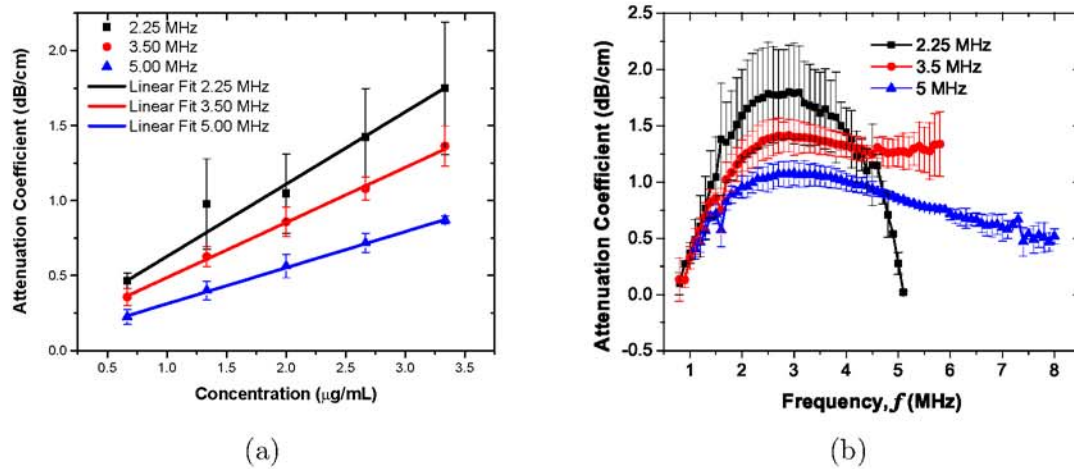


Figure 6.3: (a) Attenuation coefficient at the central frequencies of the three transducers (2.25, 3.5 and 5 MHz) as a function of microbubble concentration (averaged over five different acquisitions). (b) Frequency-dependent attenuation coefficient measured with three different transducers (with central frequencies 2.25, 3.5 and 5 MHz) averaged over five different acquisitions. Reproduced from [4] with permission from Elsevier.

Using the error minimization approach mentioned earlier for lipid coated microbubbles (See Section 5.3), the unknown parameters pertaining to each model were calculated and given in Table 6.3 using the three different size distributions noted above. Note that for the Marmottant model, we assumed that the contrast agent is initially in a buckled state with a zero surface tension; this would render them initially stable in the absence of acoustic excitation. The frequency dependent attenuation curves obtained through modeling (using each bubble size distribution) match very well with

experiment. We show the match only for the Size Dist. 3; others are very similar and not shown for brevity. However, note that unlike in our previous experience with lipid coated bubbles, using an average size and total number did not work very well in estimating the parameters for PLA microbubbles; depending on the initial guesses for the parameters at the start of the minimization, often the error minimization procedure did not converge, and when it converged, it gave rise to unphysical values for the material parameters. The inability of using an average diameter for parameter estimation indicates the importance of the polydispersity of the bubble size distribution and the limitation of the estimation process adopted here. One has to be careful in adopting such a process and interpreting the results.

The estimated parameters for three different size distributions are similar except for slightly smaller dilatational viscosity for the size distribution 3 (Note also slightly smaller surface tension value for this distribution but only for the Newtonian model). The smaller dilatational viscosity for distribution 3 can be explained by noting that damping of a bubble increases as the radius decreases [172, 175]. This can be understood by examining the encapsulation damping term given by Equation 2.28e. Since, for contrast microbubbles this term dominates the total damping decreases with increasing radius. Size distribution 3 has the largest fraction of smaller bubbles. Therefore, the same attenuation data gives rise to the smallest damping for this distribution to achieve satisfactory match during the fitting. Note that the interfacial elasticity values predicted for PLA coated microbubbles (0.02-0.07 N/m) are an order of magnitude smaller than the values reported previously for phospholipid coated bubbles ($\sim 0.5 - 1.0$ N/m) given in the Chapter 5. However, the interfacial viscosity values ($2 \times 10^{-9} - 8.5 \times 10^{-9}$ kg/s) are similar to those reported for Definity microbubbles and SonVue microbubbles. Using size distribution 3, we predicted the lowest values of surface dilatational viscosity and therefore correspondingly the lowest damping which critically affects the subharmonic response from microbubbles as discussed in a later section. Note that, unlike Sonazoid or Definity, here we obtain a reasonable value of surface tension (σ) even for the Newtonian model. For the other models, σ_0 achieves

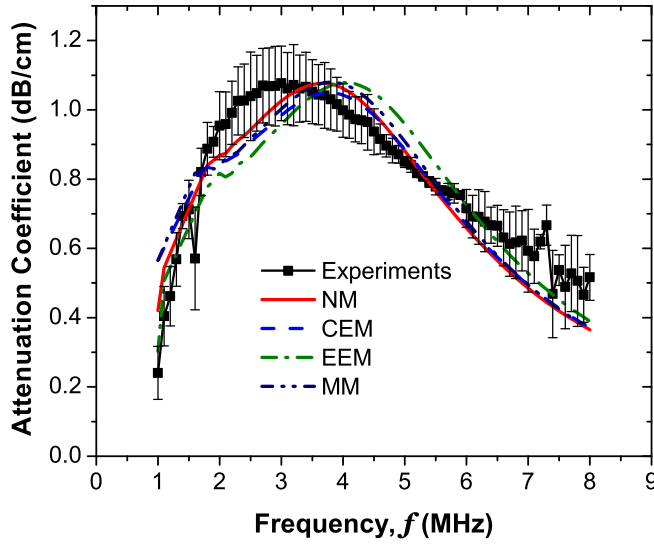


Figure 6.4: Experimentally measured and fitted attenuation data for PLA microbubbles using Size Dist. 3. Concentration was 4×10^4 bubbles/ml.

Table 6.3: Estimated model parameters of poly(DL-lactic acid)-encapsulated microbubbles for different interfacial models and using three different size distributions. Reproduced from [4] with permission from Elsevier.

Interfacial Model	Estimated Parameters			
	Size Dist. 1	Size Dist. 2	Size Dist. 3	
NM	σ (N/m)	0.08	0.06	0.03
	κ^s (10^{-9} Ns/m)	7.5	8.5	2.0
CEM	σ_0 (N/m)	0.02	0.01	0.01
	E^s (N/m)	0.07	0.05	0.01
	κ^s (10^{-9} Ns/m)	7.5	8.5	2.1
EEM	σ_0 (N/m)	0.02	0.01	0.01
	E_0^s (N/m)	0.07	0.05	0.02
	α	1.5	1.5	1.5
	κ^s (10^{-9} Ns/m)	7.5	8.5	2.1
MM	σ_0 (N/m)	0	0	0
	χ (N/m)	0.08	0.06	0.04
	κ^s (10^{-9} Ns/m)	7.5	8.5	2.0

a value which is also less than the air-water interface value of 0.072 N/m. The low surface tension along with an extremely low value of elasticity contributes to the low average resonance frequency seen for these microbubbles.

6.3.2.1.1 Resonance Frequency of PLA Bubbles

We explained in Section of this thesis, how the peak in the attenuation curve due to a monodisperse bubble population can be used as a representative of its resonance frequency. However, for a polydisperse suspension, this peak represents a weighted-average resonance frequency. Figure 6.3b indicates that the measured attenuation increases with increasing frequency reaching a peak in the range of 2.5-3 MHz — indicating the incidence of the average resonance frequency there — and decreases thereafter. The frequency for the peak response agrees well with the previously reported value of 2.28 MHz [284]. As noted before, the resonance frequency of the PLA bubble was reported to be lower than that of a same sized free bubble, in contrast to other contrast microbubbles where the elasticity of the encapsulation increases the stiffness giving rise to a higher resonance frequency seen for lipid coated microbubbles in the previous chapter. The resonance frequency of a free bubble is often estimated using the well known Minneart formula

$$f_0 = \sqrt{\frac{3.26}{R_0(\mu\text{m})}} \quad (6.1)$$

However, note that this formula is more appropriate for bubbles of size mm and above; it includes only the term due to the gas compressibility — the term in the numerator of Equation 2.38 — and neglects the contribution due to surface tension. The surface tension term becomes high for bubbles of micrometer size and is of the same order as the compressibility term. For a free air bubble in water with an average diameter of 1.9 μm , the resonance frequency computed with Minneart formula (3.43 MHz) becomes significantly smaller than that calculated (4.2 MHz) using the correct

form as given by Equation 2.38. Therefore, the decrease in resonance frequency with encapsulation is even higher than predicted earlier by [296], when one would expect the encapsulation to contribute to the stiffness of the damped mass-spring system and increase its resonance frequency. As mentioned above, this paradox was noted before [296], and several hypotheses were proposed for explaining it, e.g., presence of gas-filled cells with an average diameter less than that of the entire capsule, or a highly porous capsule where tiny chambers have a greater contribution to the actual dynamics, or a disproportionate contribution from bubbles of different sizes to the overall dynamics. The first two reasons are clearly wrong since, a smaller effective radius would lead to further increase of resonance frequency.

We argue that the result stems from several effects — the reduced effective surface tension ($\sigma(R)$), extremely small dilatational surface elasticity and the polydispersity of the size distribution, which makes the average diameter irrelevant for determining acoustic properties of the entire suspension. It explains the difficulty in the property estimation using average diameter described above. The attenuation curve with its maximum peak position results from attenuation due to bubbles of different sizes from the entire size distribution that includes small number of larger bubbles with size different from the average of the size distribution. These bubbles have their peak attenuation at a frequency lower than the one corresponding to the average size. Using only average radius therefor inevitably leads to a larger resonance frequency, as it neglects the effects of these larger bubbles. Note also that nonlinearity can decrease the resonance frequency [183, 299]; for lipid shelled microbubbles it tends to decrease with increasing acoustic excitation pressure. We will see in the subsequent sections that the strong nonlinearity, through subharmonic emissions, of PLA bubbles sets in at much lower excitation pressures (around 100-150 kPa). So even at 50 kPa nonlinear effects might be causing a decrease in the resonance frequency. One final check is to verify if the damping is causing the shift in resonance. All our resonance calculations are based on the discussion we presented in Section 2.4.3.3. We showed that, $\omega_0^2 = K$ if damping factor (b) is small. However, for present case this might not be a valid

assumption due to smaller contribution by surface tension to the stiffness term. The damped resonance frequency can be calculated using $\omega_0^2 = K - 2b^2$, which resulted in a value of ~ 4.0 MHz. Hence, the effect of damping on the resonance frequency is negligible for PLA bubbles.

6.3.2.2 PB-127 and Philips Bubbles

Similar to the PLA microbubbles, we measured attenuation through a suspension of PB-127 and Philips bubbles using our *in vitro acoustic setup*. Due to scarcity of samples, no concentration dependent measurements were performed. The multiple scattering effects were avoided by using the lowest possible concentration of bubbles for detecting a damping of the wave, which was 10 $\mu\text{g}/\text{ml}$. The corresponding bubble concentration in numbers per unit volume can be calculated using Table 6.2. Figure shows the frequency dependent attenuation coefficients corresponding five different bubble formulations obtained through our experiments. We also calculated the variation in phase velocity of a sound wave while traveling through a suspension of these bubbles, which are shown in Figure 6.6. As expected the deviation from the mean velocity of sound in water (1485 m/s) was minimal for low concentration of bubble in the suspension. This validates our assumption of the absence of multiple scattering effects. As before, the error bars in both the figures represents the standard deviations about the mean of five independent acquisitions.

As before, we can estimate an average resonance frequency of the suspension by looking at the peak in the attenuation curve. The PB-127 bubbles show a distinct peak in the 4-6 MHz range. The phase velocity also shows a considerable change near that frequency. This indicates a suspension of PB-127 bubbles has an average resonance frequency of *simMHz*, which is consistent with previous reports [300]. In contrast to the PB-127 bubbles, none of the Philips bubbles showed a distinct peak. The attenuation due to the PH37 and PH45 are much lower than PH45 and PH44 bubbles. This is indicative of the fact that the latter two has a thicker encapsulation shell [See Table 6.2] and lower number of bubbles per unit volume [See Table 6.2]. The resonance

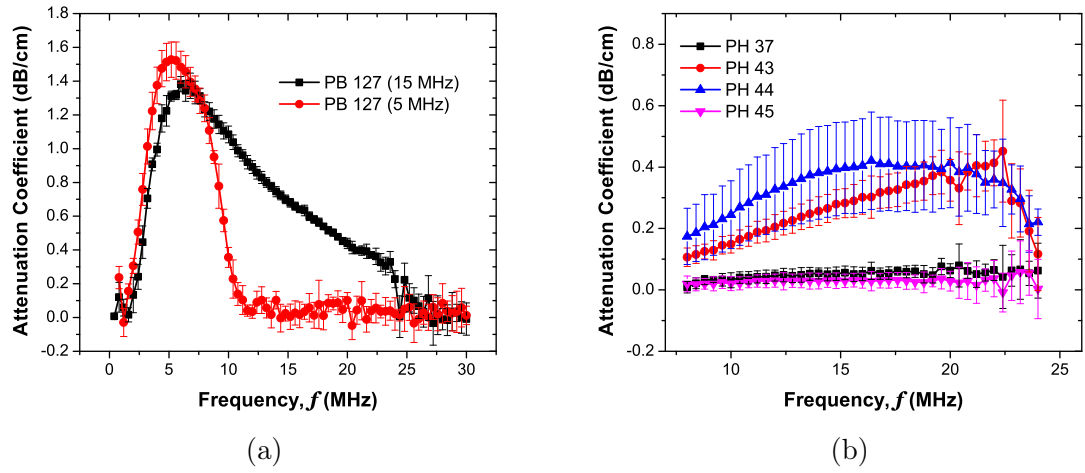


Figure 6.5: Frequency dependent attenuation coefficients measured through a suspension of (a) PB-127 bubbles using both 5 MHz and 15 MHz transducers, and (b) Philips bubbles (PH37, PH43, PH44 and PH45) using a 15 MHz transducer.

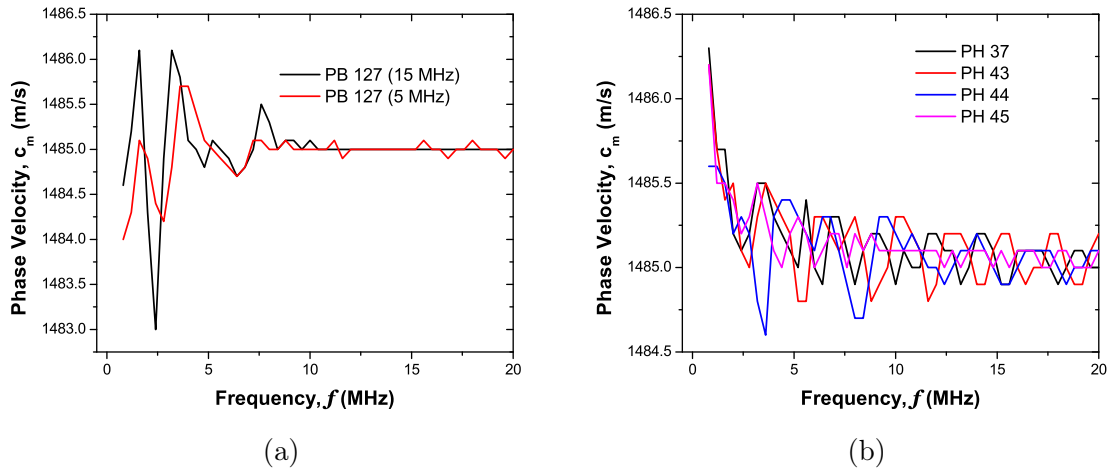


Figure 6.6: Frequency dependent dispersion measured for a suspension containing (a) PB-127 bubbles using both 5 MHz and 15 MHz transducers, and (b) Philips bubbles (PH37, PH43, PH44 and PH45) using a 15 MHz transducer.

frequency of Philips bubbles are expected to be much higher, beyond 40 MHz [241], which is consequently not be detected with the present setup. Nevertheless, the present attenuation data should be a good enough representative of the bubble behavior in the 20 MHz regime used for the model validation using nonlinear scattering experiments.

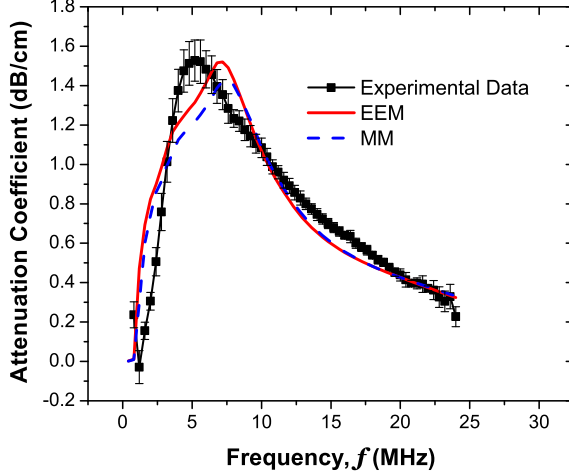


Figure 6.7: Experimentally measured and fitted attenuation data for PB-127 microbubbles.

The unknown parameters pertaining to each model were estimated using the error minimization technique. The bubble suspensions were polydisperse and hence, the estimated properties estimated with an average size from those estimated with the entire distribution. Since, we are interested in analyzing the suspension behavior, we only present the estimated parameters obtained using the entire size distribution in Table 6.4. The corresponding fitting curves are shown in Figure 6.8, which shows a very good agreement with the experimental data. The elasticity values predicted in this manner ($4\text{-}27 \text{ N/m}$) were an order of magnitude higher than those reported for lipid coated bubbles. The dilatation viscosity of the Philips bubble were much higher in the order of 10^{-7} N.s/m . The dilatational viscosity for PB-127 was however similar to those reported for lipid coated bubbles.

If the shells are considered to be homogeneous continuum, which can be a valid

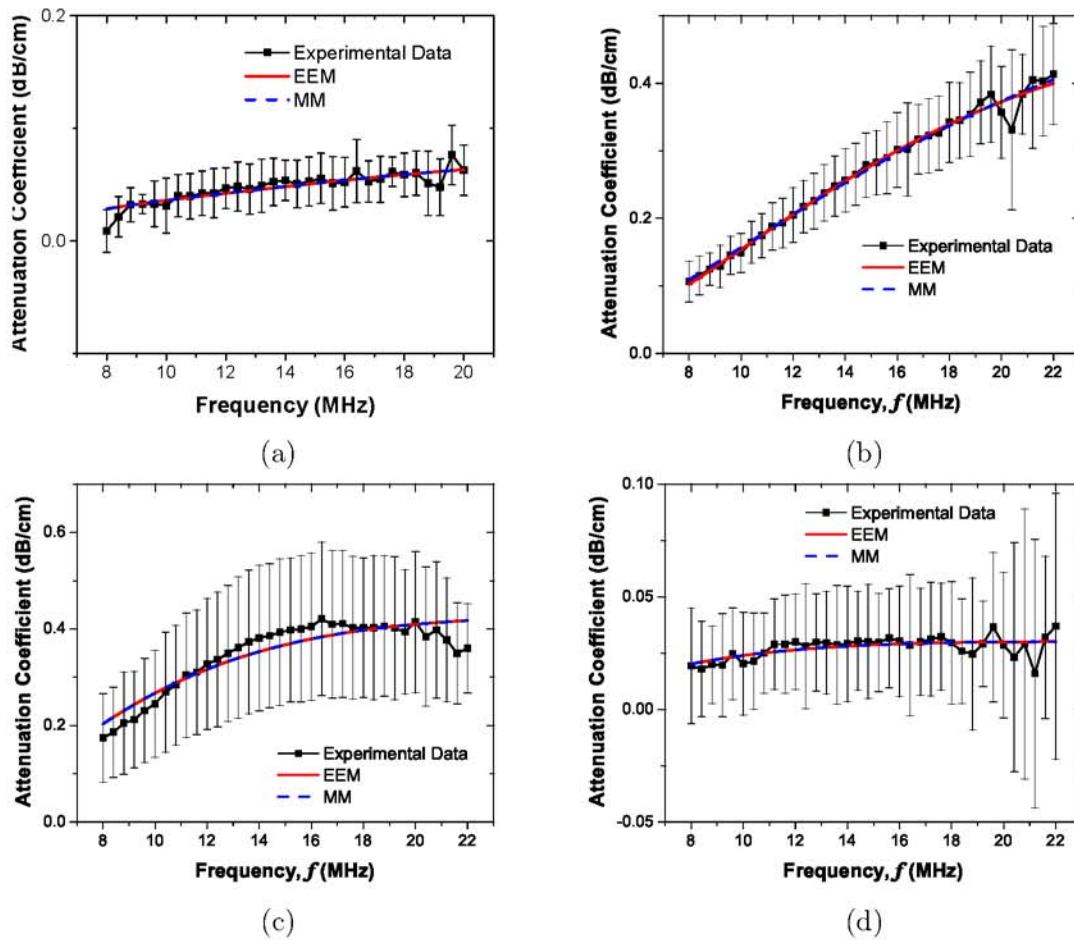


Figure 6.8: Experimentally measured and fitted attenuation data for PH37, PH43, PH44, and PH45 microbubbles.

Table 6.4: Estimated material properties of the polymeric encapsulation for PB-127 and Philips microbubbles using different interfacial models.

Interfacial Model		Estimated Parameters			
		PB-127	PH37	PH43	PH44
NM	σ (N/m)	5.0 ± 0.2	13.0 ± 0.5	27.0 ± 1.0	11.0 ± 0.5
	κ^s (10^{-7} Ns/m)	0.1 ± 0.02	1.06 ± 0.2	2.05 ± 0.2	1.65 ± 0.2
	σ_0 (N/m)	0.02 ± 0.02	0.05 ± 0.01	0.06 ± 0.01	0.02 ± 0.02
EEM	E_0^s (N/m)	4.5 ± 0.5	10.0 ± 2.0	10.0 ± 2.0	5.6 ± 0.5
	α	10 ± 10	10 ± 10	10 ± 10	5 ± 5
	κ^s (10^{-7} Ns/m)	0.1 ± 0.02	1.14 ± 0.2	2.4 ± 0.2	1.6 ± 0.2
MM	σ_0 (N/m)	0	0	0	0
	χ (N/m)	5.0 ± 0.2	13.0 ± 1.0	27.0 ± 1.0	11.0 ± 1.0
	κ^s (10^{-7} Ns/m)	0.1 ± 0.02	1.14 ± 0.2	1.06 ± 0.2	1.62 ± 0.2

assumption for thicker polymer shells studied here, the following relations can be obtained under small amplitude approximations

$$\chi = 2\epsilon\mu_s, \quad (6.2a)$$

$$\kappa^s = 3\epsilon\eta_s, \quad (6.2b)$$

where μ_s and η_s are the shear modulus and shear viscosity of the shell respectively. Note that both the elasticity and the dilatational viscosity are directly proportional to shell thickness. This explains why the elasticity for the thinner-shelled polymeric bubbles like PB-127 and PH45 elasticity values are lower (4-5 N/m). It also explains the lower viscosity predicted for the PB-127 bubbles. The thickness usually has a more pronounced effect on the dilatational viscosity. The thickness of the Philips bubbles are more than 10 times higher than that of PB-127 bubbles [See Table 6.2], which again explains the higher viscosity predictions. However, this analogy fails to explain why the PH37 bubbles have a much higher elasticity even with a thinner shell. Nevertheless, as with the PLA bubbles, these polymer-shelled bubbles predict different material properties from lipid coated bubbles that will critically affect their dynamics under ultrasonic pulsations.

6.3.3 Time Dependent Attenuation and Destruction Thresholds for PLA Microbubbles

Sustained acoustic excitation changes the state of the encapsulation which in turn affects bubble stability and lifetime of PLA microbubbles (Eisenbrey et al. 2008). To investigate the PLA bubble lifetime under acoustic excitation, attenuation was measured as a function of time and the normalized attenuation defined by Equations 3.7 and 3.6 in Section 3.3.5 plotted in 6.10. For this figure the data were averaged of consecutive 30 second intervals. It shows a steady decrease with time, as was also observed previously [69, 209, 301]. Contrast agents containing gases other than air show a transient increase in attenuation initially before its eventual decrease. The increase

in attenuation is caused by transient growth of bubble volume due to air diffusing much faster initially into them compared to the outward diffusion of low-solubility gases [50]. Air-filled PLA agents do not show any such transient increase. We notice that over the 20 min period the attenuation drops by 30-40%. Note that previous time response backscatter study with PLA [284] and PLGA (50:50) [296] contrast microbubbles also noted a 15% loss in enhancement over the same time period. Also, the range of excitation frequencies studied here show no effect on the time dependent attenuation due to PLA bubbles.

Our group had earlier device a technique to use time dependent attenuation as an indicator of the mode of destruction and utilized it to determine the various modes of destruction for Definity microbubbles [69]. They observed the following modes: a transient growth at small amplitude excitations explained above, pressure dependent decay in the attenuation at intermediate pressures mostly due to gas diffusion, and finally a rapid pressure independent decay at very high excitation pressures. For our case with PLA microbubbles, we expect to see the latter two for reasons explained above. A pressure dependent attenuation study was done and the results are shown in Figure 6.10 averaging over consecutive 1 minute intervals. We observe at very low acoustic pressure of 50 kPa there is an increase over the first one minute, followed by a slow decay. This increase indicated that bubbles take a finite amount of time to stabilize at an equilibrium radius once the powders are dissolved in the solution. Due to this initial increase there seems to be a slow decay at even at 50 kPa indicating loss of gas. However, this change is less than 15%, which indicates the bubbles are fairly stable. This trend continues at higher pressures of 280 and 400 kPa. For both these cases the decay is around 20 % indicating bubble stability. Note that this decay rate is consistent with the previous measurements at 200 kPa with three different transducers shown in Figure 6.9. At even higher acoustic excitation pressures of 550 and 800 kPa the decay rate is much faster with around 80% and 100% reductions at 550 kPa and 800 kPa acoustic pressure respectively. Note that at 800 kPa excitation pressure, normalized attenuation reaches zero within 5 minutes indicating a complete

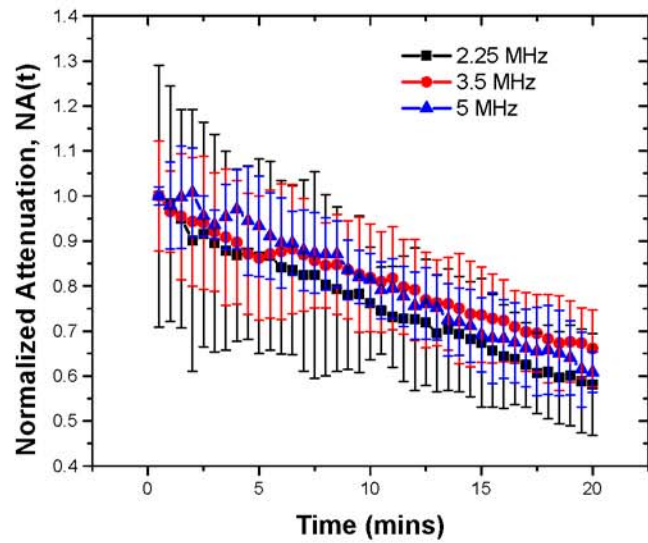


Figure 6.9: Plot of normalized total attenuation coefficient versus time measured at 200 kPa acoustic excitation pressure using three different flat faced transducers of central frequencies 2.25, 3 and 5 MHz. Reproduced from [4] with permission from Elsevier.

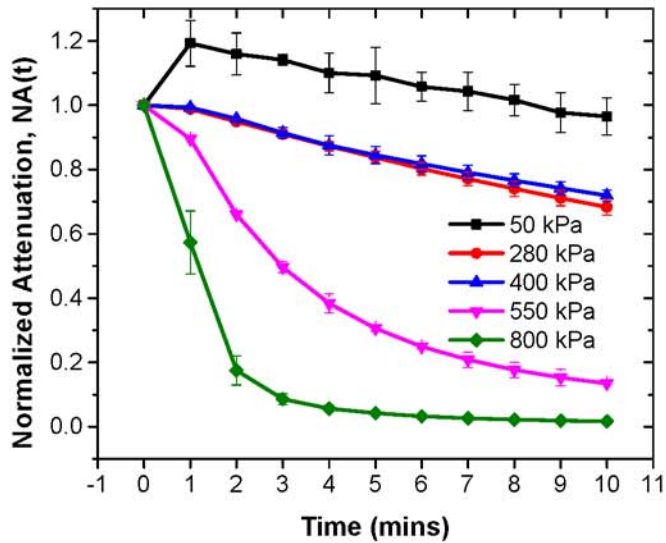


Figure 6.10: Plot of normalized total attenuation coefficient versus time measured for PLA microbubbles at different acoustic excitation pressures with a 2.25 MHz flat faced transducer.

loss of bubbles. Hence, we conclude that the PLA microbubbles are fairly stable under acoustic excitations less than 450 kPa in amplitude, beyond which they will undergo shell rupture mediated destruction.

6.3.4 Scattering and Comparison with Model Predictions

6.3.4.1 PLA Microbubbles

6.3.4.1.1 Fundamental and second harmonic responses

Scattered response from PLA shelled contrast agents was acquired varying acoustic pressure amplitudes at two different excitation frequencies of 3.5 and 2.25 MHz. Averages and standard deviations of five independent acquisitions at each pressure amplitude were then obtained through above mentioned data analysis technique. Fundamental (at excitation frequency), second-harmonic (at twice the excitation frequency) and subharmonic (at half the excitation frequency) responses for both the transducers are shown in Figure 6.11.

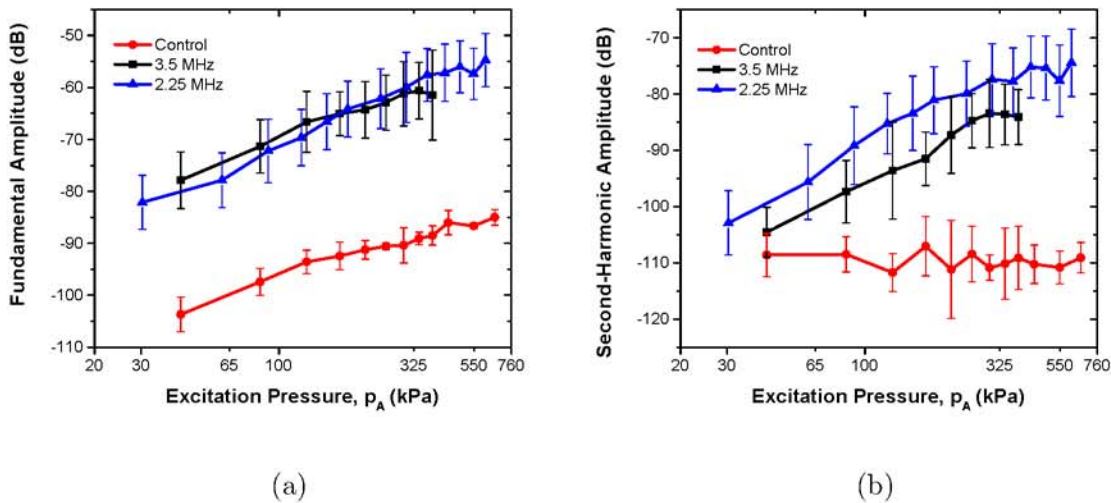


Figure 6.11: Experimentally measured scattered response from PLA microbubbles for two different excitation frequencies of 2.25 MHz and 3.5 MHz at (a) Fundamental Frequency (b) Second-harmonic frequency. Control indicates data without any bubbles introduced in the suspension. Reproduced from [4] with permission from Elsevier.

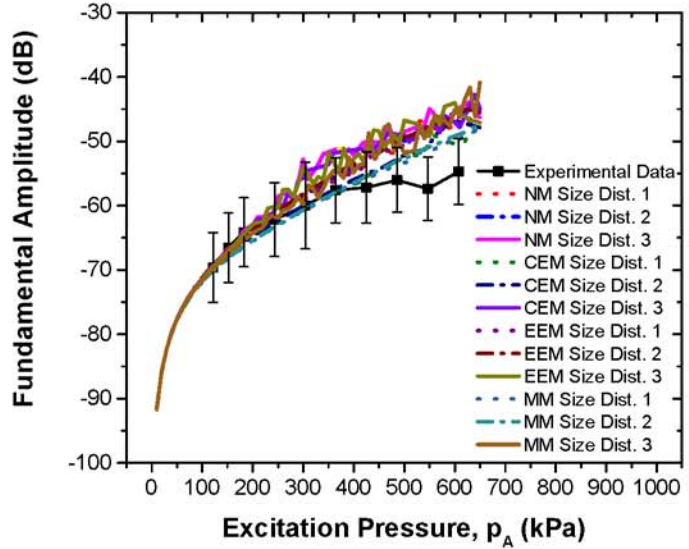
The fundamental response shows a 25-30 dB enhancement in the entire range of excitations for both frequencies. Previous *in vitro* scattering experiments with PLA

microbubbles reported similar enhancement, around 17 dB at 5 MHz and 690 kPa excitation pressure (estimated from the dose response curve for the concentration of 1.33 $\mu\text{g}/\text{ml}$) [83]. For a PLGA (50:50) microbubble, the enhancements were 10 dB at 2.25 MHz and 20 dB at 5 MHz [296]. The second harmonic shows an enhancement of 10-35 dB (2.25 MHz) and 5-25 dB (3.5 MHz). The results demonstrate the echogenicity of PLA agents, specifically their efficacy for harmonic contrast imaging, where the second harmonic response is imaged.

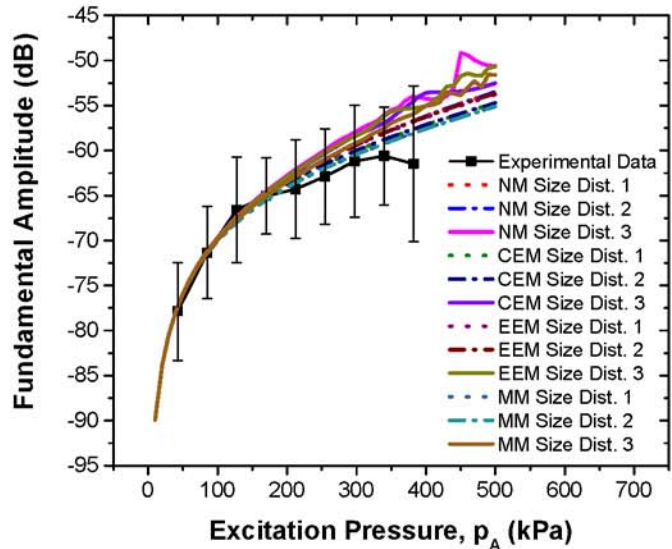
Both fundamental (Figure 6.11a) and second harmonic (6.11b) responses (plotted in a log-log scale) for each excitation frequency show an approximately linear increase with increasing acoustic pressures; They deviate from linearity at higher pressure; especially the second harmonic response curve flattens beyond 320 kPa, possibly due to bubble destruction. The slopes for the curves are found to be 0.92 at 3.5 MHz and 1.15 at 2.25 MHz for fundamental response and about 1.5 at both frequencies for second harmonic. Small amplitude perturbation analysis predicts them to be 1 (fundamental) and 2 (second harmonic). However, the experimentally measured slope of second harmonic has been shown to deviate from its theoretical value of 2 [50].

We also simulated the scattered response from the microbubbles using several models. Note that for each model, we obtained three different predictions, using three different set of parameter values obtained using the three different size distributions given in Table 6.1 and Figure 6.1. The scattered responses were computed using the corresponding size distributions and shown in Figures 6.12 and 6.13. For both excitation frequencies, predicted fundamental response from all three models shows good agreement with experimental data for all three bubble distributions (size dist. 1-3). The experimental curve deviates at higher pressures from model predictions. The deviation occurs approximately around the same pressure value (320 kPa) where the linearity of the experimental result breaks down due to possible bubble destruction mentioned above. Destruction is not accounted in any of the models which might explain the difference between the model prediction and the experimental observation.

Second harmonic responses predicted by different models show a slope of 2, as



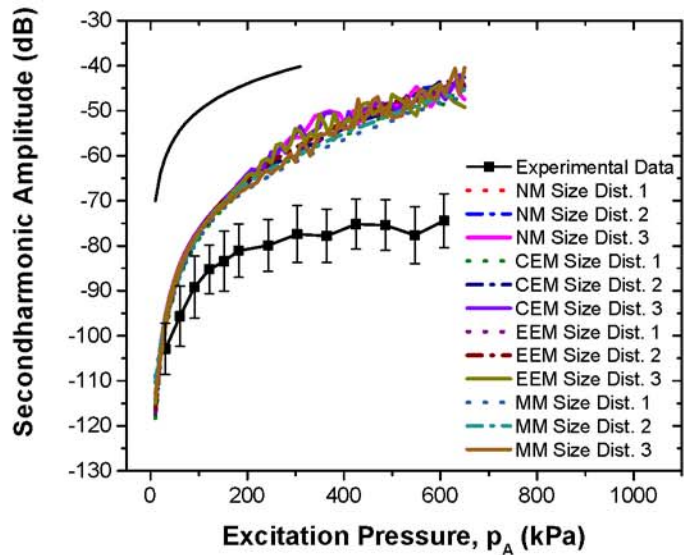
(a)



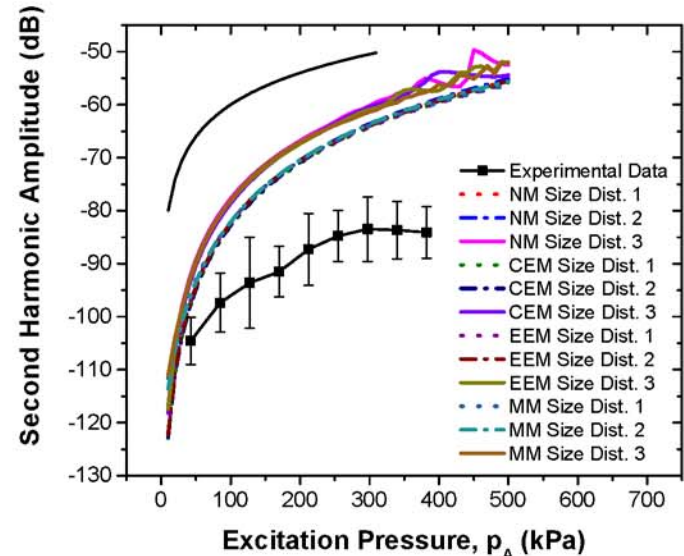
(b)

Figure 6.12: Comparison of experimentally measured and predicted scattered fundamental responses of PLA-encapsulated microbubbles for different models using three different size distributions at (a) 2.25-MHz excitation and (b) 3.5-MHz excitation. Reproduced from [4] with permission from Elsevier.

they should, in contrast to the experiments as noted before [Figure 6.13]. They do not match very well even for the lower acoustic pressures. However, the predictions



(a)



(b)

Figure 6.13: Comparison of experimentally measured and predicted scattered second-harmonic responses of PLA-encapsulated microbubbles for different models using three different size distributions at (a) 2.25-MHz excitation and (b) 3.5-MHz excitation. Reproduced from [4] with permission from Elsevier.

from all three models and three size distributions are similar. Note that the second harmonic frequencies studied here are within the receiving bandwidth of the transducer

used. The discrepancy in the model prediction points towards the inadequacies of the modeling effort. Also as mentioned before the bubble destruction that might affect the nonlinear response was not accounted for in the models.

6.3.4.1.2 Subharmonic Response

The scattered subharmonic response from PLA microbubbles measured experimentally [Figure 5.9] shows the typical characteristics of the subharmonic response at both excitation frequencies — initially no subharmonic before a threshold pressure value, at threshold a rapid rise followed by a saturation [50, 163]. The excitation threshold at excitation frequency of 2.25 MHz is 125 kPa, slightly higher than 100 kPa at 3.5 MHz. The classical bubble dynamics theory predicts minimum threshold for subharmonic generation to be at twice the resonance frequency [187, 302, 303]. Observations for two different encapsulated microbubbles — Optison [268] Definity [304] were reported to follow this theory. The frequency for minimum subharmonic threshold for PLA agents is therefore expected to be between 5 and 6 MHz. Note however that we have recently shown that the minimum threshold shifts towards resonance away from twice its value for encapsulated microbubbles due to large damping [175]. We also showed that the threshold is rather flat in the region between resonance and twice its value. We also note that the threshold at 3.5 MHz is only slightly lower than that at 2.25 MHz.

All models considered here predict very low acoustic response until the threshold is reached (Figure 6.15). Hence, model predictions are shown only when above -120 dB (above the experimental noise level of -115 dB). Unlike the fundamental response, the simulated subharmonic response does not show an unqualified match for all bubble distributions. Note that the post-threshold response level is matched well for both frequencies. However, predicted threshold value varies. For both frequencies, the size distributions 1 and 2 exhibit much higher threshold values in comparison to experimental data [See Table 6.5]. The size distribution 3, which has larger fraction of smaller bubbles (Figure 6.1) matches very well (solid curves) the threshold for 2.25

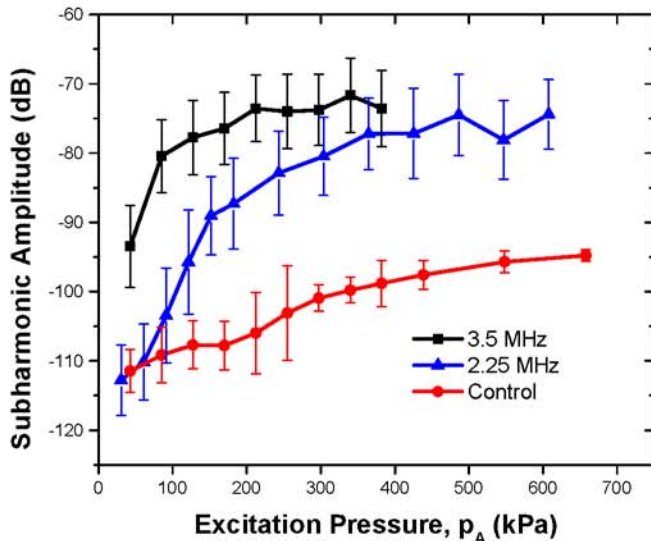
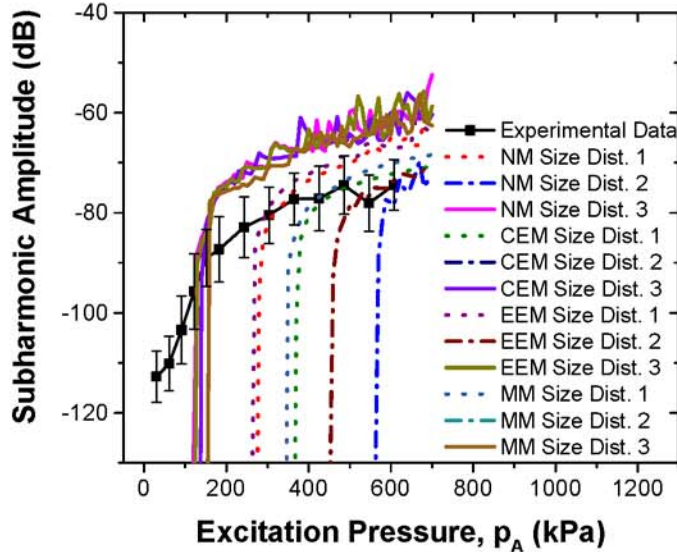


Figure 6.14: Experimentally measured subharmonic response from PLA microbubbles at two different excitation frequencies of 2.25 MHz and 3.5 MHz. Control indicates data without any bubbles introduced in the suspension. Reproduced from [4] with permission from Elsevier.

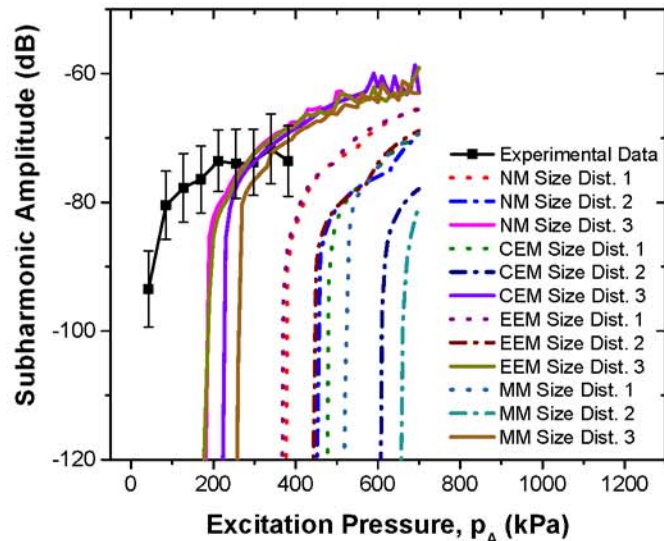
MHz excitation, and is closer to the experimental measurements for 3.5 MHz.

6.3.4.1.3 Model validation and their Predictive capability

In our previous modeling exercise for lipid coated microbubbles, we have emphasized the need for independent model validation. We determined the model parameters through linear attenuation data, as is done here, and then validated the model by investigating its ability to predict subharmonic response obtained at higher excitations. In fact, our modeling exercise led to results that dictated model improvements from Newtonian to constant elasticity model to exponential elasticity model. For Albunex, Optison Sonazoid [162] and Definity (Chapter 5), the Newtonian model resulted in an unrealistically large value of surface tension and hence deemed unsuitable for modeling encapsulated microbubbles. As a result, we introduced surface dilatational elasticity [163]. However, here we find a very low value of surface elasticity for the PLA encapsulation. Even the NM predicts low surface tension values; for size distribution 3, it predicted a value lower than that for the air–water interface. As mentioned above, only



(a)



(b)

Figure 6.15: Comparison of experimentally measured and predicted scattered subharmonic responses of PLA-encapsulated microbubbles for different models using three different size distributions at (a) 2.25-MHz excitation and (b) 3.5-MHz excitation. Reproduced from [4] with permission from Elsevier.

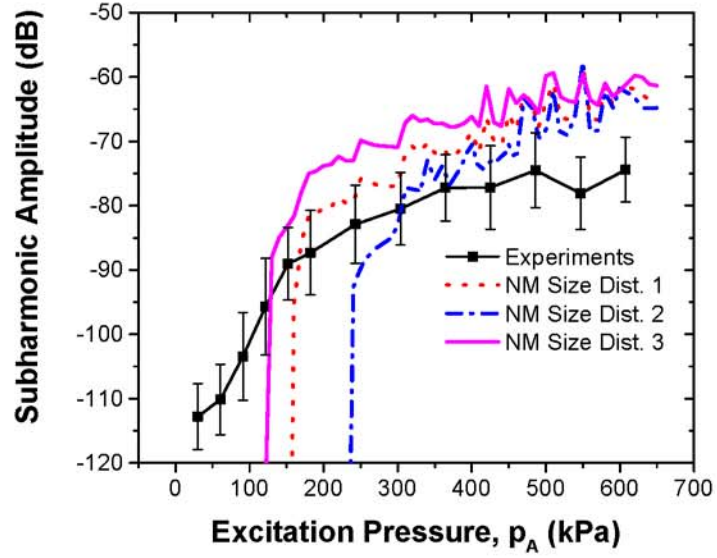
for size distribution 3 did we get a prediction that matched experimentally measured thresholds. For this distribution all models predicted similar values: the CEM and MM

predicted slightly higher values than the NM and EEM, the latter two predicting the same value. The NM therefore remains an effective model to describe PLA bubbles. We use it below to examine further certain features of PLA-encapsulated microbubbles.

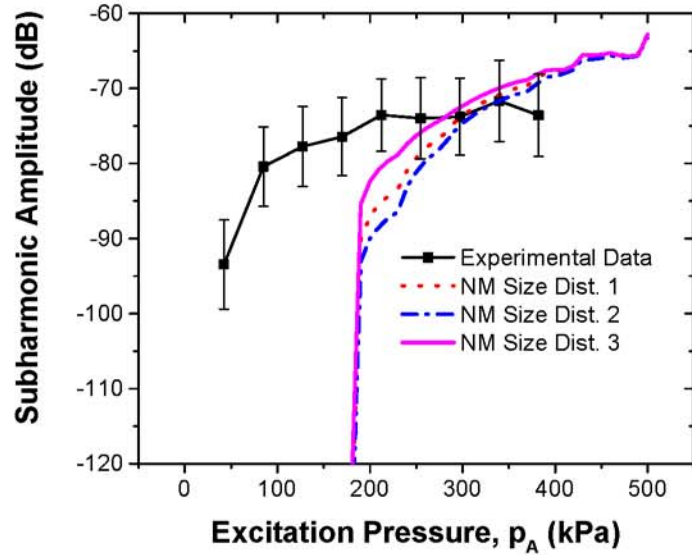
Table 6.5: Threshold pressure for subharmonic generation obtained experimentally and using three different models for all three size distributions studied. Values in bold indicate lowest threshold predictions for each model. Reproduced from [4] with permission from Elsevier.

	Threshold Pressure (kPa)	
	2.25 MHz	3.5 MHz
Experiments	125	100
Newtonian Model (NM)		
Size Dist. 1	280	380
Size Dist. 2	570	460
Size Dist. 3	130	190
Constant Elasticity Model (CEM)		
Size Dist. 1	370	480
Size Dist. 2	1500	610
Size Dist. 3	140	230
Exponential Elasticity Model (EEM)		
Size Dist. 1	270	370
Size Dist. 2	460	450
Size Dist. 3	130	190
Marmottant Model (MM)		
Size Dist. 1	350	520
Size Dist. 2	830	660
Size Dist. 3	160	250

We note that all models perform poorly in predicting second-harmonic responses, and clearly more research is needed to resolve this discrepancy. However, for predicting sub-harmonic responses, size distribution 3 fares the best (see Table 6.5 for sub-harmonic threshold), indicating that the behavior of any model describing the dynamics of encapsulated microbubbles is critically dependent on bubble size distribution. (As mentioned above, such extreme sensitivity in size distribution, where in fact the different size distributions were obtained from the same batch, also insinuates the limitations of the parameter estimation technique used.) Specifically, the subharmonic



(a)



(b)

Figure 6.16: Comparison of experimentally measured and predicted scattered subharmonic responses of PLA-encapsulated microbubbles for the Newtonian model (NM) with different size distributions and parameter values for size dist. 3 at (a) 2.25-MHz excitation and (b) 3.5-MHz excitation. Reproduced from [4] with permission from Elsevier.

threshold depends on the ratio of excitation frequency to natural frequency, and natural frequency is determined by bubble size [172]. More bubbles with lower subharmonic

threshold values would lower the overall threshold value as well. Also, as we already noted, the variation in size distribution from sample to sample affected corresponding parameters for the three samples; sample 3 had the lowest surface dilatational viscosity value: one-third to one-fourth those of the other two samples. Decreased damping lowers the sub-harmonic generation threshold [172, 175]. To further investigate the effects of material parameters and size distribution on the predicted sub-harmonic response, we used the material properties (low dilatational viscosity value, $\kappa^s = 2.0 \times 10^{-9}$ N.s/m) determined using size distribution 3, but computed subharmonic response with all distributions including distributions 1 and 2. The results illustrated in Figure 6.16 indicate that the lower dilatational viscosity predicts subharmonic responses closer to the experimentally measured value, even with the other two size distributions. We therefore conclude that the lower dilatational viscosity (albeit determined with the size distribution corresponding to sample 3) is the critical factor. This underscores the fact that accurate estimation of the average material parameters of encapsulation critically depends on the ability to measure the size distribution, and inter-sample variation has to be taken into account.

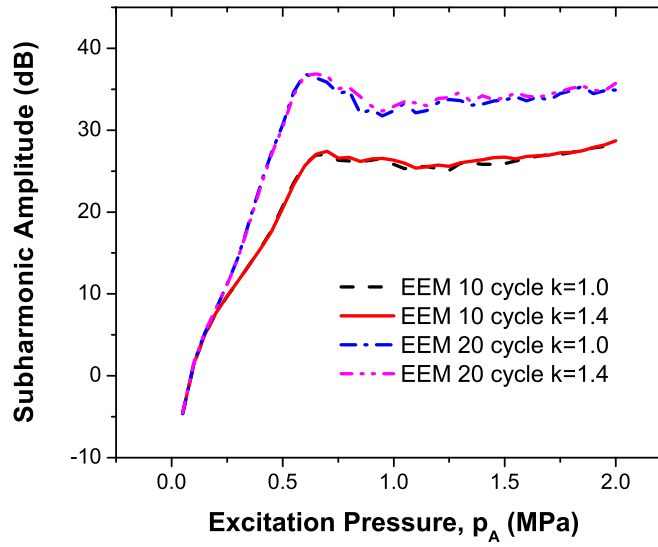
6.3.4.2 PB-127 and Philips Microbubbles

Our collaborative effort to characterize the acoustic behavior of PB-127 and Philips bubbles was motivated by the need to understand their dynamics, specifically their subharmonic generation mechanisms, at high frequencies. Hence, the model predictions were validated against subharmonic measurements acquired by our collaborators at 20 MHz excitation published previously. However, they had a different technique to analyze the subharmonic response microbubbles where they utilize a method based on singular-value decomposition (SVD) technique to obtain cumulative subharmonic scores (SHS) [See [305] for more details]. Thus, unlike PLA-encapsulated microbubbles, we could not validate model predictions with excitation pressure dependent linear and nonlinear response curves. As an alternative, we compared the experimentally observed subharmonic thresholds for the bubbles with our model predictions under similar

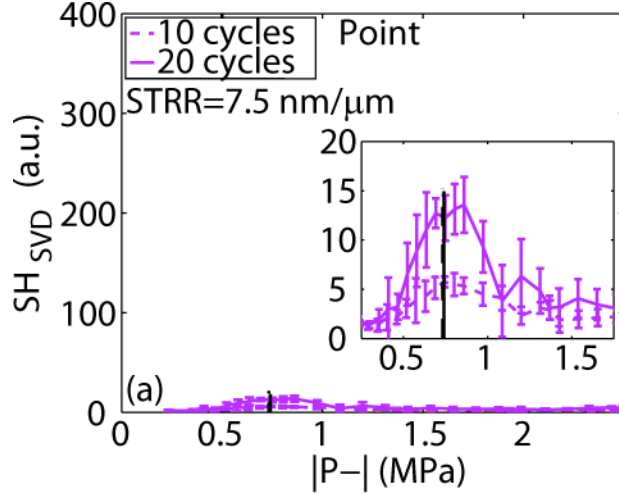
acoustic excitation conditions. Since, there is an uncertainty with the correct choice of polytropic index for these bubbles, we simulated the bubble dynamics with the largest possible variations i.e., isothermal ($\kappa = 1.0$) case and adiabatic case ($\kappa = 1.4$).

Figure 6.17 shows the predicted subharmonic response from PB-127 microbubbles at 20 MHz excitation with 10 and 20 cycle tone bursts. Both show the characteristics of the subharmonic response as mentioned earlier. The predictions from Marmottant model are not shown as they did not show any subharmonic response in the range of excitation pressures studied here. We see a good qualitative match of our predictions with experimental measurements. The threshold for subharmonic generation from our simulations was ~ 500 kPa which is close to the experimental value of ~ 600 kPa. Also, the amplitude subharmonic response increases with an increase with number of cycles. Hence, we believe our models can capture dynamics of PB-127 polymeric bubbles fairly accurately. However, this was not true for the Philips bubbles where simulations showed no subharmonic response from any of the bubbles whereas experiments clearly recorded subharmonic signature beyond 1.5 MPa acoustic pressure. We believe this is due to the unusually high values of dilatational viscosity ($\kappa^s \sim 10^{-7}$ N.s/m) predicted for Philips bubbles [See Table 6.4]. We are currently investigating the source of these discrepancies and one possible solution will be incorporate a nonlinear viscosity model with shear thinning constitutive behavior as has been proposed for lipid coated bubbles [168]. Hence, in light of the existing results discussed above, it is evident that the applicability of our model to thicker shelled polymeric bubbles with constant shell thickness to radius ratio needs further scrutiny.

Note that, similar to the lipid coated bubbles, the excitation pressure dependent bubble response also show structures for polymer-shelled microbubbles [See Section 5.4.2.3]. PLA microbubbles, which has lower damping shows the onset of such structures at relatively lower pressures consistent with previous reports. Also, the response from PH bubbles with a much larger damping contribution due to the encapsulation did not show such structures for acoustic excitation pressures less than 1.5 MPa (results not shown here).



(a)



(b)

Figure 6.17: (a) Predicted scattered subharmonic responses of PB-127 microbubbles for the exponential elasticity model(EEM) 20 MHz excitation with 10 and 20 cycle pulse length under both isothermal and adiabatic assumptions. (b) Experimentally measured singular-value decomposition (SVD) derived subharmonic score (SHS) from PB-127 microbubbles at 20 MHz excitation with 10 and 20 cycle pulse lengths. The solid black vertical line indicates the subharmonic threshold. Reproduced with permission from [241] Copyright © 2013, IEEE.

6.4 Summary and Conclusions

In this chapter, we characterized polymer-coated air-containing microbubbles through in vitro scattering and attenuation experiments. Five different bubbles were studied viz., PLA-encapsulated microcapsules prepared by double emulsification technique (PLA microbubbles), PLA-shelled constant shell thickness to radius ratio (STRR) bubbles with nominal STRRs of 7.5 (PB-127), 30 (PH45), 40 (PH37), 65 (PH44) and 100 (PH43). Four different models of microbubble encapsulation — Newtonian, constant elasticity, exponential elasticity and Marmottant — were used to determine the interfacial rheological properties of the microbubbles. Unlike our previous investigation of Sonazoid and Definity, we found significantly different values for interfacial tension and surface dilational elasticity — lower for PLA-encapsulated bubbles and higher for PB-127 and Philips bubbles. However, sample-to-sample size distribution variations for the same batch of contrast agents gives rise to variation in the parameters determined using them. Moreover, the average bubble size was found unsuitable for material characterization of these polydisperse polymer-shelled bubbles.

The peak in the attenuation spectrum indicates a weighted-average resonances at around 2.5–3 MHz and 6 MHz for PLA and PB-127 microbubbles respectively in agreement with previous measurements. However, no such resonance behavior was observed for the Philips (PH) bubbles for the range of frequencies studied (8–22 MHz). For PLA microbubble, this value of the average resonance frequency is smaller than that of a free bubble of the same size (1.9 μm in diameter). We discussed in detail the limitations of the Minneart formula for microbubbles, showing that the reduced resonance frequency stems from the reduced surface tension, extremely low surface elasticity and polydispersity; normally, the surface elasticity of an encapsulation results in enhanced stiffness of the system, thereby increasing resonance frequency. The low interfacial elasticity value distinguishes PLA-encapsulated bubbles from other lipid- and protein-coated bubbles. For the thicker shelled constant STRR microbubbles however, the resonance frequency was higher than that of a similar sized uncoated bubble as

expected. All these polymeric microbubbles have both second- and sub-harmonic scattered responses as a result of non-linear oscillations during experimental observations.

For PLA microbubbles, all models predict similar dynamics and match the fundamental scattered response very well, but fail to predict the second-harmonic response, clearly indicating the need for further research. Experimentally measured second-harmonic responses have a slope of 1.5 in contrast to the theoretical value of 2. The subharmonic response exhibits the characteristic features: it appears only above a threshold excitation level (100–150 kPa) and then sharply rises with increasing excitation strength. The models predict the characteristic features of a subharmonic response and the post-threshold response amplitude. The size variation from sample to sample gives rise to variation in parameters, in particular for surface dilatational viscosity. The lower value for surface dilatational viscosity obtained using one of the measured size distributions results in better prediction of the experimentally measured subharmonic threshold value. This experimental and modeling study of PLA microbubbles using two independent acoustic experiments — linear attenuation for model determination and non-linear scattering for validation — revealed several unique features of PLA microbubbles, such as extremely low encapsulation elasticity values and relatively low subharmonic threshold values and explains the low resonance frequency experimentally observed here as well as before. Our study also indicates that contrast microbubbles are complex polydispersed systems and underscores the importance of careful analysis of experiments performed on them.

For PB-127 and Philips bubbles, no direct comparison was possible with experimentally measured subharmonic and second-harmonic. Predictions with PB-127 microbubbles also show the typical characteristics of the subharmonic behavior. A very good qualitative match was obtained with the experiments with fairly accurate prediction of subharmonic generation thresholds. However, all the models failed to capture the experimentally observed subharmonic behavior of Philips bubbles. This was due to the order of magnitude higher dilatational viscosity predicted for these bubbles and further studies are currently being undertaken to address these issues. However, the

findings indicate that in present from the models are incapable of describing the nonlinear dynamics of thick-shelled polymeric constant STRR microbubbles and a nonlinear viscosity model with shear-thinning characteristics may be implemented in future.

Chapter 7

DESIGN AND IMPLEMENTATION OF MODIFIED *IN VITRO* EXPERIMENTAL SETUPS FOR THE CHARACTERIZATION OF ULTRASOUND CONTRAST MICROBUBBLES

7.1 Motivation

During this research, we realized the need to modify our acoustic experimental setup for addressing certain issues with the larger sample volume and also expand the scope of our experimental characterization. Herein, we discuss two such modifications undertaken during the course of study. The motivation behind them are discussed below.

A lot of our acoustic characterization experiments were performed on liposomes with custom made lipid formulations and hence were costly. The larger volume setup utilized a sample volume of 100 ml. The inherent variability of liposomal systems as will be seen in the next few chapters dictated us to use higher concentrations of liposomes in our experiments. Usually the number of liposomes formed after dissolving the lyophilized powders is a direct function of the amount of lipids present in the powder. Even for a concentration of 10 $\mu\text{g}/\text{ml}$ of lipids, use of a 100 ml sample would force use to use 1 mg of lipids per run! This severely restricted the number of experimental studies that could be performed with these liposomes. For e.g., unlike the microbubbles we did not acoustic pressure dependent characterization with liposomes to determine their subharmonic generation thresholds, if they were to be generated. This motivated us to design and optimize a smaller volume acoustic setup as described in Chapter 3. Here we will present the some validation experiments proving that the result obtained from the new setup are equivalent to those obtained using the older, larger sample volume setup.

We mentioned in Chapter 1 the use of subharmonic signals from as a potential tool for non-invasive local blood pressure estimation. This idea was developed by our collaborators at Thomas Jefferson University [306]. They reported the subharmonic response from microbubbles are particularly sensitive to changes in the ambient pressure. By varying the ambient pressure they showed that subharmonic response from several microbubble based contrast agents decreases linearly with increasing ambient pressure [55, 307–309]. If one can calibrate this decrease, the amplitude of the subharmonic response obtained using targeted microbubbles can then be used for Subharmonic Aided Pressure Estimation (SHAPE) [310]. This technique is particularly useful for diagnosis of several disease conditions related to portal hypertension [311, 312] or breast cancer lesions [313], where a local increase of blood pressure have been reported. However, during our attempts to model this behavior using the interfacial models discussed earlier revealed some interesting dynamics of bubbles under changing ambient pressure [172, 175, 314]. We found that depending on the excitation frequency, the subharmonic response from a single microbubble can either increase monotonically ($f_{\text{excitation}}/f_0 > 1.7$), decrease monotonically ($f_{\text{excitation}}/f_0 < 1.2$) or show a non-monotonic behavior ($1.2 < f_{\text{excitation}}/f_0 < 1.7$). However, till date, there has been no experimental report validating this numerical results. This motivated us to pursue detailed characterization of subharmonic behavior from contrast microbubbles with varying ambient pressure. In this chapter we will discuss the design and implementation of this setup and present some preliminary data.

7.2 Materials and Methods

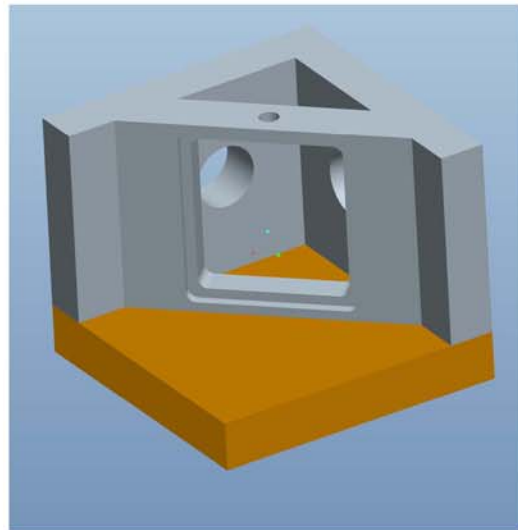
7.2.1 Smaller Sample Volume Experimental Setup

A number of small volume setup utilized in the literature either utilize a single transducer system or use two transducers directly facing each other. However, the confocal arrangement utilized in this study gives a better signal to noise ratio. Moreover, with a rigid system for fixing the transducers, as utilized in the larger volume [See Figure], usually provides more accurate alignment during the experiments. Hence,

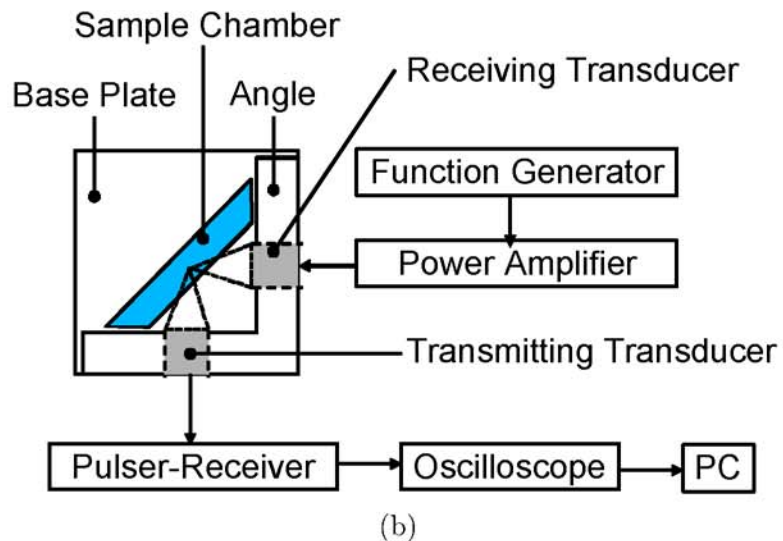
we implemented a modified version of our previous setup with a reduced sample volume. The setup utilized a 90° angle, which was made of polycarbonate, with drilled holes on each wall to allow the insertion of the transducers [See Figure 7.1a]. The angle could also be fixed to the base plate (golden colored in Figure 7.1a). An acoustically transparent film (Saran™ wrap) was wrapped around the frame to provide an enclosure for the samples. It forms two acoustically transparent windows. Care was taken to keep the film taut and well stretched to reduce reflections from the film corrupting the data in our region of interest. When both the frame (wrapped with the film) and the angle fitted with transducers were affixed to the base plate, the confocal regions of the focused transducer aligned halfway between the acoustically transparent windows [See Figure 7.1b]. The entire arrangement was placed in a large container with water to keep the sample chamber and the transducers submerged, while the water level was adjusted to ensure that it did not spill into the sample chamber. The transmit/receive circuitry and the data acquisition process remains same as the larger volume setup described in Section 3.3.4 of Chapter 3.

7.2.2 Ambient Pressure Dependent Subharmonic Measurements

Due to the requirement of a pressurized system, we could not use a small sample volume, which requires use of a thin film like Saran wrap. A more robust setup was required to sustain the overpressure applied during the experiments. Hence, we decided to modify the larger volume setup for these experiments. A three dimensional view of the assembled setup is shown in Figure 7.2. The sample chamber and transducer holding arrangement is exactly similar to the larger volume setup as was the instrumental setup and the data acquisition system. A top plate (also made of polycarbonate) was screwed to the lower assembly to seal the container. The top plate had two holes drilled through it, each with inside threading. One of them was used to connect a digital pressure gauge (SSI Technologies Inc., 1/4 bottom connection Type 316 NPT male, 0-30 psi range). The other hole was used to connect a standard wall black steel threaded pipe nipple (1/4 pipe size, McMasterCarr, Robbinsville, NJ) coupled



(a)



(b)

Figure 7.1: (a) Schematic representation of the experimental setup to measure acoustic scattering *in vitro* using (a) a large sample volume, (b) a small sample volume.

with an aluminum barbed hose fitting (1/4" NPT Male, McMasterCarr, Robbinsville, NJ) and brass check valve (1/4 NPT female, McMasterCarr, Robbinsville, NJ). This entire arrangement provided an unidirectional inlet for air, where as the pipe nipple without the check valve assembly allowed us to fill up or remove the contents from the sample chamber. All the connections were made leak proof by the use of rubber gaskets/o-rings wherever possible. The check valve and barbed hose fitting was further

connected to a plastic tubing. The check valve assembly can be removed to fill up the inside chamber, with water — complete immersion of transducer requires 100 ml of liquid. The valve and hose fitting are then fitted back and tightened properly. The plastic tube was connected to a balloon hand-pump used to pump air into the system and increase the ambient pressure above its atmospheric value. The entire setup was immersed in soap water to identify bubble generation sites indicating air leakage. Those sites were secured using a 3M marine adhesive sealant (No. 5200, Fast Cure). This process was repeated until the entire setup was leak proof. The setup was now ready for performing experiments.

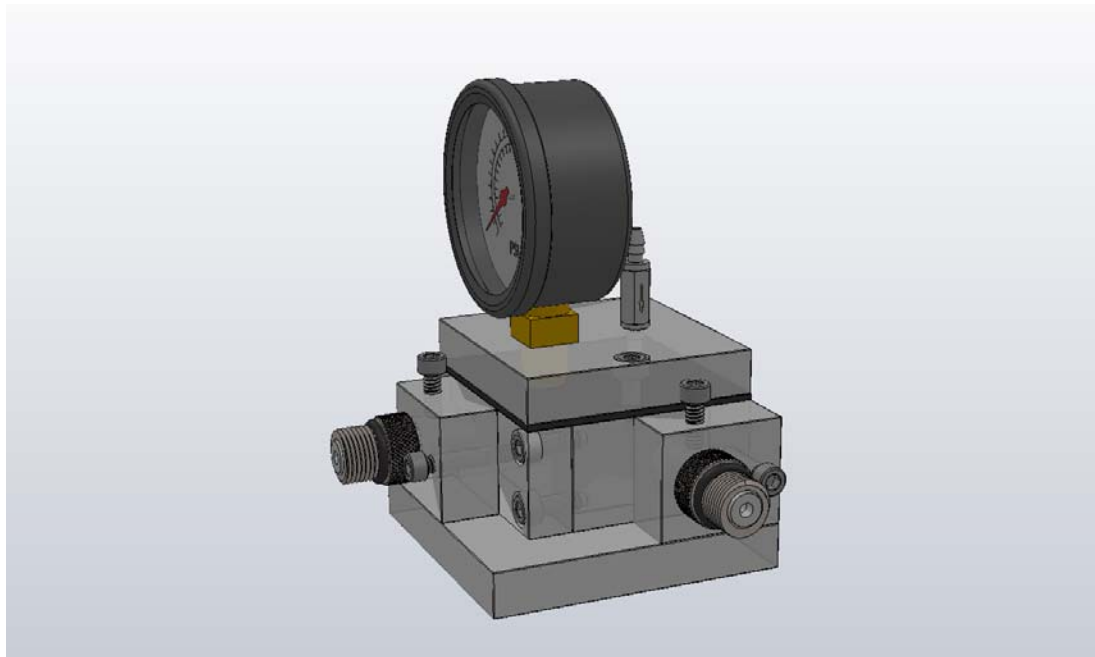


Figure 7.2: A 3-D view of the acoustic setup for measuring ambient pressure dependent subharmonic response.

The check valve and hose fitting assembly was opened and the inside content was emptied out and washed. 100 ml of PBS buffer was poured into the setup and the valve was put back on. The pump was used to increase the ambient pressure to a desired value, monitored using the pressure gauge. Control measurements were acquired using the exact same methodology used for the non-pressurized experiments and saved onto a desktop computer. The valve assembly was reopened to add the contrast microbubbles.

A magnetic stirrer, which was inserted previously before sealing the setup was turned on to obtain homogeneity of the solution. The valve assembly was put back on to seal the setup and pressurized again. The response from the bubble was now recorded using the data acquisition system and saved on the desktop for post processing. This entire process was repeated for changing ambient pressure values, which was varied from 0-200 mm of Hg ambient overpressure. Four runs were acquired at each ambient overpressure and the average of the four runs with corresponding standard deviation errors are plotted for data analysis.

For the preliminary results presented here we used both Definity and PLA microbubbles. Note that we had earlier mentioned that the resonance frequency for these bubbles are 5-6 MHz and 2-3 MHz for Definity and PLA microbubbles respectively. We studied the ambient pressure dependent response from Definity at two excitation frequencies of 3.5 MHz (below resonance) and 10 MHz (above resonance), both at an acoustic pressure amplitude of 500 kPa. The receiver for these two cases were 2.25 MHz and 5 MHz transducers respectively to have maximum sensitivity to the subharmonic response. For Definity microbubbles a dilution of 1:10000 was utilized. For PLA microbubbles we have only studied the response at 3.5 MHz excitation frequency and at an acoustic excitation pressure of 500 kPa. The concentration of PLA bubbles used are same as those employed in their characterization experiments presented in Chapter 10, which is 1.66 $\mu\text{g}/\text{ml}$. The pulse duration for all these experiments were 32 cycles.

7.3 Results and Discussion

7.3.1 Smaller Sample Volume Experimental Setup

We used Definity contrast microbubbles for our setup validation. Definity microbubbles were suspended in PBS buffer at two different dilutions of 1:10000 and 1:2000. Both the larger volume and smaller setup was utilized to acquire response from the bubbles at 3.5 MHz, 500 kPa acoustic excitation condition. Note that avoiding wall reflections from the smaller sample volume mandates the use of a smaller duration excitation — a 8 cycle pulse was used in this experiments unlike the previous

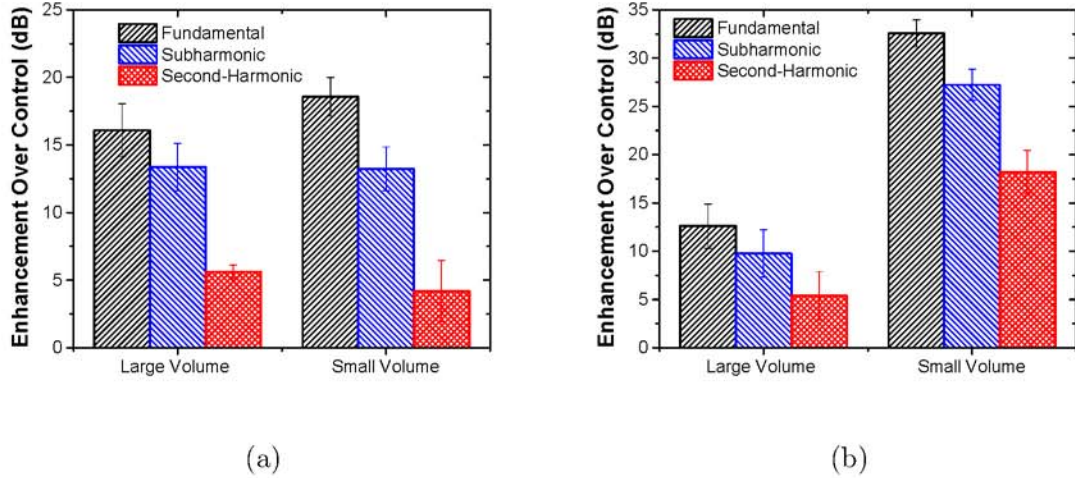


Figure 7.3: Comparison of the scattered response from Definity using the small and large sample volume acoustic setups at a dilution of (a) 1:10000 and (b) 1:2000.

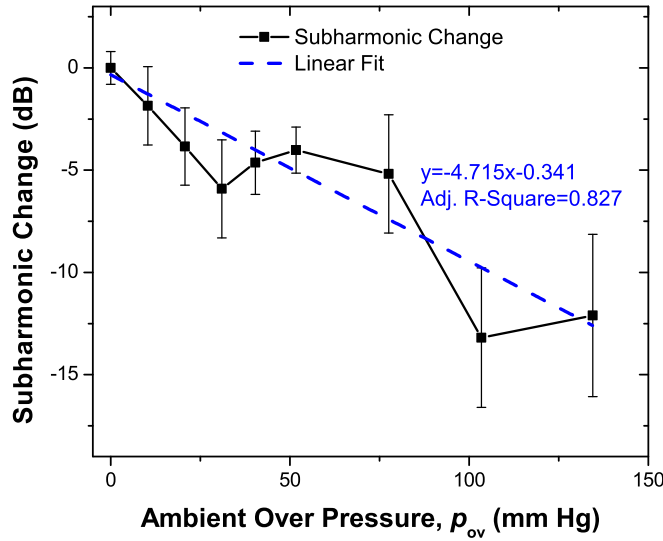
experiments where 32 cycles were used. The results for the two dilutions are shown in Figure 7.3, where we plot enhancement of fundamental, subharmonic and second-harmonic components over control in dB. This was done to ensure direct comparison of data as the baseline noise level for the two setup will be different, thereby changing absolute value of responses in dB. For the lower dilution, roughly corresponding to 1×10^6 bubbles/ml, the results obtained from the smaller and larger sample volume setup are equivalent [See Figure 7.3a]. This validates that our new setup should not play any role to change the nature of acquired data under these bubble concentration. However, as we increased the concentration by five times, the response from the two setups become completely different [See Figure 7.3b]. At this high concentration, the acoustic pulse suffers more attenuation per unit length of travel. For the larger volume setup, the pulse is traveling through a distance of around 6.1 cm through the bubble suspension in contrast to a distance of around 1.5 cm for the smaller volume setup. Hence, for the larger volume setup, almost all of the scattered pulse is damped out before it can be received. This demonstrates the ability of the smaller volume setup to acquire experimental data at higher concentration, whereas the larger volume setup is unsuitable and will give inaccurate results. We subsequently used this setup

for characterization of redox sensitive echogenic polymersomes described in Section 11.4.2.4 of Chapter 11

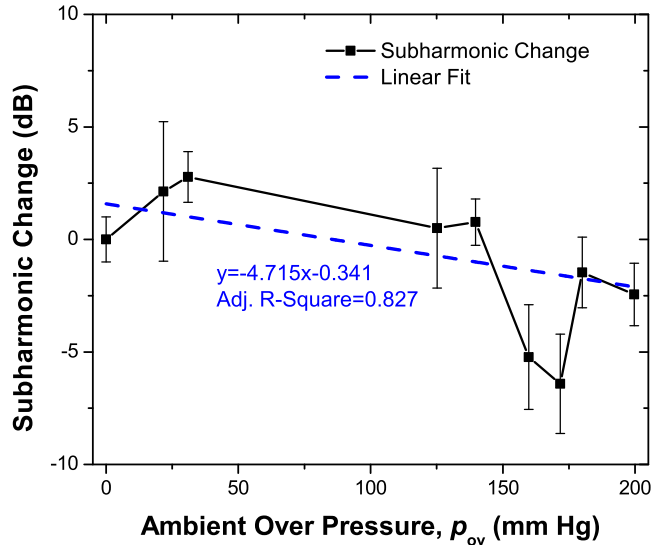
7.3.2 Ambient Pressure Dependent Subharmonic Measurements

Figure 7.4 shows the ambient overpressure (p_{ov}) dependent subharmonic response, plotted as a change (in dB) from its value at zero overpressure for both the excitation frequencies. Note that the overpressure is defined as the contribution to the ambient pressure in addition to the atmospheric pressure i.e., $p_0 = p_{atm} + p_{ov}$. The most notable result was the lack of monotonicity in the response at both the frequencies in contrast to previous reports. At 3.5 MHz excitation we saw a predominantly decreasing trend, with an overall decrease in subharmonic response by around 12 dB over the ambient overpressure range of 0-135 mm of Hg [See Figure 7.4a]. Although, a decrease was seen at 10 MHz excitation too; the trend was highly non-monotonic with maximum decrease of around 5 dB [See Figure 7.4b]. Based on our previously published and ongoing numerical simulation results [314], expected a steady decrease of the subharmonic response at 3.5 MHz excitation ($f_{excitaion}/f_0 \sim 0.7$) and a steady increase at 10 MHz excitation ($f_{excitaion}/f_0 \sim 2.0$). Note that at 10 MHz we see an initial increase upto 50 mm Hg ambient overpressure. We note that simulation results were for a monodisperse system (i.e., single bubble) and hence substantial deviation in the final experimental results are expected. Nonetheless, to the best of our knowledge, this is the first documented attempt to check the role excitation frequency on ambient pressure dependent subharmonic report. These preliminary results are definitely encouraging, justifying the need for further detailed investigations both through experiments and numerical simulations.

To investigate the role of encapsulation material on the ambient pressure dependent subharmonic response we also investigated the response from PLA, a polymer encapsulated microbubble. Figure shows change in subharmonic response (in dB) from PLA microbubbles at 3.5 MHz ($f_{excitaion}/f_0 \sim 1.0$) excitation and 500 kPa acoustic excitation pressure. For PLA microbubble a linear monotonic decrease was observed (R



(a)



(b)

Figure 7.4: Experimentally measured ambient pressure dependent subharmonic response from Definity microbubbles at 500 kPa excitation and an excitation frequency of (a) 3.5 MHz and (b) 10 MHz.

value of 0.95), atleast for the data point collected. The overall change was around 10 dB. Although, we believe more data point should be acquired before substantiating the

claim of a linear decrease, the overall trend with these polymeric bubbles are also consistent with our hypothesis based on our numerical simulations. As before, we reiterate that numerical predictions were based on monodisperse assumptions so a qualitative match should be expected.

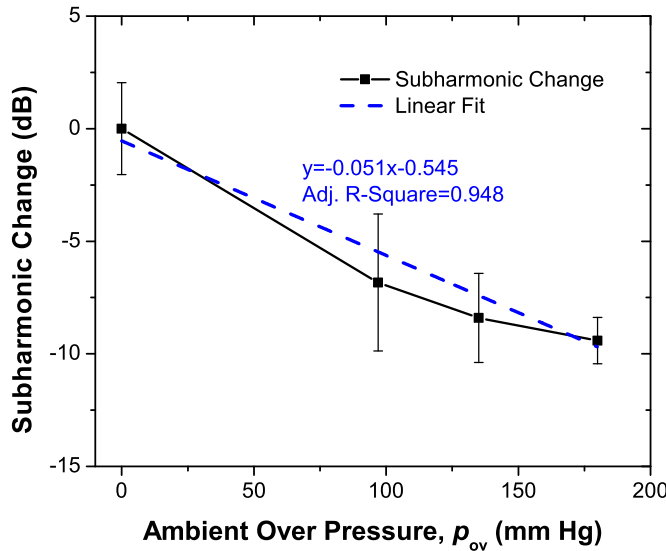


Figure 7.5: Experimentally measured ambient pressure dependent subharmonic response from PLA microbubbles at 3.5 MHz, 500 kPa excitation.

Nonetheless, to the best of our knowledge, this is the first documented attempt to check the role excitation frequency on ambient pressure dependent subharmonic response. These preliminary results are definitely encouraging, justifying the need for further detailed investigations both through experiments and numerical simulations and scope of possible future work in this area will be discussed in the final chapter of this thesis.

7.4 Summary and Conclusion

In this chapter we discussed the design and implementation of two modifications of our existing acoustic experimental setup — one for reducing the sample volume enabling us to perform higher concentration experiments and the other for experimental

measurements of ambient overpressure dependent subharmonic response contrast microbubbles. We validated that the new smaller volume setup gives same results for lower bubble concentrations. However, at higher concentration, where the attenuation of acoustic pulse becomes considerably higher, the smaller volume provides gives more accurate results. Based on the successful implementation of this setup, we utilized it to characterize redox sensitive echogenic polymersomes [Discussed later in Chapter 11]. We also presented our results for the ambient pressure dependent subharmonic response from a lipid coated (Definity) microbubble and a polymer encapsulated microbubble (PLA). Numerical simulations performed by our research group had earlier indicated the role of excitation frequency (more specifically $f_{\text{excitation}}/f_0$). Depending on the excitation frequency subharmonic response was shown to increase monotonically ($f_{\text{excitation}}/f_0 > 1.7$), decrease monotonically ($f_{\text{excitation}}/f_0 < 1.2$) or show a non-monotonic behavior ($1.2 < f_{\text{excitation}}/f_0 < 1.7$) [314]. To the best of our knowledge this is the first study that undertakes the experimental verification of these results. To this goal we two different excitation frequencies with the Definity microbubbles — one at $\sim 2f_0$ and the other at $\sim 0.7f_0$. Our results indicate an overall decrease for both these cases, with a highly non-monotonic variation for the latter case, which provide a qualitative agreement with our hypothesis based on numerical simulations with the assumption of monodispersity. Around 12 dB change observed in the subharmonic response at 3.5 MHz excitation. The change was substantially less at 10 MHz excitation, with a maximum change of around 5 dB. Our limited studies with PLA microbubbles at 3.5 MHz frequency ($f_{\text{excitation}}/f_0 \sim 1$) we saw a monotonic linear decrease with increasing overpressure. Over a overpressure range of 0-180 mm of Hg, a 10 dB decrease in subharmonic response was observed, which is also consistent with our hypothesis based on previously reported numerical simulation results. The encouraging preliminary data makes a strong case for further detailed investigation of the effect of excitation frequency of ambient pressure dependent subharmonic response.

Part II

DESIGN AND DEVELOPMENT OF ‘DUAL-PURPOSE’ ECHOGENIC LIPOSOMES AND POLYMERSOMES

Chapter 8

A REVIEW OF ECHOGENIC LIPOSOMES¹

8.1 Echogenic Liposomes

A number of innovative particulate systems — nanoparticles [43], nanoemulsions [26], quantum dots [315], ‘bubbicles’ [41], vesicles — are presently being developed for healthcare applications. They are aimed at the ‘dual-purpose’ of early accurate diagnosis of diseases — as contrast enhancing agents for medical imaging — and their rapid remediation — as delivery vehicles for therapeutic agents. The effectiveness of these agents critically depends on our ability to engineer them using sound physical principles. Echogenic liposomes, which combine the favorable properties of microbubble based contrast agents and the drug delivering liposomes, falls into this category. Echogenic liposomes were first reported in 1996 [32] and since then have been studied extensively. However, the underlying mechanisms that gives rise to their acoustic properties are still poorly understood. This motivated our research group to initiate a collaborative effort to improve our understanding of these liposome-based contrast agents and develop them as alternative options for the diagnosis and treatment of cardiac diseases and cancer. This chapter will present a detailed review of the existing work, which will provide the background for understanding the results presented in this study and will explain the motivation behind the present study.

8.1.1 The Preparation Protocol for Making Echogenic Liposomes

The echogenic properties of liposomes are critically dependent on their modified preparation protocol. Hence, we will present a detailed discussion of the modified

¹ Parts of the text in this chapter have been adapted from an article under review [7].

preparation protocol highlighting the key steps that are deemed responsible for their echogenic properties. Since the first report of echogenic liposomes in 1996, the preparation protocol has been optimized by Huang and co-workers [106, 107] through years of research to establish a standardized methodology. The updated and detailed methodology proposed by Huang and co-workers can be found in a recent publication [316].

ELIPs can be prepared in a pressurized or a non-pressurized environment. The lipids are mixed in the desired molar ratio in a round bottomed flask and dissolved in an organic solvent e.g., choloroform. The solvent is then evaporated at 40 °C , usually in a rotary evaporator, to obtain a thin film. Residual traces of the solvent are removed by placing the flask under high vacuum overnight. The lipid films are then hydrated with a 0.32 molar(M) mannitol solution in buffer. The hydrating solution can also contain hydrophilic molecules, which will subsequently be encapsulated within the aqueous core of the liposomes. The multilamellar vesicles, formed after the hydration, are bath sonicated for 10 minutes. The resulting solution of liposomes is frozen at -70 °C for 30 minutes followed by thawing at room temperature. Around 3-5 freeze-thaw cycles have been suggested as the optimum number for echogenic liposome production with good encapsulation efficiency. The liposomes are again frozen at -70 °C and lyophilized in a freeze-drying apparatus. The lyophilized dry cake thus obtained is stored at 4 °C until further use. A schematic representation of the preparation protocol is shown in Figure

For the pressurization technique, the sonicated liposomal solution is collected in a screw-cap vial and pressurized by a gas using a syringe. The gas can be air or other bioactive gases like xenon [317], nitric oxide [318–321] etc. The pressurized-gas/liposome dispersion is incubated for 30 minutes and then frozen at -78 °C on dry ice for another 30 minutes, followed by immediate depressurization. The frozen liposomes are thawed at room temperature to cause a temperature drop from -78 °C to 24 °C within 10 minutes.

The lyophilized cakes of ELIPs, obtained either way, are reconstituted in a phosphate buffered saline (PBS) solution for further investigations. Adding 5% by weight of bovine serum albumin (BSA) to the PBS prevents the aggregation of ELIPs

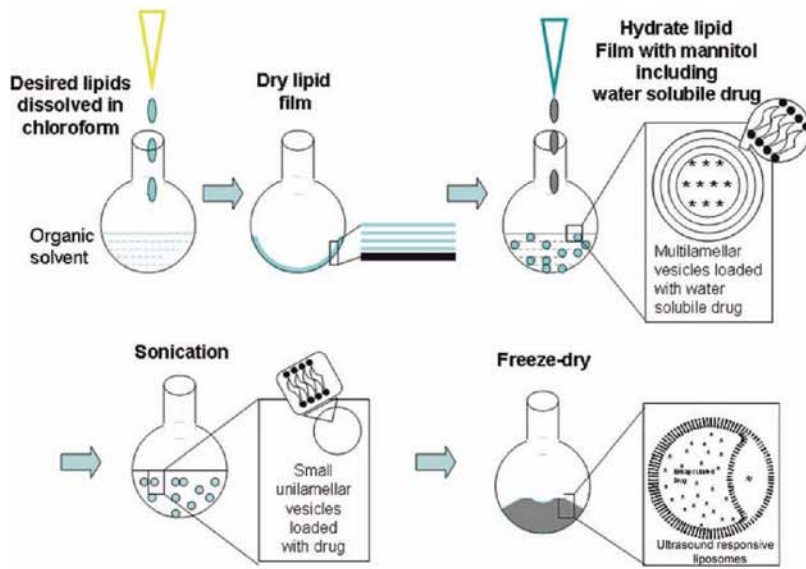


Figure 8.1: A schematic representation of the non-pressurized preparation protocol for producing echogenic liposomes. Reproduced [316] with kind permission from Springer Science and Business Media.

[109] and substantially improves the detection of their acoustic properties. The critical steps in the above-mentioned methodology for echogenicity of liposomes are the freeze-thaw cycles and lyophilization in presence of mannitol, a weak cryoprotectant, and the subsequent reconstitution process in a buffer. It has been proposed that the lipid bilayer develops defects during the freezing steps due to the weak cryo-protection abilities of mannitol [316], thereby exposing the hydrophobic portions of the lipid bilayer. The fluffy dry cake formed after lyophilization also increases the surface area of contact. The air is entrapped through these bilayer defects during the reconstitution phase to form gas pockets stabilized by lipid monolayer [108, 109]. The exact location or dimensions of such structures remains unascertained. Moreover, the protocol also does not guarantee that all the liposomes in the suspension will be associated with such a structure [316]. Nevertheless, the echogenicity of the liposomes prepared following this protocol has been conclusively demonstrated through several independent experiments including the ones in our laboratory described later. Note that the preparation protocol can be further modified to include different lipid formulations and targeting ligands or to replace the entrapped air with other bioactive gases. Two such novel ELIP formulations

with simultaneous imaging and targeted delivering capabilities have been developed by us and will be discussed in a later chapter.

8.1.2 Acoustic Characterization of Echogenic Liposomes

Earliest studies of the echogenicity of ELIPs primarily employed a 20 MHz high frequency intravascular ultrasound (IVUS) catheter for both *in vitro* [32, 106] and *in vivo* [35, 108, 322] characterization. Subsequently their protocol was optimized using the same probe as well as videodensitometry analysis [107, 323] — the mean gray scale values for the region of interest (ROI) were obtained from the quantitative analysis of pixel densities in the images obtained and then used as a measure of echogenicity of the liposomes prepared. However, detailed characterization and understanding of the mechanism of echogenicity can only be achieved through controlled *in vitro* experiments, very few of which have been undertaken when we first started this study.

The first comprehensive *in vitro* characterization of echogenic liposomes was performed by Coussios et al. [324]. They used a 3.5 MHz lightly focused immersion transducer and compared the echogenicity of ELIPs with that of the microbubble based contrast agent Optison®. They reported that the backscattering coefficient of liposomes can be even higher than that of Optison® with the liposomes having higher scattering to attenuation ratio (STAR) [See Section 2.6.1 for explanation]. This demonstrated the potential of ELIPs to be used as ultrasound contrast agents. Kopechek et al. [109] extended this study to a wider range of frequencies for both attenuation and backscattering experiments using single element immersion transducers. Unlike contrast microbubbles, ELIPs showed no defined peak in broadband attenuation in the range of 3-25 MHz. The attenuation was fitted with Church's model for encapsulated bubbles [155, 156] to predict a shear viscosity of 0.30 Pa·s and a shear modulus of 125 MPa, which are equivalent to a dilatational viscosity (κ^s) of 9×10^{-10} N.s/m and an elasticity (E^s) of 0.56 N/m. They also reported a backscattering coefficient of $0.011 - 0.023(\text{cm-str})^{-1}$ in the range of 6-30 MHz resulting in a STAR of 8 to 22%, which is comparable with the values for contrast microbubbles. It must be mentioned

that in spite of using similar preparation protocols, Coussios et al. [324] reported almost no attenuation due to echogenic liposomes, in contrast to the report of Kopechek et al. [109]. Sheng-Chieh et al. [39] followed a similar method to prepare echogenic liposomes with an average size of 1600 ± 200 nm and conducted *in vitro* acoustic studies. They also found no distinct peak in attenuation, but concluded that the resonance lies in the range 7-11 MHz. Their scattering experiments at 10 MHz excitation showed enhancement of both fundamental and second-harmonic responses. However, these liposomes were not found to be very robust with an effective operation time of 10 minutes and a destruction threshold of 150 kPa at 2.25 MHz excitation.

Echogenicity of such liposomes has also been detected with 25 MHz B-mode pulses. Using a Phillips L12-5 linear array transducer system [325], ELIPs were found to generate robust echoes for both continuous 6-9 MHz fundamental and 4-5 MHz harmonic B-mode pulses. A more recent *in vitro* study by Radhakrishnan and co-workers [326] evaluated the performance of ELIPs as a blood pool contrast agent using a physiologic flow phantom. ELIPs were found to be stable in physiologic conditions with proper care. Around 14-17 dB enhancement of echogenicity was reported in citrate-phosphate-dextrose whole blood. Echogenicity was reported to be sensitive to abnormalities of red blood cells and rapid cooling below body temperature. Suitability of ELIPs as contrast agents for passive cavitation imaging have also been reported [327].

Note that none of these above mentioned studies looked at nonlinear response from ELIPs in detail although ELIPs have been associated with cavitation effects [328]. Also, to ascertain the critical role of the various steps involved in ELIP preparation also needs to be ascertained under controlled *in vitro* experiments for a better understanding of the physical mechanisms of echogenicity. This motivated us to carefully examine acoustic properties of echogenic liposomes, which was critical first step for the proof of concept validation.

8.1.3 Ultrasound Triggered Release from Echogenic Liposomes

Since echogenic liposomes retain all favorable properties of normal liposomes, they have been extensively studied as ultrasound triggered drug delivery vehicles [93, 116, 329, 330]. Anti-intercellular adhesion molecule-1 (ICAM-1) [331–334], anti-vascular cell adhesion molecule (VCAM-1), anti-fibrin, anti-fibrinogen and anti-tissue factor conjugated with ELIPs [34, 35] have also been developed to achieve both *in vitro* and *in vivo* targeting. ELIPs can be loaded with both hydrophilic and lipophilic molecules [113]. By suitably modifying the preparation protocol, ELIPs have been made to entrap genes [40], fluorescent molecules like calcein [107, 111, 113, 114] and carboxyfluorescein [115] as drug surrogates, antibiotics [335], peroxisomal proliferator-activated receptor agonists [336], a thrombolytic enzyme rt-PA (recombinant tissue-plasminogen activator) [116, 118, 337, 338], a vasodilator papaverine [113, 339], an anti-diabetic drug rosiglitazone [340, 341] and NF- κ B decoy oligonucleotides [329]. By virtue of its preparation protocol, ELIPs can encapsulate a gaseous phase, which is usually air. However, with suitable manipulations of the preparation protocol, ELIPs can also encapsulate bioactive gases like xenon [317] and nitric oxide [318–321]. Note that in all these studies, incorporation of a payload did reduce the echogenicity of ELIPs significantly.

Fluorescent molecules like calcein [24, 342, 343] and carboxyfluorescein [102, 344] are often used as surrogates for hydrophilic drugs for evaluating triggered release from liposomes. Hence, ultrasound triggered release from ELIPs has also been studied by detecting changes in fluorescence due to the release of calcein or carboxyfluorescein. Huang and MacDonald [111] used a continuous wave ultrasound pulse at 1 MHz frequency and at an output power of 2 W/cm^2 , generated using a Sonitron ultrasound system, for a duration of 10s. Depending on the number of excitation cycles, 30-60% release of contents was reported with no mention of passive release in absence of ultrasound. Huang et al. [107] in a later study used a similar ultrasound system to excite calcein loaded ELIPs with 1 MHz continuous wave ultrasound at 8 W/cm^2 output power for a duration of 10s. Both the passive and ultrasound triggered release (over 10s) from air containing ELIPs was both around 10% indicating negligible effects from

ultrasound excitation. The release improved to about 30% with argon or perfluorocarbon encapsulated ELIPs. Note that none of these studies reported the calibration techniques for determining the actual output power. Kopechek et al. [259] did a detailed calibration of Sonitron systems to show that presence of standing waves can play a critical role in the above mentioned *in vitro* studies — the pressure field can be corrupted due to the constructive and destructive interference. A more detailed study of ultrasound mediated release of calcein was performed by Kopechek and co-workers using color Doppler ultrasound [113]. A CL15-7 linear array transducer was used to generate 6 MHz ultrasound pulses at 2 MPa peak-negative pressure and a PRF of 150 Hz. Although $47.5 \pm 33\%$ release of calcein was reported with ultrasound, no release was observed for the lipophilic drug papaverine in the same study. However, a later study by the same group concluded that the results might be erroneous due to effects of gas bubbles on fluorescence measurements [341]. In this updated study, which used 6 MHz color Doppler ultrasound pulses (1250 Hz PRF and 0.17 W/cm^2 calibrated output power) from CL15-7 transducer, reported no ultrasound mediated release of either calcein or rosiglitazone, even after detection of both inertial and stable cavitation. Smith et al. [116] have however shown therapeutically relevant release of rt-PA from ELIPs using color Doppler ultrasound. Other studies have demonstrated thrombolytic efficacy of rt-PA loaded ELIPs [330, 337, 345]. Buchanan et al. [329] had studied ultrasound mediated release of oligonucleotides (ODN) using a Sonitron 1000 system to generate 1 MHz continuous wave ultrasound at a peak negative pressure of 0.26 MPa for a duration of 60s. Around 42% release of ODN from ELIPs was reported compared to around 18% release from non-echogenic liposomes. However, it is not clear if their measurements are also susceptible to changes caused by the presence of gas bubble as mentioned earlier.

It is evident from the preceding discussion that ultrasound mediated release of liposomal contents is often uncertain and susceptible to several other factors that can critically affect the release efficiency. Moreover, the release is not always optimal, ranging from 20-50%. This motivated us to pursue the development of echogenic liposomes

with dual release triggers — a combination of a different exogenous or endogenous trigger with ultrasound — to achieve considerably higher amount of contents release. Till date we have developed two such ELIP formulations: a substrate lipopeptide conjugated ELIP formulation that can be triggered (or cleaved) by the extracellular enzyme matrix metalloproteinase-9 (MMP-9) [115] and a polymer coated redox triggered ELIP formulation capable of cytosolic drug delivery [114], which will be discussed in detail in Chapter 11. We will also discuss briefly another liposomal formulation with pH tunable echogenicity and release characteristics currently under development.

This concludes our review of the existing studies on the behavior of echogenic liposomes. In the following chapter we will discuss the research undertaken in this study for detailed characterization of the acoustic properties and release characteristics for echogenic liposomes for developing ‘dual-purpose’ ultrasound contrast agent with the simultaneous imaging and drug-delivery potential.

Chapter 9

ACOUSTIC CHARACTERIZATION OF ECHOGENIC LIPOSOMES: *IN VITRO* ATTENUATION AND SCATTERING MEASUREMENTS¹

9.1 Introduction

In the previous chapter, we discussed the research that had been undertaken to characterize the acoustic properties of ELIPs. We realized that before attempting a development ELIPs, we need a more fundamental understanding of the acoustic properties through detailed *in vitro* studies under a controlled environment. Our aim here is to understand the linear and nonlinear acoustic responses from these liposomes including the effects of components in the preparation protocol that are believed to be critical for echogenicity. Towards that goal, here we report the measurement of frequency dependent attenuation coefficient and linear and nonlinear scattered responses of ELIP prepared with varying concentrations of mannitol. Note that nonlinear responses from contrast agents are utilized for harmonic [56, 346] and subharmonic imaging [268, 347–350]. Hence, characterization of nonlinear responses can help in appraising the effectiveness of ELIP for such nonlinear imaging modalities with potentials for higher contrast-to-tissue ratio. As explained in previous chapters for lipid and polymer coated microbubbles, acoustic responses also help in determining the material properties of the encapsulating shells [163, 169], and this approach has recently been extended to ELIP [109].

¹ Figures and text in this chapter have been adapted from the a previously published [110] article.

9.2 Materials and Methods

9.2.1 Preparation of Echogenic Liposomes and Reconstitution Procedure

Stock solutions of lipids were prepared by dissolving the lipid powders in chloroform - methanol (9:1) mixture and stored at -20 °C in the following concentrations: 10 mg/ml for 1, 2 - dipalmitoyl - sn - glycero - 3 - phosphocholine (DPPC) and 1 mg/ml for 1, 2 - dipalmitoyl - sn- glycero - 3 - phospho - (1'-rac-glycerol) (DPPG), 1, 2 - dihexadecanoyl - sn - glycero - 3 - phosphoethanolamine (DPPE), cholesterol (CH) (Avanti Polar Lipids, Alabaster, AL, USA). The lipids in desired lipid molar ratio (DPPC: DPPG: DPPE: CH in 69:8:8:15) were taken in a 50 ml round bottom flask. The flask was gently shaken to form a uniform solution. A thin lipid film was obtained by evaporating this mixture in a rotary evaporator at 40 °C for about 5-10 minutes. The thin film was then dried in a vacuum desiccator overnight to remove all residual organic solvents. The dry lipid film was hydrated with 3 ml of 0.32 M mannitol (Alfa Aesar, MA, USA) solution. The solution was then sonicated for 10 minutes using a bath sonicator, and frozen at -70 °C for 30 minutes followed by thawing the frozen liposomes to room temperature. This freeze-thaw cycle is repeated 5 times. The frozen liposomes were subsequently lyophilized using a freeze-drying apparatus (Labconco, MO, USA) for 24 h. The lyophilized dry cake of echogenic liposomes were stored at 4 °C until use, when it is reconstituted at desired concentration before an experiment. ELIPS were reconstituted in a phosphate buffered saline (PBS) with 0.5% by weight bovine serum albumin (BSA). Appropriate amounts of powder were measured for each experiment and added to 150 ml of the PBS-BSA solution, already poured in the sample chamber to have the desired lipid concentration. Liposomes prepared using 320 mM mannitol has 1 mg of lipids in every 6 mg of lyophilized powder. The PBS-BSA solution is prepared by adding 2.5 g of BSA powder to 500 ml of PBS buffer. The mixture is then thoroughly shaken and kept refrigerated for a minimum of 48 hours before use.

Size measurements were acquired using dynamic light scattering instrument Zetasizer Nano-ZS described in Section 3.1.1. To determine the morphology of the

ELIPs and to have another independent measurement of vesicle size and structures, we also acquired microscopic images with both TEM and AFM using the methodology described in Sections 3.2.2 and 3.2.1.

Both attenuation and scattering measurements were performed using the larger volume setup discussed in Sections 3.3.3 and 3.3.4. For attenuation experiments, four different unfocused broadband transducers were used in transmit-receive mode with center frequencies of 2.25, 3.5, 5 and 10 MHz. Attenuation coefficients were measured for three different lipid concentrations of 3.33 $\mu\text{g}/\text{ml}$, 6.67 $\mu\text{g}/\text{ml}$ and $\mu\text{g}/\text{ml}$ at a peak negative pressure of 100 kPa. Scattering experiments employed a 3.5 MHz focused transducer as the transmit transducer and a 5 MHz focused transducer as the receiver. Scattering experiments were performed at a lipid concentration of 1.67 $\mu\text{g}/\text{ml}$. A magnetic stirrer was used to ensure homogeneity before starting acoustic excitation and during the course of experiments.

9.3 Results and Discussion

9.3.1 Size Distribution

Table 9.1: Average diameter and the polydispersity index of ELIPs (as measured by DLS) as a function of mannitol concentration. Reprinted from [110] with permission from Elsevier.

Mannitol Conc. (mM)	Averaged Diameter (nm)		Polydispersity Index
	Intensity	Number	
No mannitol	65 ± 7	64 ± 7	1.00 ± 0.00
5	1293 ± 474	125 ± 14	0.63 ± 0.03
10	733 ± 400	134 ± 15	1.00 ± 0.00
15	640 ± 466	122 ± 11	1.00 ± 0.00
50	500 ± 65	173 ± 31	0.72 ± 0.07
100	336 ± 7	171 ± 2	0.63 ± 0.04
150	512 ± 87	185 ± 8	0.73 ± 0.09
200	972 ± 129	180 ± 14	0.86 ± 0.01
250	374 ± 18	170 ± 34	0.63 ± 0.01
320	459 ± 35	152 ± 15	0.83 ± 0.07
350	623 ± 12	181 ± 14	$0.850.02$

Table 9.2: Comparison of previously reported size distribution measurements with ELIPs.

	Kopechek et al.	Paul et al.
Number averaged diameter	65 nm	150 nm
Range of particle sizes detected	30 nm-6 μ m	100 nm-2 μ m
Polydispersity Index (PDI)	Not reported	0.63-1.00

Table 9.1 shows the intensity averaged diameter, obtained by averaging the radius distribution weighted with the intensity of the scattered light, and the number averaged diameter for the ELIP prepared with varying amounts of mannitol (measured with DLS). The polydispersity from the DLS measurements are also reported in the same table. The average diameter is 125-185 nm depending on the mannitol concentration. The polydispersity indices are observed to be high (0.63 – 1.0) indicating that the liposomal formulations have a large range of sizes. In order to corroborate these observations, ELIPs prepared with 320 mM mannitol were imaged employing a transmission electron microscope (TEM) and an atomic force microscope (AFM). Although some changes to the vesicular structure are expected under the sample preparation conditions [351], the TEM image (Figure 9.1a, magnification: 7900) indicates considerable variations in the size of the liposomes. Similar results can also be observed by the AFM imaging studies (Figure 9.1b). Both show liposomes with diameters of 1 micron and above. We believe that these larger liposomes (although far less in number compared to those with diameters in the nanometer range) are crucial for the echogenicity observed below. They can contain a large enough air pocket inside the bilayer that oscillates while excited to generate the linear and nonlinear scattered responses. Size distribution of echogenic liposomes, prepared using the exact same protocol, was also measured independently by Kopechek et al to facilitate their acoustic characterization experiments. They reported similar polydisperse nature of echogenic liposomes but with significantly different size distribution [See Table 9.2]. This indicates that conventional sizing techniques like dynamic light scattering and Coulter counter measurements might not be accurate for such highly polydisperse size distribution.

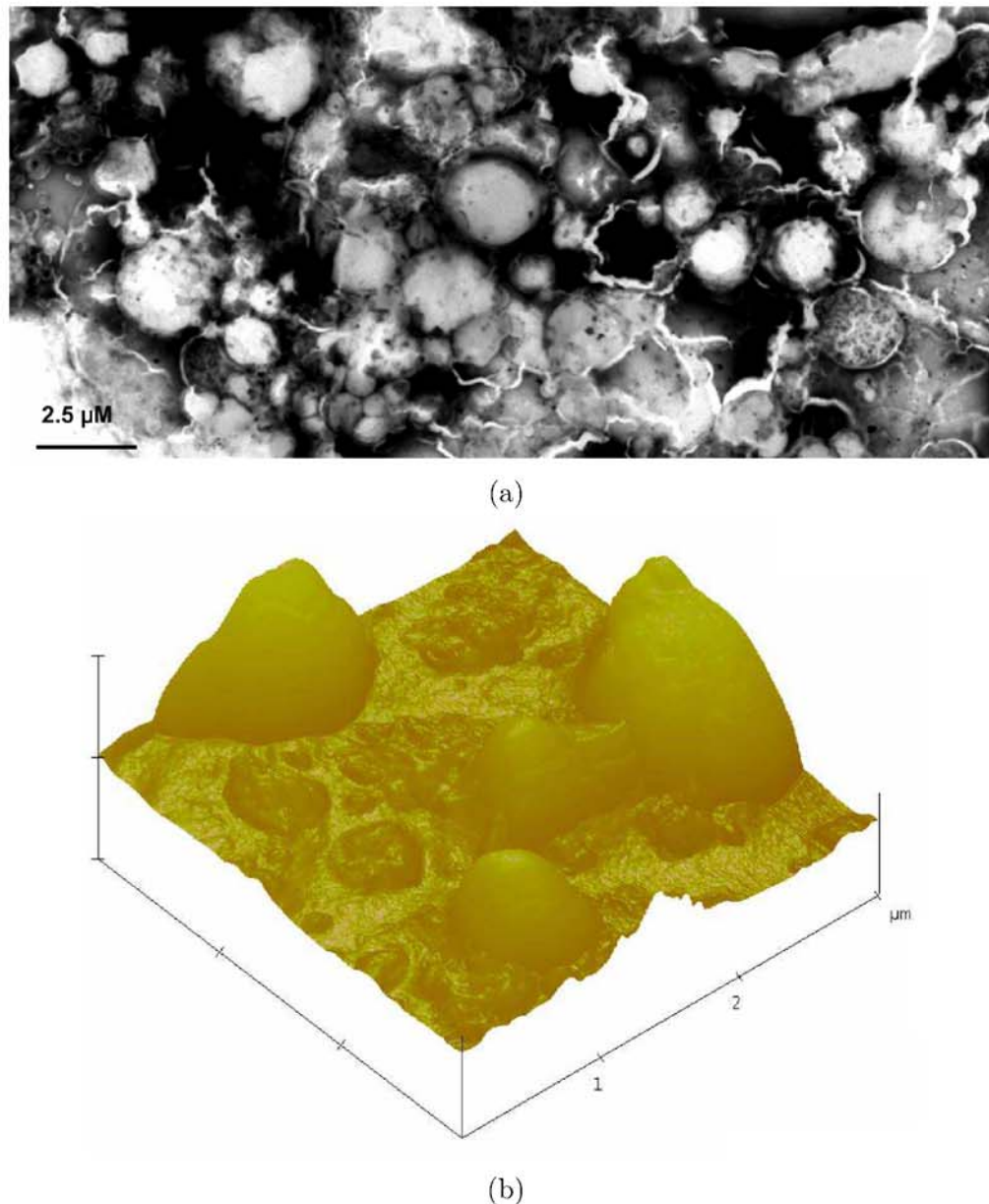


Figure 9.1: (a) TEM (b) AFM images of echogenic liposomes. Reprinted from [110] with permission from Elsevier.

9.3.2 Attenuation

The attenuation measurements conducted for echogenic liposomes were used to generate the frequency dependent attenuation using the data reduction technique described in Section 3.3.3 and shown in Figure 9.2. The attenuation coefficients are shown for each transducer within its bandwidth. The data obtained with different transducers

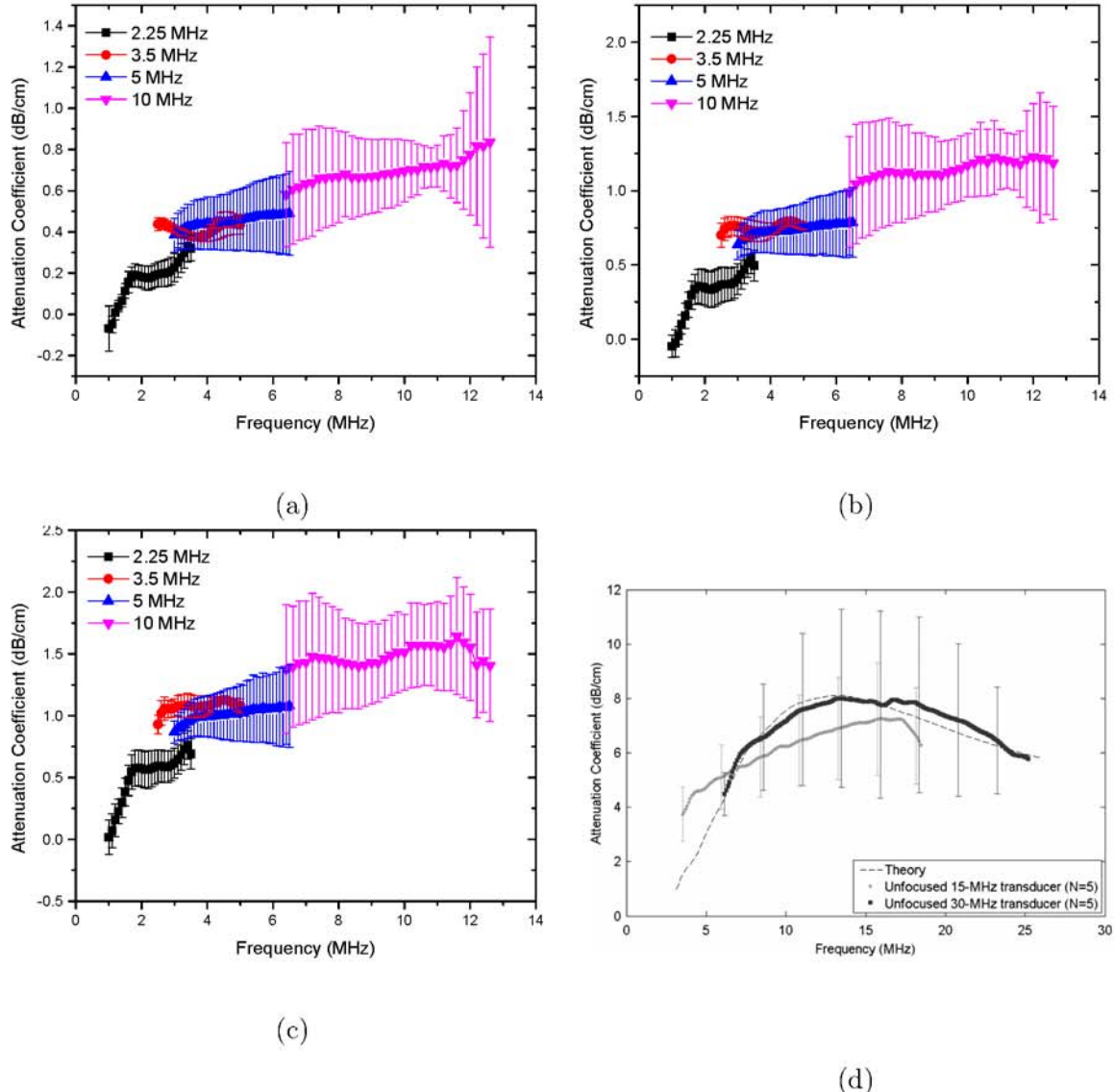


Figure 9.2: Frequency dependent attenuation coefficient of echogenic liposomes measured with four different transducers (2.25, 3.5, 5, 10 MHz) and plotted within their respective -6 dB bandwidth for lipid concentrations of (a) 3.33 $\mu\text{g}/\text{ml}$ (b) 6.67 $\mu\text{g}/\text{ml}$ and (c) 10 $\mu\text{g}/\text{ml}$. Data averaged for 5 different samples. Figures (a),(b) and (c) are reprinted from [110] with permission from Elsevier. (d) Attenuation coefficient of ELIPs measured by Kopechek et al. [109]. Reprinted from [109] with permission. Copyright [2011], Acoustical Society of America.

match in the region of overlapping frequencies. The frequency dependent attenuation coefficient shows a continuous increase with increasing frequency for frequencies lower than 5MHz. Beyond 5 MHz the frequency dependent attenuation curves show a flat

response. For the entire range of frequencies studied here (1-12 MHz), the attenuation curve does not show any peak. A peak in attenuation for a suspension of conventional contrast agents indicates the average resonance frequency for the encapsulated contrast microbubbles. Note that a free bubble with a diameter of 150 nm (average diameter of these liposomes) has a resonance frequency 40 MHz. Typically an air pocket of this size within a liposome would have an even larger resonance frequency because of the increased elasticity of the part of the bilayer. Therefore, it would lead to very little acoustic response in the range investigated here. However, note that the large polydispersity indices reported above indicate a broad size distribution including diameters over a micron (Figure 9.1 clearly shows liposomes with micron range diameters). We believe that the attenuation and scattered responses from the liposomal solution are primarily due to the air pockets entrapped in these larger liposomes. Note also that, for a broad distribution with sizes predominantly at the sub-micron level, attenuation is expected to show increase and then gradual flattening at higher frequencies. Experimental measurements of attenuation coefficients in Definity® by Goertz et al. [207] showed that for a broader size distribution, the attenuation curve is flatter in comparison to the response from a manipulated bubble population with a sharper cut-off in size distribution. Experimental observations by Gong et al. [248] using lipid coated microbubbles also showed that as the size distribution becomes broader, the attenuation curve tends to be wider and flatter, with a less distinct peak. Moreover, attenuation studies conducted by Kopechek et al. [109] also shows similar response from ELIPs in 5-25 MHz range [See Figure 9.2d]. The larger error bars associated with the attenuation data from both the previous reports can be attributed to the inherent variability in the acoustic properties of ELIPs, possibly due to their high polydispersity. It should also be mentioned that Kopechek et al. assumed the volume of the gas pocket to be 18% of the entire range of liposomal size to obtain the fitting using Church's model for encapsulation. Since, no conclusive experiments have validated this assumption, we did not attempt to fit our attenuation data with any model to obtain material parameters.

Figure 9.3 shows that the attenuation at the central frequency for each transducer increases linearly with concentration. This indicates that for the lipid concentrations used, resulting liposome concentration is dilute enough, that multiple scattering effects are negligible. Therefore, the analysis employed to obtain the attenuation data is correct. We conclude that the attenuation is primarily due to the larger liposomes, and lack of a peak in the spectra is due to the broad size distribution.

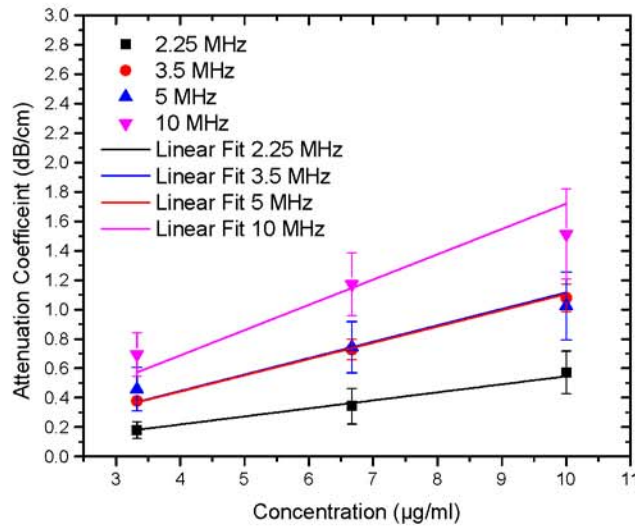


Figure 9.3: Attenuation coefficient at the central frequencies of the four transducers as a function of lipid concentration. Reprinted from [110] with permission from Elsevier.

9.3.3 Scattering

The scattered response from contrast microbubbles depends strongly on the acoustic pressure amplitude, indicating a non-linear response [50, 163, 352]. Five sets of measurements were acquired for each of the acoustic pressure amplitudes. In Figure 9.4, we show the FFT of the scattered response from ELIP for two different acoustic excitations — 50 kPa and 600 kPa. Note that, only the data corresponding to the higher pressure has a distinct third harmonic contribution. However, even at the higher pressure, we do not see a distinct subharmonic peak, in contrast to what has been observed for conventional contrast agents used in subharmonic imaging [50, 163, 268],

[352]. The mean of five data sets and the corresponding standard deviations are then plotted in Figure 9.5. The fundamental response shows around 15-20 dB enhancement over the data without any liposomes. It also shows a consistent increase (linear in the log-log plot) with increasing acoustic excitation amplitude until 400 kPa. Beyond this pressure, the response starts to saturate, indicating possible liposomal destruction at these higher acoustic excitations. The second harmonic response also shows similar enhancement, increasing linearly till acoustic pressure amplitude of 400 kPa, and then saturation. In view of the absence of subharmonic peak, ELIPs might not be suitable for non-destructive subharmonic imaging applications. However, these liposomes are clearly echogenic with a 15-20 dB enhancement in signal over control (see also Figure 9.6). Ordinary liposomes with an aqueous interior are not echogenic. We believe that the echogenicity of these liposomes is primarily due to the air entrapped in the bilayer of the liposomes with diameters larger than one micrometer as visible in Figure 9.1.

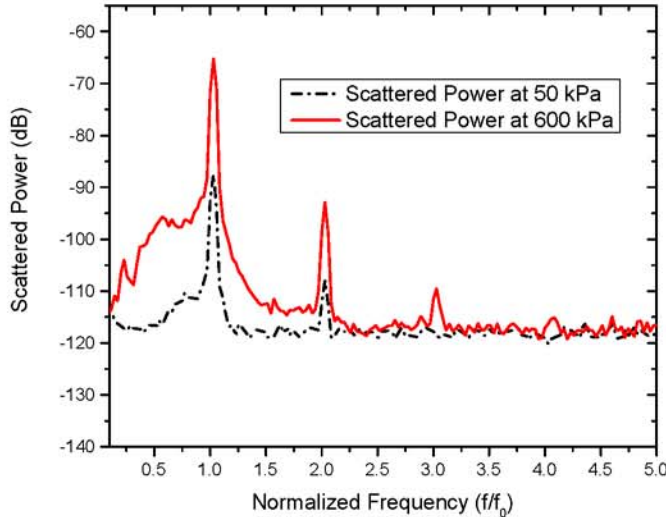


Figure 9.4: FFT of the experimentally acquired scattered signal from liposomes for acoustic pressure amplitudes of 50 kPa and 600 kPa. Reprinted from [110] with permission from Elsevier.

Mannitol and lyophilization are reported to play critical roles in the echogenicity of these liposomes [106–108]. In an effort to have a better understanding of their

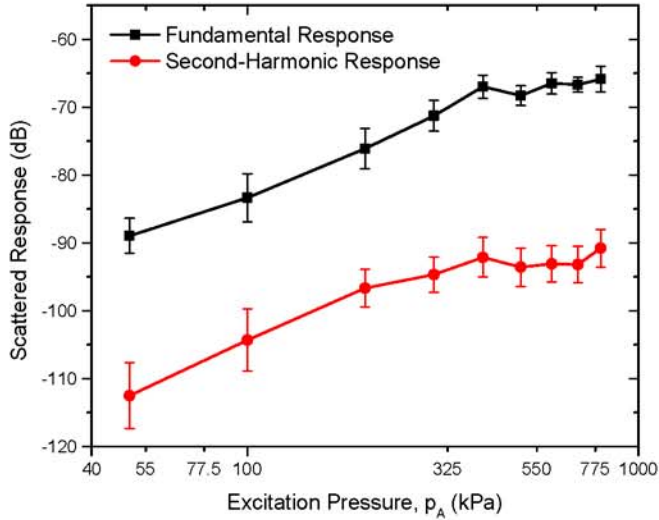


Figure 9.5: Measured scattered response from echogenic liposomes at fundamental and second harmonic frequencies. Reprinted from [110] with permission from Elsevier.

role and to determine the optimal concentration of mannitol, liposomes were prepared without lyophilization and with varying amounts of mannitol (0 mM to 350 mM), and then tested for echogenicity. Note that such studies have been performed before for echogenic liposomes, with a different chemical composition, using an IVUS catheter [106, 111]. While one of the previous studies showed existence of an optimal mannitol concentration [106], another showed consistent monotonic increase of echogenicity with increasing mannitol content [111]. It has been reported that mannitol content also affects the encapsulation efficiency [111, 316]. The adopted mannitol concentration of 320 mM for most of our studies was reported to be the optimal concentration for both echogenicity and encapsulation efficiency [107, 316]. Also note that here we investigate the effects of mannitol concentration variation on the nonlinear (second harmonic) response that has not been investigated before.

Figure 9.6 plots the fundamental and second harmonic responses from liposomes prepared with four different formulations: with and without freeze-drying (lyophilization), and with and without mannitol added during preparation. It shows that without

freeze-drying and mannitol addition, liposomes are not echogenic. In Figure 9.7, responses from liposomes prepared with different mannitol concentrations are shown. Lipid concentration used in all cases is 10 $\mu\text{g}/\text{ml}$. Both fundamental and the second harmonic responses from ELIP prepared with increasing concentrations of mannitol show increasing response till 50 mM, but above 100 mM, they show very little variation. The response from liposomes prepared without mannitol is the same as the control. Therefore, we conclude that a finite nonzero amount (100 mM) of mannitol is required for ensuring sufficient echogenicity. The lack of echogenicity without the lyophilization/reconstitution step in the preparation protocol has also been observed previously [108] .

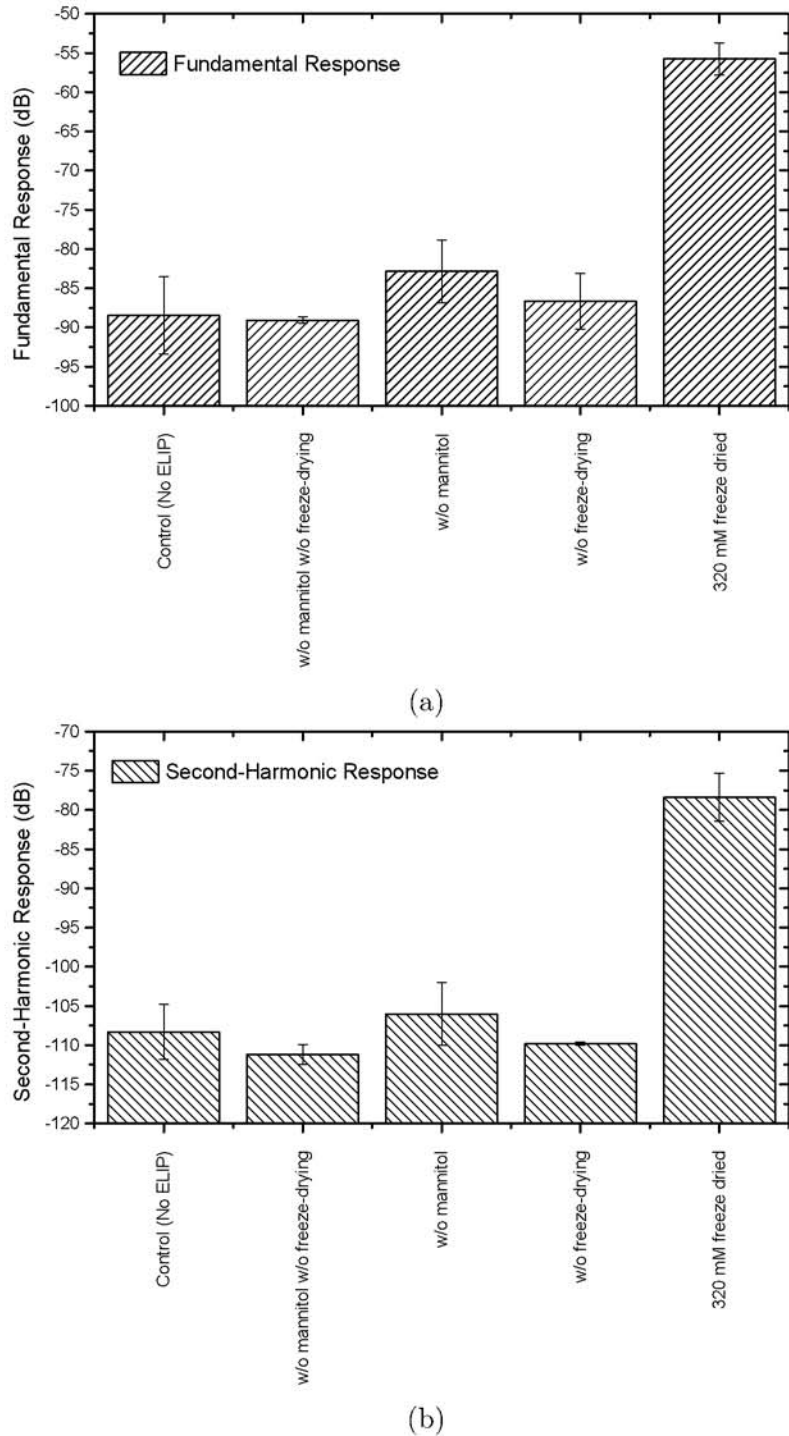


Figure 9.6: Scattered response at an acoustic excitation of 500 kPa and 3.5 MHz from liposomes prepared with and without mannitol and with and without freeze-drying (lyophilization) at: (a) fundamental and (b) second harmonic frequencies. Reprinted from [110] with permission from Elsevier.

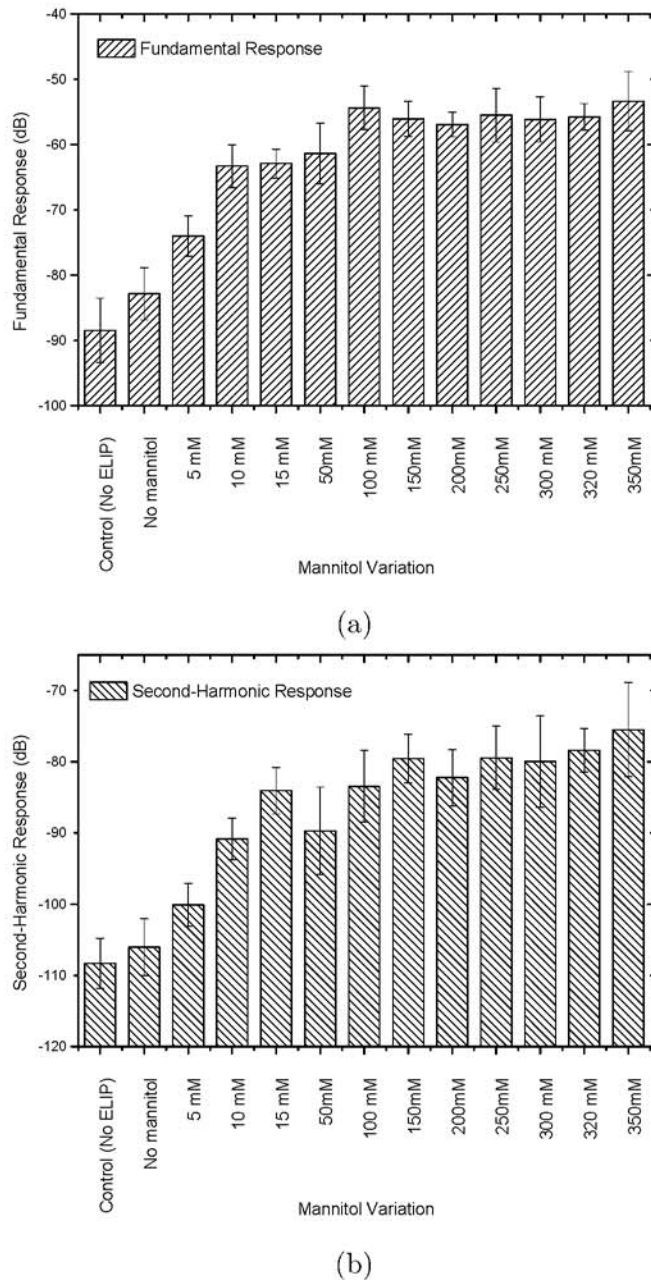


Figure 9.7: Comparison of scattered response from echogenic liposomes prepared with different amounts of mannitol at: (a) fundamental and (b) second harmonic frequencies and at an acoustic excitation of 500 kPa and 3.5 MHz. Reprinted from [110] with permission from Elsevier.

9.4 Summary and Conclusions

Echogenic liposomes prepared using a previously published technique was experimentally examined. The average diameter of these liposomes, measured using dynamic light scattering, was found to be 125-185 nm. However, the large polydispersity also indicates a broad size distribution. More specifically, TEM and AFM studies indicate many liposomes with diameters of 1-2 μm . Both frequency dependent attenuation and excitation dependent nonlinear scattered responses are measured. Attenuation of 0.1-0.7 dB/cm is measured in a liposomal solution containing 3.33 $\mu\text{g}/\text{mL}$ of lipids using four transducers with central frequencies 2.25, 3.5, 5, 10 MHz. The data show an increase and later saturation with frequency but no clear peak. Such a data is consistent with the broad size distribution of these liposomes. The scattered response shows a 15-20 dB enhancement of fundamental and second harmonic responses demonstrating conclusively that the liposomes are echogenic. Therefore, they are suitable for fundamental as well as harmonic imaging applications. However, no subharmonic response is found. We believe that the attenuation and the fundamental and harmonic responses are generated by larger liposomes (diameter $> 1 \mu\text{m}$) that are shown to be present in the size distribution. They entrap air in the lipid bilayer during the specialized preparation protocol.

Mannitol is thought to be of critical importance as a weak cryoprotectant to ensure rupture in the lipid film entrapping air and thereby making liposomes echogenic [108]. Here, by measuring scattered responses from liposomes prepared with varying mannitol concentrations (0-350 mM), we demonstrate that a low but finite amount of mannitol (~ 100 mM) is critical for ensuring echogenicity. Lyophilization is also critical since without it liposomes are found to be nonechogenic.

Although these studies have demonstrated the potential of ELIPs as ultrasound contrast agents, there remains important unanswered questions relating to the exact cause of echogenicity. There is a need to determine the exact location and dimension of gas pockets. This problem has eluded researcher since the first report of echogenic

liposomes, fueling the skepticism regarding their echogenicity. There have been microscopic pictures that suggests gas pockets [109, 114, 353]. However, those pictures are not as conclusive as one would like them to be so that it can end the decade long debate about these purported gas pockets. In our personal experience, these pictures have been extremely difficult to obtain. Even if these gas pockets exist, their dimensions will be too small to have a scattering cross-section large enough to be detected accurately by 1-10 MHz acoustic waves. Experimental evidences however, clearly show that the echogenicity is only achieved when the modified preparation protocol is followed. We believe that the echogenicity is primarily due to the existence of a smaller fraction of larger liposomes, which will have larger gas pockets. Presence of larger vesicles is indicated by the high polydispersity index of dynamic light scattering measurements with ELIP suspensions. Atomic force microscopic images (AFM), shown in 9.1b, also show the presence of different sized vesicles, even with micron range diameters. However, due to lack of conclusive evidence, existence of separate lipid monolayer coated microbubbles in the suspension, which may be created during the preparation of liposomes, cannot be completely ruled out.

Chapter 10

ACOUSTIC CHARACTERIZATION OF *POLYMERIZED ECHOGENIC LIPOSOMES*

The nonlinear scattering experiments with ELIPs presented in the previous chapter for diagnostic frequency ultrasound (less than 10 MHz) showed lack of distinct subharmonic response for the acoustic excitation pressure range of 50-800 kPa. Presence of subharmonic response in the scattered spectra can be utilized for subharmonic imaging modalities which usually offer better signal to noise ratio [268]. Hence, in this paper we investigate one such novel liposomal formulation with a polymerized bilayer that can offer superior nonlinear scattering properties and enhanced stability in circulation.

Polymerization can form a stronger association of the molecules in the stabilizing layer, which gives rise to increased stability and strength. Moreover, polymerization is a more flexible technique; it offers a much better control over the properties of the encapsulation like stiffness or elasticity. There have been many reports of polymerized liposomes for various applications like detection of antibodies [354], controlled drug delivery [355–357], colorimetric detections [358], multicolor printing [US Patent Application Number- 2008/0286483] [359] and colorimetric biosensors [360]. However, such polymerized liposomes have not yet been studied as potential multipurpose ultrasound contrast agents that can take advantage of the enhanced bilayer stability and strength. To this goal, we prepared echogenic version these polymerized liposomes (Pol-ELIPs) and characterized their acoustic properties.

The present study reports comprehensive acoustic characterization of these novel Pol-ELIPs through *in vitro* scattering and attenuation experiments along with detailed comparisons with their normal counterpart studied in the previous chapter.

10.1 Materials and Methods

10.1.1 Preparation of Polymerized Echogenic Liposomes

1, 2 - bis(10,12-tricosadiynoyl) - sn - glycero - 3 - phosphocholine (PC), 1, 2 - bis(10,12-tricosadiynoyl) - sn - glycero - 3 - phosphoethanolamine (PE) were purchased from Avanti Polar Lipids. Using a syringe, the lipids were mixed in the molar ratio of 90:10 (PC:PE) or 80:10:10 (PC:PE:cholesterol) in an amber colored round bottomed flask (RBF) and then added to 1 ml of chloroform to form an uniform solution. The RBF was then slowly rotated on rotary evaporator at 50 °C for 5-10 minutes, with the vacuum on, to evaporate all the solvent and obtain a thin film of lipid. The RBF was kept under vacuum for 3 hrs to overnight to remove any residual traces of the solvent. The dried lipid film obtained was then hydrated with 0.32 M mannitol solution (58.3 g in 1000 ml) by continuous rotation of the flask at 220 rpm for 1 hr in a water bath at 60 °C to get a final lipid concentration of 0.5 mg/ml. The lipid dispersion was then bath sonicated for 10 minutes, followed by an exposure to 3-5 freeze (-70 °C) and thaw (room temperature) cycles. The liposomal dispersion was then transferred to a quartz beaker with magnetic stirrer bar. Polymerization was achieved through ultraviolet irradiation at 254 nm for 30 minutes using a 400 W lamp resulting in a color change from clear colorless to pink-violet colored dispersion. Color change of the dispersion indicated completion of the polymerization process. Polymerized liposomal dispersion was then frozen to -70 °C and lyophilized until it dried completely. The lyophilized liposomal powder was stored at 4 °C and reconstituted at desired concentration when needed. The conventional ELIPs without polymerization were prepared following a well established protocol discussed in earlier chapters.

Size measurements were acquired using dynamic light scattering instrument Zetasizer Nano-ZS described in Section 3.1.1.

Both attenuation and scattering measurements were performed using the larger volume setup discussed in Sections 3.3.3 and 3.3.4. For attenuation experiments, two unfocused broadband transducers were used in transmit-receive mode with the center frequencies of 2.25 MHz and 10 MHz. Attenuation coefficients were measured at a lipid

concentrations of 10 $\mu\text{g}/\text{ml}$ and at a peak negative pressure of 50 kPa. The stability of the Pol-ELIPs was also examined under sustained acoustic excitation, similar to our studies using PLA microbubbles, using the time dependent attenuation experiments explained in Section 3.6. Scattering experiments employed two focused transducer as the transmitters with center frequencies of 2.25 MHz and 3.5 MHz. A 5 MHz focused transducer was used as the receiver. Scattering experiments were performed at a lipid concentration of 1 $\mu\text{g}/\text{ml}$. A magnetic stirrer was used to ensure homogeneity before starting acoustic excitation and during the course of experiments. To further verify the echogenic nature of these ELIPs, ultrasonic images of the ELIPs were also acquired using a clinical scanner as described in Section 3.3.6.

10.2 Results and Discussion

10.2.1 Size Distribution

Figure 10.1 shows the size distribution measurements using dynamic light scattering for Pol-ELIP suspensions both before and after lyophilization. We observed a significant increase in the size of particles present in the suspension after the lyophilization step. This is due to the critical lyophilization step in the preparation protocol that ensures the entrapment of air within the liposomes thereby making them echogenic [108, 109]. We also observed the presence of liposomes for a large range of sizes [1.5-7.0 μm in diameter] in the suspension. We also present here in Table 10.1 the average sizes and polydispersity indices measured for polymerized liposomal suspensions before and after lyophilization. Note that suspensions of lyophilized Pol-ELIPs have a larger average size ($\sim 3 \mu\text{m}$) compared to normal ELIPs in suspension ($\sim 152 \text{ nm}$) discussed in the previous chapter. This can play a critical role in determining their acoustic behavior for the range of excitation frequencies studied here.

10.2.2 Ultrasonic Imaging

The echogenicity of the Pol-ELIPs was confirmed using an ultrasonic medical imaging system (Terason t3200) with a 4-15 MHz transducer. Figure 10.2 shows two

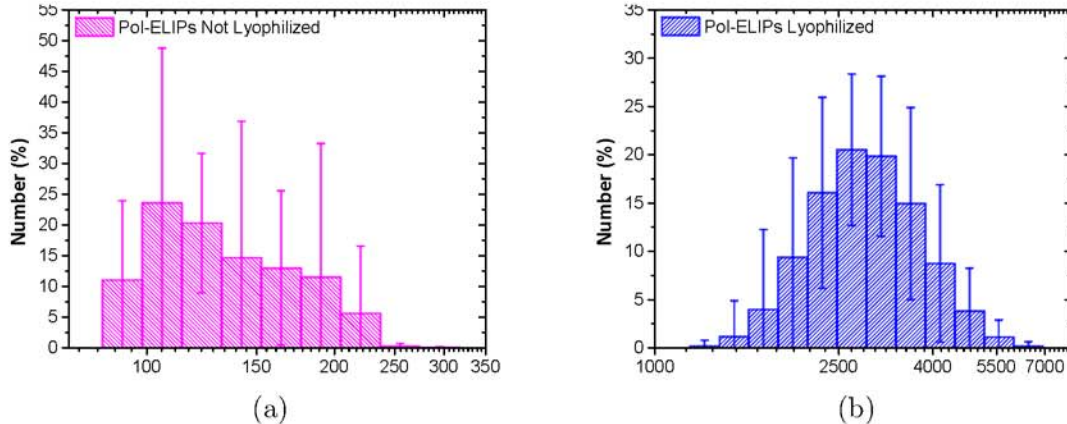


Figure 10.1: Size distributions of Pol-ELIPs measured using dynamic light scattering method. (a) Size distribution by number before lyophilization. (b) Size distribution by number after lyophilization. Data averaged for five independent measurements.

Table 10.1: Average diameters and polydispersity indices of Pol-ELIPs measured using DLS.

Type of Pol-ELIPs	Average Diameter (nm)		Polydispersity Index
	Volume Averaged	Number Averaged	
Not Lyophilized	142 ± 37	137 ± 35	0.43 ± 0.18
Lyophilized	3268 ± 685	2963 ± 538	0.24 ± 0.09

representative images acquired during our experiments with and without liposomes. Images of wells containing reconstituted Pol-ELIPs [Figure 10.2b] are clearly brighter than the control image without any liposomes [Figure 10.2a] indicating the acoustic reflectivity of the Pol-ELIPs.

10.2.3 Attenuation Measurements

Figure 10.3 shows experimentally measured frequency dependent attenuation spectra using two different transducers of central frequencies 2.25 MHz and 10 MHz. The attenuation measurements were performed at an acoustic excitation pressure of 50 kPa. The attenuation through a suspension of non-polymerized ELIPs (presented in the previous chapter) at the same lipid concentration is also shown in the same figure for comparison. The attenuation curves are only shown for the respective bandwidths

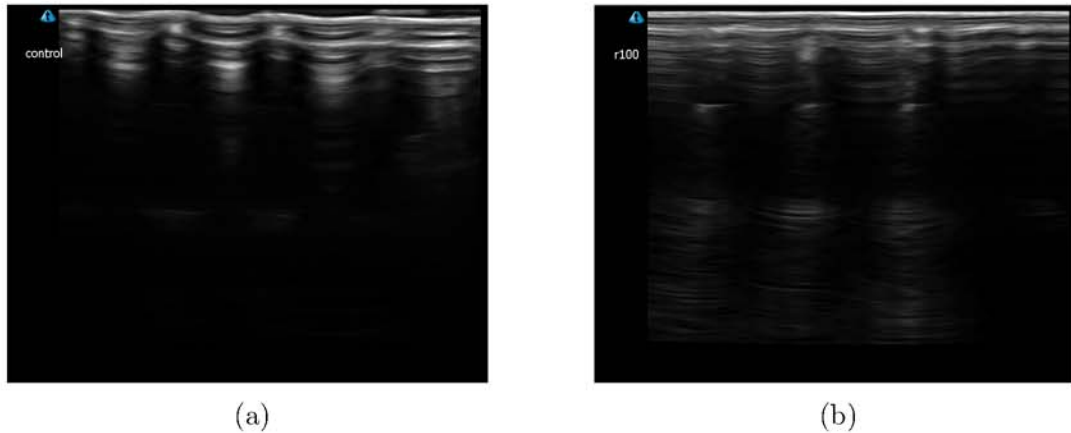


Figure 10.2: Ultrasound images of Pol-ELIPs reconstituted in 10 mM HEPES buffer pH 7.4 acquired using Terason t3200 medical imaging system. (a) Control Images without any liposomes. (b) Images in presence of reconstituted Pol-ELIPs in the suspension. Lipid concentration was 1mg/ml.

of the transducers used. For the frequency range studied here, we observed no distinct peak in the attenuation curve for Pol-ELIPs similar to that for normal ELIP suspension. We believe this stems from the fact that echogenic liposome suspensions are highly polydisperse with a large range of particle sizes present in the reconstituted suspension. We also observed that attenuation due to Pol-ELIPs is higher than attenuation due to normal ELIPs for frequencies lower than 5 MHz.

10.2.3.1 Time Dependent Attenuation Studies and Destruction

We had previously discussed the experimental method to measure ultrasound mediated destruction thresholds of contrast agents using time dependent broadband attenuation studies with varying acoustic excitation pressures in Section 3.6 and showed its application for PLA microbubbles 6.3.3. We utilize here the same methodology to study the stability and lifetime of Pol-ELIPs under sustained acoustic excitation. Figure 10.4a shows the time dependent total attenuation due to Pol-ELIPs for three different acoustic excitation pressures (50, 100 and 200 kPa) calculated from the experimentally acquired voltage-time traces. For comparison, we also present time dependent attenuation measurements with conventional ELIPs reconstituted in PBS-BSA in

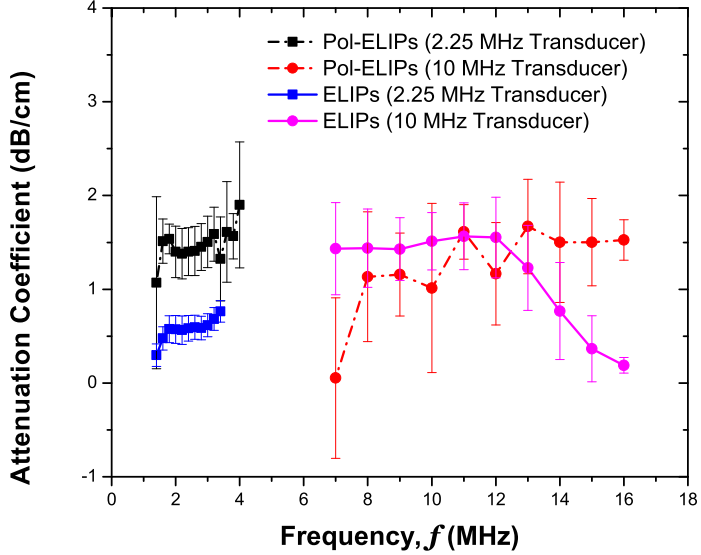


Figure 10.3: Frequency dependent attenuation coefficient for both non-polymerized and polymerized echogenic liposomes, measured using two different transducers of central frequencies of 2.25 and 10 MHz at a lipid concentration of 10 $\mu\text{g}/\text{ml}$. The average of five independent acquisitions with corresponding standard deviation error is plotted.

Figure 10.4b. In contrast to our previous findings with PLA microbubbles, the total attenuation from both liposomal formulations always show a steady decrease with time for all acoustic excitation pressures studied here. Hence, we could not estimate a definite destruction threshold for either of the liposomal formulations. Such steady decay indicates that the stability of the gas pockets associated with ELIPs are less compared to conventional microbubble based contrast agent.

The decay in attenuation was around 65-85% with Pol-ELIPs and 55% with conventional ELIPs over a period of 10 minutes. Note that in contradiction to our hypothesis, the Pol-ELIPs showed more decay under similar acoustic excitation. We believe the reconstitution of ELIPs in BSA gives this enhanced stability to normal ELIPs as has been reported previously [110, 325]. However, we also observe that the decay in attenuation with time is almost independent of the excitation pressure amplitude for ELIPs [see overlapping error bars in Figure 10.4b] unlike the attenuation decay due to Pol-ELIPs. Excitation pressure independent decay in attenuation can be attributed to a shell rupture dominated destruction [69]. The dependence of decay

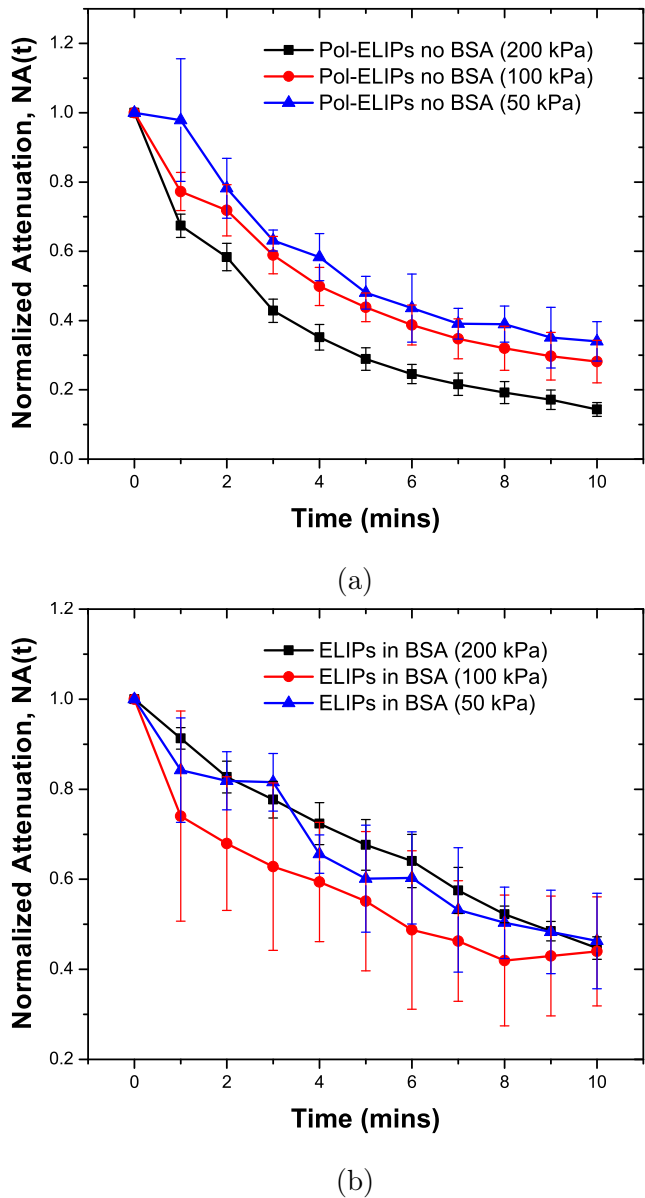


Figure 10.4: Variation of normalized total attenuation coefficient with time measured with a 2.25 MHz transducer at three different acoustic excitation pressures of 50, 100 and 200 kPa for (a) polymerized echogenic liposomes (b) conventional echogenic liposomes. Data is averaged over five independent acquisitions, and over consecutive 1 minute intervals.

in attenuation from polymerized liposomes with excitation pressure can indicate a gas diffusion dominated destruction in contrast to shell rupture. Hence, we believe that the polymerization plays an important role to provide slightly enhanced stability of echogenic liposomal formulations. However, a more comprehensive study is required to ascertain the effects of polymerization on stability and echogenicity of liposomes. Nonetheless, our results indicate that both of these liposomal formulations are susceptible to ultrasound mediated destruction even when excited by short duration broadband pulses and hence are expected to show a significant decay in their echogenic properties under sustained acoustic excitation. Previous investigations of ELIP stability have utilized both short duration pulsed ultrasound to excite single element immersion transducers [324] and clinical diagnostic ultrasound scanners to generate B-mode and pulsed Doppler acoustic pulses [325]. The former study reported almost complete loss of echogenicity within 5 minutes when excited with a 3.5 MHz pulse with 634 ns duration at a PRF of 475 Hz and at a MI of 0.25 (\sim 470 kPa). The stability study with the diagnostic scanner reported an echogenic lifetime of around 4 minutes under nondestructive continuous B-mode excitation. Our present findings are in reasonable agreement with these results except for the rapid decay even at low acoustic pressures (<100 kPa). Hence, all echogenicity measurements in this study with both of these ELIP formulations were completed within 5 minutes of sustained excitation. Recent investigation of ELIP stability as blood pool contrast agent also reported the critical dependence of ELIP echogenicity on dissolved oxygen concentration in the surrounding fluid [326]. Note that, for our experiments the liposomal suspensions were left to equilibrate with atmospheric oxygen concentration under ambient pressure. This may account for the accelerated leakage of gas out of the ELIPs even at the lowest acoustic excitation pressure amplitudes.

To test if the stability of the ELIPs can be further enhanced we prepared another batch of Pol-ELIPs with cholesterol (denoted as PC-PE-CH Pol-ELIPs). We performed attenuation measurements with them using a 2.25 MHz transducer. Both frequency

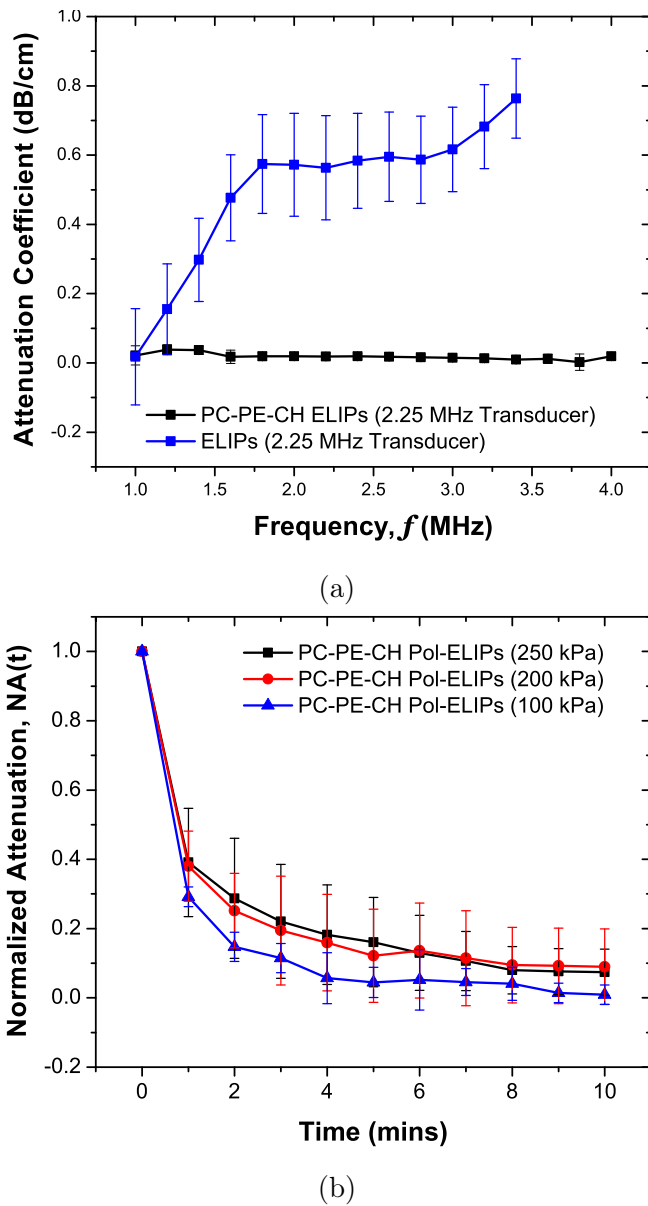


Figure 10.5: (a) Frequency dependent attenuation coefficient for PC-PE-CH polymerized echogenic liposomes, measured using 2.25 MHz transducer at a lipid concentration of 10 µg/ml. (b) Variation of normalized total attenuation coefficient with time measured with a 2.25 MHz transducer at three different acoustic excitation pressures of 100, 200 and 250 kPa for PC-PE-CH Pol-ELIPs. Data is averaged over five independent acquisitions, and over consecutive 1 minute intervals.

dependent attenuation coefficient and time dependent attenuation from the PC-PE-CH ELIPs are shown in Figure 10.5. Note that unlike PC-PE Pol-ELIPs discussed earlier, even with the same concentration of 10 μ /ml the attenuation due to PC-PE-CH Pol-ELIPs was less than the normal ELIPs [See Figure 10.5a]. Due to such low attenuation, we were not able to obtain any time dependent attenuation data from these PC-PE-CH ELIPs below 100 kPa acoustic pressure amplitude — the change in signal was too weak in comparison to the control signal. Surprisingly, an even faster decay was observed with PC-PE-CH Pol-ELIPs [See Figure 10.5b], quite opposite to what we had hypothesized. Note that cholesterol is reported to make the lipid bilayer stable for liposomes. Recently, Sax and Kodama [38] have also prepared echogenic liposomes encapsulating perfluoropropane gas to study their stability *in vitro* and *in vivo* by varying their lipid compositions. Echogenicity measurements were acquired using a high frequency US imaging system generating B-mode pulses. They reported that increasing the molar ratio polyethylene glycol (PEG) lipids significantly enhanced the half-life of the liposomes, both *in vitro* (55 MHz probe) mode and *in vivo* (40 MHz probe). However, in contrast to previous reports, cholesterol was shown to reduce stability of the liposomes by increasing membrane permeability and the gas leakage. Our results are consistent with their reports.

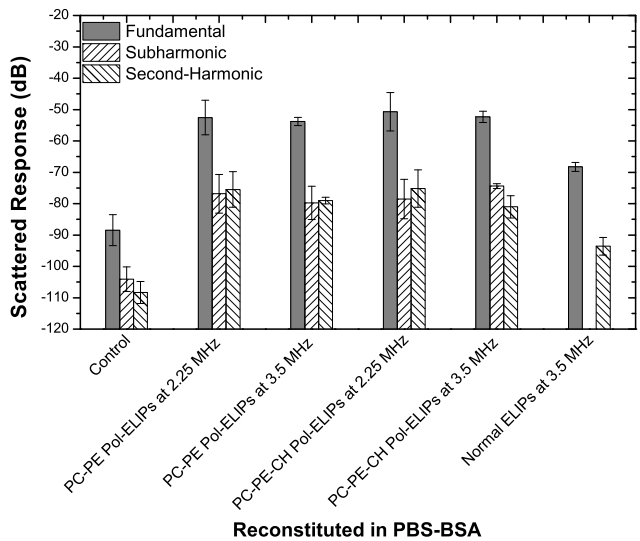
10.2.4 Scattering Measurements

The scattered response from the both PC-PE and PC-PE-CH Pol-ELIPs was measured at two different excitation frequencies (2.25 and 3.5 MHz) and at an acoustic pressure of 500 kPa. The experimentally measured scattered response data averaged for 5 independent acquisitions is plotted in Figure 10.6 with corresponding standard deviation errors. Figure 10.6a shows scattered fundamental (at the frequency of excitation), second-harmonic (at twice the frequency of excitation) and subharmonic (at half the excitation frequency) responses from the Pol-ELIPs in presence of BSA in the solution. For comparison we also include the echogenic response from a conventional

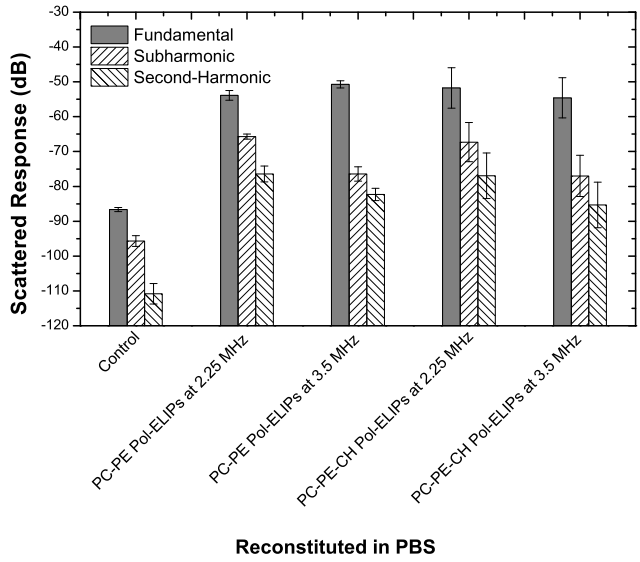
ELIP formulation we had presented in the previous chapter. Figure 10.6b shows the response from Pol-ELIPs without any BSA. Since, reconstitution in PBS-BSA was found to be an essential step for obtaining echogenic response from conventional ELIPs, we do not have any data for comparison with ELIPs in this case.

It is evident from Figure 10.6 that BSA does not play any significant role in the echogenic response from Pol-ELIPs. Note that Pol-ELIPs show a distinct subharmonic peak at both the excitation frequencies unlike conventional ELIPs. Thus, no subharmonic response is shown for the conventional ELIPs in Figure 10.6a. To further elucidate this point we present a comparison of the Fast Fourier Transforms (FFTs) of the scattered response from different ELIP formulations at 500 kPa acoustic excitation pressure in Figure 10.7. Response from Pol-ELIPs shows distinct peaks at fundamental, subharmonic, second-harmonic frequencies with up to 35, 30 and 35 dB and enhancements over control respectively. This is a stronger enhancement when compared to the response from conventional ELIPs at the same lipid concentration and can be attributed to the changes in lipid compositions used in our preparation protocol. Figure 10.6 and Figure 10.7 conclusively demonstrate the echogenicity and the non-linear scattering properties — including existence of distinct subharmonic component — of Pol-ELIPs studied here.

Subharmonic response from any contrast agent can only be detected distinctly beyond a certain acoustic pressure known as the threshold for subharmonic generation for that specific contrast agent. To determine the subharmonic generation threshold for Pol-ELIPs we performed pressure dependent scattering experiments at 3.5 MHz excitation frequency. *For this study however, only PC-PE Pol-ELIPs were utilized.* The experimentally measured scattered fundamental, second-harmonic and subharmonic responses are shown in Figures 10.8a, 10.8b and 10.9 respectively. Averages of five independent acquisitions along with corresponding standard deviation errors are plotted. Consistent with previous experimental findings for both microbubble based contrast agents and ELIPs, fundamental and second-harmonic response show a linear increase with excitation pressure on a log-log plot. The numerical values of the slope of a linear



(a)



(b)

Figure 10.6: Scattered response at two different excitation frequencies (2.25, 3.5 MHz) from different ELIP formulations reconstituted in (a) PBS-BSA (b) PBS. Lipid concentration is 1 $\mu\text{g}/\text{ml}$ for all the experiments.

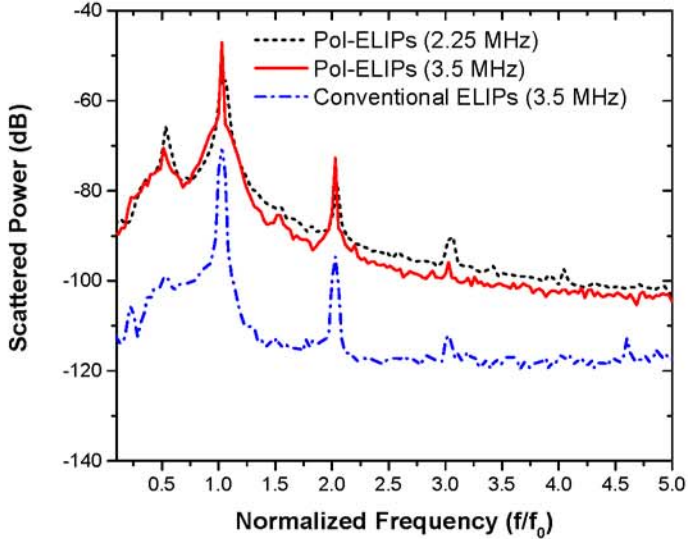


Figure 10.7: FFTs of the scattered signal from different ELIP formulations for an acoustic pressure amplitude of 500 kPa.

trendline for fundamental and second-harmonic response are 1.4 and 1.3 respectively. These values are close to the low amplitude perturbation analysis predictions of 1 and 2 for fundamental and second-harmonic response respectively. We believe the deviation from theoretical predictions is due to the non-linearity of the pressure dependent response at higher excitation pressures. It should also be mentioned that unlike the pressure dependent scattering measurements with non-polymerized ELIPs, measurements with Pol-ELIPs does not show any breakdown of this linear trend beyond 400 kPa of acoustic excitation amplitude. This can be attributed to the modified preparation protocol involving polymerization which makes Pol-ELIPs less susceptible to loss of echogenicity under acoustic excitation in comparison to conventional echogenic liposomes.

Note that, the scattered subharmonic response shown in Figure 10.9 shows all the characteristic features of a pressure dependent subharmonic response viz., initial noisy response with a sudden steep rise beyond the subharmonic generation threshold, followed by a gradual saturation. As evident from Figure 3(c), the threshold for subharmonic generation from a suspension of Pol-ELIPs at 3.5 MHz excitation is around

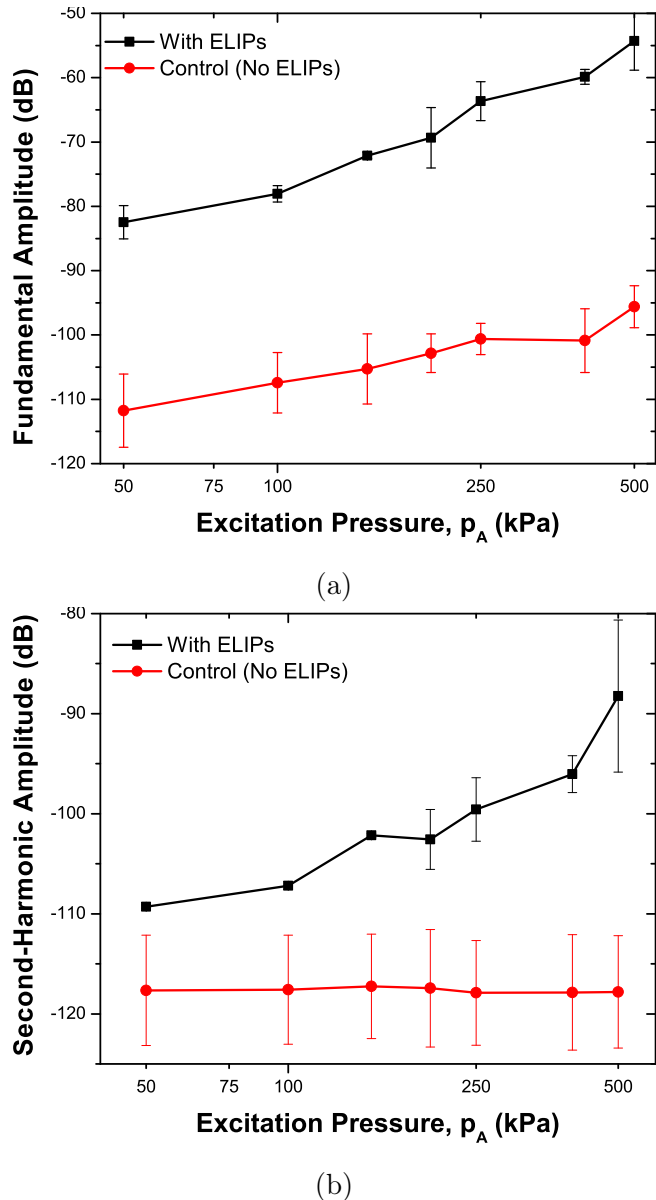


Figure 10.8: Experimentally measured scattered response at 3.5 MHz excitation from polymerized echogenic liposomes at (a) fundamental (b) second-harmonic frequencies. Lipid concentration is 1 $\mu\text{g}/\text{ml}$ for all the experiments.

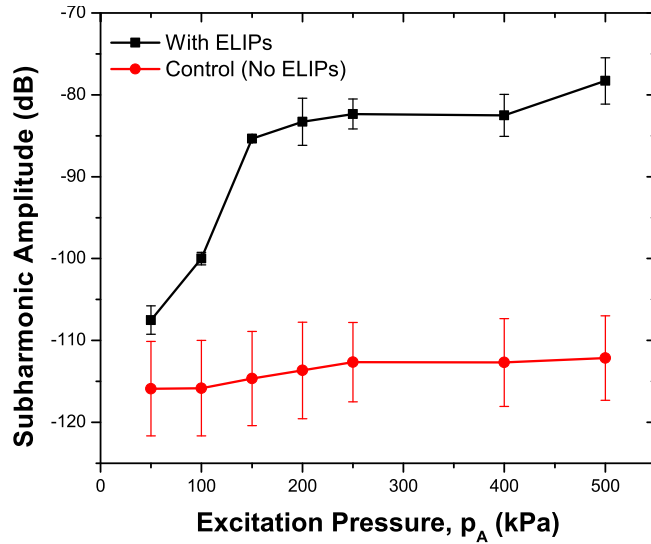


Figure 10.9: Experimentally measured scattered subharmonic response at 3.5 MHz excitation from polymerized echogenic liposomes at a lipid concentration of 1 $\mu\text{g}/\text{ml}$ for all the experiments.

150 kPa. A distinct peak at the subharmonic frequency was also observed in the scattered power spectra at this pressure and beyond. Note that we never detected any subharmonic response from the conventional ELIP suspension in our previous studies. The subharmonic generation threshold for Pol-ELIP suspension is comparable to the threshold values identified for microbubble based contrast agents discussed previously.

To study the dependence of echogenic properties on the preparation protocol, we also varied the mannitol content during the Pol-ELIP preparation. The results are shown in Figure 10.10. We had earlier presented our findings that for non-polymerized ELIPs, a finite amount of mannitol (> 50 mM) was essential for the echogenicity of the liposomes. A very similar trend was observed in our case as evident from Figure 10.10.

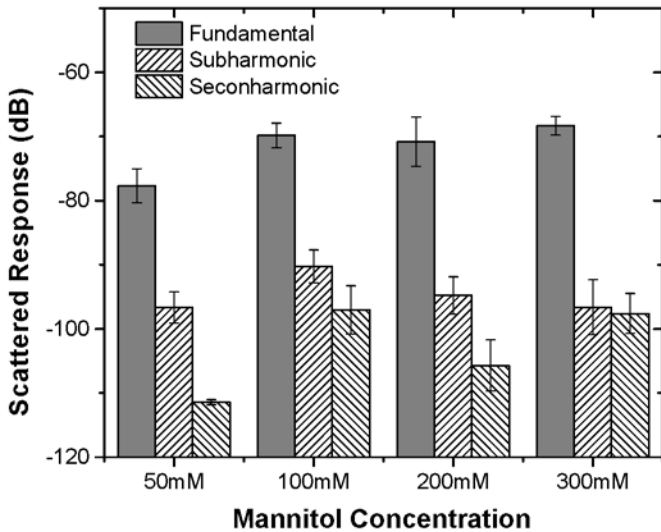


Figure 10.10: Experimentally measured scattered response at 3.5 MHz excitation from polymerized echogenic liposomes with varying mannitol content. Excitation pressure was 250 kPa and the lipid concentration was 1 $\mu\text{g}/\text{ml}$ for all the experiments.

10.3 Summary and Conclusions

We studied echogenic liposomes with a polymerized lipid bilayer that can potentially improve their stability and nonlinear behavior. These Pol-ELIPs had a very polydispersed size distribution with an average size of 3 μm . The frequency dependent attenuation experiment did not show any distinct peak due to the polydispersity. The Pol-ELIPs showed echogenicity in our *in vitro* scattering experiments, even without the presence of bovine serum albumin (BSA) in the reconstituting media. Scattered response measured from Pol-ELIP suspension showed strongly nonlinear behaviors with distinct second-harmonic and subharmonic peaks, in contrast to non-polymerized ELIPs that did not show any subharmonic response. Scattered fundamental, second-harmonic and subharmonic responses at a lipid concentration of 1 $\mu\text{g}/\text{ml}$ showed upto 35, 30 and 35 dB enhancement respectively over the control response i.e., without any liposomes in the suspension. The subharmonic response showed all its characteristic features — its appearance only above a threshold excitation level (150 kPa) and then a sharp rise with a subsequent saturation. The results conclusively demonstrate the potential of these Pol-ELIPs to be used in nonlinear ultrasound imaging.

Chapter 11

‘DUAL-PURPOSE’ ECHOGENIC LIPOSOMES AND POLYMERSOMES: PROOF OF CONCEPT¹

11.1 Motivation

Targeted drug delivery remains one of the major challenges in current pharmaceutical research. Upon injection, many drugs get distributed in the body according to their pharmacokinetic and pharmacodynamic properties, resulting in low therapeutic concentrations at the target site and unwanted side effects [362]. The drug biodistribution can be suitably altered and side effects can be minimized by employing targeted delivery systems. A wide variety of drug carriers and passive and active targeting strategies have been reported in the literature [363]. However, upon reaching the intended site, the rate of drug release from the carriers is often very slow.

Stimuli responsive drug delivery vehicles are highly attractive because of local control over payload release and consequently, reduced systemic toxicity. Both biological/endogenous (e.g., enzymes [101, 102], redox [104], pH [364]) and non-biological or exogenous (e.g., temperature [98], light [99], ultrasound [116]) triggers have been used as stimuli to release the payload these drug carriers. A combination of a biological and an external trigger can give dual levels of control for drug release at the targeted site. Incorporation of concurrent contrast imaging capability renders multimodal characteristics to the drug carrier. However, there are only a few reports of such multimodal nanocarriers responding to multiple triggering stimuli with simultaneous imaging capability [365].

¹ Figures and certain parts of the text in this chapter have been adapted from several published [114, 115] and under review [7, 361] articles with permission from respective copyright holders/publishers.

The ability of ultrasonic excitation to induce thermal and/or mechanical effects has been used to release drugs from different carriers such as polymeric assemblies [291], micelles [366], emulsions [29, 367], microcapsules [298, 368], microspheres [369] and liposomes [106]. However, majority of these studies were performed with low frequency ultrasound (LFUS) at kHz frequencies [105, 342, 343, 370–373]. Although application of kHz frequency ultrasound leads to more release compared to MHz frequency [105], it has very limited clinical applications due to the associated harmful biological effects. There are only a few reports of MHz frequency ultrasound utilized to release drugs from liposomes [113, 116, 329, 331] and microbubbles conjugated to liposomes [36]. In 9 we discussed in detail the application of diagnostic frequency ultrasound-triggered release from ELIPs, which led to the conclusion that release from ELIPs only by application of ultrasound is often less than optimum (i.e., ranging between 20-50%). This motivated us to develop ELIPs with dual-release triggers. While the previous two chapters described detailed acoustic characterization of different ELIP formulations for conclusively demonstrating their potential for use as ultrasound image contrast enhancement, this chapter will discuss the proof of concept validation of the ‘dual-purpose’ echogenic liposomes or polymersomes. Till date we have achieved *in vitro* proof of concept validation for the following liposomal formulations:

1. A substrate lipopeptide conjugated ELIP formulation that can be triggered (or cleaved) by the extracellular enzyme matrix metalloproteinase-9 (MMP-9).
2. A polymer coated redox triggered ELIP formulation capable of cytosolic drug delivery.
3. A pH sensitive liposomes with tunable echogenicity that are capable of delivering drugs in mildly acidic micro-environment of the tumors.
4. Redox sensitive echogenic polymersomes

The motivation behind pursuing the development each of these above mentioned formulations are discussed below.

11.1.1 MMP-9 Cleavable ELIPs

MMP-2 and -9 are members of Zn_2^+ and Ca_2^+ dependent family of enzymes responsible for degradation of gelatin and collagen (IV and V) in the extracellular matrix [374]. MMPs play an important role in a variety of normal physiological processes, e.g., embryonic development, tissue metamorphosis, angiogenesis, wound healing, ovulation etc [375–378]. Increased expression levels of MMP-9 and MMP-2 correlate with arthritis, atherosclerosis, cancer and other diseases [379–383]. These two enzymes hydrolyze and weaken the fibrous caps of the plaques, leading to plaque rupture [384]. MMP-9 is also involved in progression and metastasis of many cancers and are being considered as biomarkers for various types of cancers [385]. Inhibitors of these enzymes are currently in clinical trials for adjuvant therapy of various cardiovascular diseases and cancers [386].

Herein, we demonstrate that the combination of enzymatic triggering (by MMP-9) and ultrasound excitation leads to considerably higher amounts of contents release from echogenic liposomes with potential application to treatment of cancers through extracellular drug-delivery.

11.1.2 Polymer Coated Redox Triggered ELIPs

The lipid-based drug delivery systems offer excellent biocompatible vehicles for both hydrophilic and lipophilic drugs. However, in the biological system, they get destabilized due to interactions with plasma proteins and biomembranes, resulting in leakage of the encapsulated drugs in the circulation (before reaching the intended site) [387]. Thus, only a small fraction of drug actually reaches the targeted site. Polymerization of the lipid bilayer improves stability but their clinical usage is limited because of poor biocompatibility.

The tripeptide glutathione (L- γ -glutamyl-L-cysteinylglycine, GSH) functions as an important free radical scavenger and protects cells from harmful effects of reactive oxygen species, toxins, drugs and many mutagens. It is one of the most abundant organic reducing agents present in human body. GSH level is elevated in various human

cancer tissues (such as breast [388, 389], ovary [389], colon [390], lung [391], bone marrow [392], and larynx [393]) compared to normal tissues. It has been implicated in drug resistance and in tumor growth [394]. The disulfide functional group have gained attention in the preparation of stimuli-responsive drug carriers because of its stability in mildly oxidizing environments (of atmospheric oxygen and blood stream [395]) and lability in presence of reducing agents. Due to the large redox potential difference between the extracellular matrix (thiol concentration: 10 – 40 μ M) and the cytosol of cancer cells (thiol concentration: 0.5 – 10 mM because of the presence of GSH) [396], the reversible disulfide thiol conversion is being used widely for cytosolic drug delivery [397–400].

Herein, we have prepared folate conjugated, disulfide - crosslinked, polymer - coated acoustically reflective echogenic liposomes for cytosolic delivery. With further developments, these polymerized lipid nanocarriers hold promise as a vehicle for ultrasound image guided, targeted cytosolic drug delivery. To the best of our knowledge, there are no reports of using polymer-coated acoustically reflective lipid nanoparticles for simultaneous targeted drug delivery and ultrasound imaging.

11.1.3 pH Sensitive Liposomes with Tunable Echogenicity

As mentioned earlier, nanometer sized liposomes hold a definite advantage over micron sized gas bubble based contrast agents — the latter cannot extravasate through blood vessels into the tumor tissue, which leads to decreased efficacy in ultrasound assisted drug delivery [23]. However, if gas bubbles are generated inside liposomes of nanometer size only at the desired/targeted sites for ultrasound imaging with concurrent cytosolic drug delivery, they can circumvent the low stability and extravasation problems associated with the conventional microbubbles-based ultrasound contrast agents and drug carriers. This motivated to pursue this tunable strategy and combine it with the cytosolic release strategies we had developed with liposomes prepared using the freeze-thaw and lyophilization techniques.

We note that due to the Warburg effect, the cancer cells are usually more acidic than normal cells [401]. The cancerous cells are characterized by rapid growth and consequently, require more nutrition and oxygen. This causes the production of lactic acid under anaerobic respiration and hydrolysis of ATP, leading to an acidic microenvironment around the hypoxic tumor. For healthy individuals, the extracellular pH is 7.4 and the intracellular pH is 7.2. In case of tumors, this gradient is reversed with the extracellular pH lower compared to intracellular [402]. Several reports indicate that there is a wide range of pH in malignant tissues, from 5.8 to 7.6 [403]. This acidic environment aids breaks down the extracellular components and destroys the surrounding normal tissue cells. For aggressive tumors, the lysosomal pH within the cancer cells can be as low as 4.5. Here, we are exploiting this characteristic decrease in pH at tumor sites as well as in the lysosome to render the liposomes echogenic and trigger the release of encapsulated anticancer drugs in the cytosol of pancreatic cancer cells, which has been associated with one of the highest fatality rates among all types of cancer [404]. To the best of our knowledge there are no reports of similar pH tunable echogenic liposomes with dual-triggering potential.

11.1.4 Redox Sensitive Echogenic Polymersomes

Polymersomes or vesicular mesophases provide an elegant alternative to cellular targeting and cytoplasmic delivery of drugs [405–407]. Such polymersomes can protect its payload in the extracellular environment. If designed properly they can be internalized by the cells through endocytosis. Once inside these polymersomes can burst suddenly to release their contents before being exposed to the harsh conditions encountered after lysosomal fusion. Redox sensitive polymersomes capable of cytosolic delivery have already been reported in the literature [408]. Inspired by these reports of , we decided to develop an echogenic version of such polymersomes and test their potential as a ‘dual-purpose’ agent. This would combine our cytosolic release strategy employed with polymer coated ELIPs and their echogenic properties with the polymersome preparation protocol. To the best of our knowledge there has only been one

such report of echogenic polymersomes [44].

In the following sections we will discuss our findings for each of these different formulations and propose possible future work for the design and development of these liposomes/polymersomes as clinically viable agents.

11.2 Materials and Methods

11.2.1 Preparation Protocol

These liposomes were prepared by our collaborators at North Dakota State University in the form of lyophilized powders or in aqueous solutions and shipped to us overnight. They are included in this discussion since the echogenicity of these formulations is determined by the modified preparation protocol. The basic principles behind the preparation of echogenic liposomes remains similar to that described in Section 8.1.1 in Chapter 8 with modifications in the lipid composition, ligand conjugations and drug/dye loading protocols, which are elaborated below for clarification of the experimental results. For pH tunable ELIPs however, a completely different strategy was utilized, which did not require use of mannitol or lyophilization steps as explained below.

11.2.1.1 MMP-9 Cleavable ELIPs

A special substrate lipopeptide [LP4, See Table 11.1 below for amino acid sequence] was utilized in this protocol, which has a MMP-9 cleavage site is between Glycine and Isoleucine]. This lipopeptide has been developed by our collaborators to optimize the contents release from conventional liposomes in the presence of MMP-9 enzyme [101, 409]. A detailed description of the established protocol can be found in several previous publications [101, 115]. In brief, the crude LP4 was synthesized employing a microwave-assisted peptide synthesizer, purified by reverse-phase HPLC and the purity was confirmed by MALDI-TOF mass spectrometry (Calculated MH⁺: 2333.26; Observed: 2333.28). Circular dichroism (CD) spectroscopic studies confirmed triple helical structure for LP4 in phosphate buffer (pH = 4.0). Stock solutions of 1 -

palmitoyl - 2 - oleoyl - sn - glycero - 3 - phosphocholine (POPC, Avanti Polar Lipids) was prepared (1 mg/ml) by dissolving in chloroform and stored in freezer. Solutions of POPC (2 mg) and a specially prepared triple-helical substrate lipopeptides LP4 (2.6 mg) were mixed in the molar ratio of 70:30 respectively in a 10 ml round bottom flask. A thin film at the bottom of the flask was formed by evaporating the solvent at 40 °C using a rotary evaporator. In order to remove any residual solvents, the flask was placed under high vacuum overnight. Subsequently, the dried film was hydrated with 100 mM carboxyfluorescein (>90% fluorescence is quenched) in HEPES (2 - [4 - (2 - hydroxyethyl) piperazin - 1 - yl]ethanesulfonic acid) buffer (25 mM, pH = 8) with added ions (Ca^{2+} and Zn^{2+}) and 2 ml of 0.64 M mannitol (final concentration 0.32 M) at 50 °C. Mannitol is a weak cryoprotectant; we mentioned in Chapter 9 that a finite amount of mannitol during preparation is critical for ensuring the echogenicity of ELIPs. The lipids were hydrated for 3 hours and the resultant multilamellar vesicles were bath sonicated for 10 minutes. The liposomal solution was exposed to three freeze (-70 °C) and thaw cycles. Subsequently, the liposomes were extruded first through 800 nm and then 200 nm polycarbonate filters (Nuclepore, Whatman) 15 times at 60 °C using a mini-extruder (Avanti Polar Lipids). To remove the unencapsulated dye, the liposomes were gel filtered using Sephadex G-100 column conditioned with HEPES buffer (25 mM, pH = 8). The osmolarity of the eluent buffer was adjusted (540 mOsm/kg with 0.17 M NaCl solution in HEPES buffer, pH = 8) to that of the liposomal solution to ensure the minimum leakage of dye from liposomes due to osmotic shock. A similar procedure was followed to prepare the liposomes without any encapsulated dye using HEPES buffer without carboxyfluorescein. ELIPs for CD spectroscopic studies were prepared by the same method using a 4 mM phosphate buffer (pH = 4.0).

Table 11.1: Amino acid sequence of LP4.

Peptide	Amino acid seqence
LP4	$\text{CH}_3(\text{CH}_2)_{16}\text{CONH}-\text{GPQGIAGQR(GPO)}_4\text{GG}-\text{COOH}$

11.2.1.2 Polymer Coated Redox Triggered ELIPs

The gallate derivative with three propargyl groups coupled to 1 - palmitoyl - 2 - oleoyl - sn - glycerol - 3 - phosphoethanolamine (POPE-G) was synthesized following a published procedure [410]. Stock solution of 1 - palmitoyl - 2 - oleoyl - sn - glycero - 3 - phosphocholine (POPC, Avanti Polar Lipids) was prepared (1 mg/ml) by dissolving the lipid powder in chloroform and methanol (9:1) and stored in freezer (-20 °C). Solutions of POPC (3 mg), POPE-G (3.9 mg) and 1, 2 - dipalmitoyl - sn - glycero - 3 - phosphoethanolamine - N - (lissamine rhodamine B sulfonyl) ammonium salt (DPPE-LR, 0.045 mg) were mixed in the molar ratio of 50:49:1 respectively in a 10 ml round bottom flask. The mixture was swirled to ensure proper mixing of components. Solvent was evaporated using a rotary evaporator and the flask was placed under vacuum overnight to remove any residual solvent traces. Next day, the dried film was hydrated for 3 hours with 3 ml of 10 µM calcein dissolved in 10 mM HEPES buffer (pH adjusted to 7.4) and 3 ml of 0.64 M mannitol (final concentration 0.32 M). The lipid dispersion was then bath sonicated for 10 minutes with constant swirling and exposed to 3 freeze (-70 °C) and thaw (23 °C) cycles to enhance calcein encapsulation. Sequential extrusion was performed using a mini-extruder (Avanti Polar Lipids) using 800 nm, 200 nm polycarbonate filters (Nuclepore, Whatman) in succession.

For polymerization, the reported procedure [410] was modified in order to make it suitable for our experiments. To the above 6 ml liposomal solution, the cross linker CL, 150 µl of 0.04 M aqueous solution), Cu-complex (150 µl of 0.053 M aqueous solution prepared by mixing 3 ml of CuCl₂, 71.7 mg, 0.53 mmol) solution, 3 ml of PMDETA solution (442 µl, 2.1 mmol)) and sodium ascorbate (150 µl of 27 mg/mL solution, 1.4 µmol) were added together. Mixture was divided into 6 closed vials and stirred slowly at room temperature for 24 hours. After 24 hours, the mixture was passed through a Sephadex-G100 gel filtration column in order to remove unencapsulated dye and other compounds from the liposomes. Mannitol was added to the ELIPs solution to obtain 0.32M concentration, the solution was frozen and subsequently, the ELIPs were placed in a lyophilizer. The freeze dried powder was stored in a refrigerator and reconstituted

just before use.

11.2.1.3 pH Sensitive Liposomes with Tunable Echogenicity

The liposomes were prepared with POPC (1 - palmitoyl - 2 - oleoyl - sn - glycero - 3 - phosphocholine; Avanti Polar lipids) lipid solution using traditional lipid film formation, hydration and sonication method. The 4 mg of 1 mg/ml lipid solution was placed in a rotary evaporator for approximately 10 minutes to allow for the lipid film to form, and then placed under a vacuum overnight to remove of traces of chloroform. Once the film was developed, 4 ml of 100 mM carboxyfluorescein dye used was added into the film, along with 126.5 mg of ammonium bicarbonate (0.4 M) and allowed to hydrate for three hours. The lipid dispersion was then sonicated for ten minutes to form liposomes. The liposomes were then exposed to three freeze (-70 °C) and thaw (23 °C) cycles to ensure the dye encapsulation inside the aqueous interior of the liposomes. After the freeze/thaw cycles, the extrusion apparatus (Avanti Polar Lipids) was used to extrude the liposomes through an 800 nm, then 200 nm polycarbonate membrane filters. The liposomes were then placed in a Sephadex-G100 gel filtration column preconditioned with HEPES buffer pH 7.4 (osmolarity adjusted to liposomal levels) to separate unencapsulated contents surrounding the liposomes. Liposome fractions were collected and subsequently used for further studies. *Note that these liposomes do not require freeze-thaw and lyophilization steps in presence of mannitol.* These liposomes have encapsulated ammonium bicarbonate, a gas precursor, which reacts with protons diffusing from outside acidic environment generates CO₂ bubbles inside. The generation of the carbon-dioxide gas will contribute both to its echogenicity and subsequent rupture of the lipid bilayer leading to contents release.

11.2.1.4 Redox Sensitive Echogenic Polymersomes

This preparation protocol is a novel idea currently under development with our collaborators and hence cannot be included in this thesis.

11.2.2 Size Distribution Measurements and Microscopic Imaging

The size distribution and morphology of the various liposomes/polymersomes were determined using the dynamic light scattering and AFM/TEM respectively. *As mentioned earlier, all these measurements were performed by our collaborators at NDSU.* The measurements techniques are same as those described in Chapter 3. For MMP-9 cleavable ELIPs the triple helical structure of the lipopeptide was checked using Circular Dichroism (CD) Spectroscopy. The TEM measurements were critical for pH tunable ELIPs to determine that vesicles were unilamellar — this helps reducing the barrier to protons migrating inside. The AFM before and after application of triggers also substantiated our hypothesis that ELIPs were indeed ruptured, which would cause the contents release.

11.2.3 Ultrasonic Measurements

The echogenicity of the liposomes/polymersomes were tested using both *in vitro* acoustic scattering experiments explained in Section 3.3.4 and using ultrasound imaging with a clinical scanner (Terason t3200) as described in Section 3.3.6 [Images were acquired by our collaborators at NDSU]. The ultrasound mediated release studies were performed using the setup described in Section 3.3.7. During initial design and optimization phase, release from MMP-9 cleavable ELIPs were measured using the 2.25 MHz transducer (1.16 cm in diameter) operating at 1 MHz. Our final setup utilized a smaller diameter 3.5 MHz transducer, which enabled reduction amount of sample used for each run. The release was quantified using the technique described in the Section 3.3.7.2.

11.3 Triggered Release Studies

For release studies with triggers other than ultrasound the protocol varied from one formulation to another and are described below. *All the release studies with enzymes/redox/pH was performed by our collaborators at NDSU.*

For MMP-9 cleavable ELIPs, the release experiments were carried out using a microplate multidetection instrument (Spectramax-M5, Molecular devices) employing the liposomes prior to freeze drying at 25 °C. Release was monitored by recording the fluorescence emission intensity at 518 nm with excitation wavelength 480 nm. All experiments were conducted in triplicate. Each well contained 20 μ l of 0.1 mg/ml ELIPs in HEPES buffer (25 mM, pH = 8.0, osmolarity 540 mOsm/kg adjusted with 0.17 M NaCl in HEPES buffer, pH = 8) and 16 μ l of 25 μ M MMP-9 (final concentration: 2 μ M). Release of dye was observed over 60 minutes. The emission intensity was recorded in one minute interval. After 1 h, 10 μ l of Triton-X100 was added to disrupt all the liposomes and the emission intensity was measured (excitation: 480 nm). This fluorescence intensity was treated as total (100%) release.

For redox triggered ELIPs, the release studies were carried out using a fluorescence microplate multidetection instrument (Spectramax-M5, Molecular devices) using calcein and CoCl₂ quenching method. Since sub-self-quenching concentration (10 μ M) of calcein was used, we could quench external fluorescence by adding CoCl₂. CoCl₂ quenches fluorescence of unencapsulated calcein outside the ELIPs, so the fluorescence signal observed is from the encapsulated dye only. For the release studies, 0.02 mg/mL ELIPs were taken into 96 well plate and external calcein was quenched with 10 mM CoCl₂. Dithiothreitol (DTT), Glutathione (GSH) and Cysteine (CYS) were added in specific concentration to determine the release of calcein. Fluorescence was monitored at 515 nm (excitation 495 nm) for an hour and subsequently, the ELIPs were disrupted using triton-X100 to record background fluorescence (if any). Initial fluorescence intensity was treated as 100% and percent decrease in fluorescence intensity was treated as percent release accordingly.

For pH tunable ELIPs, the release studies were carried out on a spectrophotometer (Spectramax, Molecular Devices) by exciting at 460 nm and monitoring the emission at 497 nm using a 96 well plate. In each well, 20 μ l of the liposomal solution (0.02 mg/ml) was incubated with phosphate buffer saline solutions with pH adjusted to 7.4 (control), 7.0, 6.0 and 5.0. The release was monitored for two hours and reading

was taken at 30 second intervals. Each sample was taken in triplicates and each study was repeated three times in order to check the repeatability of the results.

11.4 Results and Discussion

11.4.1 Size Distribution and Microscopic Images

11.4.1.1 MMP-9 Cleavable ELIPs

We determined the average diameters of the ELIPs before and after freeze-drying employing dynamic light scattering (DLS). We observed that average diameter of the liposomes in the reconstituted powder was larger (190 ± 35 nm; Figure 11.1b) compared to that prior to freeze drying (116 ± 22 nm, Figure 11.1a). The polydispersity index also increased to 0.85 from 0.3 — indicating a large distribution of size in the reconstituted liposomes. Transmission electron microscopy corroborated these observations. TEM images show that the reconstituted ELIPs were heterogeneous (50 nm – 1 μm) with median size between 100 – 200 nm (Figures 11.1c and 11.1d). During the freeze-drying and subsequent reconstitution steps, some of the liposomes fuse with each other — leading to a more heterogeneous size distribution. Also note that the relatively high polydispersity indicates presence of larger liposomes (also seen in the inset of Figure 11.1b). These larger liposomes with air pockets of sizes around micron range are primarily responsible for the echogenicity of ELIPs. Consistent with this, we also observed that the liposome solution prior to freeze-drying was not echogenic.

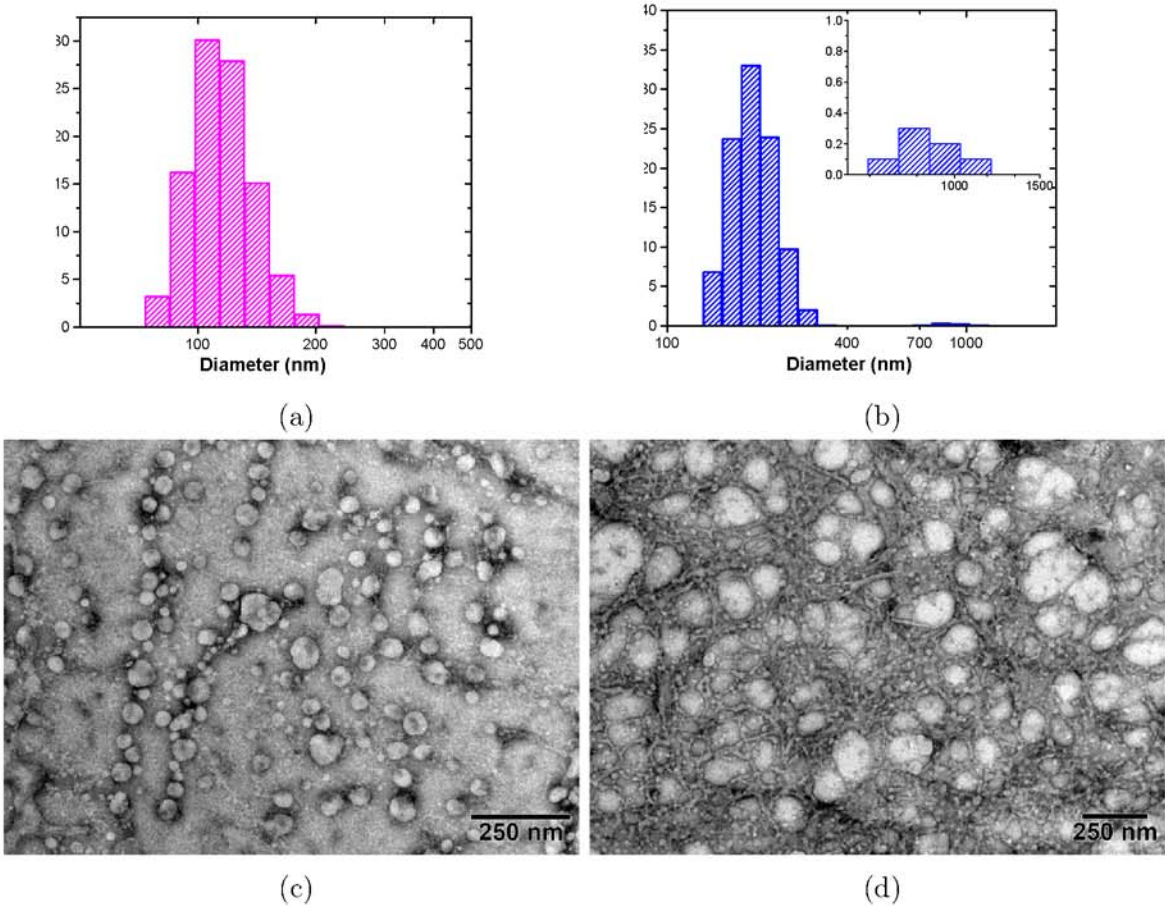


Figure 11.1: DLS size distributions (by percentage number) of carboxyfluorescein encapsulated MMP-9 cleavable ELIPs (a) before lyophilization, and (b) after lyophilization. The inset plot of panel (b) shows the presence of liposomes in the size range 700 – 1100 nm. TEM images (c) before lyophilization, and (d) after lyophilization. Reprinted with permission from [115]. Copyright (2012) American Chemical Society.

11.4.1.2 Polymer Coated Redox Triggered ELIPs

We determined the size distribution (both before and after lyophilization) using DLS. We observed that the number averaged diameter after lyophilization increased (117 ± 11 nm, Figure 11.3b) compared to the average diameter before lyophilization (78 ± 14 nm, Figure 11.2a). Polydispersity index also increased from 0.37 ± 0.04 to 0.71 ± 0.05 , indicating a more heterogeneous distribution of sizes in the lyophilized sample. This was confirmed by the TEM images with the lyophilized ELIPs (Figure 11.3b). Due to the modified preparation protocol, the ELIPs indeed entrapped air as verified by TEM images (Figure 11.3a) and gave rise to a more polydisperse suspension with a larger average diameter.

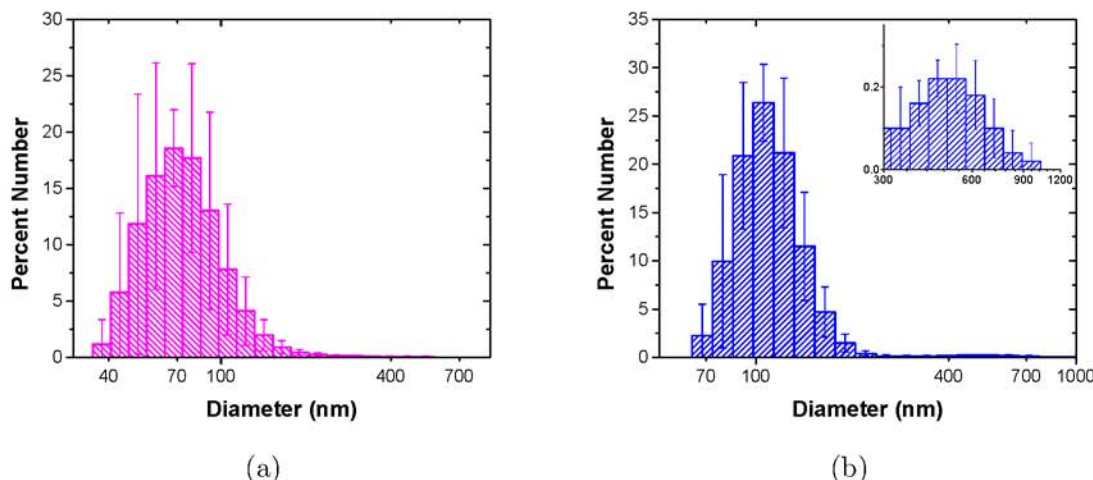


Figure 11.2: DLS size distributions (by percentage number) of calcine encapsulated polymer coated redox triggered ELIPs (a) before lyophilization, and (b) after lyophilization. The inset plot of panel (b) shows the presence of liposomes in the size range 300 – 1200 nm. Reprinted with permission from [114]. Copyright (2013) American Chemical Society.

We also studied the effect of addition of reducing agents on the morphology and size distribution of ELIPs employing atomic force microscopy (AFM). We observed that, before the treatment ELIPs look spherical with average size of 100-200 nm (Figure 11.4A); but upon addition of 5 mM reducing agents (GSH), the particles fuse with each other giving a more heterogeneous size distribution (Figure 11.4B).

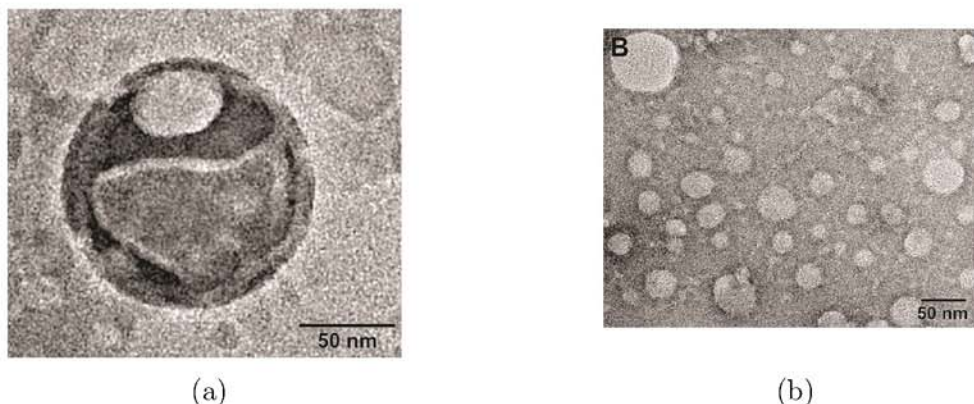


Figure 11.3: Transmission Electron Microscopic images of negatively stained redox triggered ELIPs. (a) ELIPs after lyophilization showing an entrapped bubble within the bilayer, and (b) Heterogeneous size distribution of ELIPs. Reprinted with permission from [114]. Copyright (2013) American Chemical Society.

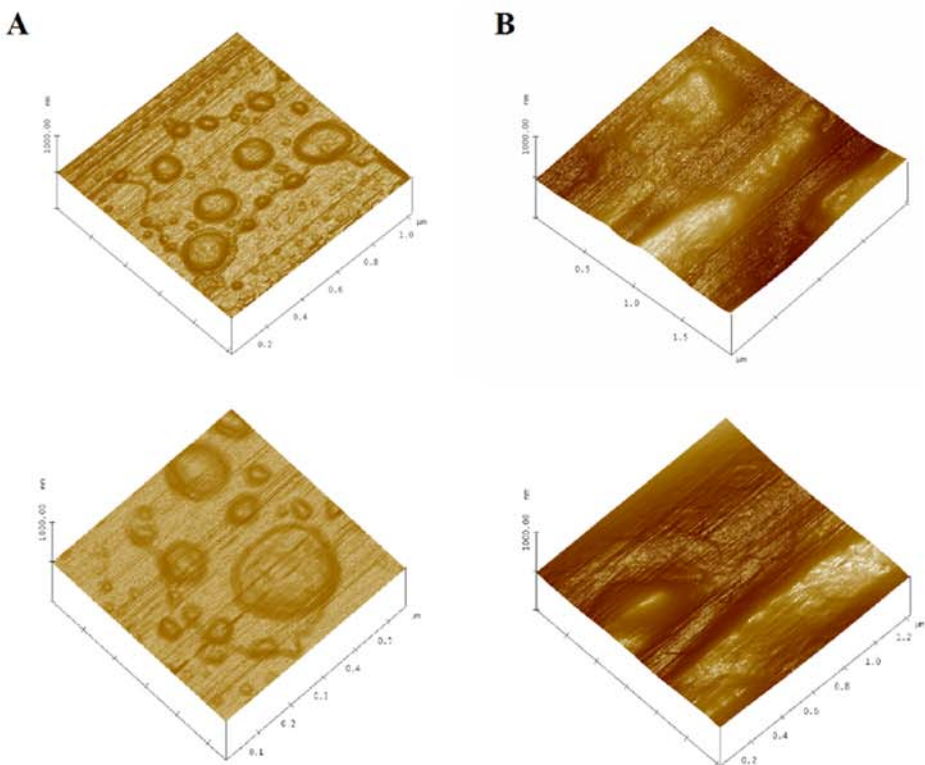


Figure 11.4: MultiMode™ Atomic Force Microscopic images of polymer coated redox triggered ELIPs before (A) and after (B) treatment with reducing agent(GSH). Reprinted with permission from [114]. Copyright (2013) American Chemical Society.

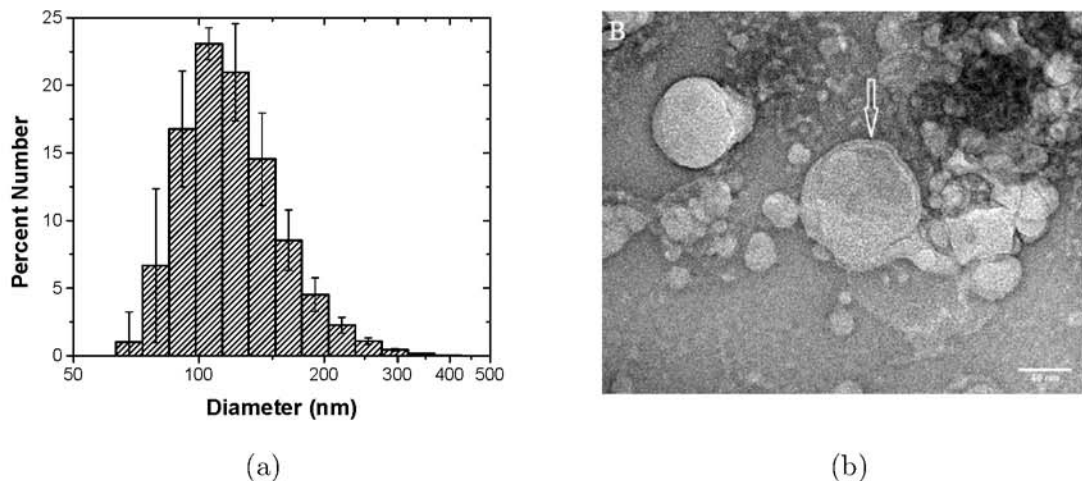


Figure 11.5: (a) Particle size distribution (by number) of the pH sensitive liposomes using dynamic light scattering instrument. (b) Transmission electron microscopic image (JEOL JEM 2100 LaB₆ 200 kV) of pH tunable echogenic liposomes using negative staining by 1% phosphotungstic acid. White arrow indicates the unilamellar bilayered structure of liposome. The white bar represents a 50 nm scale. Reproduced with permission from the under review article [361].

11.4.1.3 pH Sensitive Liposomes with Tunable Echogenicity

We hypothesized that the outside hydronium ions (H_{30}^+) need to diffuse through several lipid bilayers to generate sufficient amounts of CO_2 gas inside the liposomes. The presence of several lipid bilayers is also expected to decrease the efficiency of contents release in response to escaping gas bubbles and ultrasonic excitation. Hence, we decided to formulate unilamellar liposomes with a narrow size distribution by sonication and sequentially extruding (through 800 nm and then 200 nm polycarbonate membrane filters) the initially formed multilamellar vesicles. We observed (by DLS) that the average hydrodynamic diameter of the liposomes is 110 ± 15 nm with polydispersity index of 0.05 (Figure 11.5a). These results were corroborated by the TEM images (Figure 11.5b).

11.4.2 Proof of Echogenicity

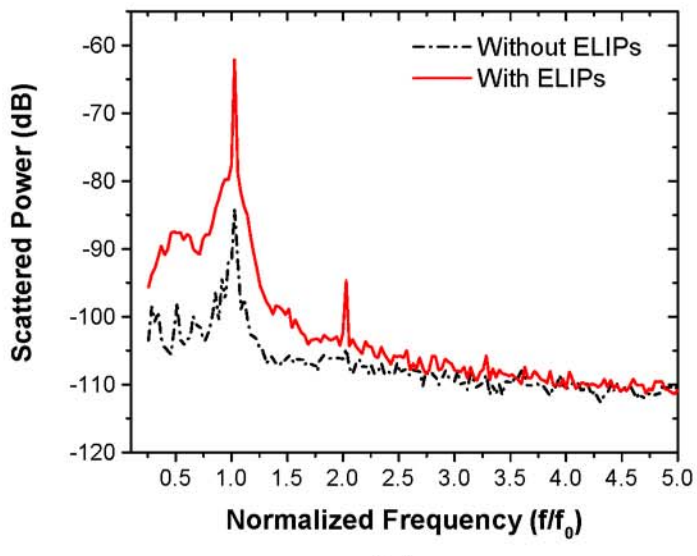
For all the different formulations, the proof of echogenicity was obtained using both *in vitro* acoustic scattering experiments and ultrasound imaging using the clinical

scanners. The results are discussed below.

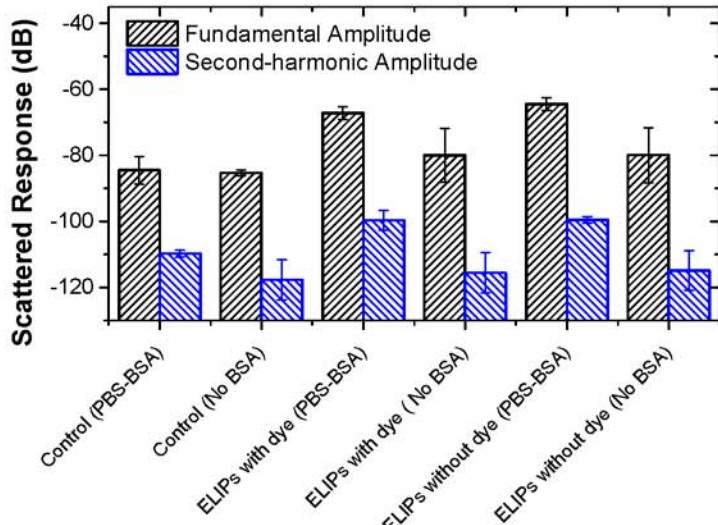
11.4.2.1 MMP-9 Cleavable ELIPs

Echogenicity of the ELIPs (reconstituted from freeze dried powders) with and without encapsulated carboxyfluorescein was investigated using the larger volume setup for scattering measurements [See Section 3.3.4]. We observed that the liposomes showed echogenicity only when freeze dried and subsequently reconstituted. However, this leads to some loss of the encapsulated dye. As mentioned above, the echogenicity is likely due to the presence of larger size liposomes with encapsulated gas in the reconstituted samples (see Figures 11.1b and 11.1d). The ELIPs were excited at a frequency of 3.5 MHz with an acoustic pressure amplitude of 500 kPa. Figure 11.6a shows the FFT of the scattered response from suspension with and without any ELIPs. At an acoustic pressure of 500 kPa, we observed distinct peaks at both fundamental frequency (i.e., at excitation frequency of 3.5 MHz) and second-harmonic frequency (i.e., at twice the excitation frequency, 7 MHz) in presence of the ELIPs. However, no distinct subharmonic peak (i.e., response at half the excitation frequency, 1.75 MHz) was observed. The nominal central frequency (5.54 MHz) of the receiving transducer is rather high compared to the subharmonic frequency (1.75 MHz). However, using a receiving transducer with a lower central frequency (2.25 MHz) did not change the result. We conclude that these ELIPs do not generate any significant subharmonic response at this excitation frequency. Figure 11.6b shows the experimentally measured echogenic response from the ELIPs (the scattered fundamental and second-harmonic components). Control measurements are acquired without any ELIPs in the sample solution. Each set of experiments was repeated five times. The mean of the five different runs is plotted along with the corresponding standard deviation. We also imaged the ELIPs (in a well plate) employing a Terason t3200 ultrasonic medical imaging system using a 4 – 15 MHz transducer (Figure 11.7).

We observed that both ELIP formulations, with and without encapsulated dye, show echogenicity with nearly 20 dB enhancement of the fundamental response when



(a)



(b)

Figure 11.6: (a) FFT of the scattered signal from a suspension with (red trace) and without (black trace) liposomes at an acoustic pressure of 500 kPa. (b) Fundamental and second-harmonic components of ultrasound scattered response from MMP-9 cleavable ELIPs prepared with or without dye-loading and reconstituted in PBS and PBS-BSA solutions. Lipid concentration was 10 $\mu\text{g}/\text{ml}$. Reprinted with permission from [115]. Copyright (2012) American Chemical Society.

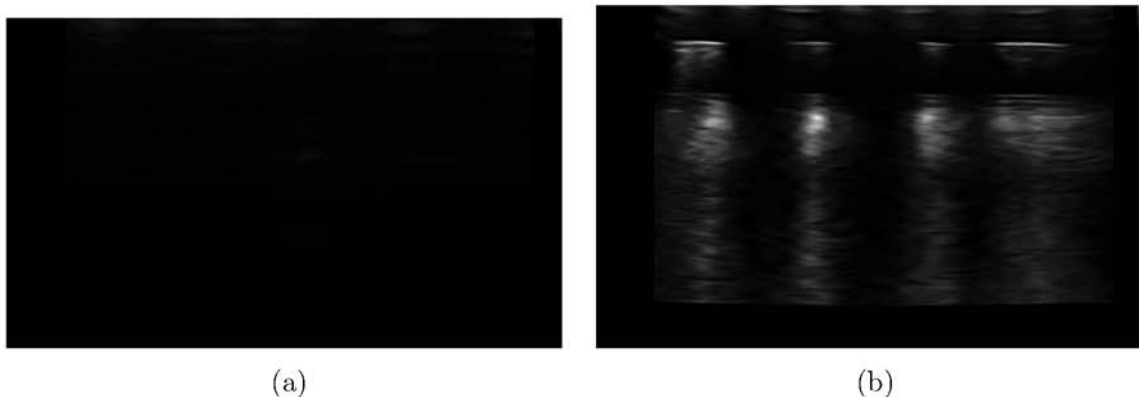


Figure 11.7: Ultrasound images (5 – 10 MHz transducer) of MMP-9 cleavable ELIPs incorporating LP4 peptide and encapsulating the dye carboxyfluorescein acquired using Terason t3200 medical imaging system. (a) Control Images without any liposomes. (b) Images in presence of reconstituted ELIPs in the suspension. Lipid concentration was 0.2 mg/ml. Reprinted with permission from [115]. Copyright (2012) American Chemical Society.

reconstituted in PBS-BSA at a lipid concentration 10 $\mu\text{g}/\text{ml}$. The preparation procedure includes addition of mannitol, a weak cryoprotectant. It has been hypothesized that lyophilization in presence of mannitol creates defects in the bilayer that serves as nucleation sites for air entrapment, which makes these ELIPs echogenic [108]. Although, the echogenicity of the ELIPs have been attributed to the presence of these purported air pockets, their exact location or dimensions still remains uncertain. Notably, there is no difference in the echogenicity of the ELIPs due to the dye-loading. The ELIPs also show nonlinear response with around 10 dB enhancement for the second-harmonic response. Note that the enhancement of scattered acoustic pressure at the fundamental frequency is considerably lower for both conventional and polymerized ELIP formulations discussed in Chapters 9 and 10 respectively. We believe this to be the cumulative effect of the modified of the preparation protocol and different size distributions. We also observe that to obtain statistically significant enhancement over control, presence of BSA in the buffer was essential. This observation is consistent with our earlier findings with conventional ELIPs.

11.4.2.2 Polymer Coated Redox Triggered ELIPs

Similar to other literature reports [32, 109], we observed by TEM the presence of air bubble either inside the aqueous interior or in the bilayer of this specific ELIP formulation (Figure 11.3a). The ELIPs prepared following freeze-drying/reconstitution in presence of mannitol also showed significant echogenicity, incontrovertibly indicating air entrapment. As with the conventional ELIPs and MMP-9 cleavable ELIPs, no sub-harmonic response was observed in the scattered power spectrum and not shown here for brevity. Figure 11.8 shows the scattered response from a suspension of these ELIPs under ultrasonic excitation for two different frequency components viz. fundamental (at frequency of excitation 3.5 MHz), and second harmonic (at twice the excitation frequency 7 MHz) at 500 kPa acoustic excitation pressure. The control data indicates the response without any ELIPs in suspension. There is an enhancement in response for both the components, which demonstrates the echogenic nature of these ELIPs. The fundamental response shows around 20 dB enhancement for the lipid concentration of 5 $\mu\text{g}/\text{ml}$. However, the nonlinear response from the ELIPs is much weaker with only 8 dB enhancement for the second-harmonic component. The enhancement of the fundamental and second-harmonic component was also weaker in comparison to the conventional and polymerized ELIP formulations. The weaker response here may be attributed to the change in the lipid composition, difference in size distribution, and increased strength of lipid shell due to polymerization. Echogenicity was also confirmed by ultrasound imaging with a Terason t3200 ultrasonic medical imaging system using a 4–15 MHz transducer. Reconstituted ELIPs reflected ultrasound indicating presence of entrapped air inside (Figure 11.9b) whereas control samples (no ELIPs) were dark due to absence of reflections (Figure 11.9a).

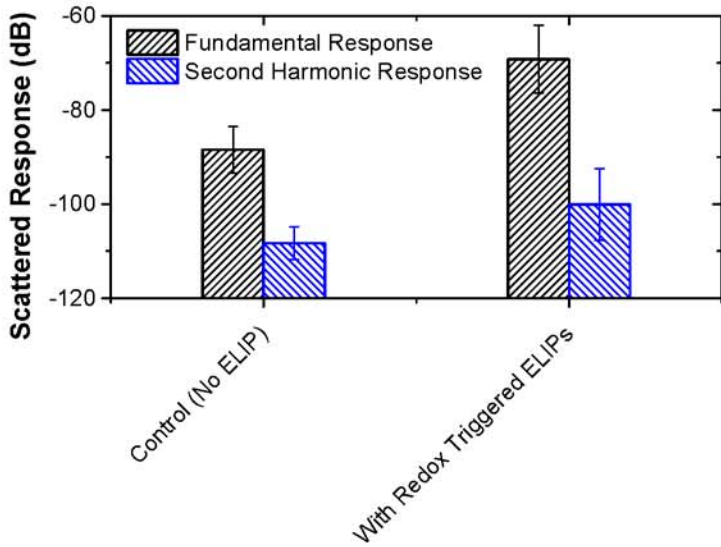


Figure 11.8: Fundamental and second-harmonic components of ultrasound scattered response from redox triggered ELIPs prepared reconstituted in PBS-BSA solutions. Lipid concentration was 5 $\mu\text{g}/\text{ml}$. Reprinted with permission from [114]. Copyright (2013) American Chemical Society.

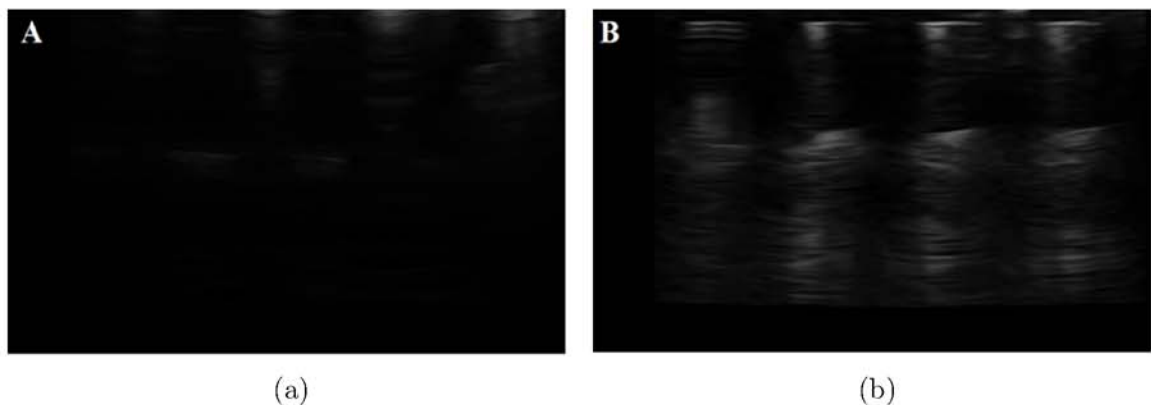
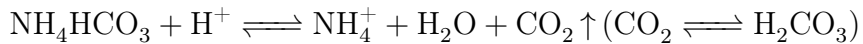


Figure 11.9: Ultrasound images (4 – 15 MHz transducer) of redox triggered ELIPs reconstituted in 10 mM HEPES buffer pH 7.4 acquired using Terason t3200 medical imaging system. (a) Control Images without any liposomes. (b) Images in presence of reconstituted ELIPs in the suspension. Lipid concentration was 0.1 mg/ml. Reprinted with permission from [114]. Copyright (2013) American Chemical Society.

11.4.2.3 pH Sensitive Liposomes with Tunable Echogenicity

Unlike the previous two liposome formulations, the acoustic properties of the pH sensitive liposomes are governed by a completely different mechanism. Our hypothesis was that the inward migration of hydronium ions into the liposomes in mild to strong acidic environment will trigger the following chemical reaction:



As the carbon dioxide gas is slowly generated within the liposomes they will grow in size and also start pulsating under acoustic excitation. Eventually, the bilayer will not be able to sustain the tension and rupture thereby releasing the gas and along with the encapsulated contents within the liposomes (fluorescent dye molecules in our case). Hence, we expect no echogenic from the liposomes under neutral to basic pH values. As soon as an acid will be added, the CO_2 generation will take and finite time during which no echogenicity should be observed, followed by a rapid rise in response and then a sudden drop. However, our previous used acoustic data acquisition mechanism relied on averaging the response over 5-10 mins, which will clearly be unsuitable for capturing such transient response. Hence, we utilized a time dependent scattering measurement as described in Section 3.3.5 of Chapter 3. The resultant data, averaged over three independent runs, are shown in Figure 11.10.

Figure 11.10 shows the time dependent scattered fundamental response pH sensitive ELIPs at pH of 6.0. At pH 5.0 we could not acquired any scattered response in our in vitro measurements, which will be explained later. The most notable observation is that the enhancement over control is very weak (2-5 dB) even with a significantly high lipid concentration of 0.01-0.05 mg/ml. Note that at such high concentration attenuation due to the bubbles will definitely contribute to the reduction of the scattered response. However, reduction of lipid concentration below these value showed no enhancement. As we can observe increasing acoustic excitation pressure to record stronger enhancement resulted in the opposite effect — See the olive colored line goes below black colored line (control) in the figure. In spite of our best efforts using our

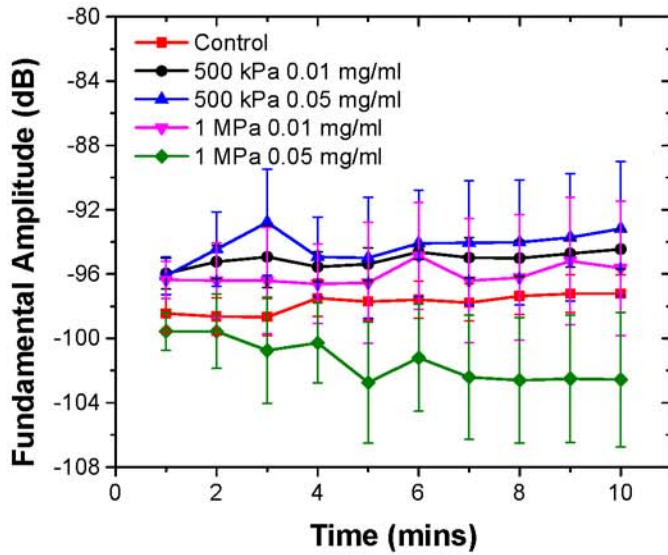


Figure 11.10: Time dependent scattered fundamental response from pH sensitive ELIPs for different lipid concentrations and acoustic excitation pressures. Excitation frequency was 5 MHz and the pH of the solution was maintained at a value of 6.

acoustic scattering setup did not give us satisfactory results to substantially validate the echogenicity of these pH sensitive ELIPs. We are currently investigating the reason behind this and have the following hypotheses.

1. Due to generation of gas bubbles inside the ELIPs they are floating up and going out of the transducer focus thereby showing no response in our scattering measurements.
2. The excitation frequency (5 MHz) is probably not optimal for the optimum acoustic response from pH sensitive ELIPs. With the existing mechanism there is no assurance we will get micron sized structures. Rather we can have a large number nanometer sized gas bubble, which will have a resonance frequency higher than 10 MHz.
3. Increasing acoustic pressure to increase enhancement will not work as they will accelerate lipid bilayer rupture leading to rapid loss of echogenicity.
4. Since the acoustic excitation wave has to travel a large distance through the suspension of bubbles, the larger volume setup will definitely result in reduction of scattered response. We have validated this hypothesis by increasing concentration of Definity microbubbles [See Section 7.3.1 for more details].

However, ultrasound imaging, which captures instantaneous images from the suspension were capable of detecting strong reflections from these ELIPs. Note that by virtue of or setup construction, we can detect signal from ELIPs even if they are floating up [See Figure 3.3.6 in Chapter 3]. It also offered us to choice of dynamic variation of frequency from 5-15 MHz. Hence, all further validations of echogenicity was pursued using ultrasound imaging and few representative results are presented below. *The images and analysis presented below for pH sensitive ELIPs were acquired by our collaborators at North Dakota State University.*

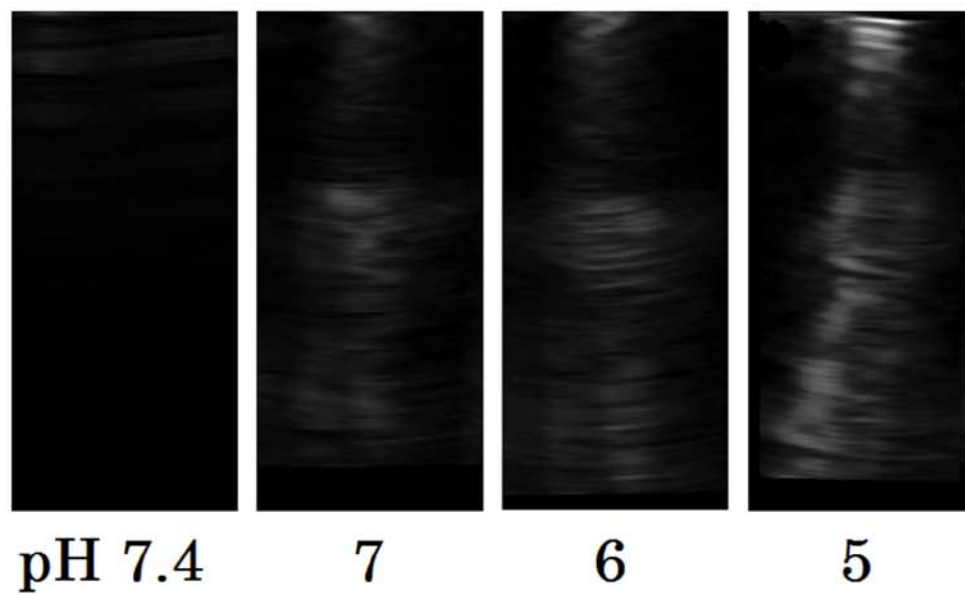


Figure 11.11: Ultrasound images of pH sensitive liposomes incubated in different acidic pH buffers, with high frequency diagnostic ultrasound transducer (12-14 MHz).

Figure 11.11 shows ultrasound images of pH sensitive liposomes incubated in series of different pH buffers. We observed that ultrasound starts reflecting after about five minutes of incubation, indicating generation of CO_2 gas bubbles inside by the reaction of ammonium bicarbonate with H^+ ions diffused from the outside environment. It is evident from the figure that with increase in acidity of the buffer images became brighter. For a more quantitative comparison, we analyzed images of each well using ImageJ software (Version 1.47; U. S. National Institutes of Health, Bethesda, Maryland, USA) to calculate mean grey scale and maximum gray scale values [See Figure 11.12].

As expected the mean and maximum grey scale value increase with decrease in pH, highest value found was 18 which becomes almost constant below pH 5 [See Figure 11.12a]. We expect that when these liposomes will get distributed throughout the body, but they will only start reflecting the ultrasound only when they reach the acidic micro-environment of cancerous tumors. Thus, the ph tunable echogenicity hypothesis is successfully validated.

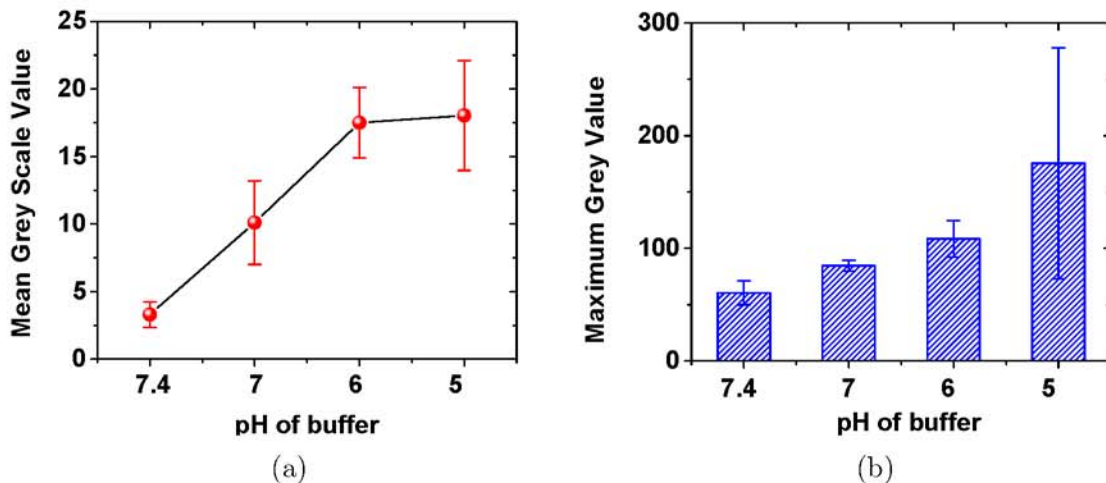


Figure 11.12: Mean gray scale value (a) and maximum gray scale value (b) of ultrasound images (Figure 11.11) of pH tunable echogenic liposomes as a function of pH of the buffer.

11.4.2.4 Redox Sensitive Echogenic Polymersomes

The polymersomes were prepared to have better control over the properties of the outer layer of the vesicle, which in turn would enable us to tune their echogenic properties. The scattered response from polymersomes was measured using the *smaller volume setup*. The excitation frequency was 3.5 MHz with an acoustic pressure amplitude of 250 kPa. A lipid concentration of 10 µg/ml was used for all experiments without any problem of signal attenuation by virtue of the setup design. Figure 11.13 shows the scattered response from two different formulations — 3600 and 5800 molecular weights. Note that for the 5800 batch both second-harmonic and subharmonic components were detected in the scattered acoustic spectra. However, unlike the nonlinear response from

microbubble based contrast agents, the detection of the nonlinear responses from 5800 polymersomes were inconsistent and varied from one run to another. Hence, all three components i.e., fundamental, subharmonic and second-harmonic are shown during comparison [See Figure 11.13b]. For the 3600 batch the nonlinear components were consistently absent in all our runs and hence not shown here [See Figure 11.13a]. The lack of or the inconsistency of nonlinear response can either be due to lower pressure amplitude (250 kPa) used here or due to the inherent acoustic properties of these polymersomes. Further studies are presently being conducted to verify these hypotheses. Note that the 5800 batch shows around 20 dB, 10 dB and 4 dB enhancement over the control (i.e., without any polymersomes) for the fundamental, subharmonic and second-harmonic components. However, the enhancement was much weaker for the 3600 batch — around 8 dB for the fundamental component. This indicates that modifying the encapsulating layer of these polymersomes will enable us to tune their acoustic properties, which is consistent with our initial hypotheses.

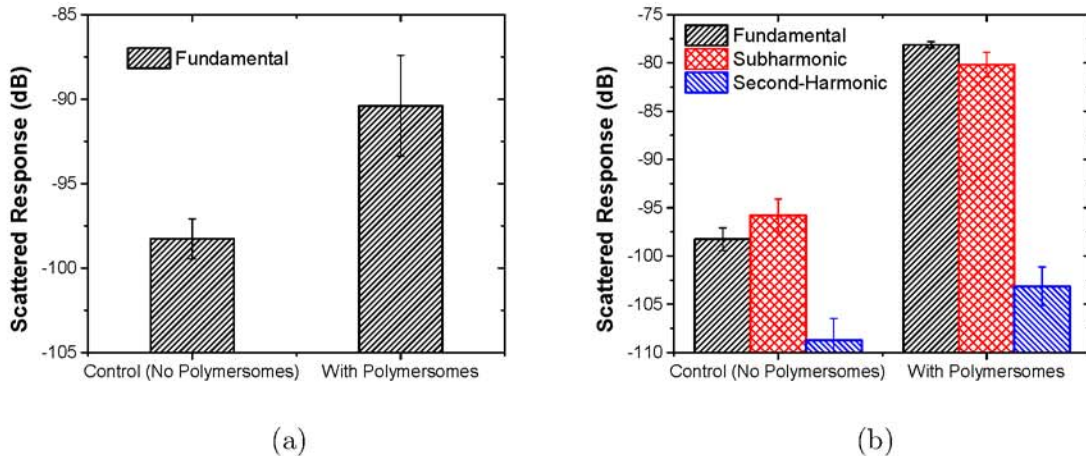


Figure 11.13: Scatter response from (a) 3600 molecular weight and (b) 5800 molecular weight batches of polymersomes. Experiments were performed at 3.5 MHz, 250 kPa excitation with a lipid concentration of 10 $\mu\text{g}/\text{ml}$. Subharmonic and second-harmonic response were not detected for 3600 batch.

We also expected these polymersomes to be fairly stable due to the polymerization involved with their preparation protocol. To test this we did a time dependent

scattering measurements with both the batches as shown in Figure 11.14. The scattered response was stable for both the batches with around 5 dB decay over 10 minutes. A more comprehensive destruction threshold measurement approach should be undertaken in future to substantiate this claim for polymersomes as was done with PLA microbubbles and polymerized ELIPs in earlier chapters.

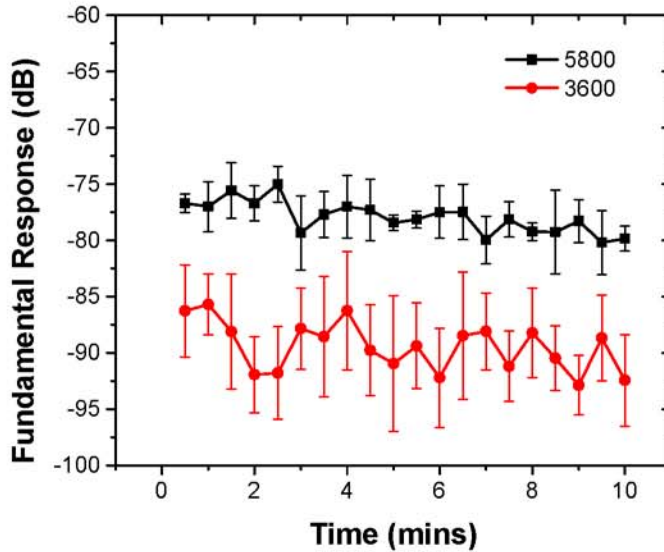


Figure 11.14: Time dependent scattered fundamental response from redox sensitive echogenic polymersomes.

The echogenicity of these polymersomes were also verified with ultrasound imaging using the Terason t3200 scanner. The images obtained are shown below in Figure 11.15. The mean gray scale values were calculated from the images in Figure 11.15 using the ImageJ software and their comparison is shown in Figure 11.16. Both 3600 and 5800 batches show higher response than control. Moreover, the response from the 5800 batch was also higher than the 3600 batch in the images obtained (a Student t-test gave a p-value of 1.65×10^{-9}), which corroborates our findings with the acoustic backscatter experiments earlier.

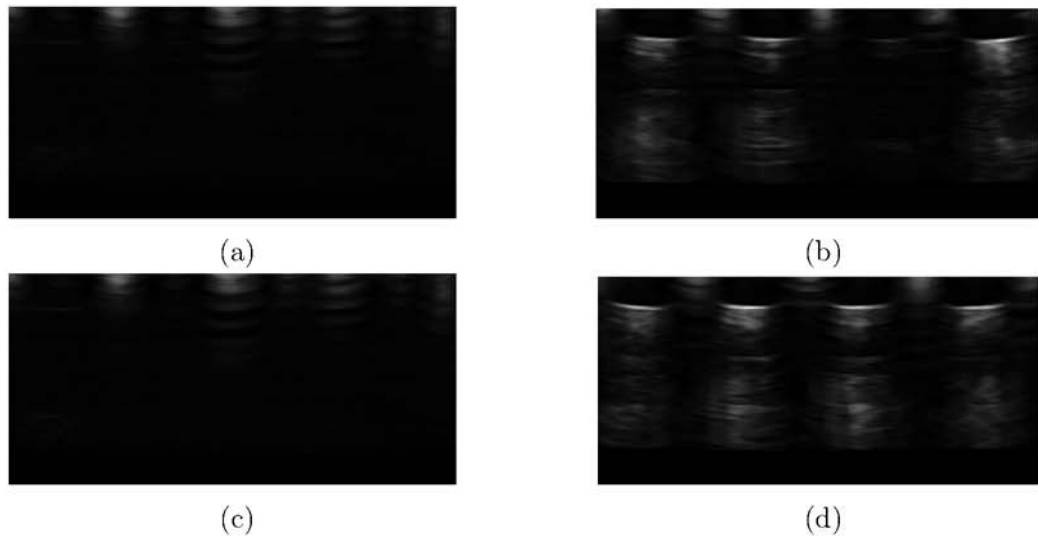


Figure 11.15: Ultrasound images of redox sensitive echogenic polymersomes acquired using Terason t3200 medical imaging system. (a) Control Images without any polymersomes. (b) Images in presence of 3600 batch of polymersomes. (c) Control Images without any polymersomes. (b) Images in presence of 5800 batch of polymersomes. Lipid concentration was 0.01 mg/ml.

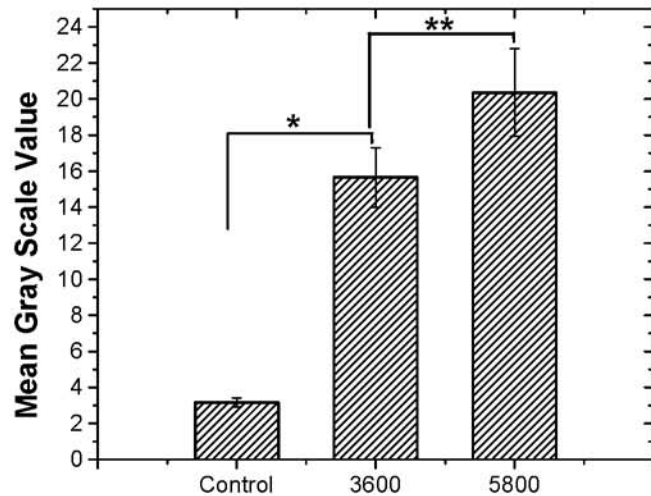


Figure 11.16: Comparison of the mean gray scale values for ultrasound images shown in Figure 11.15.

11.4.3 Proof of Ultrasound Enhanced Stimuli Responsive Release

For our drug release studies, we used a single element flat faced ultrasound transducer that was carefully calibrated to determine accurately the output energy of the ultrasound pulse. The transducer was excited with a continuous wave ultrasound pulse. The excitation frequency, output pressure and duration of excitation was chosen for optimal release of contents under static conditions [See Table 3]. For a set of positive control experiments, we also utilized a 22.5 kHz sonic dismembrator at 4 W output setting.

11.4.3.1 MMP-9 Cleavable ELIPs

For the MMP-9 cleavable ELIPs, carboxyfluorescein was encapsulated to quantify the release of liposomal contents by employing a self-quenching strategy. During initial optimization studies a larger diameter (1.27 cm) 2.25 MHz transducer was used to vary the frequency and power of excitation using the release setup described in Section 3.3.7. Figure 11.17a shows the percentage release of the dye as a function of excitation frequency and acoustic pressure amplitude. The release was almost negligible both at 1 MHz and 2.25 MHz for 2 minute exposure time. However, changing the exposure time from 2 min to 4 minutes showed a significant increase in the release [See Figure 11.17b].

Since, the larger diameter setup required use of 12 well plate a lot of sample was required for each run (2.5 ml sample volume per run), which restricted the number of runs and higher concentration experiments. A smaller diameter (1 cm) 3 MHz transducer was eventually utilized for the subsequent studies in 48 well plates. We noticed that a continuous wave excitation at 3 MPa was required for satisfactory release of contents i.e., greater than 10%, from MMP-9 cleavable ELIPs. Figure 11.18 shows the role of exposure times on the percentage release, with 3 min exposure time at 3 MHz, 3 MPa continuous wave excitation with ultrasound resulting in 20% release. Hence, for ultrasound mediated release studies for MMP-9 cleavable ELIPs we choose

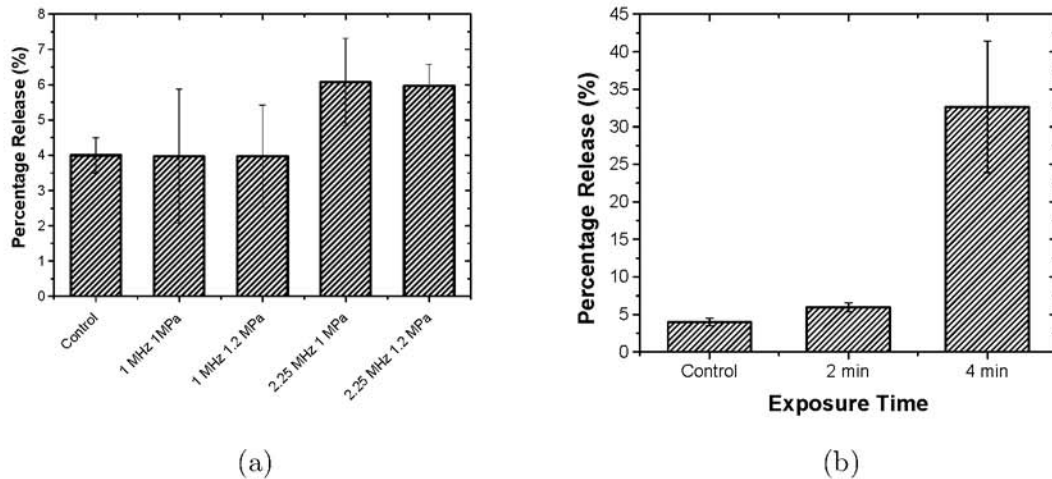


Figure 11.17: Ultrasound triggered release from MMP-9 cleavable ELIPs with a larger diameter 2.25 MHz transducer. (a) Release as a function of excitation frequency and acoustic excitation pressure for 2 min exposure. (b) Role of exposure time in ultrasound triggered release at 2.25 MHz, 1 MPa excitation.

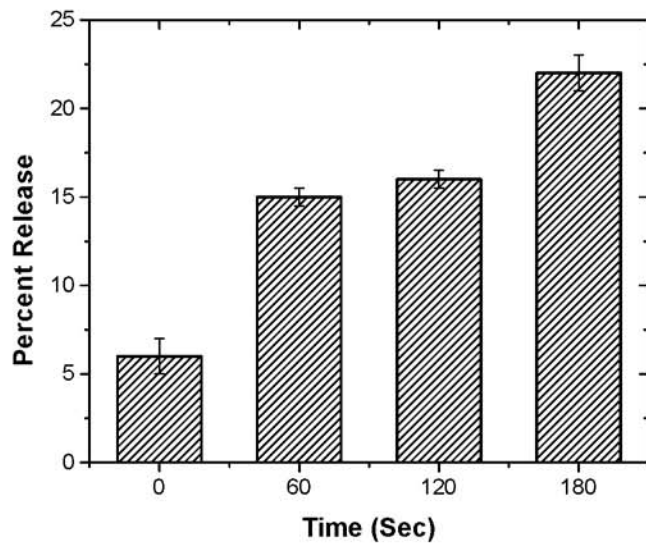
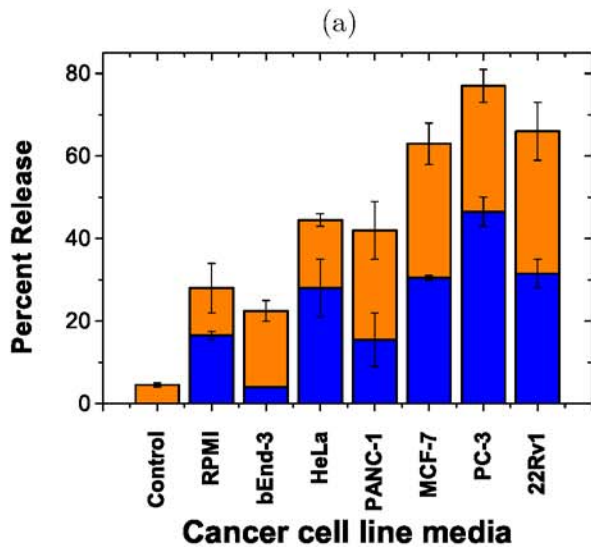
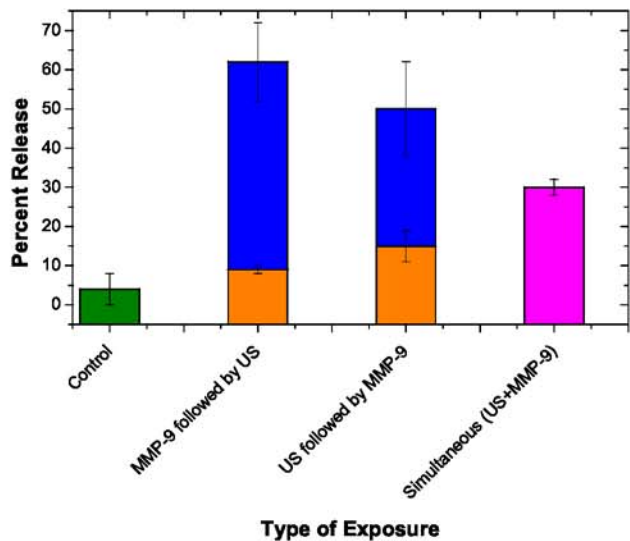


Figure 11.18: Role of exposure time in ultrasound triggered release from MMP-9 cleavable ELIPs at 3 MHz, 3 MPa continuous wave excitation. Reprinted with permission from [115]. Copyright (2012) American Chemical Society.

the following parameters for further investigations: 3 MHz continuous wave excitation at 3 MPa acoustic pressure amplitude for a duration of 3 minutes.

Figure 11.19a shows ultrasound enhanced recombinant MMP-9 triggered release



(b)

Figure 11.19: Ultrasound (US) enhanced MMP-9 triggered release of contents from ELIPs at 3 MHz, 3 MPa continuous wave excitation. (a) Release of contents in presence of recombinant MMP-9 and ultrasound. (b) Release of liposomal contents in presence of conditioned cell culture media from metastatic cancer cells and upon subsequent application ultrasound. In both the figures, the olive, orange, blue, and magenta colored bars represents the passive release in absence of any trigger, release due to US only, release due to MMP-9 only, and the release with simultaneous application of US and the MMP-9 enzymatic trigger respectively. Reprinted with permission from [115]. Copyright (2012) American Chemical Society.

of contents from the ELIPs. About 50-60% release was observed with recombinant MMP-9 enzymes, which was further enhanced by 10-20% upon application of ultrasound. The total release was slightly higher when ELIPs were exposed to recombinant MMP-9 first followed by ultrasound application. However, the simultaneous application of ultrasound and enzymatic trigger showed a reduction in release, possibly due to localized increase of temperature during ultrasonic excitation that reduced the activity of the recombinant enzymes (bulk temperature was maintained constant by using an ice bath). It should also be mentioned that we utilized the non-lyophilized version of the liposomes for our release studies. Hence, we do not expect any interference in our fluorescence measurements due to presence of gas bubbles.

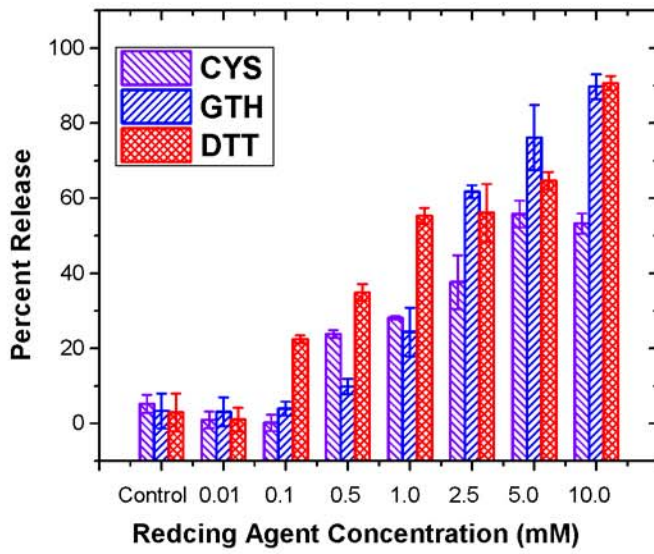
Various cancer cells are known to secrete varying amounts of MMP-9 in the extracellular matrix [411]. We decided to determine if the conditioned media from cancer cells can release the encapsulated dye from the ELIPs and if this release can be further enhanced by the application of diagnostic frequency ultrasound. In this endeavor, we cultured the cells HeLa (cervical cancer), PC-3 (prostate cancer), 22Rv1 (prostate cancer), MCF-7 (breast cancer) and PANC-1 (pancreatic cancer) in dye-free RPMI culture media. After reaching confluence, the cells were pelleted and the media was harvested. The immortalized mouse brain endothelial cell line bEnd-3 (which does not secrete MMP-9 [412]) was taken as control. Based on our observation with recombinant enzymes, we incubated the ELIPs with the conditioned media for an hour, followed by the application of ultrasound pulses for 3 min duration. Around 20-50% release was observed with conditioned cell culture media from cancer cells secreting MMP-9 [Figure 11.19b]. This release was further enhanced by 20-30% by the application of ultrasound.

11.4.3.2 Polymer Coated Redox Triggered ELIPs

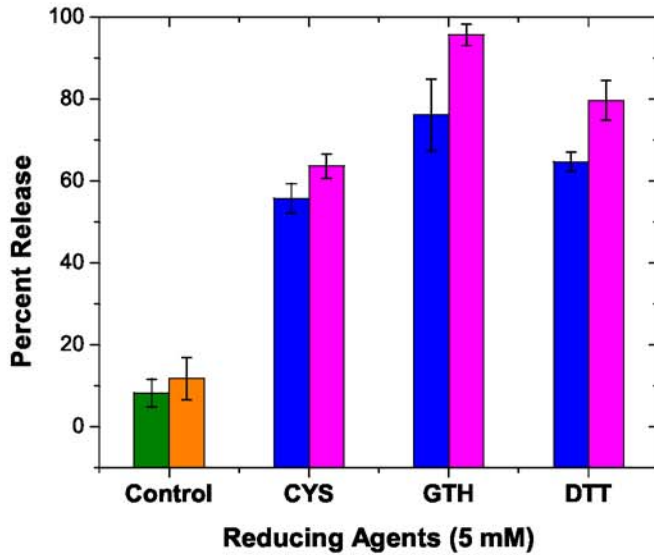
The polymer coated ELIPs had a disulfide cross-linkage that is stable in mildly oxidizing environment but unstable in presence of reducing agents. In order to achieve

active internalization of the ELIPs in cancer cells, we also incorporated a folate conjugated lipid in the ELIPs . A CoCl₂ quenching strategy [See Section 3.3.7.2] was implemented to quantify release of calcein from these polymer coated ELIPs in the presence of both redox and ultrasound triggers. Different reducing agents were also used in our study for comparison, which includes dithiothreitol (DTT), cysteine (CYS) and glutathione GSH). Negligible release (less than 5%) was observed in our control samples i.e., both without ultrasound and reducing agents. At a very low concentration of reducing agents (10 μM, which corresponds to its concentration in extracellular matrix), the release was also less than 5%, but it increased significantly with increasing reducing agent concentration [See Figure 11.20a]. We were able to obtain up to 90% release with just reducing agents at 10 mM concentrations (typical in cell cytoplasm of affected by cancer). The results for ultrasound (3 MHz, 0.53 MPa continuous wave excitation for 2 mins) enhanced release are shown in Figure 11.20b. As with the MMP-9 cleavable ELIPs, there was significantly less release with just the application of 3 MHz ultrasound. However, about 8-20% enhancement over redox triggered release was observed with simultaneous application of 5 mM redox and ultrasound.

We cannot present the ultrasound mediated release studies with pH sensitive ELIPs and polymersomes as this point of time as they currently being optimized. For pH sensitive ELIPs some preliminary data was obtained by our collaborators that validate the proposed working principle and is currently submitted for publication and awaiting review [361].



(a)



(b)

Figure 11.20: (a) Redox triggered release of calcein from polymer coated ELIPs with increasing concentration of reducing agents CYS (violet stripes), GSH (blue stripes) and DTT (red stripes). (b) Ultrasound (US) enhanced redox triggered release from polymer coated ELIPs. The olive, orange, blue, and magenta colored bars represents the passive release in absence of any trigger, release due to US only (3 MHz, 0.53 MPa, continuous wave excitation for 2 min), release due to reducing agent only (5 mM), and the release with simultaneous application of US and the redox trigger respectively. Reprinted with permission from [114]. Copyright (2013) American Chemical Society.

11.5 Summary and Conclusions

In vitro validation of the concept of ‘dual-purpose’ contrast agents was presented for various formulations involving liposomes and polymersomes. All these formulations were echogenic as verified by both acoustic measurements and ultrasound imaging, except for the pH sensitive ELIPs. Diagnostic frequency ultrasound alone was not able to cause optimal release of contents. However, a dual triggering strategy was successful showing considerable enhancement in the release due to ultrasound (8-20%). Future studies must be undertaken for an extensive parametric study of ultrasound-mediated release for enhanced release. However, the experimental data acquired till date conclusively demonstrates the potential for clinical applications of these novel formulations.

Chapter 12

CONCLUSIONS AND FUTURE WORK

12.1 A Review of the Outcomes

The primary objective of this thesis was to characterize the acoustic behavior and the contents release characteristics of ultrasound contrast agents for developing multi-functional agents. two different types of contrast agent were studied viz., conventional microbubble based contrast agents with a stabilizing layer of lipids/polymers and liposome/polymersome based formulations.

12.1.1 Characterization of Ultrasound Contrast Microbubbles

Microbubbles are nonlinear systems capable of generating subharmonic response (i.e., response at half the excitation frequency), which results in better signal to noise ratio in ultrasound images. Subharmonic imaging have also been suggested as a potential tool for local blood pressure estimation and monitoring. In spite of the staggering amount of experimental data characterizing various nonlinear behavior of encapsulated microbubbles and two decades of modeling efforts, our understanding of encapsulated bubble dynamics remains incomplete. Motivated by the need for developing reliable mathematical models of nonlinear encapsulated bubble dynamics and the subsequent improvement of the understanding of the underlying mechanisms of contrast agent behavior, observed both experimentally and numerically, we sought to characterize the behavior of contrast microbubbles. Unlike, several existing reports we attempted a suitable coupling of rigorous mathematical modeling and numerical simulations with extensive *in vitro* experimental characterization. Such concerted efforts have led to the development of a two-pronged hierarchical approach where a model is formulated

and applied to one set of experimental data to estimate model parameters (i.e., perform material characterization), and then the same model is validated against a second independent experiment. This approach was utilized for material characterization of lipid and polymeric encapsulation materials for several commercial and experimental contrast agents, which was subsequently incorporated in the bubble dynamics equation for their predicting nonlinear response. A parallel numerical investigation in our group had indicated, in contradiction to existing experimental results, the magnitude of subharmonic response from microbubbles can either increase, decrease or vary non-monotonically with increasing ambient pressure(p_0). An experimental validation of these results was also attempted by designing a modified acoustic setup for performing pressurized acoustic experiments. The results of the above mentioned studies were presented in first part of the thesis and the significant outcomes are summarized below.

12.1.2 Strain-Softening Models of Contrast Agent Encapsulation

The failure of the proposed constant elasticity models in predicting nonlinear response motivated us to incorporate nonlinear elastic models. We proposed two simple nonlinear extensions of the constant elasticity mode (Hooke’s law) — elasticity varying linearly with area fraction i.e. a quadratic elasticity model (QEM), and an exponentially varying elasticity model (EEM). Both nonlinear models represent the strain softening resulting from the decreased association between constituent molecules in the encapsulation as its area increases. Note that elasticity of the encapsulation has been shown to play a critical role in long-time microbubble stability [15, 196]. Both QEM and EEM predicted similar radial dynamics in our numerical simulations. The EEM was also capable in predicting the experimentally observed “compression-only” behavior by imposing the condition of non-negativity on the effective surface tension term, similar to another popular nonlinear elastic interfacial model proposed by [164]. However, we argue such a condition need not be imposed for contrast agents since, elasticity could be considered as a separate term independently introduced in the formulation. Moreover, an effective negative surface tension can also explain the buckling of the

encapsulation observed experimentally. Analytical subharmonic threshold predictions demonstrated the ability of nonlinear models to predict lower subharmonic thresholds.

12.1.2.1 Characterization of Lipid Coated Microbubbles

After, validating the effectiveness of the strain-softening models, we implemented them for characterization of lipid coated microbubbles — Sonazoid™ and Definity®. The estimated model parameters obtained characterizing the encapsulation of both these bubbles were very similar indicating the similarity of lipid coatings. Our estimates were also similar to the existing reports in the literature. However, it was shown that even though the consideration of polydispersity during our property estimation amplifies the ill-posed nature of the problem, they should not be neglected in our characterization protocol to avoid inaccurate and unsatisfactory predictions.

Both QEM and EEM performed equally well in predicting the subharmonic response from Sonazoid. Since the exponential variation of surface elasticity seems more physical we implemented it for all our subsequent numerical investigations of contrast agent dynamics. We were able to show good agreement with experimentally observed subharmonic behavior for both Sonazoid and Definity microbubbles, thereby demonstrating their effectiveness.

12.1.2.2 Characterization of Polymer Encapsulated Microbubbles

The interfacial models were also utilized in the characterization of polymer encapsulated microbubbles. Our investigations indicated that in spite of using the same polymer (polylactides), the material properties of the encapsulations were substantially different based on the preparation protocol.

PLA microbubbles prepared using a double-emulsification technique, was associated with very low elasticity and dilatational viscosity values. As with lipid coated microbubbles, the size distribution was shown to play a critical role in our parameter estimations indicating the pitfalls associated with erroneous approach of using an

average size to represent a polydisperse bubble suspension. Consideration of polydispersity helped us address the paradoxical observation of low resonance behavior of these microbubbles and also obtain better agreement with experimentally measured subharmonic generation thresholds. However, unlike the lipid coated bubble an unqualified match could not be obtained indicating the need for further model improvements/modifications.

The PB-127 and Philips bubble were prepared with a special protocol with the hypothesis that it will result in constant shell thickness to radius ratio for these bubbles. Our estimates, which was critically dependent on the consideration of polydispersity, was consistent with this hypothesis. However, except for thinner shelled PB-127 bubbles, our subharmonic predictions did not match with experimental measurements. Hence, the model in its present form seems incapable of predicting dynamics of thick-shelled contrast microbubbles.

12.1.2.3 Experimental Investigation of Ambient Pressure Dependent Subharmonic Response

The experimental setup developed was capable of performing pressurized acoustic experiments without any considerable loss of pressure over the course of the experiments. Ambient pressure dependent subharmonic response from “expired” Definity batches showed both consistent decrease (excited below resonance frequency) and non-monotonic behavior (excited at twice the resonance frequency) with increasing ambient overpressure, whereas PLA mcirobubbles excited at resonance frequency showed a linear decrease. Preliminary results are encouraging justifying further experimental investigations for a more extensive validation.

12.1.3 Design and Development of ‘Dual-Purpose’ Echogenic Liposomes and Polymersomes

Echogenic liposomes (ELIPs), which combine the advantages of liposomes such as, bio- compatibility, ability to encapsulate both hydrophobic and hydrophilic drugs

etc., with strong reflections of ultrasound are also an excellent candidate for concurrent ultrasound imaging and drug delivery applications. Polymersomes or vesicular mesophases provide an elegant alternative to cellular targeting and cytoplasmic delivery of drugs and offer a greater degree of control over the agent property by suitably modifying the constituent polymers. In spite of their immense potential, there has been no substantial effort to develop echogenic polymersomes. Experimental characterization of the ELIPs and polymersomes was performed with the goal of demonstrating their potential as ultrasound agents with simultaneous imaging and drug/gene delivery applications thereby validating the concept of ‘dual-purpose’ contrast agents. the significant outcomes of these studies are summarized below.

12.1.3.1 Acoustic Characterization of Conventional and Polymerized Echogenic Liposomes

The echogenicity of the conventional ELIP formulation was conclusively demonstrated through *in vitro* experiments. No subharmonic response was observed form the conventional ELIPs for the range of acoustic frequencies and pressures investigated. However, we were able to obtain subharmonic response by altering the constituents of the lipid bilayer using a polymerization process (Pol-ELIPs). The larger population of bigger liposomes detected in our size measurements were deemed responsible for this observation. The results indicate that the echogenic properties of these ELIPs can be tuned by controlling the preparation protocol.

The freeze-thaw and lyophilization-reconstitution steps in presence of a weak cryo-protectant mannitol, adopted in both the preparation protocols, were found to be critical for echogenic nature of these liposomes, which is consistent with existing hypothesis. The liposome suspensions were highly polydisperse resulting in greater variability during the experiments. The polydispersity also resulted lack of any distinct resonance behavior in the diagnostic imaging frequency regime (1-10 MHz). In spite of conclusive experimental evidence, the understanding of the underlying mechanisms behind the observed echogenicity remains incomplete. Moreover, the lack of

our knowledge of the exact location and dimension of the air pockets along with high polydispersity of the suspensions severely restricts the our ability to formulate mathematical models describing their dynamics. We believe that the echogenicity is primarily due to the existence of a smaller fraction of larger liposomes, which will have larger gas pockets.

12.1.3.2 Experimental Validation of the Concept of ‘Dual-Purpose’ Contrast Agent

For the experimental validation of the concept of ‘dual-purpose’ contrast agents, four novel formulations were investigated — a substrate lipopeptide conjugated ELIP formulation that can be triggered by the extracellular enzyme matrix metalloproteinase-9 (MMP-9), a polymer coated redox triggered ELIP formulation for cytosolic drug delivery, pH sensitive liposomes with tunable echogenicity capable of drug-release in mildly acidic micro-environment and redox sensitive echogenic polymersomes. Both *in vitro* acoustic studies and ultrasound imaging demonstrated the echogenicity of each formulation. Although, ultrasound excitation (< 5 MHz) alone was incapable of causing optimal release of contents, a dual-triggering strategy proved successful. Application of ultrasound in conjugation of other triggers (e.g., enzyme, pH, redox) showed significant enhancements (10-20%), which resulted in total release of up to 80-90%. Considering these experimental results, it can be safely concluded that these novel formulations can be potentially used for simultaneous imaging and therapeutic applications. If implemented successfully, such contrast agents can provide powerful treatment strategies for several cardiovascular diseases and cancer.

12.2 Limitations of this Study

Contrast microbubbles are developed with the final goal of *in vivo* applications in humans. The lack of *in vivo* validation of the results presented here is the biggest drawback of this study. Under those conditions several assumptions of the present study must be reconsidered through modifications like

1. Considering the effect of the capillary wall and bubble interactions instead of investigating bubble response in an infinite medium. This can be replicated *in vivo* by constructing a flow loop setup with a small diameter acoustically transparent cylindrical pipe acting as the sample chamber.
2. Considering the non-Newtonian behavior of the outside liquid (blood for practical applications).
3. Considering nonlinear propagation effects due to presence of surrounding tissues and blood and attenuation of the scattered signal due to the tissues.
4. Considering the change in the encapsulation properties due to interaction with serum proteins and other molecules in the blood stream.
5. Considering the change of size distribution due to gas content of the blood, lung filtration etc.
6. Considering the change in bubble stability and effect of recirculation under *in vivo* conditions.

Apart from these effects, contrast enhanced ultrasound images suffer from variability due to several factors like, scanner settings, changes in the local blood pressure in the vicinity of contrast agents, phagocytosis, tissue motion, contrast agent handling etc. An extensive review of the effects of such factors can be found in a recent publication by [413]. Hence, it is imperative that the present findings might not be directly equatable with *in vivo* observations using animal models or human trials. However, *in vitro* investigations like these are critically important to develop our fundamental understanding of the contrast agent behaviors. Without a sound knowledge of the physical mechanisms of the experimental observations obtained under controlled *in vitro* conditions, the applicability of contrast agents will remain prone to uncertainty and variability. Hence, we believe the results presented in this study will be an important precursor for further investigations under *in vivo* conditions.

12.3 Proposed Future Work

12.3.1 Scope for Model Improvement

As evident from the preceding discussion, the recent developments in interfacial models have significantly improved our understanding of encapsulated bubble

dynamics, and equipped us with powerful predictive tools of contrast agent behavior. However, none of the models enjoys unambiguous validity and each comes with a set of strengths and weaknesses. Moreover, emerging experimental techniques are reporting several new and interesting contrast agent behaviors. Therefore, further experiment driven model improvement is required to improve their reliability and widen their scope of applicability and few such suggestions are provided below.

- Preliminary results indicate that unlike the Marmottant model, our models cannot predict several experimentally observed nonlinear behavior for lipid coated microbubbles e.g., resonance skewing at very low acoustic pressures, thresholding behavior for the onset of bubble oscillations [183]. The reasons behind these should be investigated.
- Although, our model can predict compression-only behavior by imposing a condition of non-negativity on the effective surface tension, it results in higher sub-harmonic threshold predictions. Hence, the justification of condition of non-negativity should be reexamined. One approach might be to consider a compressive stress up to a certain limit allowing negative effective surface tension, beyond which the effective surface tension will be zero [170].
- Clinical applications of contrast agents involve polydisperse bubble population at fairly high concentrations. Model predictions are critically dependent on the bubble size distributions. Therefore, more reliable and accurate size measurements techniques are required especially those which can handle highly polydisperse systems.
- Increasing levels of sophistications and complexity can be introduced into modeling e.g., multiple scattering [414], presence of blood vessels [415–417], non-spherical bubble oscillations [227, 418], ultrasound mediated bubble destruction, and effects of drug loading or targeting ligands on bubble dynamics [419, 420], lipid shedding and acoustically induced bubble deflation [72, 198–201] etc.
- Study the model performance for monodisperse bubble populations to eliminate effects of polydispersity corrupting our analysis. We have already initiated a collaboration of with Dr. Tyrone Porter and his research group in Boston University in this regard.
- Some of the numerical modeling work performed in our lab suggests that the lowest subharmonic generation threshold can occur for an excitation near resonance frequency rather than at twice the resonance frequency as obtained through analytical predictions [172, 175]. Hence, the perturbation solutions for the modified Rayleigh-Plesset equation should be reexamined to understand the reasons behind these findings.

- The model requires suitable modifications for a better description of thick-shelled microbubbles such as, the Philips bubble studied here. One idea will be to implement a nonlinear viscosity model.

12.3.2 Possible Experiments with Contrast Microbubbles

Experimental characterization of encapsulated bubble dynamics also have several potential areas for further development e.g., devising sophisticated experimental techniques for correct estimation of shell viscoelastic properties, accounting for polydispersity of bubble suspensions during experiments, characterization of nonlinear behavior at low acoustic pressure, characterization of bubble-wall interactions, determination of the thresholds for subharmonic generation, characterization of rupture, break-up, dissolution dynamics of encapsulated bubbles etc. Few specific suggestions are given below.

- A more extensive characterization of ambient pressure dependent subharmonic response must be pursued for different types of contrast agents. Specifically, the effect of the varying the excitation frequency and excitation pressure should be determined, which has not been studied till date.
- An experimental investigation of minimum subharmonic generation threshold can be pursued to check the validity of numerical predictions mentioned earlier.
- A flow loop can be implemented [See Figure] for our acoustic scattering studies for understanding bubble response under *in vivo* conditions.
- To avoid the effects of polydiversity, we can develop experimental techniques that acquires response from single bubbles as proposed recently by various groups [232].
- Clinical ultrasound setups should be utilized to validate *in vitro* behavior observed in our experiments. A mean gray scale value can be used as a technique of quantifying the response from contrast microbubbles.

12.3.3 Possible Studies with Echogenic Liposomes

We had stressed earlier that a proper understanding of the echogenic properties of liposomes is critically dependent on our ability to obtain reliable and accurate size distribution measurements. Conventional sizing techniques utilized in this study are

restricted in their ability to handle a polydisperse system like ELIPs. We also need to ascertain the location and dimension of the purported gas pockets. Without these informations, even simple mathematical modeling studies are not possible. We had hypothesized earlier that echogenicity is primarily due to the larger diameter vesicles. Some preliminary modeling work from other groups indicate best fitting with experimental data was obtained with an assumption that each liposome has a gas pocket that occupies 18% of its total volume [109]. Hence, to have a micron sized gas pocket, we need vesicles larger than 5 μm in diameter. An alternate hypothesis could be that a large number liposomes, each with nanometer sized gas pockets, is contributing to the echogenic response [Personal Communications with Jonathan Kopechek]. Two approaches are proposed to determine the validity of these hypotheses.

- Separate out liposomes of different sizes from the suspension through a filtration process and then study their echogenic response. This way we can determine the range of liposome sizes that have the most significant contribution to echogenicity.
- The gas pockets in the liposomes are hypothesized to have lipid monolayer encapsulation similar to those implemented in contrast microbubbles. A modeling study may be performed with artificial size distribution and model parameters for lipid encapsulations to determine which of these above hypotheses is correct.

We also need to identify the exact reasons why our *in vitro* studies did not report any echogenicity of pH dependent ELIPs. The first approach can be to use the smaller volume setup to use higher concentrations. The other approach will be to modify the setup to eliminate the effect of buoyancy resulting in liposomes going out of the focus.

Finally, the ultrasound-mediated release studies presented here are not extensive. Hence, there also is a need for detailed parametric study of ultrasound mediated release form ELIPs *in vitro* using clinically relevant ultrasound pulses to ascertain the optimal excitation conditions. It will be also be beneficial to detect the role of cavitation associated with such release. Such studies will improve our understanding of the physical mechanisms, and pave the way for clinical translation of these technologies. Moreover, there has been reports that conical lipids are more sensitive to ultrasound-mediated release [343, 421]. Hence, the effect of changing the lipid structures can also

be studied to optimize ultrasound enhanced release. The echogenic polymersomes being developed by our collaborators at NDSU also utilizes this concept of changing the structure of the membrane constituents (polymers for this case).

REFERENCES

- [1] M. Postema and G. Schmitz. Bubble Dynamics Involved in Ultrasonic Imaging. *Expert Review of Molecular Diagnostics*, 6(3):493–502, 2006.
- [2] E. Stride. *Characterisation and Design of Ultrasound Contrast Agent Particles*. PhD thesis, University College London, 2005.
- [3] T. Faez, M. Emmer, K. Kooiman, M. Versluis, A. F. W. van der Steen, and N. de Jong. 20 Years of Ultrasound Contrast Agent Modeling. *Ultrasonics, Ferroelectrics and Frequency Control, IEEE Transactions on*, 60(1):7–20, 2013.
- [4] S. Paul, D. Russakow, T. Rodgers, K. Sarkar, M. Cochran, and M. A. Wheatley. Determination of the Interfacial Rheological Properties of a Poly(DL-lactic acid)-Encapsulated Contrast Agent Using In Vitro Attenuation and Scattering. *Ultrasound in Medicine & Biology*, 39(7):1277–1291, Jul 2013.
- [5] K. K.D, J. Xu, S. Murphy, A. Minino, and H. Kung. Deaths: Final Data for 2009. *National Health Statistics Report*, 30(3):1–117, 2011.
- [6] A. S. Go, D. Mozaffarian, V. L. Roger, E. J. Benjamin, J. D. Berry, W. B. Borden, D. M. Bravata, S. Dai, E. S. Ford, C. S. Fox, S. Franco, H. J. Fullerton, C. Gillespie, S. M. Hailpern, J. A. Heit, V. J. Howard, M. D. Huffman, B. M. Kissela, S. J. Kittner, D. T. Lackland, J. H. Lichtman, L. D. Lisabeth, D. Magid, G. M. Marcus, A. Marelli, D. B. Matchar, D. K. McGuire, E. R. Mohler, C. S. Moy, M. E. Mussolino, G. Nichol, N. P. Paynter, P. J. Schreiner, P. D. Sorlie, J. Stein, T. N. Turan, S. S. Virani, N. D. Wong, D. Woo, and M. B. Turner. Heart Disease and Stroke Statistics—2013 Update: A Report from the American Heart Association. *Circulation*, 127(1):e6–e245, 2013.
- [7] S. Paul, R. Nahire, S. Mallik, and K. Sarkar. Encapsulated Microbubbles and Echogenic Liposomes for Contrast Ultrasound Imaging and Targeted Drug Delivery. Under review - Computational Mechanics (Springer), 2013.
- [8] T. G. Leighton. What Is Ultrasound? *Progress in Biophysics and Molecular Biology*, 93(1-3):3–83, 2007.
- [9] P. G. Newman and G. S. Rozycski. The History of Ultrasound. *Surgical Clinics of North America*, 78(2):179–195, 1998.

- [10] I. Donald, J. Macvicar, and T. Brown. INVESTIGATION OF ABDOMINAL MASSES BY PULSED ULTRASOUND. *The Lancet*, 271(7032):1188–1195, Jun 1958.
- [11] Dale and Ensminger. *Ultrasonics: Fundamentals, Technologies, and Applications, Third Edition (Dekker Mechanical Engineering)*. CRC Press, 2012.
- [12] A. L. Klibanov. Ultrasound Contrast Agents: Development of the Field and Current Status. *Contrast Agents II*, 222:73–106, 2002.
- [13] R. Gramiak and P. M. Shah. Echocardiography of the Aortic Root. *Investigatory Radiology*, 3(3):356–366, 1968.
- [14] K. Sarkar, A. Katiyar, and P. Jain. Growth and Dissolution of an Encapsulated Contrast Microbubble. *Ultrasound in Medicine and Biology*, 35(8):1385–1396, 2009.
- [15] A. Katiyar, K. Sarkar, and P. Jain. Effects of Encapsulation Elasticity on the Stability of an Encapsulated Microbubble. *Journal of Colloid and Interface Science*, 336:519–525, 2009.
- [16] S. B. Feinstein, F. J. T. Cate, W. Zwehl, K. Ong, G. Maurer, C. Tei, P. M. Shah, S. Meerbaum, and E. Corday. Two-dimensional contrast echocardiography. I. In vitro development and quantitative analysis of echo contrast agents. *Journal of the American College of Cardiology*, 3(1):14 – 20, 1984. ISSN 0735-1097.
- [17] B. A. Carroll, R. J. Turner, E. G. Tickner, D. B. Boyle, and S. W. Young. Gelatin Encapsulated Nitrogen Microbubbles As Ultrasonic Contrast Agents. *Investigative Radiology*, 15(3):260–266, 1980.
- [18] N. C. Nanda. History of Echocardiographic Contrast Agents. *Clinical Cardiology*, 20(S1):7–11, 1997. ISSN 1932-8737.
- [19] M. J. K. Blomley. Science, Medicine, and the Future: Microbubble Contrast Agents: A New Era in Ultrasound. *BMJ*, 322(7296):1222–1225, May 2001.
- [20] D. L. Miller, M. A. Averkiou, A. A. Brayman, E. C. Everbach, C. K. Holland, J. H. Wible, and J. R. Wu. Bioeffects Considerations for Diagnostic Ultrasound Contrast Agents. *Journal of Ultrasound in Medicine*, 27(4):611–632, 2008.
- [21] M. L. Main, J. H. Goldman, and P. A. Grayburn. Ultrasound Contrast Agents: Balancing Safety Versus Efficacy. *Expert Opinion on Drug Safety*, 8(1):49–56, 2009.
- [22] G. Haar. Safety and Bio-Effects of Ultrasound Contrast Agents. *Medical & Biological Engineering & Computing*, 47(8):893–900, 2009.

- [23] K. Ferrara, R. Pollard, and M. Borden. Ultrasound Microbubble Contrast Agents: Fundamentals and Application to Gene and Drug Delivery. *Annual Review of Biomedical Engineering*, 9:415–447, 2007.
- [24] A. L. Klibanov, T. I. Shevchenko, B. I. Raju, R. Seip, and C. T. Chin. Ultrasound-Triggered Release of Materials Entrapped in Microbubble-Liposome Constructs: A Tool for Targeted Drug Delivery. *Journal of Controlled Release*, 148(1):13–17, 2010.
- [25] G. M. Lanza, K. D. Wallace, S. E. Fischer, D. H. Christy, M. J. Scott, R. L. Trousil, W. P. Cacheris, J. G. Miller, P. J. Gaffney, and S. A. Wickline. High-frequency Ultrasonic Detection of Thrombi With a Targeted Contrast System. *Ultrasound in Medicine & Biology*, 23(6):863 – 870, 1997. ISSN 0301-5629.
- [26] Z. Gao, A. Kennedy, D. Christensen, and N. Rapoport. Drug-loaded Nano/microbubbles for Combining Ultrasonography and Targeted Chemotherapy. *Ultrasonics*, 48(4):260–270, 2008.
- [27] N. Rapoport, Z. Gao, and A. Kennedy. Multifunctional Nanoparticles for Combining Ultrasonic Tumor Imaging and Targeted Chemotherapy. *Journal of the National Cancer Institute*, 99(14):1095–1106, 2007.
- [28] N. Rapoport, Z. Gao, and A. Kennedy. Drug-Loaded Nanoemulsions/Microbubbles for Combined Tumor Imaging and Therapy. *AIP Conference Proceedings*, 911(1):472–478, 2007.
- [29] N. Rapoport, K.-H. Nam, R. Gupta, Z. Gao, P. Mohan, A. Payne, N. Todd, X. Liu, T. Kim, J. Shea, C. Scaife, D. Parker, E.-K. Jeong, and A. Kennedy. Ultrasound-mediated Tumor Imaging and Nanotherapy Using Drug Loaded, Block Copolymer Stabilized Perfluorocarbon Nanoemulsions. *Journal of Controlled Release*, 153(1):4–15, 2011.
- [30] K. Wilson, K. Homan, and S. Emelianov. Biomedical Photoacoustics Beyond Thermal Expansion Using Triggered Nanodroplet Vaporization for Contrast-enhanced Imaging. *Nature Communications*, 3(618):10, 2012.
- [31] J. Correas and S. Quay. EchoGen® Emulsion: A New Ultrasound Contrast Agent Based on Phase Shift Colloids. *Clinical Radiology*, 51(SUPPL. 1):11–14, 1996.
- [32] H. AlkanOnyuksel, S. M. Demos, G. M. Lanza, M. J. Vonesh, M. E. Klegerman, B. J. Kane, J. Kuszak, and D. D. McPherson. Development of Inherently Echogenic Liposomes as an Ultrasonic Contrast Agent. *Journal of Pharmaceutical Sciences*, 85(5):486–490, 1996.

- [33] B. Geers, I. Lentacker, N. N. Sanders, J. Demeester, S. Meairs, and S. C. De Smedt. Self-Assembled Liposome-Loaded Microbubbles: The Missing Link for Safe and Efficient Ultrasound Triggered Drug-Delivery. *Journal of Controlled Release*, 152(2):249–256, 2011.
- [34] A. Hamilton, S. L. Huang, D. Warnick, A. Stein, M. Rabbat, T. Madhav, B. Kane, A. Nagaraj, M. Klegerman, R. MacDonald, and D. McPherson. Left Ventricular Thrombus Enhancement after Intravenous Injection of Echogenic Immunoliposomes - Studies in a New Experimental Model. *Circulation*, 105(23):2772–2778, 2002.
- [35] A. J. Hamilton, S. L. Huang, D. Warnick, M. Rabbat, B. Kane, A. Nagaraj, M. Klegerman, and D. D. McPherson. Intravascular Ultrasound Molecular Imaging of Atheroma Components in Vivo. *Journal of the American College of Cardiology*, 43(3):453–460, 2004.
- [36] A. Kheirolooom, P. A. Dayton, A. F. H. Lum, E. Little, E. E. Paoli, H. R. Zheng, and K. W. Ferrara. Acoustically-Active Microbubbles Conjugated to Liposomes: Characterization of a Proposed Drug Delivery Vehicle. *Journal of Controlled Release*, 118(3):275–284, 2007.
- [37] M. J. Rondeau, L. Leung, R. H. Silverman, A. Chabi, F. L. Lizzi, R. Folberg, and D. Coleman. Uveal Melanoma Imaging with Echogenic Liposomes. *Investigative Ophthalmology & Visual Science*, 44:U294–U294, 2003.
- [38] N. Sax and T. Kodama. Optimization of Acoustic Liposomes for Improved in Vitro and in Vivo Stability. *Pharmaceutical Research*, 30(1):218–224, 2013.
- [39] L. Sheng-Chieh, H. Ja-An, and Y. Chih-Kuang. Echogenic Liposomes in High-Frequency Ultrasound Imaging. In *Ultrasonics Symposium, 2007. IEEE*, pages 2203–2206, 2007.
- [40] S. D. Tiukinhoy, M. E. Mahowald, V. P. Shively, A. Nagaraj, B. J. Kane, M. E. Klegerman, R. C. MacDonald, D. D. McPherson, and J. S. Matsumura. Development of Echogenic, Plasmid-Incorporated, Tissue-Targeted Cationic Liposomes That Can Be Used for Directed Gene Delivery. *Investigative Radiology*, 35(12):732–738, 2000.
- [41] D. Phillips, X. Chen, R. Baggs, D. Rubens, M. Violante, and K. Parker. Acoustic Backscatter Properties of The Particle/bubble Ultrasound Contrast Agent. *Ultrasonics*, 36(8):883–892, 1998.
- [42] K. Parker, T. Tuthill, R. Lerner, and M. Violante. A Particulate Contrast Agent with Potential for Ultrasound Imaging of Liver. *Ultrasound in Medicine and Biology*, 13(9):555–566, 1987.

- [43] J. Liu, A. Levine, J. Mattoon, M. Yamaguchi, R. Lee, X. Pan, and T. Rosol. Nanoparticles as Image Enhancing Agents for Ultrasonography. *Physics in Medicine and Biology*, 51(9):2179–2189, 2006.
- [44] W. Zhou, F. Meng, G. Engbers, and J. Feijen. Biodegradable Polymersomes for Targeted Ultrasound Imaging. *Journal of Controlled Release*, 116(2):e62 – e64, 2006. ISSN 0168-3659.
- [45] H. Bleeker, K. Shung, and J. Barnhart. On the application of ultrasonic contrast agents for blood flowmetry and assessment of cardiac perfusion. *Journal of Ultrasound in Medicine*, 9(8):461–71, 1990.
- [46] S. L. Mulvagh, H. Rakowski, M. A. Vannan, S. S. Abdelmoneim, H. Becher, S. M. Bierig, P. N. Burns, R. Castello, P. D. Coon, M. E. Hagen, J. G. Jollis, T. R. Kimball, D. W. Kitzman, I. Kronzon, A. J. Labovitz, R. M. Lang, J. Mathew, W. S. Moir, S. F. Nagueh, A. S. Pearlman, J. E. Perez, T. R. Porter, J. Rosenbloom, G. M. Strachan, S. Thanigaraj, K. Wei, A. Woo, E. H. Yu, and W. A. Zoghbi. American Society of Echocardiography Consensus Statement on the Clinical Applications of Ultrasonic Contrast Agents in Echocardiography. *Journal of the American Society of Echocardiography*, 21(11):1179 – 1201, 2008. ISSN 0894-7317.
- [47] J.-B. Liu, G. Wansaicheong, D. A. Merton, F. Forsberg, and B. B. Goldberg. Contrast-Enhanced Ultrasound Imaging: State of the Art. *Journal of Medical Ultrasound*, 13(3):109–126, 2005.
- [48] M. Postema and O. H. Gilja. Contrast-Enhanced and Targeted Ultrasound. *World Journal of Gastroenterology*, 17(1):28–41, 2011.
- [49] E. Quaia and T. V. Bartolotta. *Contrast Media in Ultrasonography: Basic Principles and Clinical Applications*. Springer Verlag, 2005.
- [50] W. T. Shi and F. Forsberg. Ultrasonic Characterization of the Nonlinear Properties of Contrast Microbubbles. *Ultrasound in Medicine and Biology*, 26(1): 93–104, 2000.
- [51] D. Adam, M. Sapunar, and E. Burla. On the Relationship between Encapsulated Ultrasound Contrast Agent and Pressure. *Ultrasound in Medicine and Biology*, 31(5):673–686, 2005.
- [52] J. K. Dave, V. G. Halldorsdottir, J. R. Eisenbrey, J. S. Raichlen, J. B. Liu, M. E. McDonald, K. Dickie, S. M. Wang, C. Leung, and F. Forsberg. Subharmonic Microbubble Emissions for Noninvasively Tracking Right Ventricular Pressures. *American Journal of Physiology-Heart and Circulatory Physiology*, 303(1):H126–H132, 2012.

- [53] J. K. Dave, V. G. Halldorsdottir, J. R. Eisenbrey, J. B. Liu, M. E. McDonald, K. Dickie, C. Leung, and F. Forsberg. Noninvasive Estimation of Dynamic Pressures in Vitro and in Vivo Using the Subharmonic Response from Microbubbles. *Ieee Transactions on Ultrasonics Ferroelectrics and Frequency Control*, 58(10):2056–2066, 2011.
- [54] V. G. Halldorsdottir, J. K. Dave, L. M. Leodore, J. R. Eisenbrey, S. Park, A. L. Hall, K. Thomeniuv, and F. Forsberg. Subharmonic Contrast Microbubble Signals for Noninvasive Pressure Estimation under Static and Dynamic Flow Conditions. *Ultrasonic Imaging*, 33(3):153–164, 2011.
- [55] W. T. Shi, F. Forsberg, J. S. Raichlen, L. Needleman, and B. B. Goldberg. Pressure Dependence of Subharmonic Signals from Contrast Microbubbles. *Ultrasound in Medicine and Biology*, 25(2):275–283, 1999.
- [56] P. J. A. Frinking, A. Bouakaz, J. Kirkhorn, F. J. Ten Cate, and N. de Jong. Ultrasound Contrast Imaging: Current and New Potential Methods. *Ultrasound in Medicine and Biology*, 26(6):965–975, 2000.
- [57] E. Stride and N. Saffari. Microbubble Ultrasound Contrast Agents: A Review. *Proceedings of the Institution of Mechanical Engineers, Part H: Journal of Engineering in Medicine*, 217(6):429–447, 2003.
- [58] J. L. Bull. The Application of Microbubbles for Targeted Drug Delivery. *Expert Opinion on Drug Delivery*, 4(5):475–493, 2007.
- [59] J. P. Christiansen and J. R. Lindner. Molecular and Cellular Imaging with Targeted Contrast Ultrasound. *Proceedings of the Ieee*, 93(4):809–818, 2005.
- [60] A. L. Klibanov, J. J. Rychak, W. C. Yang, S. Alikhani, B. Li, S. Acton, J. R. Lindner, K. Ley, and S. Kaul. Targeted Ultrasound Contrast Agent for Molecular Imaging of Inflammation in High-Shear Flow. *Contrast Media & Molecular Imaging*, 1(6):259–266, 2006.
- [61] J. R. Lindner. Molecular Imaging with Contrast Ultrasound and Targeted Microbubbles. *Journal of Nuclear Cardiology*, 11(2):215–221, 2004.
- [62] C. C. Coussios and R. A. Roy. Applications of Acoustics and Cavitation to Noninvasive Therapy and Drug Delivery. *Annual Review of Fluid Mechanics*, 40:395–420, 2008.
- [63] J. Wu and W. L. Nyborg. Ultrasound, Cavitation Bubbles and Their Interaction with Cells. *Advanced Drug Delivery Reviews*, 60(10):1103–1116, 2008.
- [64] P. A. Dayton, J. S. Allen, and K. W. Ferrara. The Magnitude of Radiation Force on Ultrasound Contrast Agents. *Journal of the Acoustical Society of America*, 112(5):2183–2192, 2002.

- [65] P. A. Dayton, K. E. Morgan, A. L. S. Klibanov, G. Brandenburger, K. R. Nightingale, and K. W. Ferrara. A Preliminary Evaluation of the Effects of Primary and Secondary Radiation Forces on Acoustic Contrast Agents. *IEEE Transactions on Ultrasonics Ferroelectrics and Frequency Control*, 44(6):1264–1277, 1997.
- [66] P. Dayton, A. Klibanov, G. Brandenburger, and K. Ferrara. Acoustic Radiation Force in Vivo: A Mechanism to Assist Targeting of Microbubbles. *Ultrasound in Medicine and Biology*, 25(8):1195–1201, 1999.
- [67] A. F. H. Lum, M. A. Borden, P. A. Dayton, D. E. Kruse, S. I. Simon, and K. W. Ferrara. Ultrasound Radiation Force Enables Targeted Deposition of Model Drug Carriers Loaded on Microbubbles. *Journal of Controlled Release*, 111(1-2):128–134, 2006.
- [68] H. J. Vos, F. Guidi, E. Boni, and P. Tortoli. Method for Microbubble Characterization Using Primary Radiation Force. *IEEE Transactions on Ultrasonics Ferroelectrics and Frequency Control*, 54(7):1333–1345, 2007.
- [69] D. Chatterjee, P. Jain, and K. Sarkar. Ultrasound-Mediated Destruction of Contrast Microbubbles Used for Medical Imaging and Drug Delivery. *Physics of Fluids*, 17(10):100603, 2005.
- [70] P. V. Chitnis, P. Lee, J. Mamou, J. S. Allen, M. Bohmer, and J. A. Ketterling. Rupture Threshold Characterization of Polymer-Shelled Ultrasound Contrast Agents Subjected to Static Overpressure. *Journal of Applied Physics*, 109(8):084906–1–084906–10, 2011.
- [71] J. E. Chomas, P. A. Dayton, D. May, J. Allen, A. Klibanov, and K. Ferrara. Optical Observation of Contrast Agent Destruction. *Applied Physics Letters*, 77(7):1056–1058, 2000.
- [72] J. E. Chomas, P. Dayton, J. Allen, K. Morgan, and K. W. Ferrara. Mechanisms of Contrast Agent Destruction. *IEEE Transactions on Ultrasonics Ferroelectrics and Frequency Control*, 48(1):232–248, 2001.
- [73] J. E. Chomas, P. Dayton, D. May, and K. Ferrara. Threshold of Fragmentation for Ultrasonic Contrast Agents. *Journal of Biomedical Optics*, 6(2):141–150, 2001.
- [74] A. L. Klibanov, M. S. Hughes, J. K. Wojdyla, J. H. Wible, and G. H. Brandenburger. Destruction of Contrast Agent Microbubbles in the Ultrasound Field: The Fate of the Microbubble Shell and the Importance of the Bubble Gas Content. *Academic Radiology*, 9:S41–S45, 2002.
- [75] M. Ward, J. Wu, and J.-F. Chiu. Experimental Study of the Effects of Optison® Concentration on Sonoporation in Vitro. *Ultrasound in medicine & biology*, 26(7):1169–1175, 2000.

- [76] M. Ward, J. R. Wu, and J. F. Chiu. Ultrasound-Induced Cell Lysis and Sono-poration Enhanced by Contrast Agents. *Journal of the Acoustical Society of America*, 105(5):2951–2957, 1999.
- [77] A. L. Klibanov. Microbubble Contrast Agents - Targeted Ultrasound Imaging and Ultrasound-Assisted Drug-Delivery Applications. *Investigative Radiology*, 41(3):354–362, 2006.
- [78] E. C. Unger, T. Porter, W. Culp, R. Labell, T. Matsunaga, and R. Zutshi. Therapeutic Applications of Lipid-Coated Microbubbles. *Advanced Drug Delivery Reviews*, 56(9):1291–1314, 2004.
- [79] F. Xie, J. M. Tsutsui, J. Lof, E. C. Unger, J. Johanning, W. C. Culp, T. Matsunaga, and T. R. Porter. Effectiveness of Lipid Microbubbles and Ultrasound in Declotting Thrombosis. *Ultrasound in Medicine and Biology*, 31(7):979–985, 2005.
- [80] R. Suzuki, T. Takizawa, Y. Negishi, K. Hagiwara, K. Tanaka, K. Sawamura, N. Utoguchi, T. Nishioka, and K. Maruyama. Gene Delivery by Combination of Novel Liposomal Bubbles with Perfluoropropane and Ultrasound. *Journal of Controlled Release*, 117(1):130–136, 2007.
- [81] Y. Taniyama, K. Tachibana, K. Hiraoka, T. Namba, K. Yamasaki, N. Hashiya, M. Aoki, T. Ogihara, K. Yasufumi, and R. Morishita. Local Delivery of Plasmid DNA into Rat Carotid Artery Using Ultrasound. *Circulation*, 105(10):1233–1239, 2002.
- [82] L. C. Phillips, A. L. Klibanov, B. R. Wamhoff, and J. A. Hossack. Localized Ultrasound Enhances Delivery of Rapamycin from Microbubbles to Prevent Smooth Muscle Proliferation. *Journal of Controlled Release*, 154(1):42–49, 2011.
- [83] J. R. Eisenbrey, O. M. Burstein, R. Kambhampati, F. Forsberg, J. B. Liu, and M. A. Wheatley. Development and Optimization of a Doxorubicin Loaded Poly(Lactic Acid) Contrast Agent for Ultrasound Directed Drug Delivery. *Journal of Controlled Release*, 143(1):38–44, 2010.
- [84] J. R. Eisenbrey, M. C. Soulen, and M. A. Wheatley. Delivery of Encapsulated Doxorubicin by Ultrasound-Mediated Size Reduction of Drug-Loaded Polymer Contrast Agents. *IEEE Transactions on Biomedical Engineering*, 57(1):24–28, 2010.
- [85] K. H. Martin and P. A. Dayton. Current Status and Prospects for Microbubbles in Ultrasound Theranostics. *Wiley Interdisciplinary Reviews: Nanomedicine and Nanobiotechnology*, 5(4):329–345, 2013.

- [86] R. Bekeredjian, P. A. Grayburn, and R. V. Shohet. Use of Ultrasound Contrast Agents for Gene or Drug Delivery in Cardiovascular Medicine. *Journal of the American College of Cardiology*, 45(3):329–335, 2005.
- [87] K. Ferrara. Molecular Imaging Update - Ultrasound Molecular Imaging: On the Move. *Journal of Nuclear Medicine*, 48(9):22N–22N, 2007.
- [88] K. W. Ferrara. Driving Delivery Vehicles with Ultrasound. *Advanced Drug Delivery Reviews*, 60(10):1097–1102, 2008.
- [89] A. Klibanov. Ultrasound Contrast Agents: Development of the Field and Current Status. In W. Krause, editor, *Contrast Agents II*, volume 222 of *Topics in Current Chemistry*, pages 73–106. Springer Berlin Heidelberg, 2002.
- [90] J. R. Lindner. Microbubbles in Medical Imaging: Current Applications and Future Directions. *Nature Reviews Drug Discovery*, 3(6):527–532, 2004.
- [91] A. Bangham. The 1st Description of Liposomes - a Citation Classic Commentary on Diffusion of Univalent Ions across the Lamellae of Swollen Phospholipids by Bangham,A.D., Standish,M.M., and Watkins,J.C. *Current Contents/Life Sciences*, (13):14–14, 1989.
- [92] A. D. Bangham, M. M. Standish, and J. C. Watkins. Diffusion of Univalent Ions across Lamellae of Swollen Phospholipids. *Journal of Molecular Biology*, 13(1):238–&, 1965.
- [93] S. L. Huang. Liposomes in Ultrasonic Drug and Gene Delivery. *Advanced Drug Delivery Reviews*, 60(10):1167–1176, 2008.
- [94] T. Lian and R. J. Y. Ho. Trends and Developments in Liposome Drug Delivery Systems. *Journal of Pharmaceutical Sciences*, 90(6):667–680, 2001.
- [95] V. P. Torchilin. Recent Advances with Liposomes as Pharmaceutical Carriers. *Nature Reviews Drug Discovery*, 4(2):145–160, 2005.
- [96] L. Zhang, F. X. Gu, J. M. Chan, A. Z. Wang, R. S. Langer, and O. C. Farokhzad. Nanoparticles in Medicine: Therapeutic Applications and Developments. *Clinical Pharmacology & Therapeutics*, 83(5):761–769, 2008.
- [97] N. Ding, Y. Lu, R. J. Lee, C. Yang, L. Huang, J. Liu, and G. Y. Xiang. Folate Receptor-Targeted Fluorescent Paramagnetic Bimodal Liposomes for Tumor Imaging. *International Journal of Nanomedicine*, 6:2513–2520, 2011.
- [98] D. C. Turner, D. Moshkelani, C. S. Shemesh, D. Luc, and H. Zhang. Near-Infrared Image-Guided Delivery and Controlled Release Using Optimized Thermosensitive Liposomes. *Pharm Res*, 29(8):2092–103, 2012.

- [99] S. J. Leung, X. M. Kachur, M. C. Bobnick, and M. Romanowski. Wavelength-Selective Light-Induced Release from Plasmon Resonant Liposomes. *Adv Funct Mater*, 21(6):1113–1121, 2011.
- [100] F. Q. Hu, Y. Y. Zhang, J. You, H. Yuan, and Y. Z. Du. Ph Triggered Doxorubicin Delivery of Pegylated Glycolipid Conjugate Micelles for Tumor Targeting Therapy. *Molecular Pharmaceutics*, 9(9):2469–2478, 2012.
- [101] J. Banerjee, A. J. Hanson, B. Gadam, A. I. Elegbede, S. Tobwala, B. Ganguly, A. V. Wagh, W. W. Muhonen, B. Law, J. B. Shabb, D. K. Srivastava, and S. Mallik. Release of Liposomal Contents by Cell-Secreted Matrix Metalloproteinase-9. *Bioconjug Chem*, 20(7):1332–9, 2009.
- [102] N. Sarkar, J. Banerjee, A. J. Hanson, A. I. Elegbede, T. Rosendahl, A. B. Krueger, A. L. Banerjee, S. Tobwala, R. Y. Wang, X. N. Lu, S. Mallik, and D. K. Srivastava. Matrix Metalloproteinase-Assisted Triggered Release of Liposomal Contents. *Bioconjugate Chemistry*, 19(1):57–64, 2008.
- [103] N. R. Sarkar, T. Rosendahl, A. B. Krueger, A. L. Banerjee, K. Benton, S. Mallik, and D. K. Srivastava. "Uncorking" of Liposomes by Matrix Metalloproteinase-9. *Chem Commun (Camb)*, 0(8):999–1001, 2005.
- [104] W. Ong, Y. Yang, A. C. Cruciano, and R. L. McCarley. Redox-Triggered Contents Release from Liposomes. *J Am Chem Soc*, 130(44):14739–44, 2008.
- [105] A. Schroeder, J. Kost, and Y. Barenholz. Ultrasound, Liposomes, and Drug Delivery: Principles for Using Ultrasound to Control the Release of Drugs from Liposomes. *Chemistry and Physics of Lipids*, 162(1-2):1–16, 2009.
- [106] S. L. Huang, A. J. Hamilton, A. Nagaraj, S. D. Tiukinhoy, M. E. Klegerman, D. D. McPherson, and R. C. MacDonald. Improving Ultrasound Reflectivity and Stability of Echogenic Liposomal Dispersions for Use as Targeted Ultrasound Contrast Agents. *Journal of Pharmaceutical Sciences*, 90(12):1917–1926, 2001.
- [107] S. L. Huang, D. D. McPherson, and R. C. Macdonald. A Method to Co-Encapsulate Gas and Drugs in Liposomes for Ultrasound-Controlled Drug Delivery. *Ultrasound in medicine & biology*, 34(8):1272–80, 2008.
- [108] S. L. Huang, A. J. Hamilton, E. Pozharski, A. Nagaraj, M. E. Klegerman, D. D. McPherson, and R. C. MacDonald. Physical Correlates of the Ultrasonic Reflectivity of Lipid Dispersions Suitable as Diagnostic Contrast Agents. *Ultrasound in Medicine and Biology*, 28(3):339–348, 2002.
- [109] J. A. Kopechek, K. J. Haworth, J. L. Raymond, T. D. Mast, S. R. Perrin, M. E. Klegerman, S. L. Huang, T. M. Porter, D. D. McPherson, and C. K. Holland.

- Acoustic Characterization of Echogenic Liposomes: Frequency-Dependent Attenuation and Backscatter. *Journal of the Acoustical Society of America*, 130(5):3472–3481, 2011.
- [110] S. Paul, D. Russakow, R. Nahire, T. Nandy, A. H. Ambre, K. Katti, S. Mallik, and K. Sarkar. In Vitro Measurement of Attenuation and Nonlinear Scattering from Echogenic Liposomes. *Ultrasonics*, 52(7):962–969, 2012.
- [111] S. L. Huang and R. C. MacDonald. Acoustically Active Liposomes for Drug Encapsulation and Ultrasound-Triggered Release. *Biochimica Et Biophysica Acta-Biomembranes*, 1665(1-2):134–141, 2004.
- [112] J. A. Kopechek. *The Role of Acoustic Cavitation in Ultrasound-triggered Drug Release from Echogenic Liposomes*. Ph.d., University of Cincinnati, 2011.
- [113] J. A. Kopechek, T. M. Abruzzo, B. Wang, S. M. Chrzanowski, D. A. B. Smith, P. H. Kee, S. Huang, J. H. Collier, D. D. McPherson, and C. K. Holland. Ultrasound-Mediated Release of Hydrophilic and Lipophilic Agents from Echogenic Liposomes. *Journal of Ultrasound in Medicine*, 27(11):1597–1606, 2008.
- [114] R. Nahire, M. K. Haldar, S. Paul, A. Mergoum, A. H. Ambre, K. S. Katti, K. N. Gange, D. K. Srivastava, K. Sarkar, and S. Mallik. Polymer-Coated Echogenic Lipid Nanoparticles with Dual Release Triggers. *Biomacromolecules*, 14(3):841–853, 2013.
- [115] R. Nahire, S. Paul, M. D. Scott, R. K. Singh, W. W. Muhonen, J. Shabb, K. N. Gange, D. K. Srivastava, K. Sarkar, and S. Mallik. Ultrasound Enhanced Matrix Metalloproteinase-9 Triggered Release of Contents from Echogenic Liposomes. *Molecular Pharmaceutics*, 9(9):2554–2564, 2012.
- [116] D. A. B. Smith, S. S. Vaidya, J. A. Kopechek, S. L. Huang, M. E. Klegerman, D. D. Mcpherson, and C. K. Holland. Ultrasound-Triggered Release of Recombinant Tissue-Type Plasminogen Activator from Echogenic Liposomes. *Ultrasound in Medicine and Biology*, 36(1):145–157, 2010.
- [117] S. D. Tiukinhoy, A. A. Khan, S. L. Huang, M. E. Klegerman, R. C. MacDonald, and D. D. McPherson. Novel Echogenic Drug-Immunoliposomes for Drug Delivery. *Investigative Radiology*, 39(2):104–110, 2004.
- [118] S. D. Tiukinhoy-Laing, S. L. Huang, M. Klegerman, C. K. Holland, and D. D. McPherson. Ultrasound-Facilitated Thrombolysis Using Tissue-Plasminogen Activator-Loaded Echogenic Liposomes. *Thrombosis Research*, 119(6):777–784, 2007.

- [119] S. L. Huang, A. J. Hamilton, S. D. Tiukinhoy, A. Nagaraj, B. J. Kane, M. Klegerman, D. D. McPherson, and R. C. MacDonald. Liposomes as Ultrasound Imaging Contrast Agents and as Ultrasound-Sensitive Drug Delivery Agents. *Cellular & Molecular Biology Letters*, 7(2):233–235, 2002.
- [120] A. Prosperetti. Bubbles. *Physics of Fluids*, 16(6):1852–1865, 2004.
- [121] T. G. Leighton. *The Acoustic Bubble*. Academic Press, San Diego ; London, first printing pbk. edition, 1997.
- [122] C. E. Brennen. *Cavitation and Bubble Dynamics*. Oxford University Press, 1995.
- [123] Z. C. Feng and L. G. Leal. Nonlinear Bubble Dynamics. *Annual Review of Fluid Mechanics*, 29(1):201–243, 1997.
- [124] M. S. Plesset and A. Prosperetti. Bubble Dynamics and Cavitation. *Annual Review of Fluid Mechanics*, 9(1):145–185, 1977.
- [125] F. R. Young. *Sonoluminescence*. CRC PressI Llc, 2005.
- [126] F. Young. *Cavitation*. Imperial College Press, 1999. ISBN 9781860941986.
- [127] A. Doinikov. *Bubble and Particle Dynamics in Acoustic Fields: Modern Trends and Applications*. Research Signpost, 2005. ISBN 9788177362848.
- [128] M. P. Brenner, S. Hilgenfeldt, and D. Lohse. Single-Bubble Sonoluminescence. *Reviews of Modern Physics*, 74(2):425–484, 2002.
- [129] S. Hilgenfeldt, D. Lohse, and M. Zomack. Response of Bubbles to Diagnostic Ultrasound: A Unifying Theoretical Approach. *European Physical Journal B*, 4 (2):247–255, 1998.
- [130] M. Plesset. The Dynamics of Cavitation Bubbles. *ASME Journal of Applied Mechanics*, 16(3):277–282, 1949.
- [131] J. R. Blake and D. C. Gibson. Cavitation Bubbles Near Boundaries. *Annual Review of Fluid Mechanics*, 19(1):99–123, 1987.
- [132] W. Lauterborn and T. Kurz. Physics of Bubble Oscillations. *Reports on Progress in Physics*, 73(10):106501, 2010.
- [133] W. Besant. *A Treatise on Hydrostatics and Hydrodynamics*. Deighton, Bell, 1859.
- [134] L. Rayleigh. On the Pressure Development in a Liquid During the Collapse of a Spherical Cavity. *Philosophical Magazine*, 32(S8):94–98, 1917.
- [135] B. E. Noltingk. Cavitation Produced by Ultrasonics. *Proceedings of the Physical Society. Section B*, 63(9):674–685, 1950.

- [136] E. A. Neppiras. Cavitation Produced by Ultrasonics: Theoretical Conditions for the Onset of Cavitation. *Proceedings of the Physical Society. Section B*, 64(12):1032–1038, 1951.
- [137] H. Poritsky. The Collapse or Growth of a Spherical Bubble or Cavity in a Viscous Fluid. In *Proceedings of the First National Congress on Applied Mechanics*, pages 813–821, 1952.
- [138] W. Lauterborn. Numerical Investigation of Nonlinear Oscillations of Gas-Bubbles in Liquids. *Journal of the Acoustical Society of America*, 59(2):283–293, 1976.
- [139] R. Lofstedt, B. P. Barber, and S. J. Puttermann. Toward a Hydrodynamic Theory of Sonoluminescence. *Physics of Fluids A: Fluid Dynamics*, 5(11):2911–2928, 1993.
- [140] D. A. King. *Collapse Dynamics of Ultrasound Contrast Agent Microbubbles*. Ph.d., University of Illinois at Urbana-Champaign, 2012.
- [141] J. B. Keller and M. Miksis. Bubble Oscillations of Large Amplitude. *Journal of the Acoustical Society of America*, 68(2):628–633, 1980.
- [142] L. Trilling. The Collapse and Rebound of a Gas Bubble. *Journal of Applied Physics*, 23(1):14–17, 1952.
- [143] C. Herring. Theory of the Pulsations of the Gas Bubble Produced by an Underwater Explosion. Technical Report 236, 1941.
- [144] F. Gilmore. The Growth or Collapse of a Spherical Bubble in a Viscous Compressible Liquid. Technical Report 26-4, California Institute of Technology. Hydrodynamics Laboratory, 1952.
- [145] A. Lezzi and A. Prosperetti. Bubble Dynamics in a Compressible Liquid .2. 2nd-Order Theory. *Journal of Fluid Mechanics*, 185:289–321, 1987.
- [146] A. Prosperetti. The Equation of Bubble Dynamics in a Compressible Liquid. *Physics of Fluids*, 30(11):3626–3628, 1987.
- [147] A. Prosperetti and A. Lezzi. Bubble Dynamics in a Compressible Liquid .1. 1st-Order Theory. *Journal of Fluid Mechanics*, 168:457–478, 1986.
- [148] A. A. Doinikov and A. Bouakaz. Review of Shell Models for Contrast Agent Microbubbles. *Ultrasonics, Ferroelectrics and Frequency Control, IEEE Transactions on*, 58(5):981–993, 2011.
- [149] R. A. Roy, C. C. Church, and A. Calabrese. Cavitation produced by short pulses of ultrasound. In H. A. F. and B. D. T., editors, *Frontiers of Nonlinear Acoustics: Proceedings of 12th International Symposium of Nonlinear Acoustics*, pages 476–481, London, UK, 1990. Elsevier Science Publishing Company.

- [150] N. deJong, L. Hoff, T. Skotland, and N. Bom. Absorption and Scatter of Encapsulated Gas Filled Microspheres - Theoretical Considerations and Some Measurements. *Ultrasonics*, 30(2):95–103, 1992.
- [151] N. deJong and L. Hoff. Ultrasound Scattering Properties of Albunex Microspheres. *Ultrasonics*, 31(3):175–181, 1993.
- [152] N. deJong, R. Cornet, and C. T. Lancee. Higher Harmonics of Vibrating Gas-Filled Microspheres .1. Simulations. *Ultrasonics*, 32(6):447–453, 1994.
- [153] N. deJong, R. Cornet, and C. T. Lancee. Higher Harmonics of Vibrating Gas-Filled Microspheres .2. Measurements. *Ultrasonics*, 32(6):455–459, 1994.
- [154] C. C. Church. The Effects of an Elastic Solid-Surface Layer on the Radial Pulsations of Gas-Bubbles. *Journal of the Acoustical Society of America*, 97(3):1510–1521, 1995.
- [155] L. Hoff, P. C. Sontum, and J. M. Hovem. Oscillations of Polymeric Microbubbles: Effect of the Encapsulating Shell. *Journal of the Acoustical Society of America*, 107(4):2272–2280, 2000.
- [156] L. Hoff. *Acoustic Characterization of Contrast Agents for Medical Ultrasound Imaging*. Kluwer Academic, Norwell, 2001.
- [157] K. E. Morgan, J. S. Allen, P. A. Dayton, J. E. Chomas, A. L. Klibanov, and K. W. Ferrara. Experimental and Theoretical Evaluation of Microbubble Behavior: Effect of Transmitted Phase and Bubble Size. *IEEE Transactions on Ultrasonics Ferroelectrics and Frequency Control*, 47(6):1494–1509, 2000.
- [158] R. E. Glazman. Effects of Adsorbed Films on Gas Bubble Radial Oscillations. *Journal of the Acoustical Society of America*, 74(3):980–986, 1983.
- [159] D. B. Khismatullin and A. Nadim. Radial Oscillations of Encapsulated Microbubbles in Viscoelastic Liquids. *Physics of Fluids*, 14(10):3534–3557, 2002.
- [160] J. S. Allen, D. J. May, and K. W. Ferrara. Dynamics of Therapeutic Ultrasound Contrast Agents. *Ultrasound in Medicine and Biology*, 28(6):805–816, 2002.
- [161] J. S. Allen and M. M. Rashid. Dynamics of a Hyperelastic Gas-Filled Spherical Shell in a Viscous Fluid. *Journal of Applied Mechanics-Transactions of the Asme*, 71(2):195–200, 2004.
- [162] D. Chatterjee and K. Sarkar. A Newtonian Rheological Model for the Interface of Microbubble Contrast Agents. *Ultrasound in Medicine and Biology*, 29(12):1749–1757, 2003.

- [163] K. Sarkar, W. T. Shi, D. Chatterjee, and F. Forsberg. Characterization of Ultrasound Contrast Microbubbles Using in Vitro Experiments and Viscous and Viscoelastic Interface Models for Encapsulation. *Journal of the Acoustical Society of America*, 118(1):539–550, 2005.
- [164] P. Marmottant, S. van der Meer, M. Emmer, M. Versluis, N. de Jong, S. Hilgenfeldt, and D. Lohse. A Model for Large Amplitude Oscillations of Coated Bubbles Accounting for Buckling and Rupture. *Journal of the Acoustical Society of America*, 118(6):3499–3505, 2005.
- [165] A. A. Doinikov and P. A. Dayton. Maxwell Rheological Model for Lipid-Shelled Ultrasound Microbubble Contrast Agents. *Journal of the Acoustical Society of America*, 121(6):3331–3340, 2007.
- [166] K. Tsiglifis and N. A. Pelekasis. Nonlinear Radial Oscillations of Encapsulated Microbubbles Subject to Ultrasound: The Effect of Membrane Constitutive Law. *Journal of the Acoustical Society of America*, 123(6):4059–4070, 2008.
- [167] E. Stride. The Influence of Surface Adsorption on Microbubble Dynamics. *Philosophical Transactions of the Royal Society a-Mathematical Physical and Engineering Sciences*, 366(1873):2103–2115, 2008.
- [168] A. A. Doinikov, J. F. Haac, and P. A. Dayton. Modeling of Nonlinear Viscous Stress in Encapsulating Shells of Lipid-Coated Contrast Agent Microbubbles. *Ultrasonics*, 49(2):269–275, 2009.
- [169] S. Paul, A. Katiyar, K. Sarkar, D. Chatterjee, W. T. Shi, and F. Forsberg. Material Characterization of the Encapsulation of an Ultrasound Contrast Microbubble and Its Subharmonic Response: Strain-Softening Interfacial Elasticity Model. *Journal of the Acoustical Society of America*, 127(6):3846–3857, 2010.
- [170] P. Marmottant, A. Bouakaz, N. de Jong, and C. Quilliet. Buckling Resistance of Solid Shell Bubbles under Ultrasound. *Journal of the Acoustical Society of America*, 129(3):1231–1239, 2011.
- [171] Q. Li, T. J. Matula, J. Tu, X. S. Guo, and D. Zhang. Modeling Complicated Rheological Behaviors in Encapsulating Shells of Lipid-Coated Microbubbles Accounting for Nonlinear Changes of Both Shell Viscosity and Elasticity. *Physics in Medicine and Biology*, 58(4):985–998, 2013.
- [172] A. Katiyar and K. Sarkar. Excitation Threshold for Subharmonic Generation from Contrast Microbubbles. *Journal of the Acoustical Society of America*, 130(5):3137–3147, 2011.
- [173] A. Prosperetti. A General Derivation of The Subharmonic Threshold for Nonlinear Bubble Oscillations. *The Journal of the Acoustical Society of America*, 133(6):3719–3726, 2013.

- [174] M. A. Ainslie and T. G. Leighton. Review of Scattering and Extinction Cross-Sections, Damping Factors, and Resonance Frequencies of a Spherical Gas Bubble. *The Journal of the Acoustical Society of America*, 130(5):3184–3208, 2011.
- [175] A. Katiyar and K. Sarkar. Effects of Encapsulation Damping on the Excitation Threshold for Subharmonic Generation from Contrast Microbubbles. *Journal of the Acoustical Society of America*, 132(5):3576–3585, 2012.
- [176] S. M. van der Meer, B. Dollet, M. M. Voormolen, C. T. Chin, A. Bouakaz, N. de Jong, M. Versluis, and D. Lohse. Microbubble Spectroscopy of Ultrasound Contrast Agents. *Journal of the Acoustical Society of America*, 121(1):648–656, 2007.
- [177] X. Yang and C. C. Church. A Model for the Dynamics of Gas Bubbles in Soft Tissue. *The Journal of the Acoustical Society of America*, 118(6):3595–3606, 2005.
- [178] V. Kamath, A. Prosperetti, and F. N. Egolfopoulos. A Theoretical Study of Sonoluminescence. *The Journal of the Acoustical Society of America*, 94(1):248–260, 1993.
- [179] A. Prosperetti, L. A. Crum, and K. W. Commander. Nonlinear Bubble Dynamics. *Journal of the Acoustical Society of America*, 83(2):502–514, 1988.
- [180] A. T. Preston, T. Colonius, and C. E. Brennen. A Reduced-Order Model of Diffusive Effects on the Dynamics of Bubbles. *Physics of Fluids*, 19(12):123302–1–123302–12, 2007.
- [181] R. I. Nigmatulin, N. S. Khabelev, and F. B. Nagiev. Dynamics, Heat and Mass-Transfer of Vapor-Gas Bubbles in a Liquid. *International Journal of Heat and Mass Transfer*, 24(6):1033–1044, 1981.
- [182] A. Prosperetti. Thermal Effects and Damping Mechanisms in the Forced Radial Oscillations of Gas Bubbles in Liquids. *The Journal of the Acoustical Society of America*, 61(1):17–27, 1977.
- [183] M. Overvelde, V. Garbin, J. Sijl, B. Dollet, N. de Jong, D. Lohse, and M. Versluis. Nonlinear Shell Behavior of Phospholipid-Coated Microbubbles. *Ultrasound in Medicine and Biology*, 36(12):2080–2092, 2010.
- [184] A. Prosperetti. *Viscous and Nonlinear Effects in the Oscillations of Drops and Bubbles*. Ph.d., California Institute of Technology, 1974.
- [185] A. Prosperetti. Nonlinear Oscillations of Gas-Bubbles in Liquids - Transient Solutions and Connection between Subharmonic Signal and Cavitation. *Journal of the Acoustical Society of America*, 57(4):810–821, 1975.

- [186] A. Prosperetti. Subharmonics and Ultraharmonics in Forced-Oscillations of Weakly Nonlinear-Systems. *American Journal of Physics*, 44(6):548–554, 1976.
- [187] A. Prosperetti. Application of Subharmonic Threshold to Measurement of Damping of Oscillating Gas-Bubbles. *Journal of the Acoustical Society of America*, 61(1):11–16, 1977.
- [188] J. Sijl, B. Dollet, M. Overvelde, V. Garbin, T. Rozendal, N. de Jong, D. Lohse, and M. Versluis. Subharmonic Behavior of Phospholipid-Coated Ultrasound Contrast Agent Microbubbles. *The Journal of the Acoustical Society of America*, 128(5):3239–3252, 2010.
- [189] A. Mallock. The Damping of Sound by Frothy Liquids. *Proceedings of the Royal Society of London. Series A*, 84(572):391–395, 1910.
- [190] L. V. Wijngaarden. One-Dimensional Flow of Liquids Containing Small Gas Bubbles. *Annual Review of Fluid Mechanics*, 4(1):369–396, 1972.
- [191] K. W. Commander and A. Prosperetti. Linear Pressure Waves in Bubbly Liquids: Comparison Between Theory and Experiments. *The Journal of the Acoustical Society of America*, 85(2):732–746, 1989.
- [192] K. Sarkar and A. Prosperetti. Coherent and Incoherent-Scattering by Oceanic Bubbles. *Journal of the Acoustical Society of America*, 96(1):332–341, 1994.
- [193] L. L. Foldy. The Multiple Scattering of Waves. I. General Theory of Isotropic Scattering by Randomly Distributed Scatterers. *Phys. Rev.*, 67:107–119, Feb 1945.
- [194] F. S. Henyey. Corrections to Foldy’s Effective Medium Theory for Propagation in Bubble Clouds and Other Collections of Very Small Scatterers. *The Journal of the Acoustical Society of America*, 105(4):2149–2154, 1999.
- [195] D. Chatterjee, K. Sarkar, P. Jain, and N. E. Schreppler. On the Suitability of Broadband Attenuation Measurement for Characterizing Contrast Microbubbles. *Ultrasound in Medicine and Biology*, 31(6):781–786, 2005.
- [196] A. Katiyar and K. Sarkar. Stability Analysis of an Encapsulated Microbubble against Gas Diffusion. *Journal of Colloid and Interface Science*, 343(1):42–47, 2010.
- [197] F. Guidi, H. J. Vos, R. Mori, N. de Jong, and P. Tortoli. Microbubble Characterization through Acoustically Induced Deflation. *Ultrasonics, Ferroelectrics and Frequency Control, IEEE Transactions on*, 57(1):193–202, 2010.

- [198] M. A. Borden, D. E. Kruse, C. F. Caskey, S. K. Zhao, P. A. Dayton, and K. W. Ferrara. Influence of Lipid Shell Physicochemical Properties on Ultrasound-Induced Microbubble Destruction. *IEEE Transactions on Ultrasonics Ferroelectrics and Frequency Control*, 52(11):1992–2002, 2005.
- [199] M. A. Borden, M. R. Sarantos, S. M. Stieger, S. I. Simon, K. W. Ferrara, and P. A. Dayton. Ultrasound Radiation Force Modulates Ligand Availability on Targeted Contrast Agents. *Molecular Imaging*, 5(3):139–147, 2006.
- [200] M. A. Borden and M. L. Longo. Dissolution Behavior of Lipid Monolayer-Coated, Air-Filled Microbubbles: Effect of Lipid Hydrophobic Chain Length. *Langmuir*, 18(24):9225–9233, 2002.
- [201] D. H. Thomas, M. Butler, T. Anderson, M. Emmer, H. Vos, M. Borden, E. Stride, N. de Jong, and V. Sboros. The "quasi-stable" lipid shelled microbubble in response to consecutive ultrasound pulses. *Applied Physics Letters*, 101(7):071601, 2012.
- [202] D. J. Cox and J. L. Thomas. Ultrasound-Induced Dissolution of Lipid-Coated and Uncoated Gas Bubbles. *Langmuir*, 26(18):14774–14781, Sep 2010.
- [203] J.-P. O'Brien, N. Ovenden, and E. Stride. Accounting for the Stability of Microbubbles to Multi-Pulse Excitation Using a Lipid-shedding Model. *The Journal of the Acoustical Society of America*, 130(4):EL180, 2011.
- [204] D. J. Cox and J. L. Thomas. Rapid Shrinkage of Lipid-Coated Bubbles in Pulsed Ultrasound. *Ultrasound in Medicine & Biology*, 39(3):466–474, Mar 2013.
- [205] P. Looney. *Theoretical Modelling of Ultrasound Contrast Agents*. Ph.d., University of Edinburgh, 2011.
- [206] A. Bouakaz, N. De Jong, L. Gerfault, and C. Cachard. In Vitro Standard Acoustic Parameters of Ultrasound Contrast Agents: Definitions and Calculations. In *Ultrasonics Symposium, 1996. Proceedings.*, 1996 IEEE, volume 2, pages 1445–1448. IEEE, 1996.
- [207] D. E. Goertz, N. de Jong, and A. F. W. van der Steen. Attenuation and Size Distribution Measurements of Definity (T_m) and Manipulated Definity (T_m) Populations. *Ultrasound in Medicine and Biology*, 33(9):1376–1388, 2007.
- [208] T. Faez, D. Goertz, and N. De Jong. Characterization of Definity (T_m) Ultrasound Contrast Agent at Frequency Range of 5-15 Mhz. *Ultrasound in Medicine and Biology*, 37(2):338–342, 2011.
- [209] B. Krasovitski, E. Kimmel, M. Sapunar, and D. Adam. Ultrasound Attenuation by Encapsulated Microbubbles: Time and Pressure Effects. *Ultrasound in Medicine and Biology*, 30(6):793–802, 2004.

- [210] Y. Gong. *Acoustic Characterization of Ultrasound Contrast Agents with Lipid-Coated Monodisperse Microbubble*. Ph.d., Boston University, 2013.
- [211] H. Shekhar and M. M. Doyley. Improving the Sensitivity of High-Frequency Sub-harmonic Imaging with Coded Excitation: A Feasibility Study. *Medical Physics*, 39(4):2049–2060, 2012.
- [212] N. de Jong, P. J. A. Frinking, A. Bouakaz, M. Goorden, T. Schourmans, J. P. Xu, and F. Mastik. Optical Imaging of Contrast Agent Microbubbles in an Ultrasound Field with a 100-Mhz Camera. *Ultrasound in Medicine and Biology*, 26(3):487–492, 2000.
- [213] K. Chetty, E. Stride, C. A. Sennoga, J. V. Hajnal, and R. J. Eckersley. High-Speed Optical Observations and Simulation Results of Sonovue Microbubbles at Low-Pressure Insonation. *Ultrasonics, Ferroelectrics and Frequency Control, IEEE Transactions on*, 55(6):1333–1342, 2008.
- [214] C. T. Chin, C. Lancee, J. Borsboom, F. Mastik, M. E. Frijlink, N. de Jong, M. Versluis, and D. Lohse. Brandaris 128: A Digital 25 Million Frames Per Second Camera with 128 Highly Sensitive Frames. *Review of Scientific Instruments*, 74(12):5026–5034, 2003.
- [215] Y. Sun, D. E. Kruse, P. A. Dayton, and K. W. Ferrara. High-Frequency Dynamics of Ultrasound Contrast Agents. *Ieee Transactions on Ultrasonics Ferroelectrics and Frequency Control*, 52(11):1981–1991, 2005.
- [216] C. F. Caskey, S. M. Stieger, S. Qin, P. A. Dayton, and K. W. Ferrara. Direct Observations of Ultrasound Microbubble Contrast Agent Interaction with the Microvessel Wall. *Journal of the Acoustical Society of America*, 122(2):1191–1200, 2007.
- [217] Y. Sun, S. K. Zhao, P. A. Dayton, and K. W. Ferrara. Observation of Contrast Agent Response to Chirp Insonation with a Simultaneous Optical-Acoustical System. *IEEE Transactions on Ultrasonics Ferroelectrics and Frequency Control*, 53(6):1130–1137, 2006.
- [218] J. Tu, J. F. Guan, Y. Y. Qiu, and T. J. Matula. Estimating the Shell Parameters of Sonovue (R) Microbubbles Using Light Scattering. *Journal of the Acoustical Society of America*, 126(6):2954–2962, 2009.
- [219] J. Tu, J. E. Swalwell, D. Giraud, W. C. Cui, W. Z. Chen, and T. J. Matula. Microbubble Sizing and Shell Characterization Using Flow Cytometry. *Ieee Transactions on Ultrasonics Ferroelectrics and Frequency Control*, 58(5):955–963, 2011.

- [220] J. F. Guan and T. J. Matula. Using Light Scattering to Measure the Response of Individual Ultrasound Contrast Microbubbles Subjected to Pulsed Ultrasound in Vitro. *Journal of the Acoustical Society of America*, 116(5):2832–2842, 2004.
- [221] G. Renaud, J. G. Bosch, A. F. W. van der Steen, and N. de Jong. An "Acoustical Camera" for in Vitro Characterization of Contrast Agent Microbubble Vibrations. *Applied Physics Letters*, 100(10):101911–1–101911–4, 2012.
- [222] M. Postema, A. van Wamel, C. T. LancÃ©e, and N. de Jong. Ultrasound-Induced Encapsulated Microbubble Phenomena. *Ultrasound in medicine & biology*, 30(6):827–840, 2004.
- [223] M. J. Hsu, M. Eghitedari, A. P. Goodwin, D. J. Hall, R. F. Mattrey, and S. C. Esenera. Characterization of Individual Ultrasound Microbubble Dynamics with a Light-Scattering System. *Journal of Biomedical Optics*, 16(6), 2011.
- [224] N. De Jong, M. Emmer, C. T. Chin, A. Bouakaz, F. Mastik, D. Lohse, and M. Versluis. "Compression-Only" Behavior of Phospholipid-Coated Contrast Bubbles. *Ultrasound in Medicine and Biology*, 33(4):653–656, 2007.
- [225] H. J. Vos, M. Versluis, and N. de Jong. Orthogonal Observations of Vibrating Microbubbles. In *Ultrasonics Symposium, 2007. IEEE*, pages 765–768, 2007.
- [226] M. Emmer, A. Van Wamel, D. E. Goertz, and N. De Jong. The Onset of Microbubble Vibration. *Ultrasound in Medicine and Biology*, 33(6):941–949, 2007.
- [227] B. Dollet, S. M. van der Meer, V. Garbin, N. de Jong, D. Lohse, and M. Versluis. Nonspherical Oscillations of Ultrasound Contrast Agent Microbubbles. *Ultrasound in medicine & biology*, 34(9):1465–1473, 2008.
- [228] N. de Jong, M. Emmer, A. van Wamel, and M. Versluis. Ultrasonic Characterization of Ultrasound Contrast Agents. *Medical & Biological Engineering & Computing*, 47(8):861–873, 2009.
- [229] H. J. Vos, B. Dollet, J. G. Bosch, M. Versluis, and N. de Jong. Nonspherical Vibrations of Microbubbles in Contact with a Wall - a Pilot Study at Low Mechanical Index. *Ultrasound in Medicine and Biology*, 34(4):685–688, 2008.
- [230] S. K. Zhao, K. W. Ferrara, and P. A. Dayton. Asymmetric Oscillation of Adherent Targeted Ultrasound Contrast Agents. *Applied Physics Letters*, 87(13):–, 2005.
- [231] M. Versluis. Nonlinear Behavior of Ultrasound Contrast Agent Microbubbles and Why Shell Buckling Matters. In *Proceedings of 20th International Congress on Acoustics*, 2010.
- [232] J. Sijl, E. Gaud, P. J. A. Frinking, M. Arditi, N. de Jong, D. Lohse, and M. Versluis. Acoustic Characterization of Single Ultrasound Contrast Agent Microbubbles. *Journal of the Acoustical Society of America*, 124(6):4091–4097, 2008.

- [233] V. Sboros, S. D. Pye, C. A. MacDonald, J. Gomatam, C. M. Moran, and W. N. McDicken. Absolute Measurement of Ultrasonic Backscatter from Single Microbubbles. *Ultrasound in medicine & biology*, 31(8):1063–1072, 2005.
- [234] V. Sboros, S. D. Pye, T. A. Anderson, C. M. Moran, and W. N. McDicken. Acoustic Rayleigh Scattering at Individual Micron-Sized Bubbles. *Applied Physics Letters*, 90(12):–, 2007.
- [235] V. Sboros. A Review of Single Microbubble Acoustics. In *Proceedings of 20th International Congress on Acoustics*, volume 1, pages 710–714, 2010.
- [236] A. L. Klibanov, P. T. Rasche, M. S. Hughes, J. K. Wojdyla, K. P. Galen, J. H. Wible Jr, and G. H. Brandenburger. Detection of Individual Microbubbles of an Ultrasound Contrast Agent: Fundamental and Pulse Inversion Imaging. *Acad Radiol*, 9(2, Supplement):S279–S281, 2002.
- [237] A. L. Klibanov, P. T. Rasche, M. S. Hughes, J. K. Wojdyla, K. P. Galen, J. H. J. Wible, and G. H. Brandenburger. Detection of Individual Microbubbles of Ultrasound Contrast Agents: Imaging of Free-Floating and Targeted Bubbles. *Investigative Radiology*, 39(3):187–195, 2004.
- [238] J. Sijl, H. J. Vos, T. Rozendal, N. de Jong, D. Lohse, and M. Versluis. Combined Optical and Acoustical Detection of Single Microbubble Dynamics. *The Journal of the Acoustical Society of America*, 130(5):3271–3281, 2011.
- [239] D. H. Thomas, M. B. Butler, T. Anderson, R. Steel, S. D. Pye, M. Poland, T. Brock-Fisher, W. N. McDicken, and V. Sboros. Single Microbubble Response Using Pulse Sequences: Initial Results. *Ultrasound in medicine & biology*, 35(1):112–119, 2009.
- [240] D. H. Thomas, P. Looney, R. Steel, N. Pelekasis, W. N. McDicken, T. Anderson, and V. Sboros. Acoustic Detection of Microbubble Resonance. *Applied Physics Letters*, 94(24):243902–3, 2009.
- [241] P. V. Chitnis, S. Koppolu, J. Mamou, C. Chlon, and J. A. Ketterling. Influence of Shell Properties on High-Frequency Ultrasound Imaging and Drug Delivery Using Polymer-Shelled Microbubbles. *Ieee Transactions on Ultrasonics Ferroelectrics and Frequency Control*, 60(1):53–64, 2013.
- [242] J. A. Ketterling, J. Mamou, J. S. Allen, O. Aristizabal, R. G. Williamson, and D. H. Turnbull. Excitation of Polymer-Shelled Contrast Agents with High-Frequency Ultrasound. *Journal of the Acoustical Society of America*, 121(1):E148–E153, 2007.
- [243] K. P. Pancholi, U. Farook, R. Moaleji, E. Stride, and M. J. Edirisinghe. Novel Methods for Preparing Phospholipid Coated Microbubbles. *European Biophysics Journal with Biophysics Letters*, 37(4):515–520, 2008.

- [244] E. Stride and M. Edirisinghe. Novel Preparation Techniques for Controlling Microbubble Uniformity: A Comparison. *Medical & Biological Engineering & Computing*, 47(8):883–892, 2009.
- [245] E. Talu, K. Hettiarachchi, R. L. Powell, A. P. Lee, P. A. Dayton, and M. L. Longo. Maintaining Monodispersity in a Microbubble Population Formed by Flow-Focusing. *Langmuir*, 24(5):1745–1749, 2008.
- [246] K. Hettiarachchi, P. Dayton, and A. P. Lee. Formulation of Monodisperse Contrast Agents in Microfluidic Systems for Ultrasonic Imaging. In *Microtechnologies in Medicine and Biology, 2006 International Conference on*, pages 230–232, 2006.
- [247] Y. Gong, M. Cabodi, and T. Porter. Pressure-Dependent Resonance Frequency for Lipid-Coated Microbubbles at Low Acoustic Pressures. In *Ultrasonics Symposium (IUS), 2010 IEEE*, pages 1932–1935, 2010.
- [248] Y. Gong, M. Cabodi, and T. Porter. Relationship between Size and Frequency Dependent Attenuation of Monodisperse Populations of Lipid Coated Microbubbles. *Bubble Science, Engineering & Technology*, 2(2):41–47, 2010.
- [249] P. H. Chang, K. K. Shung, S. J. Wu, and H. B. Levene. Second-Harmonic Imaging and Harmonic Doppler Measurements with Albunex(R). *Ieee Transactions on Ultrasonics Ferroelectrics and Frequency Control*, 42(6):1020–1027, 1995.
- [250] J. M. Gorce, M. Ardit, and M. Schneider. Influence of Bubble Size Distribution on the Echogenicity of Ultrasound Contrast Agents - a Study of Sonovue (Tm). *Investigative Radiology*, 35(11):661–671, 2000.
- [251] K. Morgan, M. Averkiou, and K. Ferrara. The Effect of the Phase of Transmission on Contrast Agent Echoes. *IEEE Transactions on Ultrasonics Ferroelectrics and Frequency Control*, 45(4):872–875, 1998.
- [252] P. A. Dayton, K. E. Morgan, A. L. Klibanov, G. H. Brandenburger, and K. W. Ferrara. Optical and Acoustical Observations of the Effects of Ultrasound on Contrast Agents. *IEEE Transactions on Ultrasonics Ferroelectrics and Frequency Control*, 46(1):220–232, 1999.
- [253] V. Sboros, E. Glynnos, S. D. Pye, C. M. Moran, M. Butler, J. Ross, R. Short, W. N. McDicken, and V. Koutsos. Nanointerrogation of Ultrasonic Contrast Agent Microbubbles Using Atomic Force Microscopy. *Ultrasound in medicine & biology*, 32(4):579–585, 2006.
- [254] K. Kooiman, M. Emmer, T. J. A. Kokhuis, J. G. Bosch, H. M. de Gruiter, M. E. van Royen, W. A. Van Cappellen, A. B. Houtsmauller, A. F. W. Van der Steen, and N. de Jong. Lipid Distribution and Viscosity of Coated Microbubbles. In *Ultrasonics Symposium (IUS), 2010 IEEE*, pages 900–903, 2010.

- [255] N. A. Hosny, G. Mohamedi, P. Rademeyer, J. Owen, Y. Wu, M.-X. Tang, R. J. Eckersley, E. Stride, and M. K. Kuimova. Mapping Microbubble Viscosity Using Fluorescence Lifetime Imaging of Molecular Rotors. *Proceedings of the National Academy of Sciences*, 110(23):9225–9230, 2013.
- [256] M. S. Hughes, A. L. Klibanov, J. N. Marsh, J. G. Miller, and G. H. Brandenburger. Broadband Time-Domain Reflectometry Measurement of Attenuation and Phase Velocity in Highly Attenuating Suspensions with Application to the Ultrasound Contrast Medium Albunex (R). *Journal of the Acoustical Society of America*, 108(2):813–820, 2000.
- [257] D. Grishenkov, C. Pecorari, T. B. Brismar, and G. Paradossi. Characterization of Acoustic Properties of Pva-Shelled Ultrasound Contrast Agents: Linear Properties (Part I). *Ultrasound in Medicine and Biology*, 35(7):1127–1138, 2009.
- [258] A. Katiyar, K. Sarkar, and R. Duncan. Effects of Ultrasound on Osteoblast Proliferation and its Mechanisms Triggered by Calcium Transport. *Proceedings of Meetings on Acoustics*, 11(1):020002, 2011.
- [259] J. A. Kopechek, H. Kim, D. D. McPherson, and C. K. Holland. Calibration of the 1-Mhz Sonitron Ultrasound System. *Ultrasound in Medicine and Biology*, 36 (10):1762–1766, 2010.
- [260] K. Hensel, M. P. Mienkina, and G. Schmitz. Analysis of Ultrasound Fields in Cell Culture Wells for In Vitro Ultrasound Therapy Experiments. *Ultrasound in Medicine & Biology*, 37(12):2105–2115, 2011.
- [261] C. Christiansen, H. Kryvi, P. C. Sontum, and T. Skotland. Physical and Biochemical-Characterization of Albunex(Tm), a New Ultrasound Contrast Agent Consisting of Air-Filled Albumin Microspheres Suspended in a Solution of Human Albumin. *Biotechnology and Applied Biochemistry*, 19:307–320, 1994.
- [262] A. H. Myrset, H. Nicolaysen, K. Toft, C. Christiansen, and T. Skotland. Structure and Organization of Albumin Molecules Forming the Shell of Air-Filled Microspheres: Evidence for a Monolayer of Albumin Molecules of Multiple Orientations Stabilizing the Enclosed Air. *Biotechnology and Applied Biochemistry*, 24:145–153, 1996.
- [263] X. Y. Li and K. Sarkar. Front Tracking Simulation of Deformation and Buckling Instability of a Liquid Capsule Enclosed by an Elastic Membrane. *Journal of Computational Physics*, 227(10):4998–5018, 2008.
- [264] E. Lac, D. Barthes-Biesel, N. A. Pelekasis, and J. Tsamopoulos. Spherical Capsules in Three-Dimensional Unbounded Stokes Flows: Effect of the Membrane Constitutive Law and Onset of Buckling. *Journal of Fluid Mechanics*, 516:303–334, 2004.

- [265] R. Skalak, A. Tozeren, R. P. Zarda, and S. Chien. Strain Energy Function of Red Blood-Cell Membranes. *Biophysical Journal*, 13(3):245–280, 1973.
- [266] D. A. Edwards, H. Brenner, and D. T. Wasan. *Interfacial Transport Processes and Rheology*. Butterworth-Heinemann, Boston, 1991.
- [267] J. J. Rychak, J. R. Lindner, K. Ley, and A. L. Klibanov. Deformable Gas-Filled Microbubbles Targeted to P-Selectin. *Journal of Controlled Release*, 114(3):288–299, 2006.
- [268] P. M. Shankar, P. D. Krishna, and V. L. Newhouse. Subharmonic Backscattering from Ultrasound Contrast Agents. *Journal of the Acoustical Society of America*, 106(4):2104–2110, 1999.
- [269] P. J. A. Frinking, E. Gaud, J. Brochot, and M. Arditi. Subharmonic Scattering of Phospholipid-Shell Microbubbles at Low Acoustic Pressure Amplitudes. *IEEE Transactions on Ultrasonics Ferroelectrics and Frequency Control*, 57(8):1762, 2010.
- [270] O. Lotsberg, J. M. Hovem, and B. Aksum. Experimental Observation of Subharmonic Oscillations in Infoson Bubbles. *The Journal of the Acoustical Society of America*, 99(3):1366–1369, 1996.
- [271] E. Biagi, L. Breschi, E. Vannacci, and L. Masotti. Stable and Transient Subharmonic Emissions from Isolated Contrast Agent Microbubbles. *Ultrasonics, Ferroelectrics and Frequency Control, IEEE Transactions on*, 54(3):480–497, 2007.
- [272] B. L. Helfield, X. Huo, R. Williams, and D. E. Goertz. The Effect of Preactivation Vial Temperature on the Acoustic Properties of DefinityTM. *Ultrasound in Medicine & Biology*, 38(7):1298 – 1305, 2012. ISSN 0301-5629.
- [273] K. Cheung, O. Couture, P. D. Bevan, E. Cherin, R. Williams, P. N. Burns, and F. S. Foster. In Vitro Characterization of the Subharmonic Ultrasound Signal from Definity Microbubbles at High Frequencies. *Physics in Medicine and Biology*, 53(5):1209–1223, 2008.
- [274] P. C. Sontum, J. Ostensen, K. Dyrstad, and L. Hoff. Acoustic Properties of Nc100100 and Their Relation with the Microbubble Size Distribution. *Investigative Radiology*, 34(4):268–275, 1999.
- [275] V. Sboros, C. M. Moran, S. D. Pye, and W. N. McDicken. Contrast Agent Stability: A Continuous B-Mode Imaging Approach. *Ultrasound in Medicine and Biology*, 27(10):1367–1377, 2001.
- [276] T. Faez, M. Emmer, M. Docter, J. Sijl, M. Versluis, and N. de Jong. Characterizing the Subharmonic Response of Phospholipid-Coated Microbubbles for Carotid Imaging. *Ultrasound in Medicine and Biology*, 37(6):958–970, 2011.

- [277] M. D. Santin, D. A. King, J. Foiret, A. Haak, J. W. D. O'Brien, and S. L. Bridal. Encapsulated Contrast Microbubble Radial Oscillation Associated with Postexcitation Pressure Peaks. *The Journal of the Acoustical Society of America*, 127(2):1156–1164, 2010.
- [278] W. Lauterborn and J. Holzfuss. Acoustic Chaos. *International Journal of Bifurcation and Chaos*, 01(01):13–26, Mar 1991.
- [279] C. A. Macdonald and J. Gomatam. Chaotic Dynamics of Microbubbles in Ultrasonic Fields. *Proceedings of the Institution of Mechanical Engineers, Part C: Journal of Mechanical Engineering Science*, 220(3):333–343, Jan 2006.
- [280] A. J. Sojahrood and M. C. Kolios. Classification of the Nonlinear Dynamics and Bifurcation Structure of Ultrasound Contrast Agents Excited at Higher Multiples of their Resonance Frequency. *Physics Letters A*, 376(33):2222–2229, Jul 2012.
- [281] J. M. Carroll, M. L. Calvisi, and L. K. Lauderbaugh. Dynamical Analysis of the Nonlinear Response of Ultrasound Contrast Agent Microbubbles. *The Journal of the Acoustical Society of America*, 133(5):2641, 2013.
- [282] E. Pisani, N. Tsapis, J. Paris, V. Nicolas, L. Cattel, and E. Fattal. Polymeric Nano/Microcapsules of Liquid Perfluorocarbons for Ultrasonic Imaging: Physical Characterization. *Langmuir*, 22(9):4397–4402, 2006.
- [283] J. R. Eisenbrey, O. M. Burstein, and M. A. Wheatley. Effect of Molecular Weight and End Capping on Poly(Lactic-Co-Glycolic Acid) Ultrasound Contrast Agents. *Polymer Engineering and Science*, 48(9):1785–1792, 2008.
- [284] D. El-Sherif. *Development of Novel Plga Contrast Agents for Use as Ultrasound Targeted Drug Delivery Vehicles*. Ph.d., Drexel University, 2003.
- [285] D. M. El-Sherif and M. A. Wheatley. Development of a Novel Method for Synthesis of a Polymeric Ultrasound Contrast Agent. *Journal of Biomedical Materials Research Part A*, 66A(2):347–355, 2003.
- [286] F. Yang, Y. Li, Z. Chen, and N. Gu. The Preparation and Application of Microbubble Contrast Agent Combining Ultrasound Imaging and Magnetic Resonance Imaging. *Chinese Science Bulletin*, 54(17):2934–2939, 2009.
- [287] F. Forsberg, J. D. Lathia, D. A. Merton, J. B. Liu, N. T. Le, B. B. Goldberg, and M. A. Wheatley. Effect of Shell Type on the in Vivo Backscatter from Polymer-Encapsulated Microbubbles. *Ultrasound in Medicine and Biology*, 30(10):1281–1287, 2004.
- [288] S. Lavisse, A. Paci, V. Rouffiac, C. Adotevi, P. Opolon, P. Peronneau, P. Bourget, A. Roche, M. Perricaudet, E. Fattal, and N. Lassau. In Vitro Echogenicity

- Characterization of Poly[Lactide-Coglycolide] (Plga) Microparticles and Preliminary in Vivo Ultrasound Enhancement Study for Ultrasound Contrast Agent Application. *Investigative Radiology*, 40(8):536–544, 2005.
- [289] D. Grishenkov, C. Pecorari, T. B. Brismar, and G. Paradossi. Characterization of Acoustic Properties of Pva-Shelled Ultrasound Contrast Agents: Ultrasound-Induced Fracture (Part Ii). *Ultrasound in Medicine and Biology*, 35(7):1139–1147, 2009.
- [290] J. M. Lu, X. W. Wang, C. Marin-Muller, H. Wang, P. H. Lin, Q. Z. Yao, and C. Y. Chen. Current Advances in Research and Clinical Applications of Plga-Based Nanotechnology. *Expert Review of Molecular Diagnostics*, 9(4):325–341, 2009.
- [291] C. Sciallero, G. Paradossi, and A. Trucco. A Preliminary in Vitro Assessment of Polymer-Shelled Microbubbles in Contrast-Enhanced Ultrasound Imaging. *Ultrasonics*, 52(3):456–464, 2012.
- [292] M. A. Wheatley, J. D. Lathia, and K. L. Oum. Polymeric Ultrasound Contrast Agents Targeted to Integrins: Importance of Process Methods and Surface Density of Ligands. *Biomacromolecules*, 8(2):516–522, 2007.
- [293] P. Jie, H. Zhenqing, Z. Peijuan, W. Yang, W. Qian, and Z. Qiqing. Optimization of Production of Pla Microbubble Ultrasound Contrast Agents for Hydroxycamptothecin Delivery. In *BioMedical Engineering and Informatics, 2008. BMEI 2008. International Conference on*, volume 1, pages 400–406, 2008.
- [294] S. R. Sirsi, R. C. Schray, M. A. Wheatley, and G. J. Lutz. Formulation of Polylactide-Co-Glycolic Acid Nanospheres for Encapsulation and Sustained Release of Poly(Ethylene Imine)-Poly(Ethylene Glycol) Copolymers Complexed to Oligonucleotides. *Journal of nanobiotechnology*, 7:1, 2009.
- [295] X. Y. Xiong, F. L. Zhao, M. R. Shi, H. Yang, and Y. Y. Liu. Polymeric Microbubbles for Ultrasonic Molecular Imaging and Targeted Therapeutics. *Journal of Biomaterials Science-Polymer Edition*, 22(4-6):417–428, 2011.
- [296] M. A. Wheatley, F. Forsberg, K. Oum, R. Ro, and D. El-Sherif. Comparison of in Vitro and in Vivo Acoustic Response of a Novel 50 : 50 Plga Contrast Agent. *Ultrasonics*, 44(4):360–367, 2006.
- [297] J. R. Eisenbrey, P. Huang, J. Hsu, and M. A. Wheatley. Ultrasound Triggered Cell Death in Vitro with Doxorubicin Loaded Poly Lactic-Acid Contrast Agents. *Ultrasonics*, 49(8):628–633, 2009.
- [298] K. Kooiman, M. R. Bohmer, M. Emmer, H. J. Vos, C. Chlon, W. T. Shi, C. S. Hall, S. H. P. M. de Winter, K. Schroen, M. Versluis, N. de Jong, and A. van

- Wamel. Oil-Filled Polymer Microcapsules for Ultrasound-Mediated Delivery of Lipophilic Drugs. *Journal of Controlled Release*, 133(2):109–118, 2009.
- [299] A. A. Doinikov, J. F. Haac, and P. A. Dayton. Resonance Frequencies of Lipid-Shelled Microbubbles in the Regime of Nonlinear Oscillations. *Ultrasonics*, 49(2):263–268, 2009.
- [300] M. Postema, A. Bouakaz, M. Versluis, and N. de Jong. Ultrasound-Induced Gas Release from Contrast Agent Microbubbles. *Ultrasonics, Ferroelectrics and Frequency Control, IEEE Transactions on*, 52(6):1035–1041, 2005. ISSN 0885-3010.
- [301] S. Casciaro, R. P. Errico, F. Conversano, C. Demitri, and A. Distante. Experimental Investigations of Nonlinearities and Destruction Mechanisms of an Experimental Phospholipid-Based Ultrasound Contrast Agent. *Investigative Radiology*, 42(2):95–104, 2007.
- [302] A. Eller and H. G. Flynn. Generation of Subharmonics of Order One-Half by Bubbles in a Sound Field. *The Journal of the Acoustical Society of America*, 46(3B):722–727, 1969.
- [303] E. A. Neppiras. Subharmonic and Other Low-Frequency Emission from Bubbles in Sound-Irradiated Liquids. *The Journal of the Acoustical Society of America*, 46(3B):587–601, 1969.
- [304] E. Kimmel, B. Krasovitski, A. Hoogi, D. Razansky, and D. Adam. Subharmonic Response of Encapsulated Microbubbles: Conditions for Existence and Amplification. *Ultrasound in Medicine and Biology*, 33(11):1767–1776, 2007.
- [305] J. Mamou and J. A. Ketterling. Subharmonic Analysis Using Singular-Value Decomposition of Ultrasound Contrast Agents. *The Journal of the Acoustical Society of America*, 125(6):4078, 2009.
- [306] W. T. Shi, F. Forsberg, B. B. Goldberg, and J. S. Raichlen. Method and system for pressure estimation using subharmonic signals from microbubble-based ultrasound contrast agents, October 2001.
- [307] W. T. Shi, F. Forsberg, J. S. Raichlen, L. Needleman, and B. B. Goldberg. Non-invasive Pressure Estimation with Us Microbubble Contrast Agents. *Radiology*, 213P:101–101, 1999.
- [308] L. Leodore, F. Forsberg, and W. T. Shi. Subharmonic Contrast Microbubble Signals for Noninvasive Pressure Estimation: An in Vitro Study. *Circulation*, 116(16):646–646, 2007.

- [309] L. Leodore, F. Forsberg, and W. T. Shi. In Vitro Pressure Estimation Obtained from Subharmonic Contrast Microbubble Signals. In *Ultrasonics Symposium, 2007. IEEE*, pages 2207–2210, 2007.
- [310] F. Forsberg, J. B. Liu, W. T. Shi, J. Furuse, M. Shimizu, and B. B. Goldberg. In Vivo Pressure Estimation Using Subharmonic Contrast Microbubble Signals: Proof of Concept. *IEEE Transactions on Ultrasonics Ferroelectrics and Frequency Control*, 52(4):581–583, 2005.
- [311] Y. Itai and O. Matsui. Blood Flow and Liver Imaging. *Radiology*, 202(2):306–314, 1997.
- [312] P. C. Pieters, W. J. Miller, and J. H. DeMeo. Evaluation of the Portal Venous System: Complementary Roles of Invasive and Noninvasive Imaging Strategies. *Radiographics*, 17(4):879–895, 1997.
- [313] F. Forsberg, V. G. Halldorsdottir, J. Eisenbrey, J. S. Raichlen, J. B. Liu, C. Miller, J. M. Gonzalez, J. K. Dave, and D. A. Merton. Subharmonic Aided Pressure Estimation for Monitoring Neoadjuvant Chemotherapy of Locally Advanced Breast Cancer. In *Proc. Era of Hope*, page 595, August 2011.
- [314] A. Katiyar, K. Sarkar, and F. Forsberg. Modeling Subharmonic Response from Contrast Microbubbles as a Function of Ambient Static Pressure. *Journal of the Acoustical Society of America*, 129(4):2325–2335, 2011.
- [315] M. N. Rhyner, A. M. Smith, X. Gao, H. Mao, L. Yang, and S. Nie. Quantum Dots and Multifunctional Nanoparticles: New Contrast Agents for Tumor Imaging. *Nanomedicine*, 1(2):209–217, Aug 2006.
- [316] S. L. Huang. *Ultrasound-Responsive Liposomes*. Springer-Verlag, Nov 2010.
- [317] G. L. Britton, H. Kim, P. H. Kee, J. Aronowski, C. K. Holland, D. D. McPherson, and S. L. Huang. In Vivo Therapeutic Gas Delivery for Neuroprotection with Echogenic Liposomes. *Circulation*, 122(16):1578–87, 2010.
- [318] G. Britton, S. Chrzanowski, M. Moody, H. Kim, D. D. McPherson, and S. L. Huang. Nitric Oxide Loaded Echogenic Liposomes for Ultrasound Controlled Nitric Oxide Delivery and Regulation of Artery Diameter. *Stroke*, 40(4):E119–E120, 2009.
- [319] S. Chrzanowski, H. Kim, D. D. McPherson, and S. L. Huang. Ultrasound Triggered Nitric Oxide Release from Echogenic Liposomes Improves Arterial Vasodilation. *Circulation*, 118(18):S465–S465, 2008.
- [320] S. L. Huang, P. H. Kee, H. Kim, M. R. Moody, S. M. Chrzanowski, R. C. Macdonald, and D. D. McPherson. Nitric Oxide-Loaded Echogenic Liposomes for Nitric

- Oxide Delivery and Inhibition of Intimal Hyperplasia. *Journal of the American College of Cardiology*, 54(7):652–9, 2009.
- [321] S. L. Huang, P. H. Kee, M. R. Moody, D. D. McPherson, and R. C. MacDonald. Nitric Oxide Loaded Echogenic Liposomes Inhibit Intimal Hyperplasia in an Acute Arterial Injury Model. *Circulation*, 116(16):294–294, 2007.
 - [322] S. M. Demos, H. Alkan-Onyuksel, B. J. Kane, K. Ramani, A. Nagaraj, R. Greene, M. Klegerman, and D. D. McPherson. In Vivo Targeting of Acoustically Reflective Liposomes for Intravascular and Transvascular Ultrasonic Enhancement. *Journal of the American College of Cardiology*, 33(3):867–875, 1999.
 - [323] K. D. Buchanan, S. Huang, H. Kim, R. C. Macdonald, and D. D. McPherson. Echogenic Liposome Compositions for Increased Retention of Ultrasound Reflectivity at Physiologic Temperature. *Journal of Pharmaceutical Sciences*, 97(6): 2242–2249, 2008.
 - [324] C. C. Coussios, C. K. Holland, L. Jakubowska, S. L. Huang, R. C. MacDonald, A. Nagaraj, and D. D. McPherson. In Vitro Characterization of Liposomes and Optison® by Acoustic Scattering at 3.5 Mhz. *Ultrasound in Medicine and Biology*, 30(2):181–190, 2004.
 - [325] D. A. B. Smith, T. M. Porter, J. Martinez, S. L. Huang, R. C. MacDonald, D. D. McPherson, and C. K. Holland. Destruction Thresholds of Echogenic Liposomes with Clinical Diagnostic Ultrasound. *Ultrasound in Medicine and Biology*, 33(5): 797–809, 2007.
 - [326] K. Radhakrishnan, K. J. Haworth, S. L. Huang, M. E. Klegerman, D. D. McPherson, and C. K. Holland. Stability of Echogenic Liposomes as a Blood Pool Ultrasound Contrast Agent in a Physiologic Flow Phantom. *Ultrasound in Medicine and Biology*, 38(11):1970–1981, 2012.
 - [327] K. J. Haworth, T. D. Mast, K. Radhakrishnan, M. T. Burgess, J. A. Kopechek, S.-L. Huang, D. D. McPherson, and C. K. Holland. Passive Imaging with Pulsed Ultrasound Insonations. *The Journal of the Acoustical Society of America*, 132 (1):544–553, 2012.
 - [328] K. E. Hitchcock, D. N. Caudell, J. T. Sutton, M. E. Klegerman, D. Vela, G. J. Pyne-Geithman, T. Abruzzo, P. E. P. Cyr, Y. J. Geng, D. D. McPherson, and C. K. Holland. Ultrasound-Enhanced Delivery of Targeted Echogenic Liposomes in a Novel Ex Vivo Mouse Aorta Model. *Journal of Controlled Release*, 144(3): 288–295, 2010.
 - [329] K. D. Buchanan, S. L. Huang, H. Kim, D. D. McPherson, and R. C. MacDonald. Encapsulation of Nf-Kappa B Decoy Oligonucleotides within Echogenic Liposomes and Ultrasound-Triggered Release. *Journal of Controlled Release*, 141(2): 193–198, 2010.

- [330] G. J. Shaw, J. M. Meunier, S. L. Huang, C. J. Lindsell, D. D. McPherson, and C. K. Holland. Ultrasound-Enhanced Thrombolysis with Tpa-Loaded Echogenic Liposomes. *Thrombosis Research*, 124(3):306–310, 2009.
- [331] S. M. Herbst, M. E. Klegerman, H. Kim, J. B. Qi, H. Shelat, M. Wassler, M. R. Moody, C. M. Yang, X. Y. Ge, Y. J. Zou, J. A. Kopechek, F. J. Clubb, D. C. Kraemer, S. L. Huang, C. K. Holland, D. D. McPherson, and Y. J. Geng. Delivery of Stem Cells to Porcine Arterial Wall with Echogenic Liposomes Conjugated to Antibodies against Cd34 and Intercellular Adhesion Molecule-1. *Molecular Pharmaceutics*, 7(1):3–11, 2010.
- [332] A. Hamilton, M. Rabbat, P. Jain, N. Belkind, S. L. Huang, A. Nagaraj, M. Klegerman, R. MacDonald, and D. D. McPherson. A Physiologic Flow Chamber Model to Define Intravascular Ultrasound Enhancement of Fibrin Using Echogenic Liposomes. *Investigative Radiology*, 37(4):215–221, 2002.
- [333] S. M. Demos, H. Onyuksel, J. Gilbert, S. I. Roth, B. Kane, P. Jungblut, J. V. Pinto, D. D. McPherson, and M. E. Klegerman. In Vitro Targeting of Antibody-Conjugated Echogenic Liposomes for Site-Specific Ultrasonic Image Enhancement. *Journal of Pharmaceutical Sciences*, 86(2):167–171, 1997.
- [334] H. Kim, M. R. Moody, S. T. Laing, P. H. Kee, S.-L. Huang, M. E. Klegerman, and D. D. McPherson. In Vivo Volumetric Intravascular Ultrasound Visualization of Early/Inflammatory Arterial Atheroma Using Targeted Echogenic Immunoliposomes. *Investigative Radiology*, 45(10):685–691 10.1097/RLI.0b013e3181ee5bdd, 2010.
- [335] S. D. Tiukinhoy, S. L. Huang, K. Maganti, R. C. MacDonald, and D. D. McPherson. Novel Echogenic Tissue Plasminogen Activator-Loaded Liposomes for Site-Specific Thrombolysis. *Circulation*, 110(17):509–510, 2004.
- [336] S. L. Huang, P. Kee, D. D. McPherson, and R. C. MacDonald. Multi-Functional Echogenic Liposomes for Image-Guided and Ultrasound-Controlled Ppar Agonist Delivery. *Journal of the American College of Cardiology*, 49(9):365a–365a, 2007.
- [337] S. T. Laing, M. Moody, B. Smulevitz, H. Kim, P. Kee, S. L. Huang, C. K. Holland, and D. D. McPherson. Ultrasound-Enhanced Thrombolytic Effect of Tissue Plasminogen Activator-Loaded Echogenic Liposomes in an in Vivo Rabbit Aorta Thrombus Model-Brief Report. *Arteriosclerosis Thrombosis and Vascular Biology*, 31(6):1357–1359, 2011.
- [338] S. D. Tiukinhoy-Laing, K. Buchanan, D. Parikh, S. L. Huang, R. C. MacDonald, D. D. McPherson, and M. E. Klegerman. Fibrin Targeting of Tissue Plasminogen Activator-Loaded Echogenic Liposomes. *Journal of Drug Targeting*, 15(2):109–114, 2007.

- [339] P. Kee, T. Abruzzo, D. A. B. Smith, B. Wang, S. L. Huang, R. C. MacDonald, C. K. Holland, and D. D. McPherson. Synthesis and Acoustic Characterization of a Novel Ultrasound Controlled Drug Delivery System Based on Echogenic Liposomes. *Journal of the American College of Cardiology*, 49(9):120a–120a, 2007.
- [340] M. R. Moody, S. Huang, H. Kim, S. Chrzanowski, and D. D. McPherson. Bioactive Gas/Drug Co-Encapsulation and Release Improve Attenuation of Intimal Hyperplasia Following Acute Arterial Injury. In *Circulation*, volume 118, pages S573–S573. LIPPINCOTT WILLIAMS & WILKINS 530 WALNUT ST, PHILADELPHIA, PA 19106-3621 USA, 2008.
- [341] J. A. Kopecek, K. J. Haworth, K. Radhakrishnan, S. L. Huang, M. E. Klegerman, D. D. McPherson, and C. K. Holland. The Impact of Bubbles on Measurement of Drug Release from Echogenic Liposomes. *Ultrasonics Sonochemistry*, 20(4):1121–1130, 2013.
- [342] H. Y. Lin and J. L. Thomas. Factors Affecting Responsivity of Unilamellar Liposomes to 20 Khz Ultrasound. *Langmuir : the ACS journal of surfaces and colloids*, 20(15):6100–6, 2004.
- [343] T. J. Evjen, E. A. Nilssen, S. Rognvaldsson, M. Brandl, and S. L. Fossheim. Distearoylphosphatidylethanolamine-Based Liposomes for Ultrasound-Mediated Drug Delivery. *Eur J Pharm Biopharm*, 75(3):327–33, 2010.
- [344] B. Chandra, R. Subramaniam, S. Mallik, and D. Srivastava. Formulation of Photocleavable Liposomes and the Mechanism of Their Content Release. *Org Biomol Chem*, 4(9):1730–1740, 2006.
- [345] S. Laing, M. Moody, B. Smulevitz, H. Kim, S. Huang, P. Kee, D. Smith, C. Holland, and D. McPherson. Doppler Ultrasound Enhances the Thrombolytic Activity of Tissue Plasminogen Activator-Loaded Echogenic Liposomes in Vivo. *Circulation*, 118(18):S643–S643, 2008.
- [346] P. Rafter, P. Phillips, and M. A. Vannan. Imaging Technologies and Techniques. *Cardiology Clinics*, 22(2):181–+, 2004.
- [347] G. Bhagavatheeshwaran, W. T. Shi, F. Forsberg, and P. M. Shankar. Subharmonic Signal Generation from Contrast Agents in Simulated Neovessels. *Ultrasound in Medicine and Biology*, 30(2):199–203, 2004.
- [348] J. Chomas, P. Dayton, D. May, and K. Ferrara. Nondestructive Subharmonic Imaging. *IEEE Transactions on Ultrasonics Ferroelectrics and Frequency Control*, 49(7):883–892, 2002.
- [349] F. Forsberg, W. T. Shi, and B. B. Goldberg. Subharmonic Imaging of Contrast Agents. *Ultrasonics*, 38(1-8):93–98, 2000.

- [350] P. D. Krishna, P. M. Shankar, and V. L. Newhouse. Subharmonic Generation from Ultrasonic Contrast Agents. *Physics in Medicine and Biology*, 44(3):681–694, 1999.
- [351] S. Bibi, R. Kaur, M. Henriksen-Lacey, S. E. McNeil, J. Wilkhu, E. Lattmann, D. Christensen, A. R. Mohammed, and Y. Perrie. Microscopy Imaging of Liposomes: From Coverslips to Environmental SEM. *International Journal of Pharmaceutics*, 417(1-2):138–150, Sep 2011.
- [352] W. T. Shi, F. Forsberg, A. L. Hall, R. Y. Chia, J. B. Liu, S. Miller, K. E. Thomenius, M. A. Wheatley, and B. B. Goldberg. Subharmonic Imaging with Microbubble Contrast Agents: Initial Results. *Ultrasonic Imaging*, 21(2):79–94, 1999.
- [353] S. T. Laing and D. D. McPherson. Cardiovascular Therapeutic Uses of Targeted Ultrasound Contrast Agents. *Cardiovascular Research*, 83(4):626–635, 2009.
- [354] E. C. M. Cabral, P. T. Hennies, C. R. D. Correia, R. L. Zollner, and M. H. A. Santana. Preparation and Characterization of Diacetylene Polymerized Liposomes for Detection of Autoantibodies. *Journal of Liposome Research*, 13(3-4):199–211, 2003.
- [355] C. X. Guo, S. Q. Liu, C. Jiang, W. Y. Li, Z. F. Dai, H. Fritz, and X. Y. Wu. A Promising Drug Controlled-Release System Based on Diacetylene/Phospholipid Polymerized Vesicles. *Langmuir*, 25(22):13114–13119, 2009.
- [356] A. Yavlovich, A. Singh, S. Tarasov, J. Capala, R. Blumenthal, and A. Puri. Design of Liposomes Containing Photopolymerizable Phospholipids for Triggered Release of Contents. *Journal of Thermal Analysis and Calorimetry*, 98(1):97–104, 2009.
- [357] G. T. Qin, Z. Li, R. M. Xia, F. Li, B. E. O'Neill, J. T. Goodwin, H. A. Khant, W. Chiu, and K. C. Li. Partially Polymerized Liposomes: Stable against Leakage yet Capable of Instantaneous Release for Remote Controlled Drug Delivery. *Nanotechnology*, 22(15):155605, 2011.
- [358] C. X. Guo, P. Boullanger, T. Liu, and L. Jiang. Size Effect of Polydiacetylene Vesicles Functionalized with Glycolipids on Their Colorimetric Detection Ability. *Journal of Physical Chemistry B*, 109(40):18765–18771, 2005.
- [359] N. Khan and C. A. Wyres. Multi-Colour Printing, 2008.
- [360] Q. Cheng and R. C. Stevens. Charge-Induced Chromatic Transition of Amino Acid-Derivatized Polydiacetylene Liposomes. *Langmuir*, 14(8):1974–1976, 1998.

- [361] R. Nahire, R. Hossain, R. Patel, S. Paul, V. Meghnani, A. H. Ambre, K. S. Katti, K. N. Gange, E. Leclerc, D. K. Srivastava, K. Sarkar, and S. Mallik. Lipid Nanoparticles with Tunable Echogenicity for Targeted Delivery to Pancreatic Cancer Cells with Simultaneous Ultrasound Imaging. Under Review - Molecular Pharmaceutics (ACS Publications), 2013.
- [362] S. Kiani and S. Mousavi. Ultrasound assisted preparation of water in oil emulsions and their application in arsenic (V) removal from water in an emulsion liquid membrane process. *Ultrasonics Sonochemistry*, 20(1):373–377, Jan 2013.
- [363] H. Bhattacharjee, P. Balabathula, and G. C. Wood. Targeted nanoparticulate drug-delivery systems for treatment of solid tumors: a review. *Therapeutic Delivery*, 1(5):713–734, Nov 2010.
- [364] X. Liu, Y. Zheng, N. M. Samoshina, A. H. Franz, X. Guo, and V. V. Samoshin. Flipoisomes: pH-triggered conformational flip of new trans -2-aminocyclohexanol-based amphiphiles causes instant cargo release in liposomes. *Journal of Liposome Research*, 22(4):319–328, Dec 2012.
- [365] M. P. Melancon, M. Zhou, and C. Li. Cancer Theranostics with Near-Infrared Light-Activatable Multimodal Nanoparticles. *Accounts of Chemical Research*, 44(10):947–956, Oct 2011.
- [366] P. Mohan and N. Rapoport. Doxorubicin as a Molecular Nanotheranostic Agent: Effect of Doxorubicin Encapsulation in Micelles or Nanoemulsions on the Ultrasound-Mediated Intracellular Delivery and Nuclear Trafficking. *Mol Pharm*, 7(6):1959–73, 2010.
- [367] M. H. Lee, H. Y. Lin, H. C. Chen, and J. L. Thomas. Ultrasound Mediates the Release of Curcumin from Microemulsions. *Langmuir : the ACS journal of surfaces and colloids*, 24(5):1707–13, 2008.
- [368] D. Lensen, E. C. Gelderblom, D. M. Vriezema, P. Marmottant, N. Verdonschot, M. Versluis, N. de Jong, and J. C. M. van Hest. Biodegradable polymeric micro-capsules for selective ultrasound-triggered drug release. *Soft Matter*, 7(11):5417, 2011.
- [369] H. S. Min, E. Kang, H. Koo, J. Lee, K. Kim, R.-W. Park, I.-S. Kim, Y. Choi, I. C. Kwon, and M. Han. Gas-generating polymeric microspheres for long-term and continuous in vivo ultrasound imaging. *Biomaterials*, 33(3):936–944, Jan 2012.
- [370] G. A. Husseini, G. D. Myrup, W. G. Pitt, D. A. Christensen, and N. A. Y. Rapoport. Factors Affecting Acoustically Triggered Release of Drugs from Polymeric Micelles. *Journal of Controlled Release*, 69(1):43–52, 2000.

- [371] H. Y. Lin and J. L. Thomas. Peg-Lipids and Oligo(Ethylene Glycol) Surfactants Enhance the Ultrasonic Permeabilizability of Liposomes. *Langmuir : the ACS journal of surfaces and colloids*, 19(4):1098–1105, 2003.
- [372] M. Pong, S. Umchid, A. J. Guarino, P. A. Lewin, J. Litniewski, A. Nowicki, and S. P. Wrenn. In Vitro Ultrasound-Mediated Leakage from Phospholipid Vesicles. *Ultrasonics*, 45(1-4):133–145, 2006.
- [373] A. Schroeder, Y. Avnir, S. Weisman, Y. Najajreh, A. Gabizon, Y. Talmon, J. Kost, and Y. Barenholz. Controlling Liposomal Drug Release with Low Frequency Ultrasound: Mechanism and Feasibility. *Langmuir : the ACS journal of surfaces and colloids*, 23(7):4019–4025, 2007.
- [374] v. Beijnum, Judy R. Tumor endothelium is characterized by a matrix remodeling signature. *Frontiers in Bioscience*, 1(1):216, 2009.
- [375] H. Emonard and J. A. Grimaud. Matrix Metalloproteinases. A Review. *Cell Mol Biol*, 36(2):131–53, 1990.
- [376] H. Birkedal-Hansen, W. G. Moore, M. K. Bodden, L. J. Windsor, B. Birkedal-Hansen, A. DeCarlo, and J. A. Engler. Matrix Metalloproteinases: A Review. *Crit Rev Oral Biol Med*, 4(2):197–250, 1993.
- [377] H. Nagase. Matrix Metalloproteinases. A Mini-Review. *Contrib Nephrol*, 107: 85–93, 1994.
- [378] Y. Herouy. Matrix Metalloproteinases in Skin Pathology (Review). *Int J Mol Med*, 7(1):3–12, 2001.
- [379] M. Pytliak, V. Vargova, and V. Mechirova. Matrix Metalloproteinases and Their Role in Oncogenesis: A Review. *Onkologie*, 35(1-2):49–53, 2012.
- [380] M. Consolo, A. Amoroso, D. A. Spandidos, and M. C. Mazzarino. Matrix Metalloproteinases and Their Inhibitors as Markers of Inflammation and Fibrosis in Chronic Liver Disease (Review). *Int J Mol Med*, 24(2):143–52, 2009.
- [381] A. Kohrmann, U. Kammerer, M. Kapp, J. Dietl, and J. Anacker. Expression of Matrix Metalloproteinases (Mmps) in Primary Human Breast Cancer and Breast Cancer Cell Lines: New Findings and Review of the Literature. *BMC Cancer*, 9: 188, 2009.
- [382] A. L. Pereira, S. S. Veras, E. J. Silveira, F. R. Seabra, L. P. Pinto, L. B. Souza, and R. A. Freitas. The Role of Matrix Extracellular Proteins and Metalloproteinases in Head and Neck Carcinomas: An Updated Review. *Braz J Otorhinolaryngol*, 71(1):81–6, 2005.

- [383] E. Carmeli, M. Moas, A. Z. Reznick, and R. Coleman. Matrix Metalloproteinases and Skeletal Muscle: A Brief Review. *Muscle Nerve*, 29(2):191–7, 2004.
- [384] Y. Konstantino, T. T. Nguyen, R. Wolk, R. J. Aiello, S. G. Terra, and D. A. Fryburg. Potential implications of matrix metalloproteinase-9 in assessment and treatment of coronary artery disease. *Biomarkers*, 14(2):118–129, Mar 2009.
- [385] R. Roy, J. Yang, and M. A. Moses. Matrix Metalloproteinases As Novel Biomarkers and Potential Therapeutic Targets in Human Cancer. *Journal of Clinical Oncology*, 27(31):5287–5297, Oct 2009.
- [386] J. Hu, P. E. Van den Steen, Q.-X. A. Sang, and G. Opdenakker. Matrix metalloproteinase inhibitors as therapy for inflammatory and vascular diseases. *Nature Reviews Drug Discovery*, 6(6):480–498, Jun 2007.
- [387] H.-H. Hub, B. Hupfer, H. Koch, and H. Ringsdorf. Polymerizable Phospholipid Analogues - New Stable Biomembrane and Cell Models. *Angewandte Chemie International Edition in English*, 19(11):938–940, Nov 1980.
- [388] R. R. Perry, J. Mazetta, M. Levin, and S. C. Barranco. Glutathione levels and variability in breast tumors and normal tissue. *Cancer*, 72(3):783–787, Aug 1993.
- [389] M. Raderer and W. Scheithauer. Clinical trials of agents that reverse multidrug resistance. A literature review. *Cancer*, 72(12):3553–3563, Dec 1993.
- [390] S. J. Berger, D. Gosky, E. Zborowska, J. K. V. Willson, and N. A. Berger. Sensitive Enzymatic Cycling Assay for Glutathione: Measurements of Glutathione Content and Its Modulation by Buthionine Sulfoximine in Vivo and in Vitro in Human Colon Cancer. *Cancer Research*, 54(15):4077–4083, 1994.
- [391] J. A. Cook, H. I. Pass, S. N. Iype, N. Friedman, W. DeGraff, A. Russo, and J. B. Mitchell. Cellular Glutathione and Thiol Measurements from Surgically Resected Human Lung Tumor and Normal Lung Tissue. *Cancer Research*, 51(16):4287–4294, 1991.
- [392] F. Joncourt, A. Oberli-Schrammli, M. Stadler, K. Buser, L. Franscini, M. Fey, and T. Cerny. Patterns of Drug Resistance Parameters in Adult Leukemia. *Leukemia and Lymphoma*, 17(1-2):101–109, 1995. cited By (since 1996)10.
- [393] T. P. Mulder, J. J. Manni, H. M. Roelofs, W. H. Peters, and A. Wiersma. Glutathione S-transferases and Glutathione in Human Head and Neck Cancer. *Carcinogenesis*, 16(3):619–624, 1995.
- [394] I. A. Cotgreave and R. G. Gerdes. Recent Trends in Glutathione Biochemistry - Glutathione - Protein Interactions: A Molecular Link between Oxidative Stress and Cell Proliferation? *Biochemical and Biophysical Research Communications*, 242(1):1–9, Jan 1998.

- [395] G. Saito, J. A. Swanson, and K.-D. Lee. Drug Delivery Strategy Utilizing Conjugation via Reversible Disulfide Linkages: Role and Site of Cellular Reducing Activities. *Advanced Drug Delivery Reviews*, 55(2):199–215, Feb 2003.
- [396] K. R. West and S. Otto. Reversible Covalent Chemistry in Drug Delivery. *Curr Drug Discov Technol*, 2(3):123–60, 2005.
- [397] B. Goldenbogen, N. Brodersen, A. Gramatica, M. Loew, J. Liebscher, A. Herrmann, H. Egger, B. Budde, and A. Arbuzova. Reduction-Sensitive Liposomes from a Multifunctional Lipid Conjugate and Natural Phospholipids: Reduction and Release Kinetics and Cellular Uptake. *Langmuir*, 27(17):10820–9, 2011.
- [398] H. Cho, J. Bae, V. K. Garripelli, J. M. Anderson, H. W. Jun, and S. Jo. Redox-Sensitive Polymeric Nanoparticles for Drug Delivery. *Chem Commun (Camb)*, 48:6043–6045, 2012.
- [399] H. Wen, C. Dong, H. Dong, A. Shen, W. Xia, X. Cai, Y. Song, X. Li, Y. Li, and D. Shi. Engineered Redox-Responsive Peg Detachment Mechanism in Pegylated Nano-Graphene Oxide for Intracellular Drug Delivery. *Small*, 8(5):760–9, 2012.
- [400] N. Graf and S. J. Lippard. Redox Activation of Metal-based Prodrugs as a Strategy for Drug Delivery. *Advanced Drug Delivery Reviews*, 64(11):993–1004, Aug 2012.
- [401] J. Griffiths. Are Cancer Cells Acidic? *British Journal of Cancer*, 64(3):425–427, Sep 1991.
- [402] E. S. Lee, Z. Gao, and Y. H. Bae. Recent Progress in Tumor Ph Targeting Nanotechnology. *Journal of Controlled Release*, 132(3):164–170, Dec 2008.
- [403] I. F. Tannock and D. Rotin. Acid pH in Tumors and Its Potential for Therapeutic Exploitation. *Cancer Research*, 49(16):4373–4384, 1989.
- [404] Cancer Facts & Figures 2013, 2013.
- [405] B. M. Discher. Polymersomes: Tough Vesicles Made from Diblock Copolymers. *Science*, 284(5417):1143–1146, May 1999.
- [406] D. E. Discher. Polymer Vesicles. *Science*, 297(5583):967–973, Aug 2002.
- [407] D. E. Discher and F. Ahmed. Polymersomes. *Annual Review of Biomedical Engineering*, 8(1):323–341, Aug 2006.
- [408] S. Cerritelli, D. Velluto, and J. A. Hubbell. PEG-SS-PPS: Reduction-Sensitive Disulfide Block Copolymer Vesicles for Intracellular Drug Delivery. *Biomacromolecules*, 8(6):1966–1972, Jun 2007.

- [409] A. I. Elegbede, J. Banerjee, A. J. Hanson, S. Tobwala, B. Ganguli, R. Wang, X. Lu, D. K. Srivastava, and S. Mallik. Mechanistic Studies of the Triggered Release of Liposomal Contents by Matrix Metalloproteinase-9. *Journal of the American Chemical Society*, 130(32):10633–10642, Aug 2008.
- [410] S. Zhang and Y. Zhao. Controlled Release from Cleavable Polymerized Liposomes upon Redox and pH Stimulation. *Bioconjugate Chemistry*, 22(4):523–528, Apr 2011.
- [411] M. W. Roomi, J. C. Monterrey, T. Kalinovsky, M. Rath, and A. Niedzwiecki. Patterns of Mmp-2 and Mmp-9 Expression in Human Cancer Cell Lines. *Oncol Rep*, 21(5):1323–33, 2009.
- [412] F. Chen, N. Ohashi, W. Li, C. Eckman, and J. H. Nguyen. Disruptions of Occludin and Claudin-5 in Brain Endothelial Cells in Vitro and in Brains of Mice with Acute Liver Failure. *Hepatology*, 50(6):1914–23, 2009.
- [413] M.-X. Tang, H. Mulvana, T. Gauthier, A. K. P. Lim, D. O. Cosgrove, R. J. Eckersley, and E. Stride. Quantitative Contrast-enhanced Ultrasound Imaging: A Review Of Sources Of Variability. *Interface Focus*, 1(4):520–539, Jun 2011.
- [414] E. Stride and N. Saffari. Investigating the Significance of Multiple Scattering in Ultrasound Contrast Agent Particle Populations. *IEEE Trans Ultrason Ferroelectr Freq Control*, 52(12):2332–2345, 2005.
- [415] A. Qamar, R. Samtaney, and J. L. Bull. Dynamics of Micro-Bubble Sonication inside a Phantom Vessel. *Applied Physics Letters*, 102(1):013702–5, 2013.
- [416] V. Garbin, D. Cojoc, E. Ferrari, E. Di Fabrizio, M. L. J. Overvelde, S. M. van der Meer, N. de Jong, D. Lohse, and M. Versluis. Changes in Microbubble Dynamics near a Boundary Revealed by Combined Optical Micromanipulation and High-Speed Imaging. *Applied Physics Letters*, 90(11):114103–3, 2007.
- [417] A. A. Doinikov, L. Aired, and A. Bouakaz. Acoustic Scattering from a Contrast Agent Microbubble near an Elastic Wall of Finite Thickness. *Phys Med Biol*, 56(21):6951–6967, 2011.
- [418] J. Loughran, R. J. Eckersley, and M.-X. Tang. Modeling Non-Spherical Oscillations and Stability of Acoustically Driven Shelled Microbubbles. *The Journal of the Acoustical Society of America*, 131(6):4349–4357, 2012.
- [419] M. C. Pauzin, S. Mensah, and J. P. Lefebvre. Development of a Finite Element Model of Ultrasound Contrast Agent. In *Ultrasonics Symposium, 2007. IEEE*, pages 1989–1992, 2007.

- [420] T. M. Maul, D. D. Dudgeon, M. T. Beste, D. A. Hammer, J. S. Lazo, F. S. Villanueva, and W. R. Wagner. Optimization of Ultrasound Contrast Agents with Computational Models to Improve Selection of Ligands and Binding Strength. *Biotechnol Bioeng*, 107(5):854–864, 2010.
- [421] T. J. Evjen, E. A. Nilssen, R. A. Fowler, S. Rognvaldsson, M. Brandl, and S. L. Fossheim. Lipid membrane composition influences drug release from dioleoylphosphatidylethanolamine-based liposomes on exposure to ultrasound. *International Journal of Pharmaceutics*, 406(1-2):114–116, Mar 2011.

Appendix A

DERIVATION OF THE RAYLEIGH-PLESSET EQUATION

A.1 Incompressible Form

The continuity and momentum equations for an incompressible fluid with the assumption of spherical symmetry is given by

$$\frac{1}{r^2} \frac{\partial}{\partial r} (r^2 v_r) = 0, \quad (\text{A.1a})$$

$$\rho_l \left(\frac{\partial v_r}{\partial t} + v_r \frac{\partial v_r}{\partial r} \right) = -\frac{\partial p}{\partial r} + \mu \left[\frac{1}{r^2} \frac{\partial}{\partial r} \left(r^2 \frac{\partial v_r}{\partial r} \right) - \frac{2v_r}{r^2} \right], \quad (\text{A.1b})$$

Integrating A.1a we obtain the expression for the radial velocity as

$$v_r = -\frac{R^2 \dot{R}}{r^2} \quad (\text{A.2})$$

Using A.2 in A.1b and integrating it from $r = R$ to $r \rightarrow \infty$, we obtain

$$\rho_L \left(R \ddot{R} + \frac{3}{2} \dot{R}^2 \right) = p_{r=R}(t) - p_\infty(t) \quad (\text{A.3})$$

where $p_{r=R}$ is the pressure in the liquid just outside the bubble and the p_∞ is the pressure at a large distance away from the bubble. To determine the $p_{r=R}$, we can use

a simple force balance at the interface given as

$$p_G(t) + p_v(t) + (\tau_{rr})_{r=R} = \frac{2\sigma}{R} \quad (\text{A.4a})$$

$$\text{or, } p_G(t) + p_v(t) - p_{r=R}(t) + 2\mu \left(\frac{\partial v_r}{\partial r} \right)_{r=R} = \frac{2\sigma}{R} \quad (\text{A.4b})$$

$$\text{or, } p_G(t) + p_v(t) - p_{r=R}(t) - 4\mu \frac{\dot{R}}{R} = \frac{2\sigma}{R} \quad (\text{A.4c})$$

$$(\text{A.4d})$$

which gives

$$p_{r=R}(t) = p_G(t) + p_v(t) - 4\mu \frac{\dot{R}}{R} - \frac{2\sigma}{R}. \quad (\text{A.5})$$

Using A.5 in A.3, we have the following form of the incompressible Rayleigh-Plesset equation

$$R\ddot{R} + \frac{3}{2}\dot{R}^2 = \frac{1}{\rho_L} \left\{ p_i - p_\infty(t) - \frac{2\sigma}{R} - \frac{4\mu\dot{R}}{R} \right\}, \quad (\text{A.6})$$

where p_i , the interior pressure equals $p_G(t) + p_v(t)$.

A.2 Compressible Form

The complete derivation of compressible form of RP equation is beyond the scope of this thesis. A short introduction is provided here.

The velocity field for the incompressible liquid derived above can be expressed in terms of a potential function near the bubble as

$$\mathbf{v} = \nabla\phi \quad \text{such that,} \quad \phi = -\frac{R^2\dot{R}}{r^2} + A(t), \quad (\text{A.7})$$

where $A(t)$ is an arbitrary matching constant. The far field potential is also modified

due to sound emission from bubbles and can be written as

$$\phi(t) = \phi_\infty(t) - \frac{1}{r} F(t - \frac{r}{c}) \approx \phi_\infty(t) - \frac{1}{r} F(t) + \dot{F}(t)/c \quad (\text{A.8})$$

This field should match the expression of near-field velocity potential given by A.7. The matching yields $F(t) = R^2 \dot{R}$ and $A(t) = \phi_\infty(t) + F(t)/c$. Note that when radiation from the bubble is neglected, $A = \phi_\infty(t)$. With this modification the compressible form of RP equation now becomes

$$R \ddot{R} + \frac{3}{2} \dot{R}^2 = \frac{1}{\rho_L} \left\{ p_i - p_\infty(t) - \frac{2\sigma}{R} - \frac{4\mu \dot{R}}{R} \right\} + \frac{1}{c} \frac{d^2}{dt^2} \left(R^2 \dot{R} \right), \quad (\text{A.9})$$

where the last term on the right hand side is an additional term. Note that the order of this term is $|\dot{R}/c|$ times the order of the other terms of the equations and hence it only becomes important when $|\dot{R}/c| \sim 1$. Thus, consideration of sound radiation by the bubble increases the order of RP equation. Now, two approaches have been proposed to solve A.9

1. Choose a proper initial condition for \ddot{R} to suppress the spurious unstable solution.
2. Calculate $\frac{d^2}{dt^2} \left(R^2 \dot{R} \right)$ using the RP equation itself.

The latter has been suggested as a better alternative and resulting equation can be written in the following generalized form [147, 179]

$$\begin{aligned} \rho_L R \ddot{R} \left[1 - (\lambda + 1) \frac{\dot{R}}{c} \right] + \frac{3}{2} \rho_L \dot{R}^2 \left[1 - \left(\lambda + \frac{1}{3} \right) \frac{\dot{R}}{c} \right] &= \left[1 + (1 - \lambda) \frac{\dot{R}}{c} \right] (p_G - p_\infty) \\ &\quad + \frac{R}{c} \frac{dp_G}{dt} - \frac{2\sigma}{R} - \frac{4\mu \dot{R}}{R}, \end{aligned} \quad (\text{A.10})$$

where λ is an arbitrary constant. Since, the above equation often breaks down as $|\dot{R}/c|$ approaches unity due to an unphysical singularity, one can get rid of the prefactors in

the parenthesis with \dot{R}/c , which gives us the following form of A.10 [128]

$$R\ddot{R} + \frac{3}{2}\dot{R}^2 = \frac{1}{\rho_L} \left\{ p_G - \frac{2\sigma}{R} - \frac{4\mu\dot{R}}{R} - p_0 - p_A(t) - \frac{R}{c} \frac{dp_G}{dt} \right\} \quad (\text{A.11})$$

Appendix B

DERIVATION OF THE ACOUSTIC CROSS-SECTIONS

A generalized liner form of the RP equation can be written as

$$\ddot{X}_l + 2b(\omega)\dot{X}_l + K(\omega)X_l = F(\omega)e^{i\omega t}. \quad (\text{B.1})$$

The particular solution to [B.1](#) is given by

$$X_l = \frac{F}{(K/\omega^2 - 1)^2 + (2\beta/\omega)^2} \quad (\text{B.2})$$

and

$$\dot{X}_l = \frac{iF\omega}{(K/\omega^2 - 1)^2 + (2\beta/\omega)^2} \quad (\text{B.3})$$

A plane wave (p_i) incident on the bubble can be represented as

$$p_i = A_0 \exp[i\omega(t - x/c)]. \quad (\text{B.4})$$

For a spherical bubble of radius R_0 positioned such that, its center coincides with the origin, the factor F in [B.1](#) is given by

$$F = -\frac{A_0}{\rho_0 R_0}, \quad (\text{B.5})$$

where ρ_0 is the equilibrium density of the liquid. Assuming that the scattered wave

(p_s) is spherical, the following representation of the scattered wave may be written

$$p_s = (B/r)\exp[i\omega(t - r/c)]. \quad (\text{B.6})$$

where r is the radial distance from origin. The scattering cross-section (σ_s) is hence given as

$$\sigma_s = 4\pi|B/A_0|^2 \quad (\text{B.7})$$

The scattered pressure can be related to radial velocity using Euler's equation which is given by

$$-\frac{\partial p_s}{\partial r} = \rho_0 \frac{\partial u}{\partial t} \quad (\text{B.8})$$

Substituting B.6 in B.8, relates the particle radial velocity in liquid at a distance r from the origin to the acoustic pressure of the spherical radiated field. The following relation is obtained

$$u_s(r) = \left(1 - \frac{i}{\omega r/c}\right) \frac{p_s(r)}{\rho_0 c}. \quad (\text{B.9})$$

The input impedance (Z) is defined as

$$Z \equiv \frac{p_i(x=0)}{u_s(r=R_0)} = i\rho_0 c \varepsilon \left(\frac{K}{\omega^2} - 1 + 2i \frac{b}{\omega} \right), \quad (\text{B.10})$$

where $\varepsilon = \omega R_0/c$ and $u_s(r = R_0)$ was substituted from B.3. We can also obtain $u_s(r = R_0)$ from Euler's equation which can be written as

$$u_s(r = R_0) = -i \frac{1 + i\varepsilon}{\rho_0 c \varepsilon} p_s(R_0) \quad (\text{B.11})$$

Eliminating $u_s(r = R_0)$ from B.10 and B.11, we have

$$\begin{aligned}\frac{p_i(0)}{p_s(R_0)} &= -i \frac{1 + i\varepsilon}{\rho_0 c \varepsilon} Z \\ &= \left(\frac{K}{\omega^2} - 1 - \frac{2\beta\varepsilon}{\omega} \right) + i \left(\frac{K\varepsilon}{\omega^2} - \varepsilon + \frac{2\beta}{\omega} \right)\end{aligned}\quad (\text{B.12})$$

Using B.12 and recalling the definition of acoustic scattering cross-section, we can write

$$\sigma_s = \frac{4\pi R_0^2}{|p_i(0)/p_s(R_0)|^2} = \frac{4\pi R_0^2}{(1 + \varepsilon^2) [(K/\omega^2 - 1)^2 + (2b/\omega)^2]} \quad (\text{B.13})$$

B.13 is exactly the same with the expression derived by Ainslie and Leighton [174] for a more generalized case with $2b/\omega$ replacing δ_{Medwin} . In the same paper the following relation between scattering and extinction cross-section was provided

$$\begin{aligned}\sigma_e &= \sigma_s \frac{\delta_{\text{Medwin}}}{\varepsilon} (1 + \varepsilon^2) \\ \text{or} \\ \sigma_e &= \frac{4\pi R_0^2}{(K/\omega^2 - 1)^2 + (2b/\omega)^2} \frac{2b}{\varepsilon \omega}\end{aligned}\quad (\text{B.14})$$

Appendix C

DATA ACQUISITION SYSTEM AND MATLAB CODES USED IN THE ANALYSIS OF EXPERIMENTAL DATA

The LabView program interface for the data acquisition is shown below in Figure C.1.

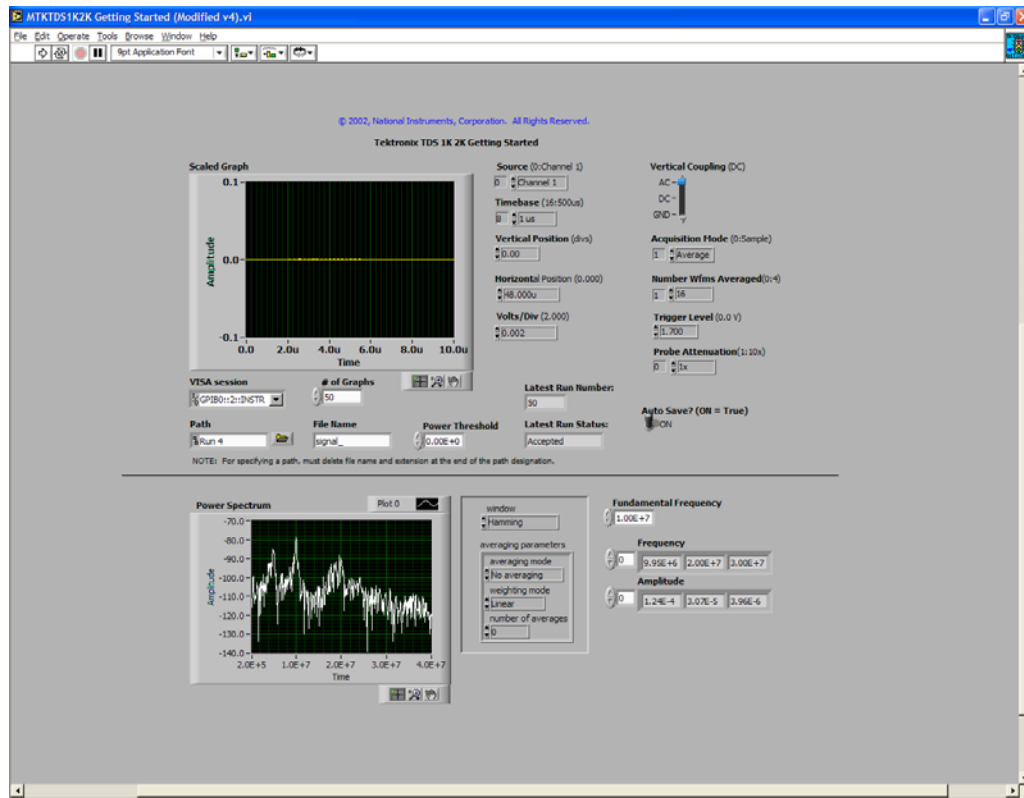


Figure C.1: The LabView program GUI interface utilized for the data acquisition.

The post experimental analysis Matlab codes utilized for this study are also included in the following pages. The purpose of each function/code is given in the table below.

Table C.1: Purpose of Matlab codes/functions included in this appendix.

Code/Function Name	Function
attenuation_calling_prog_correct	Calculates Attenuation
attenuation_called_mod	Read Data Files and Outputs Their FFTs
dblevel	Calculates and Displays Scattered Response
scattering_calling_prog_correct	Calculates Time Dependent Scattering
scattering_called	Read Data Files and Outputs Their FFTs

```

clear all
clc
global attn_coeff
k=[];
kk=[];
kk_avg=[];
k_avg=[];
hz=[];
alpha = [];
alpha_avg=[];
index=[];
signal_energy=[];
path_length=11;%path length in cm.
% for i=1:6:120
% i
% attenuation_called(10e6,6,25,'Attenuation\PC PE\10 MHz\June 8,2012\Run
1','signal_10dB','control_10dB')
[k kk k_avg kk_avg hz fo] = attenuation_called(3.5e6,20,20,'Krishna\Attenuation\June
4,2013\Run 7','signal_10dBattn','control_10dBattn');

% fft_array=vertcat(k,k_avg,kk_avg);
ratio=kk_avg./k_avg;
attn_coeff(:,1)=hz;
attn_coeff(:,2)=(20*log10(ratio(1:length(hz))))';
attn_coeff(:,2)=attn_coeff(:,2)/path_length;
save('attn.dat','attn_coeff','-ASCII');

counter=1;
for i=1:12:120 %since each acquisition takes 5 secs 12 acquisitions takes 1 min
%     k_time_avg(counter,:)=mean(k(i:i+11,1:length(hz)),1);
    k_time_avg(counter,:)=mean(k(i:i+11,:),1);%takes average of 12 consecutive
acquisitions
    ref_to_sig(counter,:)=kk_avg(1:length(hz))./k_time_avg(counter,1:length(hz));
    sum=0;
    for j=1:length(hz)
        if k_time_avg(counter,j)>0
            sum=sum+((k_time_avg(counter,j))^2);%sums of the squares of half the elements
        end
    end
    signal_energy(counter)=sum;
    counter=counter+1;
end
time_dep_spectra=(20*log10(ref_to_sig(:,1:50)))'/12

ref_energy=0;
signal_energy_initial=0;
for j=1:length(hz)
    ref_energy=ref_energy+((kk_avg(j))^2);

    signal_energy_initial=signal_energy_initial+((k(1,j))^2);%at t=0;

```

```
end
A=[ ];
% A(1)=(10*log10(ref_energy/signal_energy_initial))/path_length;% This is A(0)
A(1)=(10*log10(ref_energy/signal_energy(1)))/path_length;% This is A(0)
%Calculating A(t)
for i=1:length(signal_energy)
    A(i+1)=(10*log10(ref_energy/signal_energy(i)))/path_length;
end
Normalized_Attenuation(:,1)=(0:12:120)';
Normalized_Attenuation(:,2)=(A/A(1))';
Normalized_Attenuation(:,2)
```

```

function levels = attenuation_called_mod(fo,numFiles,dirName,fileName1,fileName2)
% folder = ['G:\Research\Summer 2010\' dirName];
close all
clc
global attn_coeff ratio k_avg kk_avg
attn_coeff=[];
%folder = ['D:\Research\Shirshendu\Experimental Data\Shirshendu Liposome data\With\
PBS+BSA\' dirName];
%folder = ['D:\Research\Shirshendu\Experimental Data\Shirshendu PLA data\Attenuation\' \
dirName];
folder = ['F:\Research\Shirshendu\Experimental Data\Shirshendu Liposome data\Shirshendu\
Pol-Ellips\' dirName];
signal = ones(numFiles,2500);
ref = ones(numFiles,2500);
%% File Acquisition
for i = 1:numFiles
    i2 = num2str(i);
    i3=num2str(i);
    fullDirName1 = [folder '\fileName1 i2 '.dat'];
    fullDirName2 = [folder '\fileName2 i3 '.dat'];
    p = load(fullDirName1);
    q = load(fullDirName2);
    signal(i,:) = p(:,2)';
    ref(i,:) = q(:,2)';
end
%% FFTs
y = length(signal(1,:));
NFFT = 2^nextpow2(y);
ts = p(2,1)-p(1,1);
fs = 1/ts;
disp(fs)
hz = ((1:y/2)/y)*fs;
hz_1 = fs/2*linspace(0,1,NFFT/2+1);
z = ones(numFiles,2500);
zz = ones(numFiles,2500);
k = ones(numFiles,2500);
kk = ones(numFiles,2500);
% db_signal = ones(numFiles,1250);
% db_ref = ones(numFiles,1250);

for l = 1:numFiles
    z(l,:) = fft(signal(l,:),y);
    zz(l,:) = fft(ref(l,:),y);
    k(l,:) = abs(z(l,:))/y;
    kk(l,:)= abs(zz(l,:))/y;
%     db_signal(l,:) = 20*log10(k(l,1:y/2));
%     db_ref(l,:) = 20*log10(kk(l,1:y/2));
end
% db_avg = mean(db,1);
% stdev = std(db,1);
k_avg = mean(k,1);

```

```
kk_avg= mean(kk,1);
ratio=kk_avg./k_avg;
attn_coeff(:,1)=hz;
attn_coeff(:,2)=(20*log10(ratio(1:y/2)))';
attn_coeff(:,2)=attn_coeff(:,2)/12; %12 cm path length
%% FFT Analysis
tol = (hz(2)-hz(1));
for n = 1:1250
    if fo/2-tol < hz(n) && fo/2+tol > hz(n)
        index1 = n;
    elseif fo-tol < hz(n) && fo+tol > hz(n)
        index2 = n;
    elseif 2*fo-tol < hz(n) && 2*fo+tol > hz(n)
        index3 = n;
    end
end
[fund location1] = max(attn_coeff(index2-1:index2+1,2));
disp(fund)
end
```

```

function levels = dblevel(fo,numFiles,dirName,fileName)
%global hz db_avg ampl_avg hz
global y fft_avg
%clear all
% folder = ['G:\Research\Summer 2010\' dirName];
close all
%folder = ['D:\Research\Shirshendu\Experimental Data\Shirshendu Liposome data\With\PBS+BSA\' dirName];
folder = ['F:\Research\Shirshendu\Experimental Data\' dirName];
% folder = ['D:\Research\Shirshendu\Experimental Data\Shirshendu PLA data\Attenuation\' dirName];
%folder = ['D:\Research\Shirshendu\Experimental Data\Shirshendu Liposome data\With\PBS+BSA\Attenuation\' dirName];
signal = ones(numFiles,2500);
%% File Acquisition
for i = 1:numFiles
    i2 = num2str(i);
    fullDirName = [folder '\\" fileName i2 '.dat'];
    p = load(fullDirName);
    signal(i,:) = p(:,2)';
end
%% FFTs
y = length(signal(1,:));
NFFT = 2^nextpow2(y);
ts = p(2,1)-p(1,1);
fs = 1/ts;
% hz = ((1:y/2)/y)*fs;
hz = ((1:NFFT/2)/NFFT)*fs;
z = ones(numFiles,NFFT);
k = ones(numFiles,NFFT);
db = ones(numFiles,NFFT/2);

for l = 1:numFiles
    % z(l,:) = fft(hamming(2500).*signal(l,:),y);
    % z(l,:) = fft((hamming(2500).*signal(l,:)),NFFT);
    z(l,:) = fft(signal(l,:),NFFT);
    k(l,:) = abs(z(l,:))/y;
    ampl(l,:)=k(l,1:y/2);
    % db(l,:) = 20*log10(k(l,1:y/2));
    db(l,:) = 20*log10(k(l,1:NFFT/2));
end
k(:,1);
db_avg = mean(db,1);
stdev = std(db,1);
%ampl_avg = mean(ampl,1);
%% FFT Analysis
tol = (hz(2)-hz(1));
for n = 1:1250
    if fo/2-tol < hz(n) && fo/2+tol > hz(n)
        index1 = n;
    elseif fo-tol < hz(n) && fo+tol > hz(n)

```

```

    index2 = n;
elseif 2*fo-tol < hz(n) && 2*fo+tol > hz(n)
    index3 = n;
end
end
% for mmm=1:numFiles
% [fund location1] = max(k(mmm,index2-1:index2+1));
% [sub location2] = max(k(mmm,index1-1:index1+1));
% [super location3] = max(k(mmm,index3-1:index3+1));
%
% %levels = [fund fund_std sub sub_std super super_std];
% %disp([fund sub super ])
% end
[fund location1] = max(db_avg(index2-2:index2+2));
[sub location2] = max(db_avg(index1-2:index1+2));
[super location3] = max(db_avg(index3-2:index3+2));
fund_std = stdev(index2-1+location1);
sub_std = stdev(index1-1+location2);
super_std = stdev(index3-1+location3);
% levels = [fund fund_std sub sub_std super super_std];
disp([fund fund_std sub sub_std super super_std])

%% Plot (Layout -> Show Plot Tools -> Edit Preferences -> Generate M-file)
% Create figure
figure1 = figure;
% Create axes
axes1 = axes('Parent',figure1, ...
    'XTick',[0 fo/2 fo 3*fo/2 2*fo 5*fo/2 3*fo 7*fo/2 4*fo], ...
    'XGrid','on');
% Uncomment the following line to preserve the X-limits of the axes
xlim([5e+005 4*fo]);
hold('all');
% Create multiple lines using matrix input to plot
plot1 = plot(hz,db_avg,'Parent',axes1);
set(plot1(1), 'DisplayName', 'Experiment', 'Color', [0 0 0]);
% Create xlabel
xlabel('Frequency');
% Create ylabel
ylabel('Amplitude (dB)');
% Create title
title('Frequency Spectrum');
% Create legend
legend(axes1,'show');
hold off
%% Saving the average data
fft_avg=[];
fft_avg(:,1)=hz/fo;
fft_avg(:,2)=db_avg;

end

```

```

clear all
clc
global attn_coeff
k=[];
kk=[];
kk_avg=[];
k_avg=[];
hz=[];
alpha = [];
alpha_avg=[];
index=[];
signal_energy=[];
path_length=11;%path length in cm.
% for i=1:6:120
% i
% attenuation_called(10e6,6,25,'Attenuation\PC PE\10 MHz\June 8,2012\Run
1','signal_10dB','control_10dB')
[k k_avg hz fo] = scattering_called(3.5e6,100,'Shirshendu Liposome data\Polymersomes\May
3,2013\5800\Run 5','signal_250kPa_');

% For Extraction of Fundamental, Second and Subharmonics
tol = (hz(2)-hz(1));
for n = 1:1250
    if fo/2-tol < hz(n) && fo/2+tol > hz(n)
        index1 = n;
    elseif fo-tol < hz(n) && fo+tol > hz(n)
        index2 = n;
    elseif 2*fo-tol < hz(n) && 2*fo+tol > hz(n)
        index3 = n;
    end
end

attn_coeff(:,1)=hz;
counter=1;
for i=1:5:100 %since each acquisition takes ***secs 5 acquisitions takes *** secs
%     k_time_avg(counter,:)=mean(k(i:i+11,1:length(hz)),1);
    k_time_avg(counter,:)=20*log10(mean(k(i:i+4,1:length(hz)),1));%takes average of 5
consecutive acquisitions

    [fund location1] = max(k_time_avg(counter,index2-1:index2+1));
    [sub location2] = max(k_time_avg(counter,index1-1:index1+1));
    [super location3] = max(k_time_avg(counter,index3-3:index3+1));
%     disp([fund sub super])
    disp(fund)
    counter=counter+1;
end
% time_dep_spectra=((k_time_avg(:,1:375))')

```

```

function [k k_avg hz fo] = scattering_called(fo,numFiles1,dirName,fileName1)
% folder = ['G:\Research\Summer 2010\' dirName];
close all

global attn_coeff ratio
attn_coeff=[];
%folder = ['D:\Research\Shirshendu\Experimental Data\John DeLucca\PLA Attenuation\' ↵
dirName];
folder = ['F:\Research\Shirshendu\Experimental Data\' dirName];
% folder = ['F:\Research\Shirshendu\Experimental Data\Shirshendu Liposome\ ↵
data\Shirshendu Pol-Elips\' dirName];
signal = ones(numFiles1,2500);
% ref = ones(numFiles2,2500);
%% File Acquisition
for i = 1:numFiles1
    i2 = num2str(i);

    fullDirName1 = [folder '\' fileName1 i2 '.dat'];

    p = load(fullDirName1);

    signal(i,:) = p(:,2)';

end
% for i = 1:numFiles2
%
%     i3 = num2str(i);
%
%     fullDirName2 = [folder '\' fileName2 i3 '.dat'];
%
%     q = load(fullDirName2);
%
%     ref(i,:) = q(:,2)';
% end

%% FFTs
y = length(signal(1,:));
ts = p(2,1)-p(1,1);
fs = 1/ts;
% hz = ((1:y/2)/y)*fs;
% z = ones(numFiles1,2500);
% zz = ones(numFiles2,2500);
% k = ones(numFiles1,2500);
% kk = ones(numFiles2,2500);
% db_signal = ones(numFiles,1250);
% db_ref = ones(numFiles,1250);
NFFT = 2^nextpow2(y);
hz = ((1:NFFT/2)/NFFT)*fs;
z = ones(numFiles1,NFFT);
k = ones(numFiles1,NFFT);

```

```
% db = ones(numFiles,NFFT/2);
for l = 1:numFiles1
%     z(l,:) = fft(signal(l,:),y);
%
%     k(l,:) = abs(z(l,:))/y;

z(l,:) = fft(signal(l,:),NFFT);
k(l,:) = abs(z(l,:))/y;

%     db_signal(l,:) = 20*log10(k(l,1:y/2));
%     db_ref(l,:)      = 20*log10(kk(l,1:y/2));
end
% for l = 1:numFiles2
%
%     zz(l,:) = fft(ref(l,:),y);
%
%     kk(l,:)= abs(zz(l,:))/y;
% %     db_signal(l,:) = 20*log10(k(l,1:y/2));
% %     db_ref(l,:)      = 20*log10(kk(l,1:y/2));
% end
% db_avg = mean(db,1);
% stdev = std(db,1);
% k(:,2)

k_avg = mean(k,1);
% kk_avg= mean(kk,1);
% ratio=kk_avg./k_avg;
% attn_coeff(:,1)=hz;
% attn_coeff(:,2)=(20*log10(ratio(1:y/2)))';
% attn_coeff(:,2)=attn_coeff(:,2)/11; %6 cm path length
% %% FFT Analysis
% tol = (hz(2)-hz(1));
% for n = 1:1250
%     if fo/2-tol < hz(n) && fo/2+tol > hz(n)
%         index1 = n;
%     elseif fo-tol < hz(n) && fo+tol > hz(n)
%         index2 = n;
%     elseif 2*fo-tol < hz(n) && 2*fo+tol > hz(n)
%         index3 = n;
%     end
% end
% [fund location1] = max(attn_coeff(index2-1:index2+1,2));
%
% disp(fund)
end
```

Appendix D

MATLAB CODES USED IN THE PARAMETER ESTIMATION AND FOR SCATTERING PREDICTIONS

The relevant Matlab codes utilized for this study are also included in the following pages [Only codes for the Exponential Model are included as the rest are similar]. The purpose of each function/code is given in the table below.

Table D.1: Purpose of Matlab codes/functions included in this appendix.

Code/Function Name	Function
trial_inverse_expm	Estimates Parameters
trial_inverse_expm1	Curve Fitting Input
exponential_model_calling	Solves the RP Equation
Viscoelastic_model_called...	Input to ODE Solver

```
%this programme estimates the parameters associated with our model
%experimental results: tried for different bubble sizes (r/ae) and frequencies (F)
%n denotes the size distribution of bubbles.
clc
clear all
close all
global r ae l n Y p0 rhol c E mul F sig k kappa Gam Pg0

% PB127
% PH37
% PH43
PH44
% PH45
l=length(n);
%-----Constant Parameters Known-----
p0=1.01325e5;
rhol=998;
mul=2*0.001;% thermal damping accounted
c=1484;
E=exp(1); %inverse of log_e;
%-----
k=1.0;%isothermal
% k=1.4;%adiabatic

X0=[1.6e-7;0.00;11.0;10];
LB=[1e-11;1e-5;1e-5;1e-2];
UB=[5e-7;0.072;inf;inf];

%options=optimset('param1',value1)'Display, TolX, TolFun, MaxFunEvals, and MaxIter
options=optimset('tolx',1e-12,'tolfun',1e-12,'maxfunevals',1e10,'maxiter',1e10);
%options=optimset('maxfunevals',1e6,'maxiter',1e4);
%[Xm,Fval]=fminsearch('trial_inverse_fun1',X0,options)

[Xm,resnorm,residual,exitflag]=lsqcurvefit('trial_inverse_expm1',X0,F,Y,LB,UB,%
options);
resnorm
kappa=Xm(1)
sig0=Xm(2)
Gam0=Xm(3)
Gam1=Xm(4)
k
Res=[];
disc=sqrt(1+(4*Gam1*sig0/Gam0));
xdx=(-1+disc)/(2*Gam1);
m=length(F);
for j=1:m,
    freq=F(j);
    sum=0;
    for i=1:l,
        %om=sqrt((3*k*p0+2*sig*(3*k-1)/ae(i))/rhol)/ae(i);
    end
end
```

```

% om=sqrt((3*k*p0+4*Gam/ae(i)-4*sig/ae(i))/rhol)/ae(i);
om=sqrt((3*k*p0+(4*Gam0*(1-xdx)*(1+2*Gaml*xdx))/ae(i))/rhol)/ae(i);
% om=sqrt((3*k*p0+x2disc/ae(i))/rhol)/ae(i);
dl=(4*mul/(om*rhol*ae(i)*ae(i)));
ds=(4*(kappa/ae(i))/(om*rhol*ae(i)*ae(i)));
OM=(2*pi*freq)/om;
Pg0=p0;
del_rad=(3*k*Pg0/c)/(rhol*ae(i)*om);
%del_rad=4*pi*pi*freq*freq*ae(i)/(om*c);
dt=dl+ds+del_rad;
sige=(4*pi*ae(i)*ae(i)*c*dt*OM*OM/(ae(i)*om*(OM*OM*dt*dt+(1-OM*OM)^2)));
al=sige*n(i);
sum=sum+al;
end
tal=10*log10(E)*sum;
%tal=log10(E)*sum/6.3;
Res=[Res;freq tal];
end
%close
plot(F/1e6,Y,'r*')
hold
plot(Res(:,1)/1e6,Res(:,2)/100,'b')

```

```

function Fn = trial_inverse_expmmod1(X,F1)
global r ae l n Y p0 rhol c E mul F k sig kappa Gam F1
%Res=[];
m=length(F1);
sum=0;
Fn1=[ ];
disc=sqrt(1+(4*X(4)*X(2)/X(3)));
xdx=(-1+disc)/(2*X(4));
for j=1:m,
sum=0;
for i=1:l,
%om=sqrt((3*k*p0+4*X(3)/ae(i)-4*X(2)/ae(i))/rhol)/ae(i);
%om=sqrt((3*k*p0+x2disc/ae(i))/rhol)/ae(i);
om=sqrt((3*k*p0+(4*X(3)*(1-xdx)*(1+2*X(4)*xdx))/ae(i))/rhol)/ae(i);
%om=sqrt((3*k*p0+4*X(2)/ae(i)+2*sig*(3*k-1)/ae(i))/rhol)/ae(i);
%om=sqrt((3*k*p0+4*X(2)/ae(i))/rhol)/ae(i);
dl=(4*mul/(om*rhol*ae(i)*ae(i)));
ds=(4*(X(1)/ae(i)))/(om*rhol*ae(i)*ae(i));
%ds=(4*(kappa/ae(i)))/(om*rhol*ae(i)*ae(i));
OM=(2*pi*F1(j))/om;
%del_rad=4*pi*pi*F1(j)*F1(j)*ae(i)/(om*c);
Pg0=p0;
del_rad=(3*k*Pg0/c)/(rhol*ae(i)*om);

%dt is total damping:

dt=dl+ds+del_rad;
sige=(4*pi*ae(i)*ae(i)*c*dt*OM*OM/(ae(i)*om*(OM*OM*dt*dt+(1-OM*OM)^2)));
al=sige*n(i);
sum=sum+al;
end
%tal=10*log10(E)*sum;
Fn1=[Fn1;10*log10(E)*sum/100];
%tal=log10(E)*sum/6.3;
%term=(Y(j)-tal)^2;
%term=(1-tal/Y(j))^2;
%sum1=sum1+term;
end
%Fn=sum1;
Fn=Fn1';

```

```
% This code is written for plotting pulse, bubble radius Vs time and
% scattered pressure multiplied by radius Vs frequency

% Most of the variables have self-explanatory names

% frequency = n * delta_f : Its required for accuracy that fundamental frequency is
% multiple of delta_f
% fmax or sampling frequency = 1/delta_t = m * delta_f, where m = # of time steps
% we fix fmax to be sufficiently larger than fundamental frequency, say x times, which
% means m/n=x.x is also the number of points taken on 1 wave.
% So we will use tmax = n/fundamental frequency;

clear all
close all
clc
tic

global polytropic_constant surface_tension_water p0 pg0 density w viscosity
surface_dialational_viscosity pa initial_radius alpha Elasticity Eqb_radius
modified_surface_tension tbar flag tbar No_of_waves

polytropic_constant          = 1.4;
density                      = 998;
viscosity                     = 0.001*2;%thermal damping considered
p0                           = 101325;
c                            = 1484;
frequency                    = 20e6;
w                            = 2*pi*frequency;

%-----Estimated Properties-----
surface_dialational_viscosity = 1.0e-8;
surface_tension_water         = 0.02;
Elasticity                   = 4.5;
alpha                         = 10;

%-----
% init_rad                    = 2e-6;
% eta                          = sqrt(1+4*surface_tension_water*alpha/Elasticity);
% disc                         = (1-eta)/(2*alpha);
% resonance_freq               = sqrt((3*polytropic_constant*p0+(2*Elasticity/init_rad)*
% *(eta/alpha)*(1+2*alpha-eta))/density)/(2*pi*init_rad);

%-----
res                           = [];
res1                          = [];

% STRR_size % file name which brings the bubble diameter and number of
bubbles information
PB127
% PH37
% PH43
% PH44
% PH45

NR                           = n;
r0                           = r;
kk                           = 0;
```

```

jmax = length(r);
%-----%
x = 64; % x is the ratio of fmax to f or total points on
one wave
maximum_frequency = x*frequency; % fmax
delta_t = 1/maximum_frequency;
= 1000;
= frequency^-1*No_of_waves;
= No_of_waves*x;
NFFT = 2^nextpow2(time_steps);
= (1/maximum_frequency)*time_steps/2;
= 0:delta_t:Total_time;
= 3;
= -x_lim:2*x_lim/(length(tspan)-1):x_lim;
= gaussian(window_x, 1, 0, 1);
= window.* (getWin(length(tspan), 'Tukey', 'Param', 0.05));
= sin(w*tspan).*window;
= cos(w*tspan-w*tbar).*exp(-((w*tspan-w*tbar)/No_of_waves).^2/2);
= sin(w*tspan).*gausswin(length(tspan));
%-----End of Pulse Data-----%

```

```

for pa = 0.6e6:0.5e5:0.601e6
No_of_waves
polytropic_constant
sum=0;
for i=1:jmax
initial_radius = r0(i);
%Eqb_radius
%Eqb_radius = initial_radius*(fsolve(@myh, -.05)+1)^-.5;
eta = sqrt(1+4*surface_tension_water*alpha/Elasticity);
disc = (1-eta)/(2*alpha);
Eqb_radius = initial_radius*((1+disc)^-.5);
modified_surface_tension_0 = surface_tension_water + Elasticity*((initial_radius/Eqb_radius)^2-1)*exp(-alpha*((initial_radius/Eqb_radius)^2-1));
sum = sum + modified_surface_tension_0;
end
%pg0 = p0;
y0 = [initial_radius 0];
tspan = 0:delta_t:Total_time;
options = odeset('RelTol',1e-8,'AbsTol',[1e-8 1e-8]);
[t,y] = ode15s(@Viscoelastic_model_called_code_w_bubble_distribution,tspan,y0,options);
L = length(t);
ps = [];
sd = diff(y(:,2))./diff(t);
ps = density*y(2:L,1).*((2*y(2:L,2).*y(2:L,2)) + (y(2:L,2)^2));

```

```

1).*sd));
    ps_hamming = ps.*hamming(time_steps);
%   z
    z = fft(ps_hamming)/(time_steps);
%   hz
    hz = fft(ps_hamming,NFFT)/time_steps;
    = ((0:time_steps/2-1)/time_steps)*maximum_frequency;
%   hz
    hz = maximum_frequency/2*linspace(0,1,NFFT/2+1);
%   Pzz
    Pzz = z.*conj(z)/1e6;
%   ratio
    ratio = NR(j)*Pzz(1:time_steps/2);
%   ratio
    ratio = NR(i)*Pzz(1:NFFT/2);

%-----%
%   z
    z = fft(ps(3*time_steps/4+1:time_steps))/
(time_steps/4);
%   hz
    hz = ((0:time_steps/8-1)/time_steps*4)*
*maximum_frequency;
%   Pzz
    Pzz = z.*conj(z)/1e6;
%   ratio
    ratio = NR(i)*Pzz(1:time_steps/8);

sum=sum+ratio;

end

dbR = 10*log10(sum);
%res = [res;pa/1e6 hz(time_steps/4/x+1)/1e6 dbR(
(time_steps/4/x+1) hz(time_steps/8/x+1)/1e6 dbR(time_steps/8/x+1))]
% res = [res;pa/1e6 hz(time_steps/8/x+1)/1e6 max(dbR(
((time_steps/8/x+1)-5:(time_steps/8/x+1)+5)) hz(time_steps/4/x+1)/1e6 max(dbR(
((time_steps/4/x+1)-5:(time_steps/4/x+1)+5)))]

% res = [res;pa/1e6 hz(time_steps/2/x+1)/1e6 max(dbR(
((time_steps/2/x+1)-2:(time_steps/2/x+1)+2)) hz(time_steps/x+1)/1e6 dbR(time_steps/x+1)]
res = [res;pa/1e6 hz(NFFT/2/x+1)/1e6 max(dbR((NFFT/2/x+1)-
2:(NFFT/2/x+1)+2)) hz(NFFT/x+1)/1e6 dbR(NFFT/x+1)]

% figure
% plot(t,y(:,1))
%res = [res;MI hz(m/2/x+1)/1e6 dbR(m/2/x+1) hz(m/x+1)/1e6]
dbR(m/x+1)

figure
% plot(t,y(:,1))
% figure
% plot(t,y(:,2))
% figure1 = figure;
% Create axes
% axes1 = axes('Parent',figure1,...
%     'XTick',[0 (NFFT/x+1)/2 (NFFT/x+1) 3*(NFFT/x+1)/2 2*(NFFT/x+1) 5*(NFFT/x+1)/2 3*(
NFFT/x+1)],...
%     'XGrid','on');
plot(hz(1:4*NFFT/x+1)./frequency,dbR(1:4*NFFT/x+1))
xlabel('f/f0')
ylabel('Amplitude (dB)')

```

```
%modified_surface_tension;
% save('EEM_PB127_10cyc_sine_k=1.dat','res','-ASCII')

end
% m
% x
% plot(tspan-tbar,signal_1)
% hold on
% plot(tspan-tbar,signal_2,'r')
% plot(tspan,signal_3,'k')
toc
```

```

function derivative = Viscoelastic_model_called_code_w_bubble_distribution(t,y)

global polytropic_constant surface_tension_water p0 pg0 density w viscosity
surface_dialational_viscosity pa initial_radius alpha Elasticity Eqb_radius
modified_surface_tension tbar No_of_waves

c=1500;
modified_surface_tension = surface_tension_water + Elasticity*((y(1)/Eqb_radius)^2-1)*
exp(-alpha*((y(1)/Eqb_radius)^2-1));
%
% if (modified_surface_tension > 0)
% modified_surface_tension = surface_tension_water + Elasticity*((y(1)-
/Eqb_radius)^2-1)*exp(-alpha*((y(1)/Eqb_radius)^2-1));
% else
% modified_surface_tension = 0;
% end
%h=1/64;
%term1 = pg0*((initial_radius/y(1))^(3*polytropic_constant));
term1 = pg0*(1-3*polytropic_constant*y(2)/c)*((initial_radius/y(1))^
(3*polytropic_constant));
term2 = (4*viscosity*y(2))/y(1);
term3 = 4*surface_dialational_viscosity*y(2)/((y(1)^2));
term4 = 2*modified_surface_tension/y(1);
term5 = p0;
term6 = pa*sin(w*t);
%term6 = pa*cos(w*t-w*tbar)*exp(-h/4*h*(w*t-w*tbar)*(w*t-w*tbar));
% term6= pa*cos(w*t-w*tbar)*exp((-((w*t-w*tbar)/No_of_waves)^2)/2);
term7 = 1.5*y(2)*y(2)*density;

derivative(1,:) = y(2);
derivative(2,:) = ((term1+term6)-(term2+term3+term4+term5+term7))/(density*y(1));

```

Appendix E

REPRINT PERMISSIONS

E.1 Reprint Permission for Figure 2.1 in Chapter 2

The relevant permission letter is included in the following pages.

**BMJ PUBLISHING GROUP LTD. LICENSE
TERMS AND CONDITIONS**

Aug 23, 2013

This is a License Agreement between Shirshendu Paul ("You") and BMJ Publishing Group Ltd. ("BMJ Publishing Group Ltd.") provided by Copyright Clearance Center ("CCC"). The license consists of your order details, the terms and conditions provided by BMJ Publishing Group Ltd., and the payment terms and conditions.

All payments must be made in full to CCC. For payment instructions, please see information listed at the bottom of this form.

License Number	3214930688631
License date	Aug 23, 2013
Licensed content publisher	BMJ Publishing Group Ltd.
Licensed content publication	British Medical Journal
Licensed content title	Microbubble contrast agents: a new era in ultrasound
Licensed content author	Martin J K Blomley, Jennifer C Cooke, Evan C Unger, Mark J Monaghan, David O Cosgrove
Licensed content date	May 19, 2001
Volume number	322
Type of Use	Thesis/Dissertation
Requestor type	Individual
Format	Print and electronic
Portion	Figure/table/extract
Number of figure/table /extracts	1
Will you be translating?	No
Circulation/distribution	50
Title of your thesis / dissertation	Acoustic Characterization of Ultrasound Contrast Microbubbles and Echogenic Liposomes: Applications to Imaging and Drug-Delivery
Expected completion date	Sep 2013
Estimated size(pages)	300
BMJ VAT number	674738491
Billing Type	Invoice
Billing address	130 Acedemy Street 126 Spencer Lab Newark, DE 19716 United States
Permissions Cost	0.00 USD
VAT (0.0%)	0.00 USD
Total	0.00 USD
Terms and Conditions	

BMJ Group Terms and Conditions for Permissions

When you submit your order you are subject to the terms and conditions set out below. You will also have agreed to the Copyright Clearance Center's ("CCC") terms and conditions regarding billing and payment <https://s100.copyright.com/App/PaymentTermsAndConditions.jsp>. CCC are acting as the BMJ Publishing Group Limited's ("BMJ Group's") agent.

Subject to the terms set out herein, the BMJ Group hereby grants to you (the Licensee) a non-exclusive, non-transferable licence to re-use material as detailed in your request for this/those purpose(s) only and in accordance with the following conditions:

1) Scope of Licence: Use of the Licensed Material(s) is restricted to the ways specified by you during the order process and any additional use(s) outside of those specified in that request, require a further grant of permission.

2) Acknowledgement: In all cases, due acknowledgement to the original publication with permission from the BMJ Group should be stated adjacent to the reproduced Licensed Material. The format of such acknowledgement should read as follows:

"Reproduced from [publication title, author(s), volume number, page numbers, copyright notice year] with permission from BMJ Publishing Group Ltd."

3) Third Party Material: BMJ Group acknowledges to the best of its knowledge, it has the rights to licence your reuse of the Licensed Material, subject always to the caveat that images/diagrams, tables and other illustrative material included within, which have a separate copyright notice, are presumed as excluded from the licence. Therefore, you should ensure that the Licensed Material you are requesting is original to BMJ Group and does not carry the copyright of another entity (as credited in the published version). If the credit line on any part of the material you have requested in any way indicates that it was reprinted or adapted by BMJ Group with permission from another source, then you should seek permission from that source directly to re-use the Licensed Material, as this is outside of the licence granted herein.

4) Altering/Modifying Material: The text of any material for which a licence is granted may not be altered in any way without the prior express permission of the BMJ Group. Subject to Clause 3 above however, single figure adaptations do not require BMJ Group's approval; however, the adaptation should be credited as follows:

"Adapted by permission from BMJ Publishing Group Limited. [publication title, author, volume number, page numbers, copyright notice year]

5) Reservation of Rights: The BMJ Group reserves all rights not specifically granted in the combination of (i) the licence details provided by you and accepted in the course of this licensing transaction, (ii) these terms and conditions and (iii) CCC's Billing and Payment Terms and Conditions.

6) Timing of Use: First use of the Licensed Material must take place within 12 months of the grant of permission.

7. Creation of Contract and Termination: Once you have submitted an order via Rightslink and this is received by CCC, and subject to you completing accurate details of your proposed use, this is when a binding contract is in effect and our acceptance occurs. As you are ordering rights from a periodical, to the fullest extent permitted by law, you will have no right to cancel the contract from this point other than for BMJ Group's material breach or fraudulent misrepresentation or as otherwise permitted under a statutory right. Payment must be made in accordance with CCC's Billing and Payment Terms and conditions. In the event that you breach any material condition of these terms and condition or any of CCC's Billing and Payment Terms and Conditions, the license is automatically terminated upon written notice from the BMJ Group or CCC or as otherwise provided for in CCC's Billing and Payment Terms and Conditions, where these apply.. Continued use of materials where a licence has been terminated, as well as any use of the Licensed Materials beyond the scope of an unrevoked licence, may constitute intellectual property rights infringement and BMJ Group reserves

the right to take any and all actions to protect its intellectual property rights in the Licensed Materials.

8. Warranties: BMJ Group makes no express or implied representations or warranties with respect to the Licensed Material and to the fullest extent permitted by law this is provided on an "as is" basis. For the avoidance of doubt BMJ Group does not warrant that the Licensed Material is accurate or fit for any particular purpose.

9. Limitation of Liability: To the fullest extent permitted by law, the BMJ Group disclaims all liability for any indirect, consequential or incidental damages (including without limitation, damages for loss of profits, information or interruption) arising out of the use or inability to use the Licensed Material or the inability to obtain additional rights to use the Licensed Material. To the fullest extent permitted by law, the maximum aggregate liability of the BMJ Group for any claims, costs, proceedings and demands for direct losses caused by BMJ Group's breaches of its obligations herein shall be limited to twice the amount paid by you to CCC for the licence granted herein.

10. Indemnity: You hereby indemnify and hold harmless the BMJ Group and their respective officers, directors, employees and agents, from and against any and all claims, costs, proceedings or demands arising out of your unauthorised use of the Licensed Material.

11. No Transfer of License: This licence is personal to you, and may not be assigned or transferred by you without prior written consent from the BMJ Group or its authorised agent(s). BMJ Group may assign or transfer any of its rights and obligations under this Agreement, upon written notice to you.

12. No Amendment Except in Writing: This licence may not be amended except in a writing signed by both parties (or, in the case of BMJ Group, by CCC on the BMJ Group's behalf).

13. Objection to Contrary Terms: BMJ Group hereby objects to any terms contained in any purchase order, acknowledgment, check endorsement or other writing prepared by you, which terms are inconsistent with these terms and conditions or CCC's Billing and Payment Terms and Conditions. These terms and conditions, together with CCC's Billing and Payment Terms and Conditions (which to the extent they are consistent are incorporated herein), comprise the entire agreement between you and BMJ Group (and CCC) and the Licensee concerning this licensing transaction. In the event of any conflict between your obligations established by these terms and conditions and those established by CCC's Billing and Payment Terms and Conditions, these terms and conditions shall control.

14. Revocation: BMJ Group or CCC may, within 30 days of issuance of this licence, deny the permissions described in this licence at their sole discretion, for any reason or no reason, with a full refund payable to you should you have not been able to exercise your rights in full. Notice of such denial will be made using the contact information provided by you. Failure to receive such notice from BMJ Group or CCC will not, to the fullest extent permitted by law, alter or invalidate the denial. For the fullest extent permitted by law in no event will BMJ Group or CCC be responsible or liable for any costs, expenses or damage incurred by you as a result of a denial of your permission request, other than a refund of the amount(s) paid by you to BMJ Group and/or CCC for denied permissions.

15. Restrictions to the license:

15.1 Promotion: BMJ Group will not give permission to reproduce in full or in part any Licensed Material for use in the promotion of the following:

- a) non-medical products that are harmful or potentially harmful to health: alcohol, baby milks and/or sunbeds
- b) medical products that do not have a product license granted by the Medicines and Healthcare products Regulatory Agency (MHRA) or its international equivalents. Marketing of the product may start only after data sheets have been released to members of the medical profession and must conform to the marketing authorization contained in the product license.

16. Translation: This permission is granted for non-exclusive world English language

rights only unless explicitly stated in your licence. If translation rights are granted, a professional translator should be employed and the content should be reproduced word for word preserving the integrity of the content.

17. **General:** Neither party shall be liable for failure, default or delay in performing its obligations under this Licence, caused by a Force Majeure event which shall include any act of God, war, or threatened war, act or threatened act of terrorism, riot, strike, lockout, individual action, fire, flood, drought, tempest or other event beyond the reasonable control of either party.

17.1 In the event that any provision of this Agreement is held to be invalid, the remainder of the provisions shall continue in full force and effect.

17.2 There shall be no right whatsoever for any third party to enforce the terms and conditions of this Agreement. The Parties hereby expressly wish to exclude the operation of the Contracts (Rights of Third Parties) Act 1999 and any other legislation which has this effect and is binding on this agreement.

17.3 To the fullest extent permitted by law, this Licence will be governed by the laws of England and shall be governed and construed in accordance with the laws of England. Any action arising out of or relating to this agreement shall be brought in courts situated in England save where it is necessary for BMJ Group for enforcement to bring proceedings to bring an action in an alternative jurisdiction.

If you would like to pay for this license now, please remit this license along with your payment made payable to "COPYRIGHT CLEARANCE CENTER" otherwise you will be invoiced within 48 hours of the license date. Payment should be in the form of a check or money order referencing your account number and this invoice number

RLNK501097100.

Once you receive your invoice for this order, you may pay your invoice by credit card. Please follow instructions provided at that time.

Make Payment To:
Copyright Clearance Center
Dept 001
P.O. Box 843006
Boston, MA 02284-3006

For suggestions or comments regarding this order, contact RightsLink Customer Support: customercare@copyright.com or +1-877-622-5543 (toll free in the US) or +1-978-646-2777.

Gratis licenses (referencing \$0 in the Total field) are free. Please retain this printable license for your reference. No payment is required.

E.2 Reprint Permissions for Chapter 3

The relevant permission letters are included in the following pages.

**ELSEVIER LICENSE
TERMS AND CONDITIONS**

Aug 26, 2013

This is a License Agreement between Shirshendu Paul ("You") and Elsevier ("Elsevier") provided by Copyright Clearance Center ("CCC"). The license consists of your order details, the terms and conditions provided by Elsevier, and the payment terms and conditions.

All payments must be made in full to CCC. For payment instructions, please see information listed at the bottom of this form.

Supplier	Elsevier Limited The Boulevard, Langford Lane Kidlington, Oxford, OX5 1GB, UK
Registered Company Number	1982084
Customer name	Shirshendu Paul
Customer address	130 Acedemy Street Newark, DE 19716
License number	3216560596063
License date	Aug 26, 2013
Licensed content publisher	Elsevier
Licensed content publication	Ultrasound in Medicine & Biology
Licensed content title	Determination of the Interfacial Rheological Properties of a Poly(DL-lactic acid)-Encapsulated Contrast Agent Using <i>In Vitro</i> Attenuation and Scattering
Licensed content author	Shirshendu Paul, Daniel Russakow, Tyler Rodgers, Kausik Sarkar, Michael Cochran, Margaret A. Wheatley
Licensed content date	July 2013
Licensed content volume number	39
Licensed content issue number	7
Number of pages	15
Start Page	1277
End Page	1291
Type of Use	reuse in a thesis/dissertation

Intended publisher of new work	other
Portion	excerpt
Number of excerpts	10
Format	both print and electronic
Are you the author of this Elsevier article?	Yes
Will you be translating?	No
Order reference number	
Title of your thesis/dissertation	Acoustic Characterization of Ultrasound Contrast Microbubbles and Echogenic Liposomes: Applications to Imaging and Drug-Delivery
Expected completion date	Sep 2013
Estimated size (number of pages)	300
Elsevier VAT number	GB 494 6272 12
Permissions price	0.00 USD
VAT/Local Sales Tax	0.0 USD / 0.0 GBP
Total	0.00 USD
Terms and Conditions	

INTRODUCTION

1. The publisher for this copyrighted material is Elsevier. By clicking "accept" in connection with completing this licensing transaction, you agree that the following terms and conditions apply to this transaction (along with the Billing and Payment terms and conditions established by Copyright Clearance Center, Inc. ("CCC"), at the time that you opened your Rightslink account and that are available at any time at <http://myaccount.copyright.com>).

GENERAL TERMS

2. Elsevier hereby grants you permission to reproduce the aforementioned material subject to the terms and conditions indicated.
3. Acknowledgement: If any part of the material to be used (for example, figures) has appeared in our publication with credit or acknowledgement to another source, permission must also be sought from that source. If such permission is not obtained then that material may not be included in your

publication/copies. Suitable acknowledgement to the source must be made, either as a footnote or in a reference list at the end of your publication, as follows:

"Reprinted from Publication title, Vol /edition number, Author(s), Title of article / title of chapter, Pages No., Copyright (Year), with permission from Elsevier [OR APPLICABLE SOCIETY COPYRIGHT OWNER]." Also Lancet special credit - "Reprinted from The Lancet, Vol. number, Author(s), Title of article, Pages No., Copyright (Year), with permission from Elsevier."

4. Reproduction of this material is confined to the purpose and/or media for which permission is hereby given.

5. Altering/Modifying Material: Not Permitted. However figures and illustrations may be altered/adapted minimally to serve your work. Any other abbreviations, additions, deletions and/or any other alterations shall be made only with prior written authorization of Elsevier Ltd. (Please contact Elsevier at permissions@elsevier.com)

6. If the permission fee for the requested use of our material is waived in this instance, please be advised that your future requests for Elsevier materials may attract a fee.

7. Reservation of Rights: Publisher reserves all rights not specifically granted in the combination of (i) the license details provided by you and accepted in the course of this licensing transaction, (ii) these terms and conditions and (iii) CCC's Billing and Payment terms and conditions.

8. License Contingent Upon Payment: While you may exercise the rights licensed immediately upon issuance of the license at the end of the licensing process for the transaction, provided that you have disclosed complete and accurate details of your proposed use, no license is finally effective unless and until full payment is received from you (either by publisher or by CCC) as provided in CCC's Billing and Payment terms and conditions. If full payment is not received on a timely basis, then any license preliminarily granted shall be deemed automatically revoked and shall be void as if never granted. Further, in the event that you breach any of these terms and conditions or any of CCC's Billing and Payment terms and conditions, the license is automatically revoked and shall be void as if never granted. Use of materials as described in a revoked license, as well

as any use of the materials beyond the scope of an unrevoked license, may constitute copyright infringement and publisher reserves the right to take any and all action to protect its copyright in the materials.

9. Warranties: Publisher makes no representations or warranties with respect to the licensed material.

10. Indemnity: You hereby indemnify and agree to hold harmless publisher and CCC, and their respective officers, directors, employees and agents, from and against any and all claims arising out of your use of the licensed material other than as specifically authorized pursuant to this license.

11. No Transfer of License: This license is personal to you and may not be sublicensed, assigned, or transferred by you to any other person without publisher's written permission.

12. No Amendment Except in Writing: This license may not be amended except in a writing signed by both parties (or, in the case of publisher, by CCC on publisher's behalf).

13. Objection to Contrary Terms: Publisher hereby objects to any terms contained in any purchase order, acknowledgment, check endorsement or other writing prepared by you, which terms are inconsistent with these terms and conditions or CCC's Billing and Payment terms and conditions. These terms and conditions, together with CCC's Billing and Payment terms and conditions (which are incorporated herein), comprise the entire agreement between you and publisher (and CCC) concerning this licensing transaction. In the event of any conflict between your obligations established by these terms and conditions and those established by CCC's Billing and Payment terms and conditions, these terms and conditions shall control.

14. Revocation: Elsevier or Copyright Clearance Center may deny the permissions described in this License at their sole discretion, for any reason or no reason, with a full refund payable to you. Notice of such denial will be made using the contact information provided by you. Failure to receive such notice will not alter or invalidate the denial. In no event will Elsevier or Copyright Clearance Center be responsible or liable for any costs, expenses or damage incurred by you as a result of a denial of your permission request, other than a refund of the amount(s) paid by you to

Elsevier and/or Copyright Clearance Center for denied permissions.

LIMITED LICENSE

The following terms and conditions apply only to specific license types:

15. Translation: This permission is granted for non-exclusive world **English** rights only unless your license was granted for translation rights. If you licensed translation rights you may only translate this content into the languages you requested. A professional translator must perform all translations and reproduce the content word for word preserving the integrity of the article. If this license is to re-use 1 or 2 figures then permission is granted for non-exclusive world rights in all languages.

16. Website: The following terms and conditions apply to electronic reserve and author websites:

Electronic reserve: If licensed material is to be posted to website, the web site is to be password-protected and made available only to bona fide students registered on a relevant course if:

This license was made in connection with a course,

This permission is granted for 1 year only. You may obtain a license for future website posting,

All content posted to the web site must maintain the copyright information line on the bottom of each image,

A hyper-text must be included to the Homepage of the journal from which you are licensing at <http://www.sciencedirect.com/science/journal/xxxx> or the Elsevier homepage for books at <http://www.elsevier.com> , and

Central Storage: This license does not include permission for a scanned version of the material to be stored in a central repository such as that provided by Heron/XanEdu.

17. Author website for journals with the following additional clauses:

All content posted to the web site must maintain the copyright information line on the bottom of each image, and the permission granted is limited to the personal version of your paper. You are not allowed to download and post the published electronic version of your article (whether PDF or HTML, proof or final version), nor may you scan the printed edition to create an electronic version. A hyper-text must be included to the Homepage of the journal from which you are licensing at

<http://www.sciencedirect.com/science/journal/xxxxx>. As part of our normal production process, you will receive an e-mail notice when your article appears on Elsevier's online service ScienceDirect (www.sciencedirect.com). That e-mail will include the article's Digital Object Identifier (DOI). This number provides the electronic link to the published article and should be included in the posting of your personal version. We ask that you wait until you receive this e-mail and have the DOI to do any posting.

Central Storage: This license does not include permission for a scanned version of the material to be stored in a central repository such as that provided by Heron/XanEdu.

18. **Author website** for books with the following additional clauses:
Authors are permitted to place a brief summary of their work online only.
A hyper-text must be included to the Elsevier homepage at
<http://www.elsevier.com>. All content posted to the web site must maintain the copyright information line on the bottom of each image. You are not allowed to download and post the published electronic version of your chapter, nor may you scan the printed edition to create an electronic version.

Central Storage: This license does not include permission for a scanned version of the material to be stored in a central repository such as that provided by Heron/XanEdu.

19. **Website** (regular and for author): A hyper-text must be included to the Homepage of the journal from which you are licensing at
<http://www.sciencedirect.com/science/journal/xxxxx>. or for books to the Elsevier homepage at <http://www.elsevier.com>

20. **Thesis/Dissertation:** If your license is for use in a thesis/dissertation your thesis may be submitted to your institution in either print or electronic form. Should your thesis be published commercially, please reapply for permission. These requirements include permission for the Library and Archives of Canada to supply single copies, on demand, of the complete thesis and include permission for UMI to supply single copies, on demand, of the complete thesis. Should your thesis be published commercially, please reapply for permission.

21. Other Conditions:

v1.6

If you would like to pay for this license now, please remit this license along with your payment made payable to "COPYRIGHT CLEARANCE CENTER" otherwise you will be invoiced within 48 hours of the license date. Payment should be in the form of a check or money order referencing your account number and this invoice number RLNK501098237.

Once you receive your invoice for this order, you may pay your invoice by credit card. Please follow instructions provided at that time.

Make Payment To:
Copyright Clearance Center
Dept 001
P.O. Box 843006
Boston, MA 02284-3006

For suggestions or comments regarding this order, contact RightsLink Customer Support: customercare@copyright.com or +1-877-622-5543 (toll free in the US) or +1-978-646-2777.

Gratis licenses (referencing \$0 in the Total field) are free. Please retain this printable license for your reference. No payment is required.

ELSEVIER LICENSE TERMS AND CONDITIONS

Aug 26, 2013

This is a License Agreement between Shirshendu Paul ("You") and Elsevier ("Elsevier") provided by Copyright Clearance Center ("CCC"). The license consists of your order details, the terms and conditions provided by Elsevier, and the payment terms and conditions.

All payments must be made in full to CCC. For payment instructions, please see information listed at the bottom of this form.

Supplier	Elsevier Limited The Boulevard, Langford Lane Kidlington, Oxford, OX5 1GB, UK
Registered Company Number	1982084
Customer name	Shirshendu Paul
Customer address	130 Acedemy Street Newark, DE 19716
License number	3216560445837
License date	Aug 26, 2013
Licensed content publisher	Elsevier
Licensed content publication	Ultrasonics
Licensed content title	<i>In vitro</i> measurement of attenuation and nonlinear scattering from echogenic liposomes
Licensed content author	Shirshendu Paul, Daniel Russakow, Rahul Nahire, Tapas Nandy, Avinash H. Ambre, Kalpana Katti, Sanku Mallik, Kausik Sarkar
Licensed content date	September 2012
Licensed content volume number	52
Licensed content issue number	7
Number of pages	8
Start Page	962
End Page	969
Type of Use	reuse in a thesis/dissertation
Intended publisher of new work	other
Portion	excerpt
Number of excerpts	10
Format	both print and electronic
Are you the author of this Elsevier article?	Yes
Will you be translating?	No
Order reference number	None

Title of your thesis/dissertation	Acoustic Characterization of Ultrasound Contrast Microbubbles and Echogenic Liposomes: Applications to Imaging and Drug-Delivery
Expected completion date	Sep 2013
Estimated size (number of pages)	300
Elsevier VAT number	GB 494 6272 12
Permissions price	0.00 USD
VAT/Local Sales Tax	0.0 USD / 0.0 GBP
Total	0.00 USD

Terms and Conditions

INTRODUCTION

1. The publisher for this copyrighted material is Elsevier. By clicking "accept" in connection with completing this licensing transaction, you agree that the following terms and conditions apply to this transaction (along with the Billing and Payment terms and conditions established by Copyright Clearance Center, Inc. ("CCC"), at the time that you opened your Rightslink account and that are available at any time at <http://myaccount.copyright.com>).

GENERAL TERMS

2. Elsevier hereby grants you permission to reproduce the aforementioned material subject to the terms and conditions indicated.

3. Acknowledgement: If any part of the material to be used (for example, figures) has appeared in our publication with credit or acknowledgement to another source, permission must also be sought from that source. If such permission is not obtained then that material may not be included in your publication/copies. Suitable acknowledgement to the source must be made, either as a footnote or in a reference list at the end of your publication, as follows:

"Reprinted from Publication title, Vol /edition number, Author(s), Title of article / title of chapter, Pages No., Copyright (Year), with permission from Elsevier [OR APPLICABLE SOCIETY COPYRIGHT OWNER]." Also Lancet special credit - "Reprinted from The Lancet, Vol. number, Author(s), Title of article, Pages No., Copyright (Year), with permission from Elsevier."

4. Reproduction of this material is confined to the purpose and/or media for which permission is hereby given.

5. Altering/Modifying Material: Not Permitted. However figures and illustrations may be altered/adapted minimally to serve your work. Any other abbreviations, additions, deletions and/or any other alterations shall be made only with prior written authorization of Elsevier Ltd. (Please contact Elsevier at permissions@elsevier.com)

6. If the permission fee for the requested use of our material is waived in this instance, please be advised that your future requests for Elsevier materials may attract a fee.

7. Reservation of Rights: Publisher reserves all rights not specifically granted in the combination of (i) the license details provided by you and accepted in the course of this licensing transaction, (ii) these terms and conditions and (iii) CCC's Billing and Payment terms and conditions.

8. License Contingent Upon Payment: While you may exercise the rights licensed immediately upon issuance of the license at the end of the licensing process for the transaction, provided that you have disclosed complete and accurate details of your proposed use, no license is finally effective unless and until full payment is received from you (either by publisher or by CCC) as provided in CCC's Billing and Payment terms and conditions. If full payment is not received on a timely basis, then any license preliminarily granted shall be deemed automatically revoked and shall be void as if never granted. Further, in the event that you breach any of these terms and conditions or any of CCC's Billing and Payment terms and conditions, the license is automatically revoked and shall be void as if never granted. Use of materials as described in a revoked license, as well as any use of the materials beyond the scope of an unrevoked license, may constitute copyright infringement and publisher reserves the right to take any and all action to protect its copyright in the materials.

9. Warranties: Publisher makes no representations or warranties with respect to the licensed material.

10. Indemnity: You hereby indemnify and agree to hold harmless publisher and CCC, and their respective officers, directors, employees and agents, from and against any and all claims arising out of your use of the licensed material other than as specifically authorized pursuant to this license.

11. No Transfer of License: This license is personal to you and may not be sublicensed, assigned, or transferred by you to any other person without publisher's written permission.

12. No Amendment Except in Writing: This license may not be amended except in a writing signed by both parties (or, in

the case of publisher, by CCC on publisher's behalf).

13. Objection to Contrary Terms: Publisher hereby objects to any terms contained in any purchase order, acknowledgment, check endorsement or other writing prepared by you, which terms are inconsistent with these terms and conditions or CCC's Billing and Payment terms and conditions. These terms and conditions, together with CCC's Billing and Payment terms and conditions (which are incorporated herein), comprise the entire agreement between you and publisher (and CCC) concerning this licensing transaction. In the event of any conflict between your obligations established by these terms and conditions and those established by CCC's Billing and Payment terms and conditions, these terms and conditions shall control.

14. Revocation: Elsevier or Copyright Clearance Center may deny the permissions described in this License at their sole discretion, for any reason or no reason, with a full refund payable to you. Notice of such denial will be made using the contact information provided by you. Failure to receive such notice will not alter or invalidate the denial. In no event will Elsevier or Copyright Clearance Center be responsible or liable for any costs, expenses or damage incurred by you as a result of a denial of your permission request, other than a refund of the amount(s) paid by you to Elsevier and/or Copyright Clearance Center for denied permissions.

LIMITED LICENSE

The following terms and conditions apply only to specific license types:

15. **Translation:** This permission is granted for non-exclusive world **English** rights only unless your license was granted for translation rights. If you licensed translation rights you may only translate this content into the languages you requested. A professional translator must perform all translations and reproduce the content word for word preserving the integrity of the article. If this license is to re-use 1 or 2 figures then permission is granted for non-exclusive world rights in all languages.

16. **Website:** The following terms and conditions apply to electronic reserve and author websites:

Electronic reserve: If licensed material is to be posted to website, the web site is to be password-protected and made available only to bona fide students registered on a relevant course if:

This license was made in connection with a course,

This permission is granted for 1 year only. You may obtain a license for future website posting,

All content posted to the web site must maintain the copyright information line on the bottom of each image,

A hyper-text must be included to the Homepage of the journal from which you are licensing at

<http://www.sciencedirect.com/science/journal/xxxxx> or the Elsevier homepage for books at <http://www.elsevier.com> , and

Central Storage: This license does not include permission for a scanned version of the material to be stored in a central repository such as that provided by Heron/XanEdu.

17. **Author website** for journals with the following additional clauses:

All content posted to the web site must maintain the copyright information line on the bottom of each image, and the permission granted is limited to the personal version of your paper. You are not allowed to download and post the published electronic version of your article (whether PDF or HTML, proof or final version), nor may you scan the printed edition to create an electronic version. A hyper-text must be included to the Homepage of the journal from which you are licensing at <http://www.sciencedirect.com/science/journal/xxxxx> . As part of our normal production process, you will receive an e-mail notice when your article appears on Elsevier's online service ScienceDirect (www.sciencedirect.com). That e-mail will include the article's Digital Object Identifier (DOI). This number provides the electronic link to the published article and should be included in the posting of your personal version. We ask that you wait until you receive this e-mail and have the DOI to do any posting.

Central Storage: This license does not include permission for a scanned version of the material to be stored in a central repository such as that provided by Heron/XanEdu.

18. **Author website** for books with the following additional clauses:

Authors are permitted to place a brief summary of their work online only.

A hyper-text must be included to the Elsevier homepage at <http://www.elsevier.com> . All content posted to the web site must maintain the copyright information line on the bottom of each image. You are not allowed to download and post the published electronic version of your chapter, nor may you scan the printed edition to create an electronic version.

Central Storage: This license does not include permission for a scanned version of the material to be stored in a central repository such as that provided by Heron/XanEdu.

19. **Website** (regular and for author): A hyper-text must be included to the Homepage of the journal from which you are licensing at <http://www.sciencedirect.com/science/journal/xxxxx> . or for books to the Elsevier homepage at <http://www.elsevier.com>

20. **Thesis/Dissertation:** If your license is for use in a thesis/dissertation your thesis may be submitted to your institution

in either print or electronic form. Should your thesis be published commercially, please reapply for permission. These requirements include permission for the Library and Archives of Canada to supply single copies, on demand, of the complete thesis and include permission for UMI to supply single copies, on demand, of the complete thesis. Should your thesis be published commercially, please reapply for permission.

21. Other Conditions:

v1.6

If you would like to pay for this license now, please remit this license along with your payment made payable to "COPYRIGHT CLEARANCE CENTER" otherwise you will be invoiced within 48 hours of the license date. Payment should be in the form of a check or money order referencing your account number and this invoice number RLINK501098235.

Once you receive your invoice for this order, you may pay your invoice by credit card. Please follow instructions provided at that time.

Make Payment To:
Copyright Clearance Center
Dept 001
P.O. Box 843006
Boston, MA 02284-3006

For suggestions or comments regarding this order, contact RightsLink Customer Support:
customercare@copyright.com or +1-877-622-5543 (toll free in the US) or +1-978-646-2777.

Gratis licenses (referencing \$0 in the Total field) are free. Please retain this printable license for your reference. No payment is required.

**RightsLink®****Home** **Account Info** **Help****ACS Publications**
High quality. High impact.**Title:**

Ultrasound Enhanced Matrix
Metalloproteinase-9 Triggered
Release of Contents from
Echogenic Liposomes

Logged in as:
Shirshendu Paul
Account #:
3000652960

Author:

Rahul Nahire, Shirshendu Paul,
Michael D. Scott, Raushan K.
Singh, Wallace W. Muhonen,
John Shabb, Kara N. Gange, D.
K. Srivastava, Kausik Sarkar,
and Sanku Mallik

LOGOUT**Publication:** Molecular Pharmaceutics**Publisher:** American Chemical Society**Date:** Sep 1, 2012

Copyright © 2012, American Chemical Society

PERMISSION/LICENSE IS GRANTED FOR YOUR ORDER AT NO CHARGE

This type of permission/license, instead of the standard Terms & Conditions, is sent to you because no fee is being charged for your order. Please note the following:

- Permission is granted for your request in both print and electronic formats, and translations.
- If figures and/or tables were requested, they may be adapted or used in part.
- Please print this page for your records and send a copy of it to your publisher/graduate school.
- Appropriate credit for the requested material should be given as follows: "Reprinted (adapted) with permission from (COMPLETE REFERENCE CITATION). Copyright (YEAR) American Chemical Society." Insert appropriate information in place of the capitalized words.
- One-time permission is granted only for the use specified in your request. No additional uses are granted (such as derivative works or other editions). For any other uses, please submit a new request.

BACK**CLOSE WINDOW**

Copyright © 2013 [Copyright Clearance Center, Inc.](#). All Rights Reserved. [Privacy statement](#).
Comments? We would like to hear from you. E-mail us at customercare@copyright.com

**RightsLink®****Home** **Account Info** **Help****ACS Publications**
High quality. High impact.**RightsLink®****Title:**Polymer-Coated Echogenic Lipid
Nanoparticles with Dual Release
TriggersLogged in as:
Shirshendu Paul
Account #:
3000652960**Author:**Rahul Nahire, Manas K. Haldar,
Shirshendu Paul, Anaas
Mergoum, Avinash H. Ambre,
Kalpana S. Katti, Kara N. Gange,
D. K. Srivastava, Kausik Sarkar,
and Sanku Mallik**LOGOUT****Publication:** Biomacromolecules**Publisher:** American Chemical Society**Date:** Mar 1, 2013

Copyright © 2013, American Chemical Society

PERMISSION/LICENSE IS GRANTED FOR YOUR ORDER AT NO CHARGE

This type of permission/license, instead of the standard Terms & Conditions, is sent to you because no fee is being charged for your order. Please note the following:

- Permission is granted for your request in both print and electronic formats, and translations.
- If figures and/or tables were requested, they may be adapted or used in part.
- Please print this page for your records and send a copy of it to your publisher/graduate school.
- Appropriate credit for the requested material should be given as follows: "Reprinted (adapted) with permission from (COMPLETE REFERENCE CITATION). Copyright (YEAR) American Chemical Society." Insert appropriate information in place of the capitalized words.
- One-time permission is granted only for the use specified in your request. No additional uses are granted (such as derivative works or other editions). For any other uses, please submit a new request.

BACK**CLOSE WINDOW**

Copyright © 2013 Copyright Clearance Center, Inc. All Rights Reserved. [Privacy statement](#).
Comments? We would like to hear from you. E-mail us at customercare@copyright.com

E.3 Reprint Permissions for Chapter 4

The relevant permission letters are included in the following pages.

**AIP PUBLISHING LLC LICENSE
TERMS AND CONDITIONS**

Aug 22, 2013

All payments must be made in full to CCC. For payment instructions, please see information listed at the bottom of this form.

License Number	3214480665567
Order Date	Aug 22, 2013
Publisher	AIP Publishing LLC
Publication	The Journal of the Acoustical Society of America
Article Title	Material characterization of the encapsulation of an ultrasound contrast microbubble and its subharmonic response: Strain-softening interfacial elasticity model
Author	Shirshendu Paul, Amit Katiyar, Kausik Sarkar, Dhiman Chatterjee, et al.
Online Publication Date	Jun 1, 2010
Volume number	127
Issue number	6
Type of Use	Thesis/Dissertation
Requestor type	Author (original article)
Format	Print and electronic
Portion	Figure/Table
Number of figures/tables	21
Title of your thesis / dissertation	Acoustic Characterization of Ultrasound Contrast Microbubbles and Echogenic Liposomes: Applications to Imaging and Drug-Delivery
Expected completion date	Sep 2013
Estimated size (number of pages)	300
Total	0.00 USD

Terms and Conditions

Acoustic Society of America -- Terms and Conditions: Permissions Uses

Acoustic Society of America ("ASA") hereby grants to you the non-exclusive right and license to use and/or distribute the Material according to the use specified in your order, on a one-time basis, for the specified term, with a maximum distribution equal to the number that you have ordered. Any links or other content accompanying the Material are not the subject of this license.

1. You agree to include the following copyright and permission notice with the reproduction of the Material: "Reprinted with permission from [FULL CITATION]. Copyright [PUBLICATION YEAR], Acoustic Society of America." For an article, the copyright and permission notice must be printed on the first page of the article or book chapter. For photographs, covers, or tables, the copyright and permission notice may appear with the Material, in a footnote, or in the reference list.
2. If you have licensed reuse of a figure, photograph, cover, or table, it is your responsibility to ensure that the material is original to ASA and does not contain the copyright of another entity, and that the copyright notice of the figure, photograph, cover, or table does not indicate that it was reprinted by ASA, with permission, from another source. Under no circumstances does ASA, purport or intend to grant

- permission to reuse material to which it does not hold copyright.
3. You may not alter or modify the Material in any manner. You may translate the Material into another language only if you have licensed translation rights. You may not use the Material for promotional purposes. ASA reserves all rights not specifically granted herein.
 4. The foregoing license shall not take effect unless and until ASA or its agent, Copyright Clearance Center, receives the Payment in accordance with Copyright Clearance Center Billing and Payment Terms and Conditions, which are incorporated herein by reference.
 5. ASA or the Copyright Clearance Center may, within two business days of granting this license, revoke the license for any reason whatsoever, with a full refund payable to you. Should you violate the terms of this license at any time, ASA, Acoustic Society of America, or Copyright Clearance Center may revoke the license with no refund to you. Notice of such revocation will be made using the contact information provided by you. Failure to receive such notice will not nullify the revocation.
 6. ASA makes no representations or warranties with respect to the Material. You agree to indemnify and hold harmless ASA, Acoustic Society of America, and their officers, directors, employees or agents from and against any and all claims arising out of your use of the Material other than as specifically authorized herein.
 7. The permission granted herein is personal to you and is not transferable or assignable without the prior written permission of ASA. This license may not be amended except in a writing signed by the party to be charged.
 8. If purchase orders, acknowledgments or check endorsements are issued on any forms containing terms and conditions which are inconsistent with these provisions, such inconsistent terms and conditions shall be of no force and effect. This document, including the CCC Billing and Payment Terms and Conditions, shall be the entire agreement between the parties relating to the subject matter hereof.

This Agreement shall be governed by and construed in accordance with the laws of the State of New York. Both parties hereby submit to the jurisdiction of the courts of New York County for purposes of resolving any disputes that may arise hereunder.

If you would like to pay for this license now, please remit this license along with your payment made payable to "COPYRIGHT CLEARANCE CENTER" otherwise you will be invoiced within 48 hours of the license date. Payment should be in the form of a check or money order referencing your account number and this invoice number RLINK501096412.

Once you receive your invoice for this order, you may pay your invoice by credit card. Please follow instructions provided at that time.

Make Payment To:
Copyright Clearance Center
Dept 001
P.O. Box 843006
Boston, MA 02284-3006

For suggestions or comments regarding this order, contact RightsLink Customer Support: customercare@copyright.com or +1-877-622-5543 (toll free in the US) or +1-978-646-2777.

Gratis licenses (referencing \$0 in the Total field) are free. Please retain this printable license for your reference. No payment is required.

**AIP PUBLISHING LLC LICENSE
TERMS AND CONDITIONS**

Aug 22, 2013

All payments must be made in full to CCC. For payment instructions, please see information listed at the bottom of this form.

License Number	3214480894985
Order Date	Aug 22, 2013
Publisher	AIP Publishing LLC
Publication	The Journal of the Acoustical Society of America
Article Title	Material characterization of the encapsulation of an ultrasound contrast microbubble and its subharmonic response: Strain-softening interfacial elasticity model
Author	Shirshendu Paul, Amit Katiyar, Kausik Sarkar, Dhiman Chatterjee, et al.
Online Publication Date	Jun 1, 2010
Volume number	127
Issue number	6
Type of Use	Thesis/Dissertation
Requestor type	Author (original article)
Format	Print and electronic
Portion	Excerpt (> 800 words)
Will you be translating?	No
Title of your thesis / dissertation	Acoustic Characterization of Ultrasound Contrast Microbubbles and Echogenic Liposomes: Applications to Imaging and Drug-Delivery
Expected completion date	Sep 2013
Estimated size (number of pages)	300
Total	0.00 USD

Terms and Conditions

Acoustic Society of America -- Terms and Conditions: Permissions Uses

Acoustic Society of America ("ASA") hereby grants to you the non-exclusive right and license to use and/or distribute the Material according to the use specified in your order, on a one-time basis, for the specified term, with a maximum distribution equal to the number that you have ordered. Any links or other content accompanying the Material are not the subject of this license.

1. You agree to include the following copyright and permission notice with the reproduction of the Material: "Reprinted with permission from [FULL CITATION]. Copyright [PUBLICATION YEAR], Acoustic Society of America." For an article, the copyright and permission notice must be printed on the first page of the article or book chapter. For photographs, covers, or tables, the copyright and permission notice may appear with the Material, in a footnote, or in the reference list.
2. If you have licensed reuse of a figure, photograph, cover, or table, it is your responsibility to ensure that the material is original to ASA and does not contain the copyright of another entity, and that the copyright notice of the figure, photograph, cover, or table does not indicate that it was reprinted by ASA, with permission, from another source. Under no circumstances does ASA, purport or intend to grant

- permission to reuse material to which it does not hold copyright.
3. You may not alter or modify the Material in any manner. You may translate the Material into another language only if you have licensed translation rights. You may not use the Material for promotional purposes. ASA reserves all rights not specifically granted herein.
 4. The foregoing license shall not take effect unless and until ASA or its agent, Copyright Clearance Center, receives the Payment in accordance with Copyright Clearance Center Billing and Payment Terms and Conditions, which are incorporated herein by reference.
 5. ASA or the Copyright Clearance Center may, within two business days of granting this license, revoke the license for any reason whatsoever, with a full refund payable to you. Should you violate the terms of this license at any time, ASA, Acoustic Society of America, or Copyright Clearance Center may revoke the license with no refund to you. Notice of such revocation will be made using the contact information provided by you. Failure to receive such notice will not nullify the revocation.
 6. ASA makes no representations or warranties with respect to the Material. You agree to indemnify and hold harmless ASA, Acoustic Society of America, and their officers, directors, employees or agents from and against any and all claims arising out of your use of the Material other than as specifically authorized herein.
 7. The permission granted herein is personal to you and is not transferable or assignable without the prior written permission of ASA. This license may not be amended except in a writing signed by the party to be charged.
 8. If purchase orders, acknowledgments or check endorsements are issued on any forms containing terms and conditions which are inconsistent with these provisions, such inconsistent terms and conditions shall be of no force and effect. This document, including the CCC Billing and Payment Terms and Conditions, shall be the entire agreement between the parties relating to the subject matter hereof.

This Agreement shall be governed by and construed in accordance with the laws of the State of New York. Both parties hereby submit to the jurisdiction of the courts of New York County for purposes of resolving any disputes that may arise hereunder.

If you would like to pay for this license now, please remit this license along with your payment made payable to "COPYRIGHT CLEARANCE CENTER" otherwise you will be invoiced within 48 hours of the license date. Payment should be in the form of a check or money order referencing your account number and this invoice number RLINK501096413.

Once you receive your invoice for this order, you may pay your invoice by credit card. Please follow instructions provided at that time.

Make Payment To:
Copyright Clearance Center
Dept 001
P.O. Box 843006
Boston, MA 02284-3006

For suggestions or comments regarding this order, contact RightsLink Customer Support: customercare@copyright.com or +1-877-622-5543 (toll free in the US) or +1-978-646-2777.

Gratis licenses (referencing \$0 in the Total field) are free. Please retain this printable license for your reference. No payment is required.

E.4 Reprint Permissions for Chapter 5

The relevant permission letters are included in the following pages.

**AIP PUBLISHING LLC LICENSE
TERMS AND CONDITIONS**

Aug 22, 2013

All payments must be made in full to CCC. For payment instructions, please see information listed at the bottom of this form.

License Number	3214480665567
Order Date	Aug 22, 2013
Publisher	AIP Publishing LLC
Publication	The Journal of the Acoustical Society of America
Article Title	Material characterization of the encapsulation of an ultrasound contrast microbubble and its subharmonic response: Strain-softening interfacial elasticity model
Author	Shirshendu Paul, Amit Katiyar, Kausik Sarkar, Dhiman Chatterjee, et al.
Online Publication Date	Jun 1, 2010
Volume number	127
Issue number	6
Type of Use	Thesis/Dissertation
Requestor type	Author (original article)
Format	Print and electronic
Portion	Figure/Table
Number of figures/tables	21
Title of your thesis / dissertation	Acoustic Characterization of Ultrasound Contrast Microbubbles and Echogenic Liposomes: Applications to Imaging and Drug-Delivery
Expected completion date	Sep 2013
Estimated size (number of pages)	300
Total	0.00 USD

Terms and Conditions

Acoustic Society of America -- Terms and Conditions: Permissions Uses

Acoustic Society of America ("ASA") hereby grants to you the non-exclusive right and license to use and/or distribute the Material according to the use specified in your order, on a one-time basis, for the specified term, with a maximum distribution equal to the number that you have ordered. Any links or other content accompanying the Material are not the subject of this license.

1. You agree to include the following copyright and permission notice with the reproduction of the Material: "Reprinted with permission from [FULL CITATION]. Copyright [PUBLICATION YEAR], Acoustic Society of America." For an article, the copyright and permission notice must be printed on the first page of the article or book chapter. For photographs, covers, or tables, the copyright and permission notice may appear with the Material, in a footnote, or in the reference list.
2. If you have licensed reuse of a figure, photograph, cover, or table, it is your responsibility to ensure that the material is original to ASA and does not contain the copyright of another entity, and that the copyright notice of the figure, photograph, cover, or table does not indicate that it was reprinted by ASA, with permission, from another source. Under no circumstances does ASA, purport or intend to grant

- permission to reuse material to which it does not hold copyright.
3. You may not alter or modify the Material in any manner. You may translate the Material into another language only if you have licensed translation rights. You may not use the Material for promotional purposes. ASA reserves all rights not specifically granted herein.
 4. The foregoing license shall not take effect unless and until ASA or its agent, Copyright Clearance Center, receives the Payment in accordance with Copyright Clearance Center Billing and Payment Terms and Conditions, which are incorporated herein by reference.
 5. ASA or the Copyright Clearance Center may, within two business days of granting this license, revoke the license for any reason whatsoever, with a full refund payable to you. Should you violate the terms of this license at any time, ASA, Acoustic Society of America, or Copyright Clearance Center may revoke the license with no refund to you. Notice of such revocation will be made using the contact information provided by you. Failure to receive such notice will not nullify the revocation.
 6. ASA makes no representations or warranties with respect to the Material. You agree to indemnify and hold harmless ASA, Acoustic Society of America, and their officers, directors, employees or agents from and against any and all claims arising out of your use of the Material other than as specifically authorized herein.
 7. The permission granted herein is personal to you and is not transferable or assignable without the prior written permission of ASA. This license may not be amended except in a writing signed by the party to be charged.
 8. If purchase orders, acknowledgments or check endorsements are issued on any forms containing terms and conditions which are inconsistent with these provisions, such inconsistent terms and conditions shall be of no force and effect. This document, including the CCC Billing and Payment Terms and Conditions, shall be the entire agreement between the parties relating to the subject matter hereof.

This Agreement shall be governed by and construed in accordance with the laws of the State of New York. Both parties hereby submit to the jurisdiction of the courts of New York County for purposes of resolving any disputes that may arise hereunder.

If you would like to pay for this license now, please remit this license along with your payment made payable to "COPYRIGHT CLEARANCE CENTER" otherwise you will be invoiced within 48 hours of the license date. Payment should be in the form of a check or money order referencing your account number and this invoice number RLINK501096412.

Once you receive your invoice for this order, you may pay your invoice by credit card. Please follow instructions provided at that time.

Make Payment To:
Copyright Clearance Center
Dept 001
P.O. Box 843006
Boston, MA 02284-3006

For suggestions or comments regarding this order, contact RightsLink Customer Support: customercare@copyright.com or +1-877-622-5543 (toll free in the US) or +1-978-646-2777.

Gratis licenses (referencing \$0 in the Total field) are free. Please retain this printable license for your reference. No payment is required.

**AIP PUBLISHING LLC LICENSE
TERMS AND CONDITIONS**

Aug 22, 2013

All payments must be made in full to CCC. For payment instructions, please see information listed at the bottom of this form.

License Number	3214480894985
Order Date	Aug 22, 2013
Publisher	AIP Publishing LLC
Publication	The Journal of the Acoustical Society of America
Article Title	Material characterization of the encapsulation of an ultrasound contrast microbubble and its subharmonic response: Strain-softening interfacial elasticity model
Author	Shirshendu Paul, Amit Katiyar, Kausik Sarkar, Dhiman Chatterjee, et al.
Online Publication Date	Jun 1, 2010
Volume number	127
Issue number	6
Type of Use	Thesis/Dissertation
Requestor type	Author (original article)
Format	Print and electronic
Portion	Excerpt (> 800 words)
Will you be translating?	No
Title of your thesis / dissertation	Acoustic Characterization of Ultrasound Contrast Microbubbles and Echogenic Liposomes: Applications to Imaging and Drug-Delivery
Expected completion date	Sep 2013
Estimated size (number of pages)	300
Total	0.00 USD

Terms and Conditions

Acoustic Society of America -- Terms and Conditions: Permissions Uses

Acoustic Society of America ("ASA") hereby grants to you the non-exclusive right and license to use and/or distribute the Material according to the use specified in your order, on a one-time basis, for the specified term, with a maximum distribution equal to the number that you have ordered. Any links or other content accompanying the Material are not the subject of this license.

1. You agree to include the following copyright and permission notice with the reproduction of the Material: "Reprinted with permission from [FULL CITATION]. Copyright [PUBLICATION YEAR], Acoustic Society of America." For an article, the copyright and permission notice must be printed on the first page of the article or book chapter. For photographs, covers, or tables, the copyright and permission notice may appear with the Material, in a footnote, or in the reference list.
2. If you have licensed reuse of a figure, photograph, cover, or table, it is your responsibility to ensure that the material is original to ASA and does not contain the copyright of another entity, and that the copyright notice of the figure, photograph, cover, or table does not indicate that it was reprinted by ASA, with permission, from another source. Under no circumstances does ASA, purport or intend to grant

- permission to reuse material to which it does not hold copyright.
3. You may not alter or modify the Material in any manner. You may translate the Material into another language only if you have licensed translation rights. You may not use the Material for promotional purposes. ASA reserves all rights not specifically granted herein.
 4. The foregoing license shall not take effect unless and until ASA or its agent, Copyright Clearance Center, receives the Payment in accordance with Copyright Clearance Center Billing and Payment Terms and Conditions, which are incorporated herein by reference.
 5. ASA or the Copyright Clearance Center may, within two business days of granting this license, revoke the license for any reason whatsoever, with a full refund payable to you. Should you violate the terms of this license at any time, ASA, Acoustic Society of America, or Copyright Clearance Center may revoke the license with no refund to you. Notice of such revocation will be made using the contact information provided by you. Failure to receive such notice will not nullify the revocation.
 6. ASA makes no representations or warranties with respect to the Material. You agree to indemnify and hold harmless ASA, Acoustic Society of America, and their officers, directors, employees or agents from and against any and all claims arising out of your use of the Material other than as specifically authorized herein.
 7. The permission granted herein is personal to you and is not transferable or assignable without the prior written permission of ASA. This license may not be amended except in a writing signed by the party to be charged.
 8. If purchase orders, acknowledgments or check endorsements are issued on any forms containing terms and conditions which are inconsistent with these provisions, such inconsistent terms and conditions shall be of no force and effect. This document, including the CCC Billing and Payment Terms and Conditions, shall be the entire agreement between the parties relating to the subject matter hereof.

This Agreement shall be governed by and construed in accordance with the laws of the State of New York. Both parties hereby submit to the jurisdiction of the courts of New York County for purposes of resolving any disputes that may arise hereunder.

If you would like to pay for this license now, please remit this license along with your payment made payable to "COPYRIGHT CLEARANCE CENTER" otherwise you will be invoiced within 48 hours of the license date. Payment should be in the form of a check or money order referencing your account number and this invoice number RLINK501096413.

Once you receive your invoice for this order, you may pay your invoice by credit card. Please follow instructions provided at that time.

Make Payment To:
Copyright Clearance Center
Dept 001
P.O. Box 843006
Boston, MA 02284-3006

For suggestions or comments regarding this order, contact RightsLink Customer Support: customercare@copyright.com or +1-877-622-5543 (toll free in the US) or +1-978-646-2777.

Gratis licenses (referencing \$0 in the Total field) are free. Please retain this printable license for your reference. No payment is required.

**ELSEVIER LICENSE
TERMS AND CONDITIONS**

Aug 23, 2013

This is a License Agreement between Shirshendu Paul ("You") and Elsevier ("Elsevier") provided by Copyright Clearance Center ("CCC"). The license consists of your order details, the terms and conditions provided by Elsevier, and the payment terms and conditions.

All payments must be made in full to CCC. For payment instructions, please see information listed at the bottom of this form.

Supplier	Elsevier Limited The Boulevard, Langford Lane Kidlington, Oxford, OX5 1GB, UK
Registered Company Number	1982084
Customer name	Shirshendu Paul
Customer address	130 Acedemy Street Newark, DE 19716
License number	3215010976174
License date	Aug 23, 2013
Licensed content publisher	Elsevier
Licensed content publication	Ultrasound in Medicine & Biology
Licensed content title	Characterization of Definity™ Ultrasound Contrast Agent at Frequency Range of 5–15 MHz
Licensed content author	Telli Faez, David Goertz, Nico De Jong
Licensed content date	February 2011
Licensed content volume number	37
Licensed content issue number	2
Number of pages	5
Start Page	338
End Page	342
Type of Use	reuse in a thesis/dissertation
Intended publisher of new work	other
Portion	figures/tables/illustrations
Number of figures/tables /illustrations	4
Format	both print and electronic
Are you the author of this Elsevier article?	No
Will you be translating?	No
Order reference number	

Title of your thesis/dissertation	Acoustic Characterization of Ultrasound Contrast Microbubbles and Echogenic Liposomes: Applications to Imaging and Drug-Delivery
Expected completion date	Sep 2013
Estimated size (number of pages)	300
Elsevier VAT number	GB 494 6272 12
Permissions price	0.00 USD
VAT/Local Sales Tax	0.0 USD / 0.0 GBP
Total	0.00 USD

[Terms and Conditions](#)

INTRODUCTION

1. The publisher for this copyrighted material is Elsevier. By clicking "accept" in connection with completing this licensing transaction, you agree that the following terms and conditions apply to this transaction (along with the Billing and Payment terms and conditions established by Copyright Clearance Center, Inc. ("CCC"), at the time that you opened your Rightslink account and that are available at any time at <http://myaccount.copyright.com>).

GENERAL TERMS

2. Elsevier hereby grants you permission to reproduce the aforementioned material subject to the terms and conditions indicated.

3. Acknowledgement: If any part of the material to be used (for example, figures) has appeared in our publication with credit or acknowledgement to another source, permission must also be sought from that source. If such permission is not obtained then that material may not be included in your publication/copies. Suitable acknowledgement to the source must be made, either as a footnote or in a reference list at the end of your publication, as follows:

"Reprinted from Publication title, Vol /edition number, Author(s), Title of article / title of chapter, Pages No., Copyright (Year), with permission from Elsevier [OR APPLICABLE SOCIETY COPYRIGHT OWNER]." Also Lancet special credit - "Reprinted from The Lancet, Vol. number, Author(s), Title of article, Pages No., Copyright (Year), with permission from Elsevier."

4. Reproduction of this material is confined to the purpose and/or media for which permission is hereby given.

5. Altering/Modifying Material: Not Permitted. However figures and illustrations may be altered/adapted minimally to serve your work. Any other abbreviations, additions, deletions and/or any other alterations shall be made only with prior written authorization of Elsevier Ltd. (Please contact Elsevier at permissions@elsevier.com)

6. If the permission fee for the requested use of our material is waived in this instance, please be advised that your future requests for Elsevier materials may attract a fee.

7. Reservation of Rights: Publisher reserves all rights not specifically granted in the combination of (i) the license details provided by you and accepted in the course of this

licensing transaction, (ii) these terms and conditions and (iii) CCC's Billing and Payment terms and conditions.

8. License Contingent Upon Payment: While you may exercise the rights licensed immediately upon issuance of the license at the end of the licensing process for the transaction, provided that you have disclosed complete and accurate details of your proposed use, no license is finally effective unless and until full payment is received from you (either by publisher or by CCC) as provided in CCC's Billing and Payment terms and conditions. If full payment is not received on a timely basis, then any license preliminarily granted shall be deemed automatically revoked and shall be void as if never granted. Further, in the event that you breach any of these terms and conditions or any of CCC's Billing and Payment terms and conditions, the license is automatically revoked and shall be void as if never granted. Use of materials as described in a revoked license, as well as any use of the materials beyond the scope of an unrevoked license, may constitute copyright infringement and publisher reserves the right to take any and all action to protect its copyright in the materials.

9. Warranties: Publisher makes no representations or warranties with respect to the licensed material.

10. Indemnity: You hereby indemnify and agree to hold harmless publisher and CCC, and their respective officers, directors, employees and agents, from and against any and all claims arising out of your use of the licensed material other than as specifically authorized pursuant to this license.

11. No Transfer of License: This license is personal to you and may not be sublicensed, assigned, or transferred by you to any other person without publisher's written permission.

12. No Amendment Except in Writing: This license may not be amended except in a writing signed by both parties (or, in the case of publisher, by CCC on publisher's behalf).

13. Objection to Contrary Terms: Publisher hereby objects to any terms contained in any purchase order, acknowledgment, check endorsement or other writing prepared by you, which terms are inconsistent with these terms and conditions or CCC's Billing and Payment terms and conditions. These terms and conditions, together with CCC's Billing and Payment terms and conditions (which are incorporated herein), comprise the entire agreement between you and publisher (and CCC) concerning this licensing transaction. In the event of any conflict between your obligations established by these terms and conditions and those established by CCC's Billing and Payment terms and conditions, these terms and conditions shall control.

14. Revocation: Elsevier or Copyright Clearance Center may deny the permissions described in this License at their sole discretion, for any reason or no reason, with a full refund payable to you. Notice of such denial will be made using the contact information provided by you. Failure to receive such notice will not alter or invalidate the denial. In no event will Elsevier or Copyright Clearance Center be responsible or liable for any costs, expenses or damage incurred by you as a result of a denial of your permission request, other than a refund of the amount(s) paid by you to Elsevier and/or Copyright Clearance Center for denied permissions.

LIMITED LICENSE

The following terms and conditions apply only to specific license types:

15. Translation: This permission is granted for non-exclusive world English rights only unless your license was granted for translation rights. If you licensed translation rights you may only translate this content into the languages you requested. A professional translator must perform all translations and reproduce the content word for word preserving the integrity of the article. If this license is to re-use 1 or 2 figures then permission is granted for non-exclusive world rights in all languages.

16. Website: The following terms and conditions apply to electronic reserve and author websites:

Electronic reserve: If licensed material is to be posted to website, the web site is to be password-protected and made available only to bona fide students registered on a relevant course if:

This license was made in connection with a course,

This permission is granted for 1 year only. You may obtain a license for future website posting,

All content posted to the web site must maintain the copyright information line on the bottom of each image,

A hyper-text must be included to the Homepage of the journal from which you are licensing at <http://www.sciencedirect.com/science/journal/xxxx> or the Elsevier homepage for books at <http://www.elsevier.com>, and

Central Storage: This license does not include permission for a scanned version of the material to be stored in a central repository such as that provided by Heron/XanEdu.

17. Author website for journals with the following additional clauses:

All content posted to the web site must maintain the copyright information line on the bottom of each image, and the permission granted is limited to the personal version of your paper. You are not allowed to download and post the published electronic version of your article (whether PDF or HTML, proof or final version), nor may you scan the printed edition to create an electronic version. A hyper-text must be included to the Homepage of the journal from which you are licensing at <http://www.sciencedirect.com/science/journal/xxxx>. As part of our normal production process, you will receive an e-mail notice when your article appears on Elsevier's online service ScienceDirect (www.sciencedirect.com). That e-mail will include the article's Digital Object Identifier (DOI). This number provides the electronic link to the published article and should be included in the posting of your personal version. We ask that you wait until you receive this e-mail and have the DOI to do any posting.

Central Storage: This license does not include permission for a scanned version of the material to be stored in a central repository such as that provided by Heron/XanEdu.

18. Author website for books with the following additional clauses:

Authors are permitted to place a brief summary of their work online only.

A hyper-text must be included to the Elsevier homepage at <http://www.elsevier.com>. All content posted to the web site must maintain the copyright information line on the bottom of each image. You are not allowed to download and post the published electronic version of your chapter, nor may you scan the printed edition to create an electronic version.

Central Storage: This license does not include permission for a scanned version of the

material to be stored in a central repository such as that provided by Heron/XanEdu.

19. **Website** (regular and for author): A hyper-text must be included to the Homepage of the journal from which you are licensing at <http://www.sciencedirect.com/science/journal/xxxxx>. or for books to the Elsevier homepage at <http://www.elsevier.com>

20. **Thesis/Dissertation:** If your license is for use in a thesis/dissertation your thesis may be submitted to your institution in either print or electronic form. Should your thesis be published commercially, please reapply for permission. These requirements include permission for the Library and Archives of Canada to supply single copies, on demand, of the complete thesis and include permission for UMI to supply single copies, on demand, of the complete thesis. Should your thesis be published commercially, please reapply for permission.

21. Other Conditions:

v1.6

If you would like to pay for this license now, please remit this license along with your payment made payable to "COPYRIGHT CLEARANCE CENTER" otherwise you will be invoiced within 48 hours of the license date. Payment should be in the form of a check or money order referencing your account number and this invoice number RLINK501097213.

Once you receive your invoice for this order, you may pay your invoice by credit card. Please follow instructions provided at that time.

Make Payment To:
Copyright Clearance Center
Dept 001
P.O. Box 843006
Boston, MA 02284-3006

For suggestions or comments regarding this order, contact RightsLink Customer Support: customercare@copyright.com or +1-877-622-5543 (toll free in the US) or +1-978-646-2777.

Gratis licenses (referencing \$0 in the Total field) are free. Please retain this printable license for your reference. No payment is required.

E.5 Reprint Permissions for Chapter 6

The relevant permission letters are included in the following pages.

ELSEVIER ORDER DETAILS

Aug 22, 2013

Order Number	500784534
Order Date	Aug 22, 2013
Licensed content publisher	Elsevier
Licensed content publication	Ultrasound in Medicine & Biology
Licensed content title	Determination of the Interfacial Rheological Properties of a Poly(DL-lactic acid)-Encapsulated Contrast Agent Using <i>In Vitro</i> Attenuation and Scattering
Licensed content author	Shirshendu Paul, Daniel Russakow, Tyler Rodgers, Kausik Sarkar, Michael Cochran, Margaret A. Wheatley
Licensed content date	July 2013
Licensed content volume number	39
Licensed content issue number	7
Number of pages	15
Start Page	1277
End Page	1291
Type of Use	reuse in a thesis/dissertation
Intended publisher of new work	other
Portion	full article
Format	both print and electronic
Are you the author of this Elsevier article?	Yes
Will you be translating?	No
Order reference number	
Title of your thesis/dissertation	Acoustic Characterization of Ultrasound Contrast Microbubbles and Echogenic Liposomes: Applications to Imaging and Drug-Delivery
Expected completion date	Sep 2013
Estimated size (number of pages)	
Elsevier VAT number	GB 494 6272 12
Permissions price	Not Available
VAT/Local Sales Tax	Not Available
Total	Not Available



RightsLink®

[Home](#) [Account Info](#) [Help](#)


Title: Influence of shell properties on high-frequency ultrasound imaging and drug delivery using polymer-shelled microbubbles
Author: Chitnis, P.V.; Koppolu, S.; Mamou, J.; Chion, C.; Ketterling, J.A.
Publication: Ultrasonics, Ferroelectrics and Frequency Control, IEEE Transactions on
Publisher: IEEE
Date: January 2013
 Copyright © 2013, IEEE

 Logged in as:
 Shirshendu Paul
 Account #: 3000652960

[LOGOUT](#)

Thesis / Dissertation Reuse

The IEEE does not require individuals working on a thesis to obtain a formal reuse license, however, you may print out this statement to be used as a permission grant:

Requirements to be followed when using any portion (e.g., figure, graph, table, or textual material) of an IEEE copyrighted paper in a thesis:

- 1) In the case of textual material (e.g., using short quotes or referring to the work within these papers) users must give full credit to the original source (author, paper, publication) followed by the IEEE copyright line © 2011 IEEE.
- 2) In the case of illustrations or tabular material, we require that the copyright line © [Year of original publication] IEEE appear prominently with each reprinted figure and/or table.
- 3) If a substantial portion of the original paper is to be used, and if you are not the senior author, also obtain the senior author's approval.

Requirements to be followed when using an entire IEEE copyrighted paper in a thesis:

- 1) The following IEEE copyright/ credit notice should be placed prominently in the references: © [year of original publication] IEEE. Reprinted, with permission, from [author names, paper title, IEEE publication title, and month/year of publication]
- 2) Only the accepted version of an IEEE copyrighted paper can be used when posting the paper or your thesis on-line.
- 3) In placing the thesis on the author's university website, please display the following message in a prominent place on the website: In reference to IEEE copyrighted material which is used with permission in this thesis, the IEEE does not endorse any [university/educational entity's name goes here]'s products or services. Internal or personal use of this material is permitted. If interested in reprinting/republishing IEEE copyrighted material for advertising or promotional purposes or for creating new collective works for resale or redistribution, please go to http://www.ieee.org/publications_standards/publications/rights/rights_link.html to learn how to obtain a License from RightsLink.

If applicable, University Microfilms and/or ProQuest Library, or the Archives of Canada may supply single copies of the dissertation.

[BACK](#)
[CLOSE WINDOW](#)

Copyright © 2013 Copyright Clearance Center, Inc. All Rights Reserved. [Privacy statement](#).
 Comments? We would like to hear from you. E-mail us at customercare@copyright.com

E.6 Reprint Permission for Figure 8.1 in Chapter 8

The relevant permission letter is included in the following pages.

**SPRINGER LICENSE
TERMS AND CONDITIONS**

Aug 23, 2013

This is a License Agreement between Shirshendu Paul ("You") and Springer ("Springer") provided by Copyright Clearance Center ("CCC"). The license consists of your order details, the terms and conditions provided by Springer, and the payment terms and conditions.

All payments must be made in full to CCC. For payment instructions, please see information listed at the bottom of this form.

License Number	3215051494963
License date	Aug 23, 2013
Licensed content publisher	Springer
Licensed content publication	Springer eBook
Licensed content title	Ultrasound-Responsive Liposomes
Licensed content author	Shao-Ling Huang
Licensed content date	Jan 1, 2010
Type of Use	Thesis/Dissertation
Portion	Figures
Author of this Springer article	No
Order reference number	
Title of your thesis / dissertation	Acoustic Characterization of Ultrasound Contrast Microbubbles and Echogenic Liposomes: Applications to Imaging and Drug-Delivery
Expected completion date	Sep 2013
Estimated size(pages)	300
Total	0.00 USD

Terms and Conditions**Introduction**

The publisher for this copyrighted material is Springer Science + Business Media. By clicking "accept" in connection with completing this licensing transaction, you agree that the following terms and conditions apply to this transaction (along with the Billing and Payment terms and conditions established by Copyright Clearance Center, Inc. ("CCC"), at the time that you opened your Rightslink account and that are available at any time at <http://myaccount.copyright.com>).

Limited License

With reference to your request to reprint in your thesis material on which Springer Science and Business Media control the copyright, permission is granted, free of charge, for the use indicated in your enquiry.

Licenses are for one-time use only with a maximum distribution equal to the number that you identified in the licensing process.

This License includes use in an electronic form, provided its password protected or on the university's intranet or repository, including UMI (according to the definition at the Sherpa website: <http://www.sherpa.ac.uk/romeo/>). For any other electronic use, please contact Springer at (permissions.dordrecht@springer.com or permissions.heidelberg@springer.com).

The material can only be used for the purpose of defending your thesis, and with a maximum of 100 extra copies in paper.

Although Springer holds copyright to the material and is entitled to negotiate on rights, this license is only valid, subject to a courtesy information to the author (address is given with the article/chapter) and provided it concerns original material which does not carry references to other sources (if material in question appears with credit to another source, authorization from that source is required as well).

Permission free of charge on this occasion does not prejudice any rights we might have to charge for reproduction of our copyrighted material in the future.

Altering/Modifying Material: Not Permitted

You may not alter or modify the material in any manner. Abbreviations, additions, deletions and/or any other alterations shall be made only with prior written authorization of the author(s) and/or Springer Science + Business Media. (Please contact Springer at (permissions.dordrecht@springer.com or permissions.heidelberg@springer.com)

Reservation of Rights

Springer Science + Business Media reserves all rights not specifically granted in the combination of (i) the license details provided by you and accepted in the course of this licensing transaction, (ii) these terms and conditions and (iii) CCC's Billing and Payment terms and conditions.

Copyright Notice:Disclaimer

You must include the following copyright and permission notice in connection with any reproduction of the licensed material: "Springer and the original publisher /journal title, volume, year of publication, page, chapter/article title, name(s) of author(s), figure number(s), original copyright notice) is given to the publication in which the material was originally published, by adding: with kind permission from Springer Science and Business Media"

Warranties: None

Example 1: Springer Science + Business Media makes no representations or warranties with respect to the licensed material.

Example 2: Springer Science + Business Media makes no representations or warranties with respect to the licensed material and adopts on its own behalf the limitations and disclaimers established by CCC on its behalf in its Billing and Payment terms and conditions for this licensing transaction.

Indemnity

You hereby indemnify and agree to hold harmless Springer Science + Business Media and CCC, and their respective officers, directors, employees and agents, from and against any and all claims arising out of your use of the licensed material other than as specifically

authorized pursuant to this license.

No Transfer of License

This license is personal to you and may not be sublicensed, assigned, or transferred by you to any other person without Springer Science + Business Media's written permission.

No Amendment Except in Writing

This license may not be amended except in a writing signed by both parties (or, in the case of Springer Science + Business Media, by CCC on Springer Science + Business Media's behalf).

Objection to Contrary Terms

Springer Science + Business Media hereby objects to any terms contained in any purchase order, acknowledgment, check endorsement or other writing prepared by you, which terms are inconsistent with these terms and conditions or CCC's Billing and Payment terms and conditions. These terms and conditions, together with CCC's Billing and Payment terms and conditions (which are incorporated herein), comprise the entire agreement between you and Springer Science + Business Media (and CCC) concerning this licensing transaction. In the event of any conflict between your obligations established by these terms and conditions and those established by CCC's Billing and Payment terms and conditions, these terms and conditions shall control.

Jurisdiction

All disputes that may arise in connection with this present License, or the breach thereof, shall be settled exclusively by arbitration, to be held in The Netherlands, in accordance with Dutch law, and to be conducted under the Rules of the 'Netherlands Arbitrage Instituut' (Netherlands Institute of Arbitration). **OR:**

All disputes that may arise in connection with this present License, or the breach thereof, shall be settled exclusively by arbitration, to be held in the Federal Republic of Germany, in accordance with German law.

Other terms and conditions:

v1.3

If you would like to pay for this license now, please remit this license along with your payment made payable to "COPYRIGHT CLEARANCE CENTER" otherwise you will be invoiced within 48 hours of the license date. Payment should be in the form of a check or money order referencing your account number and this invoice number RLINK501097240.

Once you receive your invoice for this order, you may pay your invoice by credit card. Please follow instructions provided at that time.

Make Payment To:
Copyright Clearance Center
Dept 001
P.O. Box 843006
Boston, MA 02284-3006

For suggestions or comments regarding this order, contact RightsLink Customer Support: customercare@copyright.com or +1-877-622-5543 (toll free in the US) or +1-978-646-2777.

Gratis licenses (referencing \$0 in the Total field) are free. Please retain this printable license for your reference. No payment is required.

Rightslink Printable License

<https://s100.copyright.com/App/PrintableLicenseFrame.jsp?publisherID...>

E.7 Reprint Permissions for Chapter 9

The relevant permission letters are included in the following pages.

**ELSEVIER LICENSE
TERMS AND CONDITIONS**

Aug 22, 2013

This is a License Agreement between Shirshendu Paul ("You") and Elsevier ("Elsevier") provided by Copyright Clearance Center ("CCC"). The license consists of your order details, the terms and conditions provided by Elsevier, and the payment terms and conditions.

All payments must be made in full to CCC. For payment instructions, please see information listed at the bottom of this form.

Supplier	Elsevier Limited The Boulevard, Langford Lane Kidlington, Oxford, OX5 1GB, UK
Registered Company Number	1982084
Customer name	Shirshendu Paul
Customer address	130 Acedemy Street Newark, DE 19716
License number	3214481338563
License date	Aug 22, 2013
Licensed content publisher	Elsevier
Licensed content publication	Ultrasonics
Licensed content title	<i>In vitro</i> measurement of attenuation and nonlinear scattering from echogenic liposomes
Licensed content author	Shirshendu Paul, Daniel Russakow, Rahul Nahire, Tapas Nandy, Avinash H. Ambre, Kalpana Katti, Sanku Mallik, Kausik Sarkar
Licensed content date	September 2012
Licensed content volume number	52
Licensed content issue number	7
Number of pages	8
Start Page	962
End Page	969
Type of Use	reuse in a thesis/dissertation
Intended publisher of new work	other
Portion	full article
Format	both print and electronic
Are you the author of this Elsevier article?	Yes
Will you be translating?	No
Order reference number	

Title of your thesis/dissertation	Acoustic Characterization of Ultrasound Contrast Microbubbles and Echogenic Liposomes: Applications to Imaging and Drug-Delivery
Expected completion date	Sep 2013
Estimated size (number of pages)	300
Elsevier VAT number	GB 494 6272 12
Permissions price	0.00 USD
VAT/Local Sales Tax	0.0 USD / 0.0 GBP
Total	0.00 USD

[Terms and Conditions](#)

INTRODUCTION

1. The publisher for this copyrighted material is Elsevier. By clicking "accept" in connection with completing this licensing transaction, you agree that the following terms and conditions apply to this transaction (along with the Billing and Payment terms and conditions established by Copyright Clearance Center, Inc. ("CCC"), at the time that you opened your Rightslink account and that are available at any time at <http://myaccount.copyright.com>).

GENERAL TERMS

2. Elsevier hereby grants you permission to reproduce the aforementioned material subject to the terms and conditions indicated.

3. Acknowledgement: If any part of the material to be used (for example, figures) has appeared in our publication with credit or acknowledgement to another source, permission must also be sought from that source. If such permission is not obtained then that material may not be included in your publication/copies. Suitable acknowledgement to the source must be made, either as a footnote or in a reference list at the end of your publication, as follows:

"Reprinted from Publication title, Vol /edition number, Author(s), Title of article / title of chapter, Pages No., Copyright (Year), with permission from Elsevier [OR APPLICABLE SOCIETY COPYRIGHT OWNER]." Also Lancet special credit - "Reprinted from The Lancet, Vol. number, Author(s), Title of article, Pages No., Copyright (Year), with permission from Elsevier."

4. Reproduction of this material is confined to the purpose and/or media for which permission is hereby given.

5. Altering/Modifying Material: Not Permitted. However figures and illustrations may be altered/adapted minimally to serve your work. Any other abbreviations, additions, deletions and/or any other alterations shall be made only with prior written authorization of Elsevier Ltd. (Please contact Elsevier at permissions@elsevier.com)

6. If the permission fee for the requested use of our material is waived in this instance, please be advised that your future requests for Elsevier materials may attract a fee.

7. Reservation of Rights: Publisher reserves all rights not specifically granted in the combination of (i) the license details provided by you and accepted in the course of this

licensing transaction, (ii) these terms and conditions and (iii) CCC's Billing and Payment terms and conditions.

8. License Contingent Upon Payment: While you may exercise the rights licensed immediately upon issuance of the license at the end of the licensing process for the transaction, provided that you have disclosed complete and accurate details of your proposed use, no license is finally effective unless and until full payment is received from you (either by publisher or by CCC) as provided in CCC's Billing and Payment terms and conditions. If full payment is not received on a timely basis, then any license preliminarily granted shall be deemed automatically revoked and shall be void as if never granted. Further, in the event that you breach any of these terms and conditions or any of CCC's Billing and Payment terms and conditions, the license is automatically revoked and shall be void as if never granted. Use of materials as described in a revoked license, as well as any use of the materials beyond the scope of an unrevoked license, may constitute copyright infringement and publisher reserves the right to take any and all action to protect its copyright in the materials.

9. Warranties: Publisher makes no representations or warranties with respect to the licensed material.

10. Indemnity: You hereby indemnify and agree to hold harmless publisher and CCC, and their respective officers, directors, employees and agents, from and against any and all claims arising out of your use of the licensed material other than as specifically authorized pursuant to this license.

11. No Transfer of License: This license is personal to you and may not be sublicensed, assigned, or transferred by you to any other person without publisher's written permission.

12. No Amendment Except in Writing: This license may not be amended except in a writing signed by both parties (or, in the case of publisher, by CCC on publisher's behalf).

13. Objection to Contrary Terms: Publisher hereby objects to any terms contained in any purchase order, acknowledgment, check endorsement or other writing prepared by you, which terms are inconsistent with these terms and conditions or CCC's Billing and Payment terms and conditions. These terms and conditions, together with CCC's Billing and Payment terms and conditions (which are incorporated herein), comprise the entire agreement between you and publisher (and CCC) concerning this licensing transaction. In the event of any conflict between your obligations established by these terms and conditions and those established by CCC's Billing and Payment terms and conditions, these terms and conditions shall control.

14. Revocation: Elsevier or Copyright Clearance Center may deny the permissions described in this License at their sole discretion, for any reason or no reason, with a full refund payable to you. Notice of such denial will be made using the contact information provided by you. Failure to receive such notice will not alter or invalidate the denial. In no event will Elsevier or Copyright Clearance Center be responsible or liable for any costs, expenses or damage incurred by you as a result of a denial of your permission request, other than a refund of the amount(s) paid by you to Elsevier and/or Copyright Clearance Center for denied permissions.

LIMITED LICENSE

The following terms and conditions apply only to specific license types:

15. Translation: This permission is granted for non-exclusive world English rights only unless your license was granted for translation rights. If you licensed translation rights you may only translate this content into the languages you requested. A professional translator must perform all translations and reproduce the content word for word preserving the integrity of the article. If this license is to re-use 1 or 2 figures then permission is granted for non-exclusive world rights in all languages.

16. Website: The following terms and conditions apply to electronic reserve and author websites:

Electronic reserve: If licensed material is to be posted to website, the web site is to be password-protected and made available only to bona fide students registered on a relevant course if:

This license was made in connection with a course,

This permission is granted for 1 year only. You may obtain a license for future website posting,

All content posted to the web site must maintain the copyright information line on the bottom of each image,

A hyper-text must be included to the Homepage of the journal from which you are licensing at <http://www.sciencedirect.com/science/journal/xxxx> or the Elsevier homepage for books at <http://www.elsevier.com>, and

Central Storage: This license does not include permission for a scanned version of the material to be stored in a central repository such as that provided by Heron/XanEdu.

17. Author website for journals with the following additional clauses:

All content posted to the web site must maintain the copyright information line on the bottom of each image, and the permission granted is limited to the personal version of your paper. You are not allowed to download and post the published electronic version of your article (whether PDF or HTML, proof or final version), nor may you scan the printed edition to create an electronic version. A hyper-text must be included to the Homepage of the journal from which you are licensing at <http://www.sciencedirect.com/science/journal/xxxx>. As part of our normal production process, you will receive an e-mail notice when your article appears on Elsevier's online service ScienceDirect (www.sciencedirect.com). That e-mail will include the article's Digital Object Identifier (DOI). This number provides the electronic link to the published article and should be included in the posting of your personal version. We ask that you wait until you receive this e-mail and have the DOI to do any posting.

Central Storage: This license does not include permission for a scanned version of the material to be stored in a central repository such as that provided by Heron/XanEdu.

18. Author website for books with the following additional clauses:

Authors are permitted to place a brief summary of their work online only.

A hyper-text must be included to the Elsevier homepage at <http://www.elsevier.com>. All content posted to the web site must maintain the copyright information line on the bottom of each image. You are not allowed to download and post the published electronic version of your chapter, nor may you scan the printed edition to create an electronic version.

Central Storage: This license does not include permission for a scanned version of the

material to be stored in a central repository such as that provided by Heron/XanEdu.

19. **Website** (regular and for author): A hyper-text must be included to the Homepage of the journal from which you are licensing at <http://www.sciencedirect.com/science/journal/xxxxx>. or for books to the Elsevier homepage at <http://www.elsevier.com>

20. **Thesis/Dissertation:** If your license is for use in a thesis/dissertation your thesis may be submitted to your institution in either print or electronic form. Should your thesis be published commercially, please reapply for permission. These requirements include permission for the Library and Archives of Canada to supply single copies, on demand, of the complete thesis and include permission for UMI to supply single copies, on demand, of the complete thesis. Should your thesis be published commercially, please reapply for permission.

21. Other Conditions:

v1.6

If you would like to pay for this license now, please remit this license along with your payment made payable to "COPYRIGHT CLEARANCE CENTER" otherwise you will be invoiced within 48 hours of the license date. Payment should be in the form of a check or money order referencing your account number and this invoice number RLINK501096418.

Once you receive your invoice for this order, you may pay your invoice by credit card. Please follow instructions provided at that time.

Make Payment To:
Copyright Clearance Center
Dept 001
P.O. Box 843006
Boston, MA 02284-3006

For suggestions or comments regarding this order, contact RightsLink Customer Support: customercare@copyright.com or +1-877-622-5543 (toll free in the US) or +1-978-646-2777.

Gratis licenses (referencing \$0 in the Total field) are free. Please retain this printable license for your reference. No payment is required.

**AIP PUBLISHING LLC LICENSE
TERMS AND CONDITIONS**

Aug 23, 2013

All payments must be made in full to CCC. For payment instructions, please see information listed at the bottom of this form.

License Number	3215060983202
Order Date	Aug 23, 2013
Publisher	AIP Publishing LLC
Publication	The Journal of Acoustical Society of America
Article Title	Acoustic characterization of echogenic liposomes: Frequency-dependent attenuation and backscatter
Author	Jonathan A. Kopechek, Kevin J. Haworth, Jason L. Raymond, T. Douglas Mast, et al.
Online Publication Date	Nov 1, 2011
Volume number	130
Issue number	5
Type of Use	Thesis/Dissertation
Requestor type	Student
Format	Print and electronic
Portion	Figure/Table
Number of figures/tables	1
Title of your thesis / dissertation	Acoustic Characterization of Ultrasound Contrast Microbubbles and Echogenic Liposomes: Applications to Imaging and Drug-Delivery
Expected completion date	Sep 2013
Estimated size (number of pages)	300
Total	0.00 USD

Terms and Conditions

Acoustic Society of America -- Terms and Conditions: Permissions Uses

Acoustic Society of America ("ASA") hereby grants to you the non-exclusive right and license to use and/or distribute the Material according to the use specified in your order, on a one-time basis, for the specified term, with a maximum distribution equal to the number that you have ordered. Any links or other content accompanying the Material are not the subject of this license.

1. You agree to include the following copyright and permission notice with the reproduction of the Material: "Reprinted with permission from [FULL CITATION]. Copyright [PUBLICATION YEAR], Acoustic Society of America." For an article, the copyright and permission notice must be printed on the first page of the article or book chapter. For photographs, covers, or tables, the copyright and permission notice may appear with the Material, in a footnote, or in the reference list.
2. If you have licensed reuse of a figure, photograph, cover, or table, it is your responsibility to ensure that the material is original to ASA and does not contain the copyright of another entity, and that the copyright notice of the figure, photograph, cover, or table does not indicate that it was reprinted by ASA, with permission, from another source. Under no circumstances does ASA, purport or intend to grant permission to reuse material to which it does not hold copyright.

3. You may not alter or modify the Material in any manner. You may translate the Material into another language only if you have licensed translation rights. You may not use the Material for promotional purposes. ASA reserves all rights not specifically granted herein.
4. The foregoing license shall not take effect unless and until ASA or its agent, Copyright Clearance Center, receives the Payment in accordance with Copyright Clearance Center Billing and Payment Terms and Conditions, which are incorporated herein by reference.
5. ASA or the Copyright Clearance Center may, within two business days of granting this license, revoke the license for any reason whatsoever, with a full refund payable to you. Should you violate the terms of this license at any time, ASA, Acoustic Society of America, or Copyright Clearance Center may revoke the license with no refund to you. Notice of such revocation will be made using the contact information provided by you. Failure to receive such notice will not nullify the revocation.
6. ASA makes no representations or warranties with respect to the Material. You agree to indemnify and hold harmless ASA, Acoustic Society of America, and their officers, directors, employees or agents from and against any and all claims arising out of your use of the Material other than as specifically authorized herein.
7. The permission granted herein is personal to you and is not transferable or assignable without the prior written permission of ASA. This license may not be amended except in a writing signed by the party to be charged.
8. If purchase orders, acknowledgments or check endorsements are issued on any forms containing terms and conditions which are inconsistent with these provisions, such inconsistent terms and conditions shall be of no force and effect. This document, including the CCC Billing and Payment Terms and Conditions, shall be the entire agreement between the parties relating to the subject matter hereof.

This Agreement shall be governed by and construed in accordance with the laws of the State of New York. Both parties hereby submit to the jurisdiction of the courts of New York County for purposes of resolving any disputes that may arise hereunder.

If you would like to pay for this license now, please remit this license along with your payment made payable to "COPYRIGHT CLEARANCE CENTER" otherwise you will be invoiced within 48 hours of the license date. Payment should be in the form of a check or money order referencing your account number and this invoice number RLINK501097243.

Once you receive your invoice for this order, you may pay your invoice by credit card. Please follow instructions provided at that time.

Make Payment To:
Copyright Clearance Center
Dept 001
P.O. Box 843006
Boston, MA 02284-3006

For suggestions or comments regarding this order, contact RightsLink Customer Support: customercare@copyright.com or +1-877-622-5543 (toll free in the US) or +1-978-646-2777.

Gratis licenses (referencing \$0 in the Total field) are free. Please retain this printable license for your reference. No payment is required.

E.8 Reprint Permissions for Chapter 11

The relevant permission letters are included in the following pages.

**RightsLink®****Home** **Account Info** **Help****ACS Publications**
High quality. High impact.**Title:**Ultrasound Enhanced Matrix
Metalloproteinase-9 Triggered
Release of Contents from
Echogenic LiposomesLogged in as:
Shirshendu Paul
Account #:
3000652960**Author:**Rahul Nahire, Shirshendu Paul,
Michael D. Scott, Raushan K.
Singh, Wallace W. Muhonen,
John Shabb, Kara N. Gange, D.
K. Srivastava, Kausik Sarkar,
and Sanku Mallik**LOGOUT****Publication:** Molecular Pharmaceutics**Publisher:** American Chemical Society**Date:** Sep 1, 2012

Copyright © 2012, American Chemical Society

PERMISSION/LICENSE IS GRANTED FOR YOUR ORDER AT NO CHARGE

This type of permission/license, instead of the standard Terms & Conditions, is sent to you because no fee is being charged for your order. Please note the following:

- Permission is granted for your request in both print and electronic formats, and translations.
- If figures and/or tables were requested, they may be adapted or used in part.
- Please print this page for your records and send a copy of it to your publisher/graduate school.
- Appropriate credit for the requested material should be given as follows: "Reprinted (adapted) with permission from (COMPLETE REFERENCE CITATION). Copyright (YEAR) American Chemical Society." Insert appropriate information in place of the capitalized words.
- One-time permission is granted only for the use specified in your request. No additional uses are granted (such as derivative works or other editions). For any other uses, please submit a new request.

If credit is given to another source for the material you requested, permission must be obtained from that source.

BACK**CLOSE WINDOW**

Copyright © 2013 Copyright Clearance Center, Inc. All Rights Reserved. [Privacy statement](#).
Comments? We would like to hear from you. E-mail us at customercare@copyright.com

**RightsLink®****Home** **Account Info** **Help****ACS Publications**
High quality. High impact.**Title:**Ultrasound Enhanced Matrix
Metalloproteinase-9 Triggered
Release of Contents from
Echogenic LiposomesLogged in as:
Shirshendu Paul
Account #:
3000652960**Author:**Rahul Nahire, Shirshendu Paul,
Michael D. Scott, Raushan K.
Singh, Wallace W. Muhonen,
John Shabb, Kara N. Gange, D.
K. Srivastava, Kausik Sarkar,
and Sanku Mallik**LOGOUT****Publication:**

Molecular Pharmaceutics

Publisher: American Chemical Society**Date:** Sep 1, 2012

Copyright © 2012, American Chemical Society

PERMISSION/LICENSE IS GRANTED FOR YOUR ORDER AT NO CHARGE

This type of permission/license, instead of the standard Terms & Conditions, is sent to you because no fee is being charged for your order. Please note the following:

- Permission is granted for your request in both print and electronic formats, and translations.
- If figures and/or tables were requested, they may be adapted or used in part.
- Please print this page for your records and send a copy of it to your publisher/graduate school.
- Appropriate credit for the requested material should be given as follows: "Reprinted (adapted) with permission from (COMPLETE REFERENCE CITATION). Copyright (YEAR) American Chemical Society." Insert appropriate information in place of the capitalized words.
- One-time permission is granted only for the use specified in your request. No additional uses are granted (such as derivative works or other editions). For any other uses, please submit a new request.

BACK**CLOSE WINDOW**

Copyright © 2013 [Copyright Clearance Center, Inc.](#). All Rights Reserved. [Privacy statement](#).
Comments? We would like to hear from you. E-mail us at customercare@copyright.com

**RightsLink®****Home** **Account Info** **Help****ACS Publications**
High quality. High impact.**Title:**Polymer-Coated Echogenic Lipid
Nanoparticles with Dual Release
Triggers**Author:**Rahul Nahire, Manas K. Haldar,
Shirshendu Paul, Anaas
Mergoum, Avinash H. Ambre,
Kalpana S. Katti, Kara N. Gange,
D. K. Srivastava, Kausik Sarkar,
and Sanku Mallik**Publication:** Biomacromolecules**Publisher:** American Chemical Society**Date:** Mar 1, 2013

Copyright © 2013, American Chemical Society

Logged in as:
Shirshendu Paul
Account #:
3000652960**LOGOUT****PERMISSION/LICENSE IS GRANTED FOR YOUR ORDER AT NO CHARGE**

This type of permission/license, instead of the standard Terms & Conditions, is sent to you because no fee is being charged for your order. Please note the following:

- Permission is granted for your request in both print and electronic formats, and translations.
- If figures and/or tables were requested, they may be adapted or used in part.
- Please print this page for your records and send a copy of it to your publisher/graduate school.
- Appropriate credit for the requested material should be given as follows: "Reprinted (adapted) with permission from (COMPLETE REFERENCE CITATION). Copyright (YEAR) American Chemical Society." Insert appropriate information in place of the capitalized words.
- One-time permission is granted only for the use specified in your request. No additional uses are granted (such as derivative works or other editions). For any other uses, please submit a new request.

If credit is given to another source for the material you requested, permission must be obtained from that source.

BACK**CLOSE WINDOW**

Copyright © 2013 [Copyright Clearance Center, Inc.](#). All Rights Reserved. [Privacy statement](#).
Comments? We would like to hear from you. E-mail us at customercare@copyright.com

**RightsLink®****Home** **Account Info** **Help****ACS Publications**
High quality. High impact.**RightsLink®****Title:**Polymer-Coated Echogenic Lipid
Nanoparticles with Dual Release
TriggersLogged in as:
Shirshendu Paul
Account #:
3000652960**Author:**Rahul Nahire, Manas K. Haldar,
Shirshendu Paul, Anaas
Mergoum, Avinash H. Ambre,
Kalpana S. Katti, Kara N. Gange,
D. K. Srivastava, Kausik Sarkar,
and Sanku Mallik**LOGOUT****Publication:** Biomacromolecules**Publisher:** American Chemical Society**Date:** Mar 1, 2013

Copyright © 2013, American Chemical Society

PERMISSION/LICENSE IS GRANTED FOR YOUR ORDER AT NO CHARGE

This type of permission/license, instead of the standard Terms & Conditions, is sent to you because no fee is being charged for your order. Please note the following:

- Permission is granted for your request in both print and electronic formats, and translations.
- If figures and/or tables were requested, they may be adapted or used in part.
- Please print this page for your records and send a copy of it to your publisher/graduate school.
- Appropriate credit for the requested material should be given as follows: "Reprinted (adapted) with permission from (COMPLETE REFERENCE CITATION). Copyright (YEAR) American Chemical Society." Insert appropriate information in place of the capitalized words.
- One-time permission is granted only for the use specified in your request. No additional uses are granted (such as derivative works or other editions). For any other uses, please submit a new request.

BACK**CLOSE WINDOW**

Copyright © 2013 Copyright Clearance Center, Inc. All Rights Reserved. [Privacy statement](#).
Comments? We would like to hear from you. E-mail us at customercare@copyright.com